The regolith expression of gold mineralisation in the Central Gawler Craton, South Australia: examples from the Tunkillia Gold Prospect and the surrounding region

BENJAMIN G. VAN DER HOEK

University of Adelaide
School of Earth and Environmental Sciences
Department of Geology and Geophysics

This thesis is submitted in fulfilment of the requirements for
the degree of Doctor of Philosophy in the Faculty of Science,
The University of Adelaide

May 2014

Contents

Abstract

Transported and typically weathered material that covers much of Australia presents a challenge to the successful application of surficial geochemical exploration methods. The Gawler Craton of South Australia is host to world-class IOCG-U style (viz. Olympic Dam and Prominent Hill) and Au (Challenger) deposits. Exploration in this region is a challenging enterprise, where 90% of the crystalline basement is under sedimentary cover. Geochemical sampling of regolith materials, such as pedogenic carbonate, has been attempted across the Gawler Craton to target buried mineralisation. However, results have been equivocal because the calcrete is potentially transported, poorly developed, or absent. Plant biogeochemistry has also emerged as a tool for mineral exploration, as it has been attributed to the discovery of mineralisation in regional-scale surveys in Canada, however, Australian applications have been limited.

The Tunkillia Au Prospect (*Mungana Goldmines Ltd.*), in the central Gawler Craton, was first recognised on a 50 km² area of elevated Au-in-calcrete (> 10 ppb). The Prospect has a challenging exploration context: pervasive sand dunes and leached saprolite cover mineralisation that is at depths greater than 50 m. Gold content in the surface materials does not always represent underlying mineralisation, and this has misled previous exploration targeting in the area.

In this thesis I show that a detailed analysis of the transported and residual regolith in three profiles to a depth of 50 m indicates that despite deep weathering, geochemical and mineralogical indicators of mineralisation are retained. The saprolite is predominantly kaolinite with relic feldspar in each of the profiles. White mica (muscovite and phengite) is abundant in the saprolite from the site of main mineralisation (Area-223). The white mica is distinguished using Hylogger™ and/or X-ray diffraction, and is characterised by Rb concentrations > 175 ppm using portable XRF instruments. Results from biogeochemical and calcrete sampling conducted across parts of the Tunkillia Au Prospect are interpreted in the context of landscape setting. Plant and calcrete Au results are similar at the prospect scale that suggests that the plants are accessing the Au from calcrete. The Au-in-calcrete anomaly is controlled by palaeo-drainage. Gold within calcrete is restricted to detrital sand pods, indicating the Au is transported within sediments from an upslope source. Silver and Te in plant leaves also indicate upslope mineralisation, highlighting areas of the Prospect that warrant further investigation.

Biogeochemical pathfinders of metre-scale mineralised veins in the Glenloth and Earea Dam goldfields west of Lake Harris I found were Au, Ag, Bi, Cu, Sn, Te and U. Biogeochemical sampling was implemented in regional surveys (20 – 200 km²) alongside regolith geochemical sampling. Calcrete development is generally irregular, whereas plant samples could be collected at regular intervals. Biogeochemical sampling was able to delineate underlying geology, particularly the Gawler Range Volcanics (high Pb) and Deception Hill basalt (high Re). Biogeochemical results were also found to be influenced by landscape processes such as mechanical and hydromorphic element mobility along drainage and aeolian contamination in open chenopod shrublands and near unsealed roads.

Keywords: *Tunkillia, Gawler Craton, biogeochemistry, calcrete geochemistry, Yellabinna, Glenloth, Earea Dam.*

Statement of originality

This work contains no material which has been accepted for the award of any other degree or diploma in any university or other tertiary institution and, to the best of my knowledge and belief, contains no material previously published or written by another person, except where due reference has been made in the text.

I give consent to this copy of my thesis when deposited in the University Library, being made available for loan and photocopying, subject to the provisions of the *Copyright Act 1968*.

I also give permission for the digital version of my thesis to be made available on the web, via the University's digital research repository, the Library catalogue, and also through web search engines, unless permission has been granted by the University to restrict access for a period of time.

Benjamin van der Hoek

Acknowledgements

Thanks to Steven Hill, Robert Dart, and David Giles from the University of Adelaide for their supervision, financial, and moral support. The following companies, organisations, and people are thanked:

Minotaur Exploration Ltd. for financial and technical support, digital databases, and accommodation for research at Tunkillia: in particular, Barry van der Stelt, Richard Flint and Tony Belperio. Mungana Goldmines Ltd., the new owners of the Tunkillia Au Prospect (from Jan 2012), for their continued support: in particular, Adrian McArthur and Pat Scott.

Endeavour Discoveries Ltd. for financial and technical support: in particular, Duncan Chessell, Nikki Galloway-Warland, Gerard Pagliaro, and Kim Petherick.

Deep Exploration Technologies Cooperative Research Centre (DET CRC) for financial and technical support, and the opportunity to be involved in the DET CRC community: in particular, Richard Hillis and David Giles; and, Program 3 researchers for feedback and suggestions; Caroline Forbes, James Cleverley, Yulia Uvarova, Adrian Fabris, John Keeling, Georgina Gordon, and Alan Mauger. Stephen Fraser (CSIRO) for the chance encounter on the bus at the first annual DET CRC conference and introducing me to Self-Organising Maps. CSIRO hydrogeochemical mapping team for the opportunity to experience regional groundwater sampling in the Yilgarn Craton WA: in particular, Nathan Reid, David Gray and Ryan Noble. David Haddow for assistance with the use of Leapfrog software. Tony Hall and Robyn Williamson for their assistance with X-Ray Diffraction analysis at the University of Adelaide.

The fellow PhD students: in particular, Ashlyn Johnson and the guys in the Continental Evolution Research Group (CERG) in the Mawson Labs – Frank Robinson and Russell Smits – for being around to provide a balance and discuss work and/or life over a burger and lemonade at the pub!

Special thanks to the late Keith Scott for his invaluable discussions and willingness to visit the PhD office at the University of Adelaide. Keith will be sadly missed as a mentor and friend.

Publications and conference proceedings derived from this research

VAN DER HOEK B. G., HILL S. M. & DART R. C. 2012. Calcrete and plant inter-relationships for the expression of concealed mineralization at the Tunkillia gold prospect, central Gawler Craton, Australia. *Geochemistry: Exploration, Environment, Analysis* **12**, 361-372. (TRaX Record 229).

VAN DER HOEK B. G., HILL S. M. & DART R. C. 2011. Regolith carbonate geochemical and plant biogeochemical inter-relationships for the expression of deeply buried mineralisation at the Tunkillia gold prospect, central Gawler Craton, Australia. International Applied Geochemistry Symposium, Rovaniemi, Finland.

VAN DER HOEK B. G., HILL S. M. & DART R. C. 2011. How deep is deep? Plant biogeochemistry for detecting deep mineralisation. Goldschmidt 2011, Prague, Czech Republic.

1. Introduction

Foreword

Since discovery of the Challenger Au Deposit in 1995 (Bonwick 1997) there has been a perception that calcrete is the holy grail of sampling materials for gold exploration in the central Gawler Craton. This has confused exploration in transported landscape settings (e.g., Tunkillia Au Prospect) and has effectively sterilised areas where there is low Au in calcrete response regardless of calcrete development. The processes of Au transport, enrichment, and preservation in calcrete (inclusive of *in situ* weathering, aeolian and alluvial transport processes, and biogeochemical cycling) is poorly understood. This thesis presents new data from biogeochemical sampling, and soil and calcrete sampling conducted as a series of case studies at sites of known mineralisation and in areas that are underexplored for mineralisation within the calcrete-dominated landscape of the central Gawler Craton. The data are presented with a discussion on the processes that redistribute bedrock geochemistry within the cover sequence. The overarching aims are to identify the indicators of mineralisation in surface materials (plants and calcrete) in the central Gawler Craton, and discuss the regolith processes that control their distribution in the landscape.

1.1. Exploration and mineral prospectivity

Regolith is soil and weathered material that sits atop fresh rock and covers most of the terrestrial Earth. Regolith is widely considered an impediment to mineral exploration. Nevertheless, regolith can host supergene or placer mineralisation and regolith processes facilitate the dispersion of elements from primary mineralisation, potentially magnifying the size of the exploration target. The chemistry of the regolith has a complex combination of hydrological, physical, and chemical dispersion. The processes driving movement of elements through this system, between fresh air and fresh rock, is still not fully understood.

The Australian minerals industry has been largely based on deposits discovered in the 1960s and 70s (CSIRO 2010b). The depletion of these and the exhaustion of exposed or near-surface mineralisation occurrences has forced mineral explorers into the challenging realm of exploration through transported and deep regolith, typical of much of Australia. This has yielded a limited number of discoveries to date. Efficient and effective targeting in mineral exploration therefore demands the development and application of new technologies and approaches.

Mineral prospectivity of the Gawler Craton is demonstrated by world-class mineral deposits (e.g., Olympic Dam and Challenger), and other projects at various stages of development such as the Tunkillia Au Prospect and the Fe-oxide-Cu-Au (IOCG) province on the Yorke Peninsula. Despite the limited bedrock exposure, mineral prospectivity evaluations of the region have been positive (Ferris *et al.* 2003).

1.2. Exploring with calcrete

Calcrete sampling and geochemical analysis has been a widely used exploration method in southern Australia since the late 1980s, following the discovery of Au mineralisation in South Australia: sub-economic (e.g., Barns, Boomerang, and Nuckulla Hill) and the world-class Challenger Au deposit. The Au affinity with calcrete has received great interest amongst the mineral explorers and researchers (who have proposed some models of association; Lintern & Butt 1993, Gray & Lintern 1994, Lintern 1999, Dart 2009, Lintern *et al.* 2009). Regolith carbonates are highly variable in composition and morphology across the landscape. The indurated form, calcrete, is commonly used as a sample medium for mineral exploration. A dependence on the perception of success from calcrete geochemical exploration has biased the approach of mineral exploration on the Gawler Craton, even in locations where calcrete is poorly developed or absent (McConachy 2001).

1.3. The biogeochemical frontier

Plants have long been used as a tool in prospecting for mineralisation (e.g., Lungwitz 1900). They source solutes from a large volume of regolith at various depths via their roots (Canadell *et al.* 1996), and accumulate these elements within the leaves. Plant biogeochemical exploration has resulted in the discovery of concealed mineralisation in Canada (Dunn *et al.* 2009, Ringrose 2011), and has been able to indicate presence of mineralisation in Australia in follow-up studies (e.g., Lowrey 2007). The Australian applications have been largely through research institutions.

Dunn *et al*. (1995) produced a comprehensive guide on using plant biogeochemical methods for mineral exploration with a few Australian examples. However, there has been limited application in Australia by the mineral exploration industry. Reluctance to use plant sampling methods is likely due to a poor understanding of: species-specific chemistry (Reid 2008); element pathways from fresh rock through the regolith to the plant; and minimal published examples of plant biogeochemistry in relation to mineralisation. Plant biogeochemical exploration has also been overshadowed by the faith placed in other regolith geochemical methods (e.g., calcrete sampling; Lintern 1997).

Biogeochemical techniques in arid Australia have had significant development in recent years (e.g., Reid 2008, Hulme 2010). A pilot biogeochemical sampling program conducted over mineralisation at Tunkillia Prospect had encouraging results indicating mineralisation underlying transported siliciclastic sediments and deeply weathered *in-situ* regolith (Lowrey 2007). Similar results have been reported from other small-scale mineral occurrences in southern Australia (Lintern *et al.* 1997, Lintern & Scott 1998, Arne *et al.* 1999, Lintern *et al.* 2006b, Lintern 2007, Lottermoser *et al.* 2008).

Advantages of developing biogeochemical methods in semi-arid Australia include wide sample coverage across many regolith types, low environmental impact, and new cost-effective exploration approaches in areas where results from calcrete sampling methodology have been inconclusive.

1.4. Project location

For this research I have chosen case studies at the Tunkillia Au Prospect and other parts of the central Gawler Craton. The case studies provide data that are specific to the processes of the redistribution of elements in the regolith, calcrete, and plants. The case studies were chosen because they will provide answers to the problems of redistribution of elements within the regolith and plants in the context of known Au mineralisation and in areas that have been underexplored because of the absence of calcrete.

This study is focussed west of Lake Harris and south of Tarcoola in the central Gawler Craton (Figure 1.1). Samples for the regional surveys are contained within the mineral exploration licence (EL) boundaries as marked. Regional studies include the Earea Dam and Glenloth Goldfields, Area 3, Area, 7, Glenloth North, and Yellabinna. Samples have been collected for detailed studies at the Tunkillia Au Prospect. Multiple studies at a particular location (e.g., Tunkillia Au Prospect, or the goldfields) are identified in their respective sections. The locations of other key regolith studies discussed throughout the text are marked in Figure 1.1: Challenger, Boomerang, Barns, Paris, Mawson, and a regolith study of the Harris Greenstone Belt (HGB).

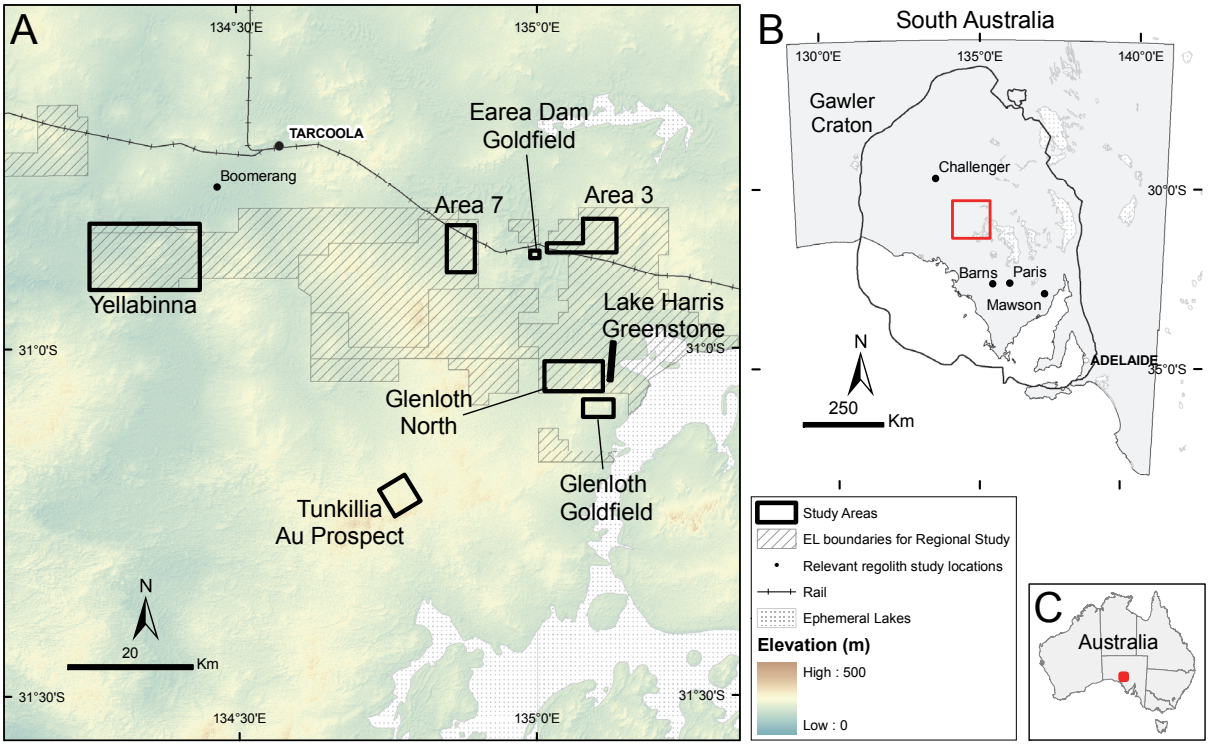

Figure 1.1: Locations of the study areas (A) within the central Gawler Craton, South Australia (B), and Australia (C). Black points denote external studies that are cited throughout the text. Study areas within the exploration licences (Endeavour Discoveries Ltd.) are part of the regional study. Multiple studies at a particular site (e.g., Tunkillia Au Prospect) are identified in their respective sections.

1.5. Project objectives

This study has two modules: (1) a detailed case study of the regolith processes at the Tunkillia Au Prospect; and, (2) broad-scale biogeochemical sampling and conventional regolith geochemical sampling regional mineral exploration in under-explored areas within the central Gawler Craton – Yellabinna-Lake Harris region.

Module 1: This module is a discussion of the geochemistry of *in-situ* and transported regolith at the Tunkillia Au Prospect, and the use of biogeochemistry for identifying mineralisation in this regolith setting. Existing drill hole data (Au assays and lithology), modelled with Leapfrog 3D geological modelling software, provides the basis for discussion with airborne electromagnetic (AEM) data, and digital elevation model (DEM) for the effectiveness of biogeochemical and geochemical sampling for exploration in this landscape and geological setting. This module aims to address the following points:

1. What characteristics of the regolith profile (*in-situ* and transported) can indicate the presence of underlying mineralisation, and are these indicators transferrable to biogeochemical and regolith (calcrete) sampling programs?
2. What is the relationship between plant and calcrete chemistry?
3. Discuss new and existing biogeochemical datasets with existing calcrete geochemistry, AEM and aeromagnetic data, and data collected from drilling.
4. What are the landscape processes and mechanisms that control the surface Au anomaly at Tunkillia?

Module 2: This module is a discussion of plant biogeochemical and regolith geochemical methods applied in regional mineral exploration with a broader context to Tunkillia. It is presented as a series of small surveys within the central Gawler Craton. Selection criteria for survey areas are: (1) underexplored by calcrete geochemistry, (2) in areas with prospective geophysical signals, and (3) within the exploration licences held by Endeavour Discoveries Ltd. This module aims to address the following points:

1. Can plant biogeochemistry be used to indicate narrow Au mineralisation over known occurrences (Glenloth and Earea Dam goldfields); and,
2. Can plant biogeochemistry be used to map regional trends and target potential mineralisation in favourable geophysical features of bedrock geology in parallel with regolith geochemistry where possible (e.g., calcrete and soil). Study areas are: Area-3, Area 7, Glenloth North, Yellabinna, and Lake Harris Greenstone.

By doing this I will provide examples with discussion on the considerations, effectiveness and outcomes of using biogeochemistry for mineral exploration at various scales and landscape settings within South Australia. It will also build on the regional biogeochemical data available for the central Gawler Craton.

2. Plant and regolith background

Foreword

This chapter provides a review of regolith, indurated materials and basic plant form and function, and terminology relevant to this study. It also provides an explanation as to how these materials can be used in geochemical mineral exploration with examples from mineral exploration throughout South Australia and globally. The review informs the sampling and analytical methodology of this study which are detailed in Chapter 3.

2.1. What is regolith?

Regolith is composed of minerals, biota, water, solutes and gases (McQueen 2006b) and can be defined as the unconsolidated or cemented material between fresh bedrock and the land surface (Eggleton 2001). It is formed from weathering, erosion, and sedimentary or chemical deposition of *in-situ* or transported material (Fraser 1997). Regolith can be broadly classified into pedolith and saprolith (Figure 2.1). Pedolith is the upper part of the regolith that has been subjected to soil-forming processes resulting in the addition of exotic material and the loss of the fabric of the underlying parent material (Eggleton 2001, p.93). Saprolith is weathered bedrock that has retained the fabric of the parent rock, with *in-situ* weathering. Saprolith can be further classified based on the degree of weathering of the labile minerals. Saprolite is defined by Eggleton (2001, pp. 105-106) as weathered bedrock in which the fabric of the parent rock is retained, and > 20% of the weatherable minerals have been altered. Saprock is slightly weathered rock, of which < 20% of the weatherable minerals have been altered.

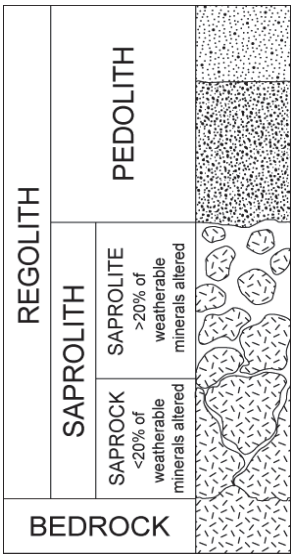

Figure 2.1: Components of the regolith profile in the central Gawler Craton. Adapted from Dart (2009) and Eggleton (2001).

The accumulation of Fe, Si and Ca within the upper parts of the regolith is common and can result in cementation to form various "cretes" (Wopfner 1978, Butt *et al.* 2009). Lamplugh (1902) originally coined the terms calcrete, silcrete, and ferricrete, to describe

these indurated materials. This nomenclature has since been applied to a range of other materials including aluminous (alcrete), gypseous (gypcrete), manganiferous (manganocrete), or saline (salcrete) indurations (Eggleton 2001). Highly indurated regolith is resistive to further weathering and erosion, and can have a significant control on subsequent landscape evolution. These indurated materials can form a prominent capping to plateaus or mesas in Australia (Langford-Smith 1978).

Mineral explorers have collected indurated regolith materials for geochemical analysis with mixed success. Silcrete is abundant in the central Gawler Craton in SA and has been tested as a geochemical sample medium for mineral exploration with minimal expression of underlying mineralisation (Butt *et al.* 2009). Similar investigations have been conducted on ferricrete. Anand & Paine (2002) suggest that there is generally no genetic relationship between ferricrete and the underlying weathered or fresh rock, but also that ferricrete is more strongly developed over Fe-rich rocks (Anand & Paine 2002, Butt *et al.* 2009), which are typical of the Yilgarn Craton in Western Australia. Calcrete, which is also widespread on the Gawler Craton and many other areas of semi-arid southern Australia, has also been sampled by mineral explorers with some resulting geochemical expression and discovery of buried mineralisation: this is detailed in *Section 2.3.1*.

2.2. Plant form and function

Since the mid-Silurian (c. 420 Ma) vascular plants have adapted to inhabit a vast range of terrestrial settings (Dunn 2007, p.10). An estimated 19% of the Australian continent is forested by species capable of achieving heights > 2 m (Moroni 2012), and has been vastly colonised by *Eucalyptus sp.* and *Acacia sp.* since the Miocene (c. 24 Ma; Morton *et al.* 2011).

Plants acquire the bulk of organic material from atmospheric gases (CO_2) and are an appreciable global storage for C in both living and dead material (Moroni 2012). Organic substances account for 96% of dry plant mass. The remaining 4% includes inorganic substances, which can contain more than 50 elements (Campbell & Reece 2005, p.757). Not all of these elements are essential for plant growth. Elements essential for growth can be categorised as macro- or micro-nutrients (Table 2.1).

Table 2.1: Elements essential for plant growth: macro-, and micro-nutrients. Adapted from Campbell & Reece (2005, p.758) and Dunn *et al*. (1995).

	Element	Form available to plants	% dry mass
Macronutrients	Carbon	CO_2	45*
	Oxygen	CO_2	45*
	Hydrogen	H_2O	6*
	Nitrogen	NO_3^-,NH_4^+	1.5*
	Potassium	K^+	1.0
	Calcium	Ca^{2+}	0.5
	Magnesium	Mg^{2+}	0.2
	Phosphorous	$H_2PO_4^-$, HPO_4^{2-}	0.2
	Sulfur	SO_4^{2-}	0.1
Micronutrients	Chlorine	Cl^-	0.01*
	Iron	Fe^{3+}, Fe^{2+}	0.01
	Manganese	Mn^{2+}	0.005
	Boron	$H_2BO_3^-$	0.002
	Zinc	Zn^{2+}	0.002
	Copper	Cu^+, Cu^{2+}	< 0.001
	Nickel	Ni^{2+}	< 0.001
	Molybdenum	MoO_4^{2-}	< 0.0001

*Not included for biogeochemical analysis in this study.

Movement of elements through the soil-plant continuum is greatly influenced by plant function (Burgess *et al.* 2001). Primary interaction that vascular plants have with the regolith is via the roots through three main processes: uptake; respiration; and, exudation (Hinsinger *et al.* 2006). Uptake of macro and micro nutrients (< 6% of total mass) from the regolith is a passive (non-metabolic) or active (metabolic) process, depending on the element (Kabata-Pendias & Pendias 2001). Passive uptake is the diffusion of ions from soil solution into the root (e.g., Ni and Pb). Active uptake requires metabolic energy for ion uptake (e.g., Cu, Mo, and Zn) where metal ions (cations) are exchanged for H^+ at the root surface (Hinsinger *et al.* 2006). Exudates produced by the plant during this process are weakly acid and facilitate the breakdown of primary minerals in the immediate root vicinity (Reid *et al.* 2009).

Plants and their associated micro-organisms actively modify the physical and chemical properties of their rooting environment known as the illuvial zone (Verboom & Pate 2006b). Redistribution of nutrients and water in this zone is important for pedogenic processes and the development of features such as Si- or Fe-linings of conduits, clay-based hardpans and precipitation of Si, Fe or Ca-indurated horizons (Verboom & Pate 2006a).

Some elements can be present in the regolith at concentrations potentially toxic to the plant. Mechanisms to manage an over-abundance of an element have been developed by some species. A barrier mechanism at the root surface can use an exudate to demobilise an element and prevent uptake (Hinsinger *et al.* 2006). Sequestration is another mechanism within subaerial organs that partition toxic metals into vacuoles (inter-cellular space).

Calcium-rich crystals are a common inclusion in plant vacuoles and have been hypothesised to play a central role in a variety of important functions: primarily Ca-regulation, plant protection, and metal detoxification (Nakata 2003). Crystal

morphologies vary with function: needle-like raphides serve as a defence against herbivory (Franceschi & Schueren 1986, Naudé & Naidoo 2007), and, druse crystals[1] evenly distribute light to cells (Franceschi 2001). Sequestration of Ca and heavy metals by plants means Ca-oxalate crystals have a potentially pivotal role in cycle of Ca and associated metals in the near-surface regolith (Goudie 1983), with particular implications for the formation of pedogenic calcrete and geochemically sampling regolith material in many mineral exploration programs.

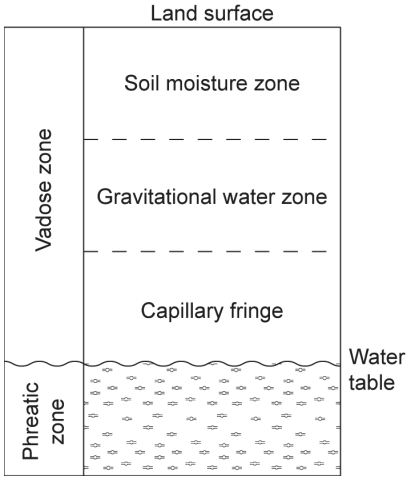

Figure 2.2: Hydrogeological zones within the regolith. Adapted from Carlisle (1980)

Deep-rooted plants (phreatophytes) can send roots down to the water table (phreatic zone) or capillary fringe (Figure 2.2; Meinzer 1923, 1927) securing a temporally-reliable water supply (Noy-Meir 1973). Xerophytes, in contrast, have adapted to conditions with minimal water supply and long periods of drought through efficient water use and near-dormant behaviour. The capillary fringe could be several to tens of metres above the water table through capillary rise, depending on the composition and porosity of the regolith (Keeling 2004).

Plant roots can make up greater than 80% of the total plant biomass (Caldwell & Richards 1986). An accurate assessment of plant root distribution and depth is therefore necessary for the understanding and prediction of water, solute and carbon fluxes in arid ecosystems (Canadell *et al.* 1996, Jackson *et al.* 1996). Plants in desert and shrub-land biomes, typical of inland Australia, have 53 to 67% of root biomass in the top 30 cm, in contrast to greater than 80% in boreal or tropical forests (Jackson *et al.* 1996). This suggests that plants inhabiting semi-arid environments are reliant on a deeper water source. In these biomes, the root biomass typically far exceeds the above-ground biomass. Maximum rooting depth at the global scale is probably best documented by Canadell *et al*. (1996, Figure 2.3), although there is limited published material, particularly with Australian examples.

[1] A spherical aggregate of individual crystals (Franceschi & Horner 1980, p.381)

Deserts and tropical savannah environments are host to deeper-rooted plant species to survive periods of drought (McCulley *et al.* 2004). Jackson *et al*. (1999) report root depths of 5 – 65 m and corresponding species (determined by DNA sequencing) of root material collected from caves in Texas, USA. Reid *et al*. (2009) report roots of *Triodia sp.* (Spinifex) extending to a depth beyond 30 m from observations in the Tanami Mine pit, Northern Territory, Australia.

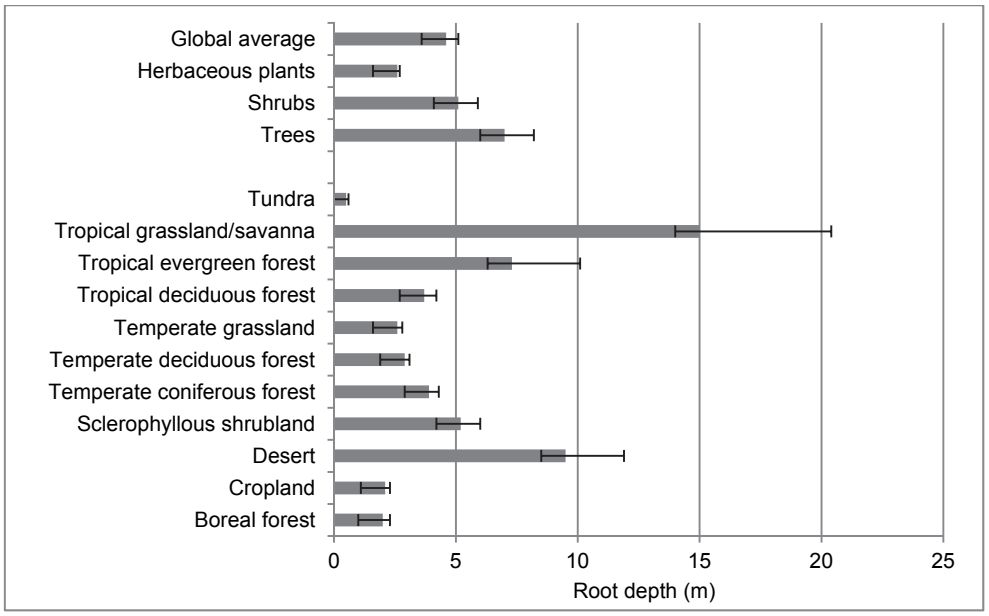

Figure 2.3: Average global root depths (with errors). Data are from Canadell *et al*. (1996).

There is ambiguity with use of 'deep' to describe root penetration depth. Deep has been used to describe root systems that extend below 1 m (McCulley *et al.* 2004). Using this definition, root-depth data from Canadell *et al*. (1996; Figure 2.3) indicates that plants from all environments (with the exception of tundra) are classed as deep rooted. However, the depth of root penetration and relationship to soil composition may not be critical in obtaining subtle responses to concealed bedrock geology (Dunn *et al.* 2009). This is because the processes invoked for explaining partial leach soil anomalies (e.g., extracting weakly adsorbed ions in soil) are relevant for the process of roots extracting anomalous elements from soil.

Plant root systems actively control the distribution of water and solutes in the regolith from depth through a hypothesised process of hydraulic lift (Figure 2.4; Richards & Caldwell 1987). Burgess *et al*. (1998) supplement the definition of this phenomenon with 'hydraulic redistribution' in which soil moisture is redistributed in the direction of water potential (up or down the profile). Through this process, water, major-, and trace-elements are extracted from a large volume of soil and saprolith through direct contact (Cohen *et al.* 1999), and are transferred between soil horizons.

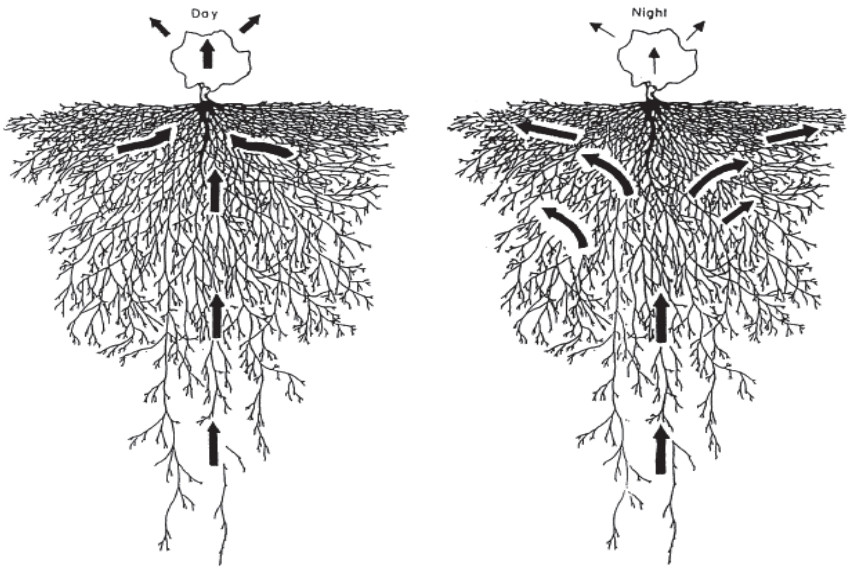

Figure 2.4: Water flow pathway through the root system during the day and night according to the hydraulic lift hypothesis. From Cadwell (1998).

2.2.1. Plants and mineral exploration

The potential for the use of plants in mineral exploration has been realised since the beginning of the last century when Lungwitz (1900) suggested the possibility of using Au content in vegetation as an indicator of concealed Au mineralisation (Girling *et al.* 1978). Many of the early studies used geobotanical associations, but as analytical technologies have improved there is an increasing application of chemical analysis methods (biogeochemistry).

Biogeochemistry is the integration of the sciences of biology (plants), geology and chemistry by the collection and chemical analysis of plant material to assess the presence and nature of underlying mineralisation, bedrock composition and structure, and soil, substrate and associated groundwater chemistry (Dunn 2007). The method is based on plant function, where certain metals or characteristic elements present in the substrate are extracted by the roots and concentrated in the tissues (Dorr *et al.* 1971).

Plant chemistry is a well-researched topic with the bulk of published information coming from agronomic species: corn, tomatoes, beans, peas, cucumbers, and grains (Dunn *et al.* 1995). These studies provide information for plant physiology, nutrition (Kabata-Pendias & Pendias 2001, Ch.5), and environmental contamination, and have applications in the environmental management and mineral exploration industries (Overall & Parry 2004, Thiry *et al.* 2005, Lottermoser *et al.* 2008).

Case studies that have shown plant biogeochemistry to have successfully identified sites of concealed U and base-metal mineralisation in Canada (Dunn 1986, Cohen *et al.* 1987, Dunn *et al.* 2009, Ringrose 2011), Papua New Guinea (McInnes *et al.* 1996), Russia (Kovalevskii & Kovalevskaya 1989), United Kingdom (Girling *et al.* 1978), with applications in South Africa (Ilja Knesl, pers. comm. 2011). A particularly encouraging case study (for the use of biogeochemistry) is the discovery of high-grade Zn mineralisation in British Columbia, Canada, which was accomplished by a "single tree-top anomaly" of Tl (Dunn 2011, Ringrose 2011).

There are many examples of biogeochemical sampling in various landscape and mineralised settings throughout Australia over known mineralisation and in prospective areas (Lintern *et al.* 1997, Cohen *et al.* 1998, Cohen *et al.* 1999, Hulme & Hill 2003, Lintern 2004a, Lintern *et al.* 2006b, Lowrey & Hill 2006, Reid *et al.* 2010, Tanti 2011). Biogeochemical sampling had a significant research investment from the Cooperative Research Centre for Landscape Environments and Mineral Exploration (CRC LEME; from between 2001 – 2008). Cohen *et al*. (1999) compare provincial vegetation and stream sediment surveys from New South Wales and found that vegetation was more dependent on hydromorphic dispersion and has a longer dispersion train from mineralisation. The authors also report cases where Au mineralisation is expressed by vegetation only, but other cases where stream sediments prevail over vegetation.

The advantages of plant biogeochemical methods include: low cost of sampling and analysis (compared to drilling); widespread sample coverage; negligible environmental

impact; minimal remediation post-sampling; and, low sample weight (Hulme & Hill 2003). However, there is yet to be a major discovery of concealed mineralisation solely from the use of vegetation in Australia. This is attributable to the limited application of biogeochemical methods, which is likely due to the lack of knowledge surrounding the standard chemistry of Australian plant species and biogeochemical pathfinders, and potentially the complication caused by an increased species diversity than the northern hemisphere (Lintern *et al.* 1997, Cohen *et al.* 1999, Reid 2008).

2.3. Regolith carbonate and calcrete

Calcium carbonate is a widespread and abundant component of coastal and inland southern Australian soils. Calcium carbonate-infused soil occupies up to 21% of the mainland (Figure 2.5; Quade *et al.* 1995, Chen & Roach 2002) and is amongst the most significant rainwater-soluble salts, with gypsum and halite, in dry regions (McKenzie 2004). Gypcrete and evaporite accumulations tend to predominate in very arid environments, however, their distribution is further controlled by local geomorphology (Goudie 1983). Other regolith carbonates include: dolomite ($CaMg(CO_3)_2$), magnesite ($MgCO_3$), and the less common siderite ($FeCO_3$) and ankerite ($Ca(Mg,Fe)(CO_3)_2$).

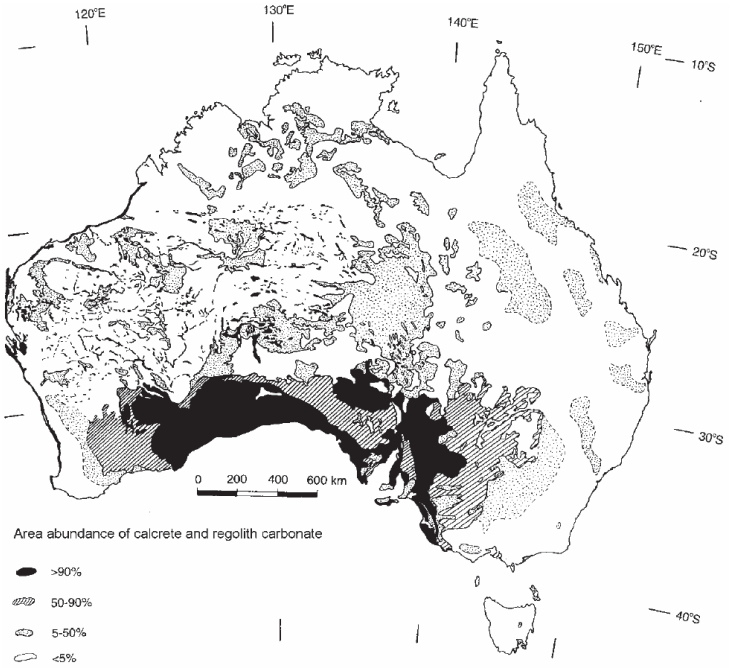

Figure 2.5: Interpretive map of Australian calcrete and regolith carbonate. From Chen *et al.* (2002b).

Calcrete is a general term used for near-surface accumulations of Ca-carbonate resulting in the cementation of sediments or bedrock (Wright 2008). In Australia the terminology used in the classification of calcrete has been the subject of much debate, where the acknowledgement of induration morphologies and extent, as well as chemical and mineralogical composition, may be significant for mineral exploration programs (Hill *et al.* 1998, McQueen *et al.* 1999). Previously, the necessity for a systematic calcrete classification came from the need to accurately describe and predict the engineering performance of materials composed of cemented particles used for construction and foundation in arid and semi-arid regions (Netterberg & Caiger 1983).

The term 'calcrete' has been most specifically used to describe Ca-carbonate cementation in regolith materials, a nomenclature used for its compatibility with other indurated materials: silcrete (silica) and ferricrete (Fe oxide; e.g., Lamplugh 1902). It has also been contentiously applied to a broader range of regolith carbonate compositions (including dolomitic) and degree of induration ranging from highly indurated to powdery and disseminated materials (Goudie 1973), for which the more general term 'regolith carbonate' may be more suitable (Hill *et al.* 1998, Chen *et al.* 2002a, Hill *et al.* 2003).

Composition

Geochemistry can be used to characterise calcrete (Goudie 1973, Netterberg 1980, McQueen 2006a, Alonso-Zarza & Wright 2010), with Ca unanimously being the dominant cation. Calcrete from Australia and worldwide have, on average, 1.8% Mg (Goudie 1973), whereas Mg concentrations > 5% are suggested to represent dolomitic regolith materials (Netterberg 1980). More recently, Australian calcrete has been defined by both geochemistry and morphology (McQueen 2006a), and Sr isotope composition to distinguish the source of Ca.

The distribution of Ca-carbonate in soils is widespread and its presence in soils developed from non-Ca-carbonate-rich parent materials indicates that there are external sources of Ca (Wright 2008). Sources of Ca in Australian pedogenic carbonate have been studied using Sr isotopes ($^{87}Sr/^{86}Sr$) as surrogate (Lintern *et al.* 2006a, Dart *et al.* 2007, Dart 2009). Samples were collected from overlying Au mineralisation in the Gawler Craton to ascertain if there was a link between the source of Au and Ca. Samples were found to contain an unexpected atmospheric source of Sr (> 94%) and by inference Ca (> 98% Ca is atmospherically-sourced; Lintern *et al.* 2006a). Also using $^{87}Sr/^{86}Sr$ isotopes, Dart *et al*. (2007) investigated the source of Ca in carbonates at 8 sites throughout inland Australia. Results revealed a bedrock Sr (and by inference, Ca) source of up to 32% in northern Australia, and less than 5% at the Tunkillia Au Prospect in the central Gawler Craton, and at Clarendon, near Adelaide (Figure 2.6).

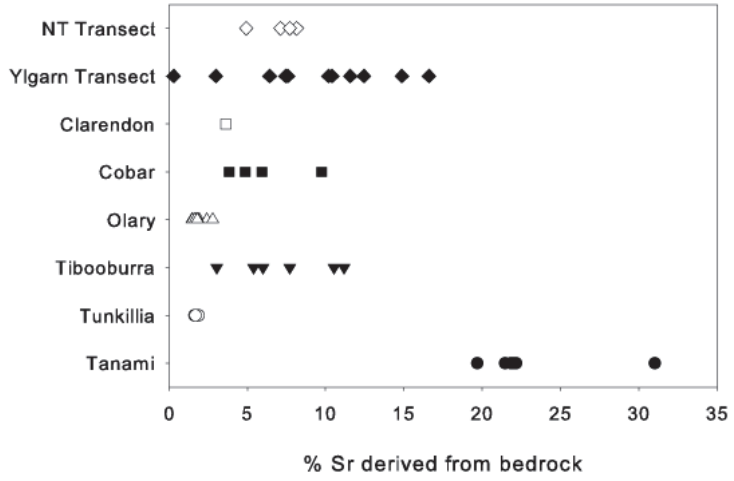

Figure 2.6: Plot showing the percentage of Sr derived from bedrock, taken from Dart *et al*. (2007)

Morphology

At least five distinct genetic types of calcrete have been proposed worldwide, including calcareous soil; powdery, nodular, honeycomb, hardpan, and boulder calcrete (Figure 2.7; Goudie 1973, Carlisle 1980, Netterberg & Caiger 1983), however there are two general types in southern Australia (Anand *et al.* 1997): groundwater (phreatic) and pedogenic (vadose). The latter two classifications are generally based on the position in the regolith, and the hydrogeological regime under which they have formed (Figure 2.2). These can be further classified by macro- and micro-morphology, internal structure, and geochemistry.

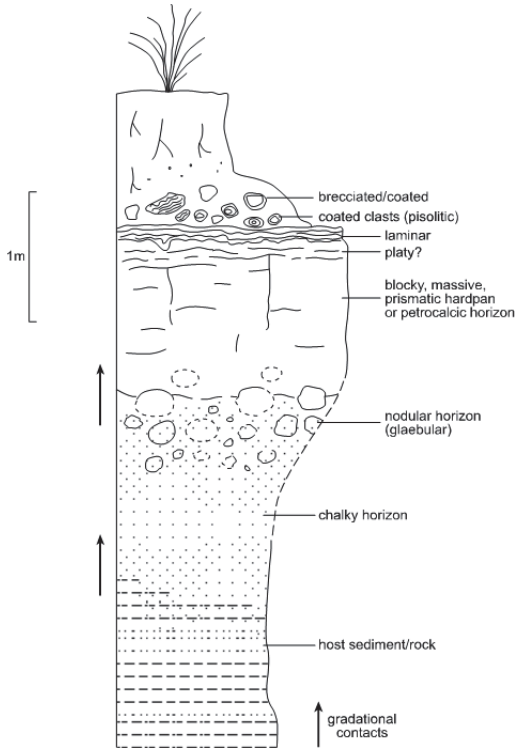

Figure 2.7: Idealised calcrete profile, from (Wright 2008, Alonso-Zarza & Wright 2010)

Mechanism of formation

Precipitation of Ca-carbonate typically occurs in regions with 400-600 mm of annual precipitation. At a local scale, however, landscape setting can be more significant than climate in controlling the distribution and depth of precipitation (Goudie 1983). Depth of precipitation is typically at the depth of seasonal wetting and drying (Wright & Tucker 1991).

The process of precipitation and dissolution of Ca-carbonate can be simplified as follows (e.g., Carlisle *et al.* 1978, p.24):

$$H_2O + CO_2 + CaCO_3 \quad \leftrightarrow \quad Ca^{2+} + 2HCO_3^- \qquad [1]$$

Calcium carbonate will precipitate from solution by driving the reaction (equation [1]) to the left. This can be achieved by increasing the concentration of Ca^{2+} and HCO^{3-} in solution, or by the removal of either H_2O or CO_2 from solution.

Pedogenic calcrete formation

Pedogenic calcrete is predominantly Ca-carbonate that occurs as a powdery to highly indurated morphology within the soil profile (Wright & Tucker 1991, Alonso-Zarza & Wright 2010). Calcium content typically has an asymmetric vertical distribution representing changes in morphology with depth (Figure 2.7), which is well-recognised in studies investigating the Au-in-calcrete phenomenon in mineralisation-endowed regions (Wright & Tucker 1991, Gibbons 1997, Lintern 1999).

The formation of pedogenic calcrete is a result of accumulation, through predominantly vertical redistribution, of Ca, Mg, carbonate, and trace elements within the soil moisture zone of the pedolith (Carlisle 1980, p.7). On the Gawler Craton, a predominantly atmospheric source of Ca has been determined for calcrete (Lintern *et al.* 2006a, Dart *et al.* 2007) indicating a top-down model of formation (or per-descensum; Goudie 1983). Other Ca sources include bedrock, vegetation litter, atmospheric dust, rainfall, lakes, surface run-off, and groundwater (Goudie 1983).

Various models of calcrete formation have been proposed (e.g., Gile *et al.* 1966, Goudie 1973, 1983, Klappa 1983, Wright & Tucker 1991, Lintern 2007) that typically involve the controls on the components in equation [1], and a left-shift in the equilibrium: removal of H_2O and/or CO_2. Evapotranspiration is regarded as the dominant process in formation, in which water is extracted from the soil via plant roots. Degassing of CO_2 is also a driver of Ca-carbonate precipitation (Salomons & Mook 1986). Calcium-carbonate precipitation is a multi-cyclical process (Wright & Tucker 1991, Gibbons 1997, Chen & Roach 2002) and follows the general sequence of formation illustrated by Figure 2.8 (Gile *et al.* 1966, Wright 2008). The process initiates with the calcification of roots and formation of rhizomorphs within existing sediments. Calcium-carbonate precipitates as coatings to sediments and eventually plugs pores and solution pathways, producing a 'hardpan' calcrete horizon. These horizons are subject to cracking, dissolution pathways, and reworking (Gile *et al.* 1966).

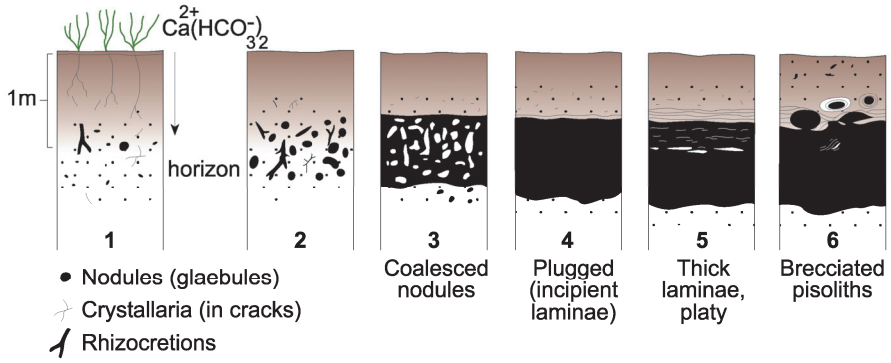

Figure 2.8: Stages of calcrete formation based on model from Gile *et al.* (1966). Diagram from Wright (2008).

2.3.1. Calcrete and mineral exploration

Calcrete is a popular geochemical sampling material in many mineral, particularly Au and U (Chen & Roach 2002), exploration programs in semi-arid regions of southern Australia (Anand *et al.* 1997, Lintern 1997, Martin 1997, McQueen *et al.* 1999, Schmidt Mumm & Reith 2007). This is largely due to its successful case-history of concealed Au mineralisation discovery (Figure 2.9; Bonwick 1997, Martin 1997, Drown 2003), and also for being easily recognisable in the 'B' or illuvial soil horizon (Lintern 2002). Despite some successes, however, the understanding of processes and mechanisms responsible for the generation of elevated Au in calcrete are poorly constrained. Of particular concern to exploration companies are situations where high concentrations of Au in calcrete have a poorly constrained association with underlying mineralisation (e.g., Gibbons 1997, Klingberg 2009).

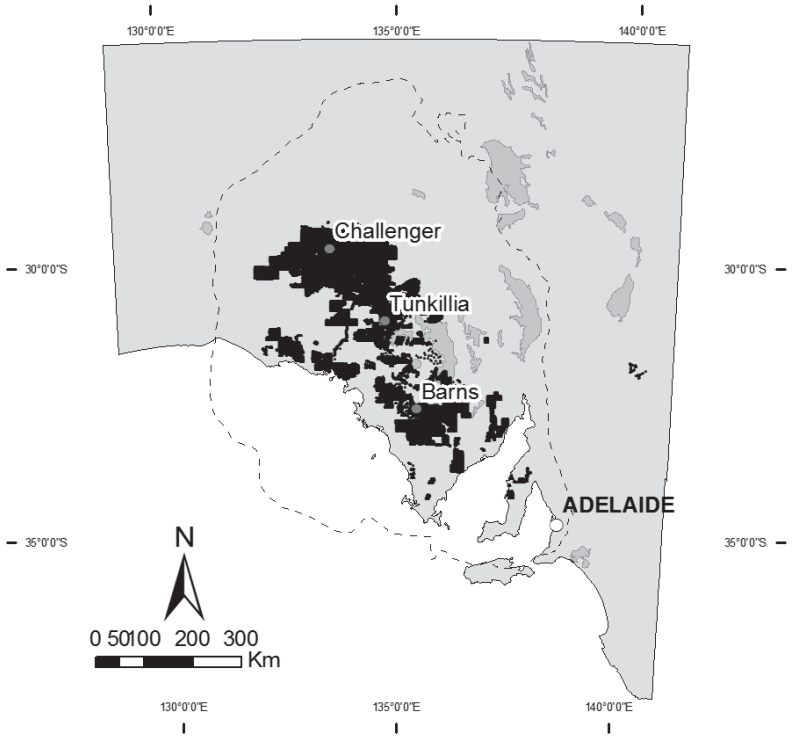

Figure 2.9: South Australian calcrete data locations (total of 180,000) on the Gawler Craton (dotted; PIRSA 2011)

Calcrete (typically nodular and hardpan; Figure 2.7) has received significant interest amongst mineral explorers since the late 1980s with the discovery of the Au-Ca (and Mg) association in the upper regolith horizons. One of the earliest published investigations of the distribution of Au in soils is from the Bounty Au deposit, Mount Hope area, Western Australia; originally an internal/restricted report from 1989, was released ten years later within the Cooperative Research Centre for Landscapes Environments and Mineral Exploration (CRC LEME; Lintern 1999). This study found an accumulation of Au, Ca, and Mg in the near surface horizons and that the concentration of these elements decreased descending the profile. The Au-Ca association was recognised on the Gawler Craton in 1993 (Wills 1997), has since been acknowledged in other regolith profile studies (e.g., Gibbons 1997, Lintern 1999, Lintern *et al.* 2006a, Dart 2009). An overwhelming application of the calcrete sampling method ensued in South Australia

resulting in the discovery of a several significant Au prospects, deposits, and sub-economic occurrences of mineralisation: Tunkillia (Martin 1997); Barns (Drown 2003); Challenger (Bonwick 1997, Edgecombe 1997), Boomerang (Lintern *et al.* 2006b), and possibly more that are not reported in the scientific literature (Lintern *et al.* 2006a).

Discovery examples

A shallow drilling program conducted by Dominion Mining Ltd. in South Australia during the early 1990s (1993-1994) revealed elevated Au in the surface horizons, which appeared to be associated with Ca (Edgecombe 1997). Application of regolith carbonate sampling in the region, either by shallow auger drilling or the collection of surface indurated carbonate material led to the discovery of the Challenger Au mineralisation. At Challenger the elevated Au-in-calcrete results span 400 m with a peak of 296 ppb Au (Edgecombe 1997, Ferris *et al.* 2003). Mineralised bedrock practically reaches the surface at Challenger: highly weathered bedrock (saprolite, quartz and clays) is situated at a depth of less than 10 m (see photo in Appendix B).

Discovery of the Barns Au mineralisation was a result of a regional reconnaissance calcrete sampling program (1 km spacing) conducted by Newcrest Mining Ltd. between 1996 – 1997 that revealed high Au-in-calcrete concentrations (Figure 2.10). Follow-up calcrete sampling at 500-m intervals defined a large Au-in-calcrete anomaly with a peak of 31 ppb Au and even further sampling at 400, 200 and 100-m spacing produced a peak of 49 ppb Au and significant areas greater than 10 ppb Au (Drown 2003). Primary Au, although sub-economic, is hosted by coarse granodiorite (visually similar to the Tunkillia Suite), with an extensive envelope of hydrothermal alteration. Transported aeolian cover, of thickness less than 10 m, conceals the Barns prospect and significant drill intersections of primary mineralisation at depths greater than 30 m (Drown 2003). Barns has also been the subject of various plant biogeochemistry, and, microbial-mediation of Au in calcrete studies (Lintern 2004a, 2005, Lintern 2007, Schmidt Mumm & Reith 2007).

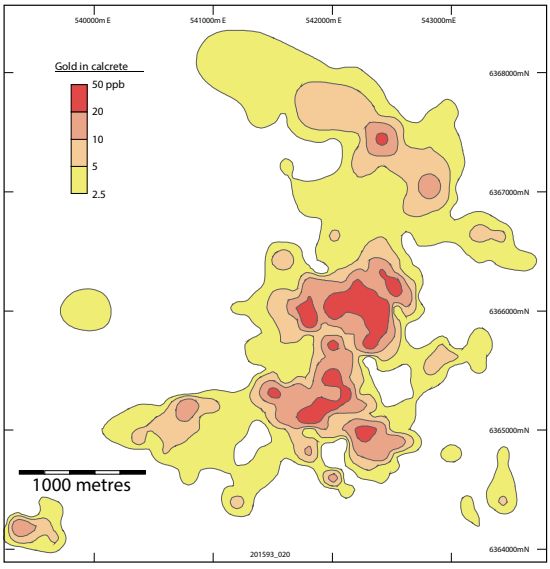

Figure 2.10: Au-in-calcrete anomaly associated with the Barns Au mineralisation. From Drown (2003).

3. Methods

Foreword

This chapter describes the methods and rationale used for the collection and chemical analysis of each of the sample materials (vegetation, calcrete, and soil) as part of several field programs conducted in collaboration with mineral exploration companies. The data that are presented in this thesis were produced using these methods and are exclusive to this study, unless stated otherwise. Data that are used from other sources, where the methods of collection and chemical analysis differ from those described for this study, are noted in the relevant sections below and reference is made to their respective source where used and discussed in the text.

3.1. Scale of geochemical mapping

Many economic mineralisation occurrences can be closely related to a series of larger target areas that can be characterised by some geological, physical or chemical feature that is diagnostic of the mineral system (Hawkes & Webb 1962, p.322). Mapping the distribution of elements in different parts of the regolith is needed for recognising the relative importance of, and understanding of these physical and geochemical features and their relation to 'background' levels (Reimann 2005, Garrett *et al.* 2008).

Carrying out geochemical mapping on a large scale can be a challenging enterprise, beginning with survey design, and includes: choice of a suitable sample material, and appropriate sample density (Reimann 2005) that depend on the size and shape of the target feature. Additional challenges arise from the spatial and temporal variation of the abundance and the chemistry of the sample material (from *Chapter 2, Section 2.3*).

Scale

Levinson (1974, p.10) proposes that geochemical surveys are classified as *detailed* or *reconnaissance* according to their scope (Table 3.1). A *reconnaissance* survey is typically used to evaluate a large area for mineral prospectivity, delineating mineralised areas for follow-up studies, and eliminating barren ground, often through low density sampling. A *detailed* survey, in contrast, is suited to a local smaller area of higher density sampling, and may include regolith or vegetation sampling, depending on the scale of the target being sought (e.g., narrow vein or highly dispersed).

Regional reconnaissance surveys should employ a practicable and cost effective configuration, yet maintain sample spacing suitable for the type of target (Hawkes & Webb 1962). Mineralisation in the central Gawler Craton Au province can be up to 200 m wide and have a surficial footprint of many hundreds of metres (e.g., Tunkillia Au Prospect), or can be as narrow as a few metres and have a strike length of a few hundred metres (e.g., Earea Dam goldfield).

Table 3.1: Classification of geochemical patterns according to size of feature, from Xuejing & Binchuan (1993).

Sizes	Geochemical Patterns
0.n km^2	LOCAL
n km^2	
n x 10 km^2	REGIONAL
n x 100 km^2	
n x 1,000 km^2	GEOCHEMICAL PROVINCE
n x 10,000 km^2	
n x 100,000 km^2	MEGA PROVINCE
n x 1,000,000 km^2	

Pattern

In the context of soil sampling, Hawkes and Webb (1962, pp.211-214) suggest the best sample pattern and spacing is determined primarily by the size and shape of the target. For vegetation surveys, however, the authors cannot recommend a universal system and strongly suggest a review of previous studies in similar areas or a carefully planned orientation survey. Fortunately there is a large amount of existing information available for the sample materials used in the area: calcrete from the South Australian geological survey (DMITRE) database; and vegetation and soil studies from published and unpublished sources (see *Chapter 2*).

Sampling material

Biogeochemistry has been used at a regional to provincial scale in Canada (e.g., 1 km; Dunn *et al.* 2009), and various local scales at mineral prospects in Australia (Barns, Boomerang, and Tunkillia; Figure 1.1). A sample spacing of 200 m was adequate to delineate mineralisation at Barns on the Eyre Peninsula (Lintern 2007), a spacing of 60 m could not delineate mineralisation at Boomerang (Lintern *et al.* 2006b), and 50 m was able to delineate mineralisation at Tunkillia (Lowrey & Hill 2006, Lowrey 2007, Belperio 2009a). These prospects were all discovered through regional sampling programs showing elevated concentrations of Au in calcrete.

Calcrete has been sampled for geochemical exploration in South Australia at 1000 m spacing for regional programs ranging to 25 m spacing for local, follow-up surveys. The calcrete sampling attributable to the discovery of Challenger was conducted on a staggered grid at a spacing of 1.6 km between centres (Edgecombe 1997): the highest result of 180 ppb Au was supported by 5 – 7 ppb Au in adjacent samples either side. A deviation of sample location by 200 m would have received a lower priority and potentially missed the mineralisation.

Samples collected for this study can be classified as detailed (or local): geochemistry and mineralogy of the saprolite, and expression of mineralisation by plants and other regolith material at Tunkillia; and, biogeochemical expression of mineralisation at the historic Glenloth and Earea Dam goldfields, or reconnaissance (or regional): exploration target generation using biogeochemistry and regolith materials within active exploration tenements (Figure 1.1).

3.2. Biogeochemical methods

An overview of biogeochemical sampling methodology is provided by Dunn *et al*. (1995) in the short course notes entitled *Applied biogeochemistry in mineral exploration and environmental studies*, and is discussed further in *Biogeochemistry in mineral exploration* by Dunn (2007). Some Australian adaptations based on these methods are detailed by Hill (2002), Hulme *et al.* (2006), and Sheard *et al*. (2007, pp.102-106 & Appendix 6), and these adapted methods have been used by researchers in Australian studies (Lowrey 2007, Hopkinson 2009, Vasey 2009, Hicks 2010, Mitchell 2010, Tanti 2011, Thomas 2011). These sources and other published Australian applications of biogeochemistry in mineral exploration (e.g., M.J. Lintern and others), have been reviewed and adapted to the planning and execution of the collection of biogeochemical data included in this study. Plant samples have been collected by various personnel especially students from the University of Adelaide, and research sponsors from the mineral exploration industry.

Material description Plant species and the target plant organs used for biogeochemical sampling in the central Gawler Craton are listed in Table 3.2. These species are used due to their previous applications in similar biogeochemical studies: mulga (Reid *et al.* 2010), black oak (Lowrey 2007), having a widespread distribution, and being easily identifiable – even by the non-botanist.

Since each species has a characteristic chemistry, selecting a widespread and abundant species helps to maintain spatial coverage and a consistent biogeochemical background. Further chemical differences throughout the plant means consistency with plant organ is also important (e.g., bark, twigs, and leaves; Dunn *et al.* 1995).

Table 3.2: Plant species and tissue sampled. New data sourced for this study and compiled from Minotaur Exploration Ltd. and Ames (2010) and Hopkinson (2009).

Plant	Scientific name	Organ sampled	No. samples
Black oak	*Casuarina pauper*	Branchlet	574
Pearl bluebush	*Maireana sedifolia*	Twig & leaf	563
Mulga (various)	*Acacia aneura, Acacia ramulosa*	Phyllode	216
Victoria Desert mallee	*Eucalyptus concinna*	Leaf	335
Woody Cassia	*Senna artemisioides*	Leaf	28
			Total: 1716

Survey layout **Tunkillia Au Prospect** biogeochemical surveys align with previous exploration drilling on an uneven grid (50 by 200 m). The smallest interval (50 m) is on a traverse perpendicular to the strike of the regional shear zone hosting mineralisation. Details of these surveys are contained in *Chapter 5*.

Narrow mineralisation biogeochemical surveys at the historic Glenloth and Earea Dam goldfields are samples collected at 25-m intervals along a single traverse perpendicular to the mineralised structure. Details of these surveys are contained in *Section 6.1.2*.

Regional biogeochemical surveys use an uneven grid pattern with a spacing

of 250 by 500 m, or 250 by 1000 m (depending on the area). The smallest interval (250 m) is on a traverse perpendicular to linear features on the South Australian aeromagnetic imagery (SARIG 2012).

Collection Particular attention was given to precautions detailed by Dunn (2007, pp. 106-114) regarding the removal of personal jewellery (precious metals) prior to the handling of samples, and avoiding contact with metallic objects and sunscreen.

Branch terminals, predominantly leaves, were targeted (Table 3.2) minimising branch material and avoiding, new growth, reproductive organs (flowers, fruit, nuts) or tissues with ill-heath. Samples included 100 g of combined leaf and branch material (no more than 10 cm of branch) collected from around the circumference (360°, where possible) of the canopy. Low hanging branches on shrubs (e.g., bluebush) are avoided to minimise contamination from aeolian and alluvial detritus.

Plant material was collected with leather-gloved hands and stored in paper (Tunkillia) or canvas bags (regional surveys). Storage in paper bags with folded top, or tied-off canvas bags inhibits further contamination, while allowing some aeration and impedes decomposition prior to drying. This is particularly important for some of the more succulent samples. For example, the *Maireana spp.* can contain 25-60% moisture (Hill 2004, p.78) and without sufficient ventilation, the paper bags will rapidly disintegrate.

Timing Plant biogeochemistry can exhibit considerable seasonal variation (Dunn 2007, pp. 66-73), and it is recommended that sampling programs are conducted over no more than a few weeks. Single surveys here were conducted over no more than a few days. Table 3.3 shows the collection dates of individual surveys that span several seasons over a period of 4 years.

Table 3.3: Biogeochemical sample collection dates, by survey.

Collection date	Location	Data source
April 2009	Tunkillia (Tomahawk)	Hopkinson (2009)
April 27-30, 2010	Centurion and Area-191 to Tomahawk	Ames (Centurion only; 2010)
February 14-24, 2011	Area 3 (southern 2 lines), Glenloth North	
June 14-28, 2011	Yellabinna, Area-3, Area-7, Glenmarkie	
February 17-22, 2012	Goldfields and Lake Harris drill line	

Preparation Samples were not washed to ensure the data were compatible with those from previous Honours' studies at the Tunkillia Au Prospect and other locations in South Australia. Possible consequences of not washing samples are discussed in *Section 3.6.3*.

Plant samples were dried at 60°C (within paper bags) to minimise

volatilization of elements, for at least 48 hours. Note: dry samples can be stored in a dry location without deteriorating.

Plant samples collected from the Tunkillia Au Prosepct during 2009 (Hopkinson 2009), and Glenloth (Jay Jay & Fabians No.3) and Earea Dam goldfield (2012) were sorted to isolate leaf material from any large branch fragments, pulverised using a rotating stainless still blade mill (Breville® coffee grinder), and placed into Kraft paper envelopes. Compressed air was used to clean the mill, and ethanol to remove residual oils between samples.

Regional samples were dispatched to Acme Analytical Laboratories, Canada for maceration using a rotating blade mill.

Analysis A 5 g portion of the milled sample underwent nitric acid and *Aqua-regia* digest, and was analysed using ICP-MS (product code: PM, 1VE2+1E6) at Acme Analytical Laboratories, Canada. The full analytical suite, with lower detection limit in parentheses is listed below. Concentrations are in ppm unless indicated otherwise.

Au (0.2 ppb), Ag (2 ppb), Al (0.01 %), As (0.1), B (1), Ba (0.1), Be (0.1), Bi (0.02), Ca (0.01 %), Cd (0.01), Ce (0.01), Co (0.01), Cr (0.1), Cs (0.005), Cu (0.01), Fe (0.001 %), Ga (0.1), Ge (0.01), Hf (0.001), Hg (1 ppb), In (0.02), K (0.01 %), La (0.01), Li (0.01), Mg (0.001 %), Mn (1), Mo (0.01), Na (0.001 %), Nb (0.01), Ni (0.1), P (0.001 %), Pb (0.01), Pd (2 ppb), Pt (1 ppb), Rb (0.1), Re (1 ppb), S (0.01 %), Sb (0.02), Sc (0.1), Se (0.1), Sn (0.02), Sr (0.5), Ta (0.001), Te (0.02), Th (0.01), Ti (1), Tl (0.02), U (0.01), V (2), W (0.1), Y (0.001), Zn (0.1), Zr (0.01).

3.3. Regolith methods

3.3.1. Calcrete

A review of the literature on the use of calcrete sampling provides an insight into various survey configurations and ideal sample morphologies. In the literature, physical collection methods are often implicit: methods typically include opportunistic surface sampling (Klingberg 2009), or hand-augering and auger-drilling (Wills 1997). Calcrete samples discussed in this study are from multiple field programs in collaboration with research sponsor companies and have been collected by one of these methods (Table 3.4). The methods described in this section are for the multi-element geochemical data from Tomahawk (Klingberg 2009) and the Regional surveys at Area-3, Area-7 and Glenloth North.

Table 3.4: Calcrete data location, sample collection methods and data source.

Location (spacing)	Section	Collection Method	Collection Date	Source
Tomahawk (50 x 200 m)	6.2, 6.5	Hand, from surface	April 2009	Klingberg (2009)
Tunkillia (400 m) Regional survey	5, 6.4	Unknown	Unknown (Accessed 2012)	South Australian Resources Information Geo-server
Tunkillia Prospect (25 x 100 m) Area-223 Area-191, Tomahawk	6.3, 6.5	Unknown	1996 - 1998	Minotaur Exploration Ltd.
Regional (500 x 500 m) Area-3 Area-7 Glenloth North	8.2	Vehicle-mounted mechanically- powered 4-inch auger	2011	Collected for this study in co-operation with Endeavour Discoveries Ltd.

Material description

Tomahawk calcrete samples are highly indurated nodules (Klingberg 2009). **Regional** sample morphologies range from highly indurated, well-developed hardpan to friable nodules or calcareous soil.

Programs & collection method

Tomahawk calcrete samples were collected opportunistically from the surface (predominantly swales) within small drainage depressions, root mats of overturned trees, and excavations and other exposures from drill-pad clearance as part of a University of Adelaide Honours' study by Klingberg (2009).

Regional samples were collected from a gridded sample array using a vehicle-mounted mechanically-powered 4-inch auger from depths generally < 2.5 m. The auger typically produced a powdered sample upon contact with an indurated (carbonate and/or silica) horizon. The first appearance of pale carbonaceous material was tested for effervescence with cold 10% w/v HCl. If the regolith from the auger contained fragments of calcrete, a bottom-of-hole sample was collected. If the regolith from the auger contained fragments of silcrete, the calcrete was often reduced to powder. In this case, the sample was sieved (< 5 mm mesh) to remove the diluting silcrete fragments and a powdered carbonate sample was collected. Samples were stored in snap-seal plastic sample bags.

Timing See Table 3.4

Preparation & analysis Regolith carbonate samples were processed and pulverised by the commercial laboratories: Genalysis Laboratory Services, Perth; and, ALS, Adelaide. Two different laboratories were used by the company geologist who supplied the data.

Genalysis (April, 2009 & February, 2011)

Samples were dried and pulverised and a 10 g sub-sample underwent *Aqua regia* digestion. The analytical process used solution ICP-OES and ICP-MS (product code: AR10/OM10). The full analytical suite, with lower detection limit in parentheses is listed below. Concentrations are in ppm unless indicated otherwise.

Au (1 ppb), Ag (0.02), Al (20), As (0.5), Ba (1), Be (0.5), Bi (0.05), Ca (0.01 %), Cd (0.05), Ce (0.01), Co (0.1), Cr (2), Cs (0.02), Cu (1), Fe (0.01 %), Ga (0.1), Hf (0.05), In (0.05), K (20), La (0.01), Li (0.1), Mg (0.01 %), Mn (1), Mo (0.1), Na (0.01 %), Nb (0.2), Ni (1), P (20), Pb (0.5), Pd (10 ppb), Pt (5 ppb), Rb (0.05), Re (0.05), Sb (0.05), Sc (1), Se (1), Sn (0.5), Sr (0.2), Ta (0.05), Te (0.05), Th (0.05), Ti (5), Tl (0.05), U (0.05), V (2), W (0.1), Y (0.05), Zn (1), Zr (0.5).

ALS (June, 2011)

Samples were dried and pulverised and a 0.5 g sub-sample underwent *Aqua regia* digestion prior to multi-element analysis using ICP-MS. The full analytical suite, with lower detection limit in parentheses is:

Au (0.2 ppb), Ag (0.01), Al (0.01 %), As (0.1), B (10), Ba (10), Be (0.05), Bi (0.01), Ca (0.01 %), Cd (0.01), Ce (0.02), Co (0.1), Cr (1), Cs (0.05), Cu (0.2), Fe (0.01 %), Ga (0.05), Ge (0.05), Hf (0.02), Hg (0.01), In (0.005), K (0.01 %), La (0.2), Li (0.1), Mg (0.01 %), Mn (5), Mo (0.05), Na (0.01 %), Nb (0.05), Ni (0.2), P (10), Pb (0.2), Rb (0.1), Re (0.001), S (0.01 %), Sb (0.05), Sc (0.1), Se (0.2), Sn (0.2), Sr (0.2), Ta (0.01), Te (0.01), Th (0.2), Ti (0.005 %), Tl (0.02), U (0.05), V (1), W (0.05), Y (0.05), Zn (2), Zr (0.5).

3.3.2. Soil

Partial extraction (Mobile Metal Ion)

Weakly attached or unbound mobile metal ions (MMI) in soils can be extracted and analysed. It is a method that has been a favourable exploration tool due to the high contrast anomalies over mineralisation (Mann *et al.* 1998). Elements are extracted using weak solutions of organic and inorganic compounds rather than an aggressive acid digest (SGS 2011a). The process targets loosely bound ions that are thought to have ascended from potentially mineralised basement. Field studies over mineralisation have found vertical transport of ions can produce anomalies 10 to 25 cm below the surface. The position of the anomaly is believed to be a factor of capillary rise, evaporation, evapotranspiration, and gaseous transport (Mann *et al.* 1998, Mann *et al.* 2005). Discovery of mineralisation at the Paris Ag prospect in South Australia can be attributed to the use of partial extraction methods on soils (Anderson 2011a, b, 2012). Partial extractions on soil fractions (< 75 µm and < 200 µm) were trialled at Tunkillia (Fabris 2009, Fabris & Keeling 2010). The study found that samples collected in the swales had higher Au concentrations than samples from the dune crests, and that the < 75 µm fraction has higher Au concentrations than the < 200 µm fraction. Both size fractions were able to delineate mineralisation.

Material description 141 bulk soil samples of c. 100 g were collected at 500 by 1000 m intervals along nine north-south survey lines in the Yellabinna Regional Reserve. The samples were aligned with a biogeochemical survey at 250 by 1000 m spacing.

Collection Soil samples were collected from a depth of 10 to 25 cm (B soil horizon clay accumulation) using a small hand-trowel, a methodology adapted from Mann *et al*. (2005) and used by Fabris (2010), and Fabris & Keeling (2010), in similar landscape settings at the Tunkillia Au Prospect. Soil samples from the Yellabinna Regional Reserve were collected laterally adjacent to vegetation where the dune was free from plant litter (Figure 3.1), avoiding roots and humic material.

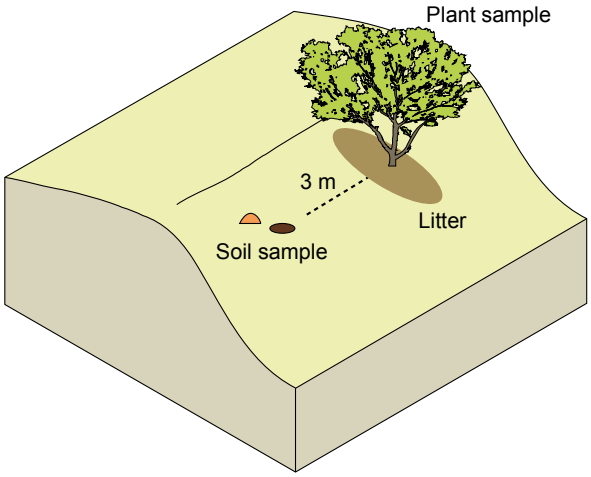

Figure 3.1: Soil sample relative to plant sample in the Yellabinna Regional Reserve survey

Timing 20-25 June, 2011

Preparation No pre-analysis preparation of soil samples. Samples were not separated into size fractions, and although this was considered, the moisture-content of the soils at the time of collection would have impeded sieving in the field. A discussion of the particle size distribution of soil samples from the Yellabinna Regional Reserve is included in Appendix B.

Analysis 'Mobile Metal Ion' analysis is an SGS Australia Pty. Ltd propriety method and, therefore, the details are not disclosed. The process possibly uses strong complexing ligands to detach or dissolve weakly attached cations from the soil matrix without the dissolution of the matrix (e.g., Mann 2009). The solution is then analysed using ICP-MS. The full analytical suite with lower detection limit in parentheses is listed below. Concentrations are in ppb unless indicated otherwise.

Au (0.1), Ag (1), Al (1 ppm), As (10), Ba (10), Bi (1), Ca (10 ppm), Cd (1),Ce (5), Co (5), Cr (1), Cu (10), Dy (1), Er (0.5), Fe (1 PPM), Gd (1), La (1), Li (5), Mg (1 ppm), Mn (5), Mo (5), Nb (0.5), Nd (1), Ni (5), Pb (10), Pd (1), Pr (1), Pt (1), Rb (0.25), S (5 ppm), Sb (1), Sc (5), Se (2), Sm (1), Sn (1), Sr (10), Ta (1), Tb (1), Te (10), Th (0.5), Ti (3), Tl (0.5), U (1), V (1), W (1), Y (5), Yb (1), Zn (20), Zr (5).

3.3.3. Drill cuttings

A total of 140 drill-cutting samples were collected from three regolith profiles to a depth 50 m from the Tunkillia Au Prospect: Area-223 (477600 mE, 6545300 mN GDA94 zone 53), Area-191 (478500 mE, 6547900 mN GDA94 zone 53), and Tomahawk (479900 mE, 6546100 mN GDA94 zone 53).

Material description Air core drilling at the Tunkillia Au Prospect has returned cuttings from the top 50 m (at 1-m intervals) of the regolith profile predominantly as powders. Sand samples at the top of the profile occasionally contain small fragments (< 1 cm) of Ca and Si indurated material. Residual regolith is a highly weathered saprolite and as cuttings has a flour-like consistency with small grains (< 2 mm) of residual quartz. The residual regolith grades from highly weathered saprolite to saprock at a depth of 50 m. Some of the basal saprock samples consist of coarse grains (< 1 mm) of weathered primary minerals (felsdpars) with some larger friable clasts of saprock. Samples are contained in large sample bags from 2010-2012.

Collection Drill cuttings are fine to coarse powders and were considered homogenous, therefore taking a 200-g subsample in the field using a plastic trowel was deemed suitable and representative for the quantity used in the analyses. A subsample was taken from the original 200-g sample using a plastic spoon for whole-rock geochemical analysis, Hylogger™ analysis, and X-Ray Diffraction (XRD) analysis of powders.

Preparation & analysis **Whole-rock geochemistry** was determined for every metre interval using two analytical methods at Acme Analytical Laboratories, Canada. 70 g of sample was transferred to a small snap-seal bag and dispatched to the laboratory, where they were dried, pulverised and fused and/or digested by acid prior to multi-element analysis using ICP-MS. Two analytical methods were used to measure concentrations of 45 trace elements for every metre interval and 12 major elements for every second metre interval (even-numbered intervals).

Every metre interval was analysed for a suite of 45 trace elements. A 0.2 g sample underwent $LiBO_2$ fusion and nitric acid digestion and was analysed using ICP-MS. The full analytical suite, with lower detection limit in parentheses is listed below. Concentrations are in ppm unless indicated otherwise.

La (0.1), Ce (0.1), Pr (0.02), Nd (0.3), Sm (0.05), Eu (0.02), Gd (0.05), Tb (0.01), Dy (0.05), Ho (0.02), Er (0.03), Tm (0.01), Yb (0.05), Lu (0.01), Ba (1), Be (1), Co (0.2), Cs (0.1), Ga (0.5), Hf (0.1), Nb (0.1), Rb (0.1), Sn (1),
Sr (0.5), Ta (0.1), Th (0.2), U (0.1), V (8), W (0.5), Y (0.1), Zr (0.1).

A 0.5 g sample underwent an *Aqua regia* digest and was measured for the precious and base metals. The analytical suite, with lower detection limit in parentheses is listed below. Concentrations are in ppm unless indicated otherwise.

Ag (0.1), As (0.5), Au (0.5 ppb), Bi (0.1), Cd (0.1), Cu (0.1), Hg (0.01), Mo (0.1), Ni (0.1), Pb (0.1), Sb (0.1), Se (0.5), Tl (0.1), Zn (1).

Every second metre interval was analysed for a suite of 45 trace elements but with the additional analysis of major oxides. A 12 g sample underwent $LiBO_2$ fusion and was analysed using X-Ray Fluorescence. The full analytical suite, with lower detection limit in parentheses is listed below. Concentrations are in per cent (%).

Si (0.1), Al (0.01), Fe (0.01), Ca (0.01), Mg (0.01), Na (0.01), K (0.01), Mn (0.01), Ti (0.01), P (0.01), Cr (0.001), Ba (0.01).

Spectral analysis (Hylogger™) was conducted for every 1-m composite sample (140 in total) at the DMITRE core library, Glenside, South Australia. Approximately 2 tablespoons of each sample was transferred to black plastic 20-segment chip tray for spectral analysis using the Hylogger™ for wavelengths between 400 – 2500 nm (visible – to short wavelength infrared; SWIR). The Hylogger™ is based on the TerraSpec™ spectroscopic device and measures the reflectance of wavelengths from between 350 – 2500 nm from three spots (< 5 mm²) of each sample. The resolution is 3 nm @ 700 nm and 6 nm up to 2100 nm (Analytical Spectral Devices 2011). The Hylogger™ also provides a photographic image of the samples. In the case of drill cuttings, these images represent how the sample would appear to a person logging at the back of a drill rig.

X-Ray Diffraction (XRD) analysis was conducted at the University of Adelaide for select samples from even-numbered intervals to align with the full geochemical analysis (major and trace elements). These intervals are: 2, 6, 16, 30, 32, and 40 m from Area-223; and, 2, 16, 32, and 50 m from Area-191 and Tomahawk. The intervals were selected to evenly divide the profile, and also to provide mineralogical constraints on abrupt changes in the abundances of some elements at depths between 16 and 32 metres. Samples from 6 and 30 m at Area-223 were selected due to an unusual yellow colour.

Approximately 2 tablespoons of sample was taken from the original 200 g sample and crushed using a tungsten-carbide ring mill to achieve a flour-like powder: residual quartz grains in the drill powders made the bulk sample too course for immediate XRD analysis. Powders were then loaded onto stages using a mechanical vibrator to achieve randomly orientated mineral surfaces. XRD analysis of powders was conducted using a Bruker

D8 Advance. CuK-alpha radiation was used with scans conducted from 2 theta (3.5 – 75°), with a step width of 0.02° and 190 ms per step operating at 40 kV and 40 mA. Diffrac*plus* Eva™ was used for phase analysis and interpretation.

X-Ray Fluorescence (XRF) analysis (portable instrument) was conducted at the University of Adelaide for the intervals: 2, 6, 16, 30, 32, and 40 m from Area-223; and, 2, 16, 32, and 50 m from Area-191 and 2, 16, 19, 32, and 50 m Tomahawk. Samples were excess powders used in the XRD analysis. Instruments used were Olympus Innov-X X-5000 desktop XRF, and Olympus Delta-X handheld XRF and use methods from Fisher *et al*. (2011). 'Soil' mode was used to detect trace elements and a 60-second beam count was used to maximise precision. Three beams are used resulting in a total count time of 180 seconds. Beam X-ray energy and the measured elements are listed below. Not all the data from the elements below are discussed.

Beam 1 – 50 kV: As, Sr, Zr, Th, Mo, Ag, Cd, Sn, Sb, Ba, Ti, V, Cr, Mn, Fe, Co, Ni, Cu, Zn, W, Hg, Se, Au, Pb, Bi, Rb, U
Beam 2 – 35 kV: Fe, Co, Ni, Cu, Zn, Se, Au, Pb, Bi, Rb, Ti, V, Cr, Mn, W, Hg, As, U, Zr, Th, Mo
Beam 3 – 15 kV: P, S, Cl, K, Ca, Ti, Cr, Mn V, Fe

3.4. Microscopic analysis

3.4.1. Calcrete

Surplus nodular calcrete samples from the study of Klingberg (2009) were used. Samples selected for analysis are from locations with previously identified as having high Au-in-calcrete results: a sand plain with 194 ppb Au (sample THKLK033), and a drainage depression with 43 ppb Au (sample THKLK075).

Preparation Samples were cut at the University of Adelaide using a rotating diamond-insert blade to produce a 1 cm^2 section that included the outer-most lamination. Each specimen was individually set into a one-inch diameter mount using a two-pack epoxy resin.

Analysis Calcrete specimens were analysed at Adelaide Microscopy using laser ablation ICP-MS (Agilent 7500cx with attached New Wave UP-213 laser ablation system); electron microprobe (CAMECA SX51); and electron microscope (Philips XL 30) Field Emission Gun Scanning Electron Microscope (SEM) fitted with thin film Energy Dispersive Spectroscopy (EDS) detector.

Sample THLK075 was analysed on the electron microprobe to determine the average Ca content of the matrix (34% Ca). The sample was then analysed using Laser-ablation ICP-MS along a single transect using an 80 μm ablation spot size. Measurements were taken at 500 μm spacing for a length of 10 mm. The results are discussed in *Section 5.5*. Calcium was used as a calibration standard for the LA-ICP-MS.

Elements analysed were the common isotopes of Al, Au, Ba, Bi, C, Ca, Ce, Co, Cu, Dy, Er, Eu, Fe, Gd, Ho, K, La, Lu, Mg, Mn, Mo, Na, Nd, Ni, P, Pb, Pr, Rb, Sc, Si, Sm, Sr, Ta, Tb, Th, Ti, Tm, U, Yb, Zn.

LA-ICP-MS mapping for samples THKLK033 and THKLK075 was carried out on a Resonetics M-50-LR 193-nm Excimer laser microprobe coupled to an Agilent 7700cx quadrupole ICP-MS housed at Adelaide Microscopy, University of Adelaide.

Data collection for image creation was performed by ablating sets of parallel rasters across the area of interest. A beam size of 14 μm was used for broad maps and 5 μm was used for detailed maps. The spacing between the lines was matched to the particular beam size for each map. A scan speed of 20 μm/s was selected, providing the desired sensitivity of elements of interest, and spatial resolution. A laser repetition of 10 Hz was selected at a constant energy output of 100 mJ, resulting in an energy density of ~7 J/cm^2 at the target. Using these beam conditions, depth of ablation during mapping was around 10 μm. A set of 15 elements were

analysed with dwell time for all masses set to 0.005 s, resulting in a total sweep time of ~0.1 s including settling time. A 30 s background acquisition was acquired at the start of every raster, and to allow for cell wash-out, gas stabilisation, and computing processing, a delay of 30 s was used after each line. Identical rasters were done on the standard glass NIST 612, and the USGS reference material MACS-3 at the start and end of a mapping run.

Images were compiled and processed using the program Iolite developed by the Melbourne Isotope Group at Melbourne University (e.g., Woodhead *et al.* 2007). Average background was subtracted from its corresponding raster signal for each element, then a linear fit between the bounding sets of standards was applied to correct for instrument drift. Rasters were then compiled into a 2-D image displaying combined background/drift corrected intensity for each element.

3.4.2. Vegetation

Surplus samples of Victoria Desert mallee leaves and black oak twigs and branchlets material from the study of Hopkinson (2009) were selected for microscopic analysis based on the multi-element biogeochemistry: high Au; high Ca; low Au; and low Ca.

Preparation Samples were cut using a razor blade to produce a long and cross section. Multiple specimens were fixed to a one-inch diameter stage using super glue (Figure 3.2). Stages were carbon-coated at Adelaide Microscopy prior to Scanning Electron Microscope imaging.

Figure 3.2 - Plant material from Hopkinson (2009) on one-inch stages (prior to carbon coating). Left-right: Black oak, black oak, Victoria Desert mallee.

Analysis Images of plant material were captured at Adelaide Microscopy, University of Adelaide using optical and electron microscopes. **Optical images** of loose pearl bluebush twigs and leaves were captured using a Leica MZ16FA Stereomicroscope. Images are discussed in *Section 3.7.3: Detrital contamination.* **Scanning Electron Microscope (SEM) images** were captured using a Philips XL 30 Field Emission Gun SEM fitted with thin film Energy-dispersive X-ray spectroscopic (EDS) detector. Images are discussed in *Section 5.2*.

3.5. Data analysis

3.5.1. Detection limits

Element concentrations less than the lower analytical detection limit (DL) are reported by the laboratory as either "<DL" or "X". These values are replaced with half the value of the detection limit (e.g., < 0.2 becomes 0.1) to prevent import conflicts and/or calculation errors. Elements that are below analytical detection limit in all samples in a survey area are noted and removed from the tabulated data in the respective section: these variables have a variance of zero and result in convergence errors in SiroSOM and Principle Component Analysis (PCA) calculations.

3.5.2. Drilling database visualisation

Geological modelling software package Leapfrog Mining 2.4 is used for the 3-D visualisation of geochemistry and lithology data from drilling at the Tunkillia Au Prospect. Data are made accessible by Minotaur Exploration Ltd. and Mungana Goldmines Ltd. to aid in the interpretation of regolith geochemical and plant biogeochemical data.

3.5.3. Mapping

Data presentation

Point and layer data are presented using ArcGIS 9.3 with a UTM GDA94 zone 53 projection. Symbol sizes used for element concentrations (point data) are determined by the 'natural breaks' function in ArcGIS. Layer data are sourced from Minotaur Exploration Ltd. (airborne electromagnetic and aeromagnetic), South Australian Resources Information Geo-server (SA aeromagnetic, 1:2M-scale geology). The 1 arc-second (30 m pixel) digital elevation model (DEM) from the Shuttle Radar Topography Mission (SRTM; Slater *et al.* 2006) is used under the Creative Commons agreement with Geoscience Australia. The DEM is used for the generation of topographic contours and flow-path modelling. Flow-paths were calculated using the hydrology tools in ArcToolbox in ArcGIS 9.3 (see Appendix B for procedure).

Regolith-landform

A regolith-landform map was produced at 1:500,000 scale using Adobe® Illustrator® CS3, Google Earth imagery, and observations made during sample collection (Appendix B). The map provides a regolith landform context for surveys conducted in close proximity to contemporary and historic activity on production leases associated with some of the historic workings. Covering an area of 95 x 65 km, the map provides information on the landforms, dispersion patterns and the subsequent development of the surface materials throughout the Yellabinna region, west of Lake Harris. Regolith-landform maps are constructed for Glenloth and Earea Dam goldfields to assist with interpretation of local chemical and physical dispersion of regolith components and the influence on the sampling material.

Key observational data for the generation of a regolith-landform map are:

- Landform, topography, and slope gradients (drainage, plain, rise, hill);
- Surface dispersion mechanism (alluvial, colluvial, sheet wash);
- Surface regolith material (substrate and lag); and,
- Vegetation community.

An alpha-numeric code after Pain *et al*. (2007) is used to depict the landforms and comprises two components: the first part (in uppercase) represents the dominant regolith material; and, the second part (in lowercase) represents the dominant landform, often a topographical feature. For example, the regolith landform unit (RLU):

$CHep_1$

Signifies a sheet wash (CH) erosional plain (ep), and is predominantly a colluvial (gravity assisted) process on a plain with low relief (0-9 m). The subscript modifier allows for subdivision of classes with similar major regolith and landform, but with differing details of minor components such as lag proportions or vegetation (Pain 2009, Hill & Chittleborough 2011).

3.5.4. Self-Organising Maps (SOM)

The "Self-Organising Map" (SOM) is a powerful software tool for the visualisation of relationships within large, high-dimensional datasets as a low-dimensional display (Kohonen 1998). The algorithm is based on unsupervised learning and vector quantization where each sample is treated as a vector in multi-dimensional space represented by the number of input variables (e.g., element concentrations; Kohonen 1998). The SOM consists of a set of cells arranged in a 2-D grid, where each cell represents a vector in the same n-dimensional space as the data vectors (Gulson *et al.* 2007). The SOM is then trained by adding the original data vectors in a random sequence. During this incremental learning process, the cell vectors' position is adjusted in n-dimensional space to more closely represent the data vectors. Data vectors are assigned to cell vectors (or Best-Matching Unit; BMU), which are subsequently ordered to produce the 'Map' – it is essentially a map of similarity of the samples, all variables considered.

SOM analysis has applications in many fields, for example: speech analysis, neural signal analysis, bioinformatics, organisation and retrieval from document collections, financial, and industrial control (Fraser 2006). There have been several SOM application in the environmental and geo-sciences (e.g., Gulson *et al.* 2007, Barnett & Williams 2009, Fraser & Hodgkinson 2009, Fraser 2012). Fraser (2012) presents examples of SOM used to analyse a diverse range of datasets, viz. regional surface geochemistry (Barnett & Williams 2009, Fraser & Hodgkinson 2009), drill-hole geochemistry, mineral and satellite imaging spectra, and, geophysics.

Software The SOM tool used in this study is the CSIRO Exploration and Mining division-developed algorithm, SiroSOM. SiroSOM is a user-friendly graphical user interface (GUI) with a MATLAB back-end for the analysis and visualisation of high-dimensional exploration datasets. Full terminology is included in Appendix C.

Data format Input data is geochemical data from drill cuttings (*Section 4.3.3.*) that has samples in rows (total of 140) and element concentrations (total of 57) in columns. Data labels, that are not included in the SOM analysis, are hole coordinates, hole ID, and sample ID.

Process The optimal number of nodes represented by the map is defined by equation [2] (Vesanto 2005). An asymmetric map is recommended to avoid edge effects and is suggested to be approximately the short side of the map equal to half the length of the long side (Kohonen 1990). This can be calculated using equation [3], where $\boldsymbol{x}$ represents the dimension of the short side of the map, and $2\boldsymbol{x}$ represents the dimension of the long side of the map.

$$\text{nodes} = 5 \times \sqrt{samples \times variables} \qquad [2]$$

$$\boldsymbol{x} = \sqrt{\frac{nodes}{2}} \qquad [3]$$

From the equations above, the suggested optimum number of nodes to represent the geochemical data is 447, using map dimensions of 15 by 30 (see figures in *Section 4.3.3.*).

It has been argued that most geochemical datasets approximate a normal to log-normal distribution (Reimann & Filzmoser 2000, McQueen 2009), and this is particularly evident for trace element concentrations. Upon import to SiroSOM, element concentrations (variables) are $\log_{10}$-transformed to reduce skewness of the data and the relative influence of high values that were not removed from the dataset prior to analysis.

Data clustering Cell vectors, and the samples they represent, are clustered using a K-means approach. Clustering is an iterative process where the number clusters in this study are defined by the lowest achieved Davies-Bouldin Index. At the lowest index value, the variance of data within clusters is minimised and the variance of data between clusters is maximised arriving at an estimated number of true populations within the data. The number of clusters is variable due to initial random seeding and the number of iterations. Five iterations is the default input and may need alteration to achieve a lower index and appropriate number of clusters.

Output data Output data are plots (e.g., U-matrix, XY-scatter of components), and as tables of original data appended with SOM-calculated variables (e.g., BMU number, cluster number, and QER).

3.6. Quality control

Modern analytical instruments are capable of generating large volumes of multi-element data. Once the data are acquired, there is a tendency to go straight to looking at the high values (Dunn *et al.* 1995, Ch.6). Subtle trends or single outliers may be an artefact of the analytical process (e.g., incomplete cell wash-out and analyte carry over; Rodushkin & Axelsson 2000) or the result of detrital contamination prior to analysis (e.g., Hill 2004, Hulme 2010). Reference materials are typically inserted into the analytical queue after the analysis of 10 to 30 unknowns to monitor drift of the measurements by the instrument over time. Reference materials can contain elements at concentrations much higher than the unknowns (samples). It is recommended that the data are reviewed in the order in which they are received from the laboratory (Dunn *et al.* 1995) to identify anomalous element concentrations that have carried-over from the analysis of unknowns or reference materials that may have a high concentration of a particular element. Since anomalous element concentrations in sampling materials could also be a response to the environment, results require interpretation and discussion with geospatial context. Carry-over issues are therefore not discussed in this section.

This section includes a discussion of:

3.6.1 Errors associated with the laboratory reference materials used during the biogeochemical analysis of plant samples from 2009 – 2012, and during the geochemical analysis of regolith samples;
3.6.2 The value of sample duplicates in biogeochemical studies; and,
3.6.3 Susceptibility and effects of detrital contamination of biogeochemical samples

3.6.1. Laboratory reference materials

Analytical laboratories use internal reference materials (V14 & V16) and internationally Certified Reference Materials (CRMs), blanks for cell wash out, and repeat analysis of sample pulps at regular intervals during the analysis of a batch of unknowns. The use of reference materials allows the laboratory (and also the client) to monitor the precision and accuracy of the instrument and to make an assessment of the overall quality of results. Laboratories recommend that clients submit ‘blind’ reference materials and sample duplicates with each batch of samples. In this study sample duplicates were submitted with some batches. No reference materials were submitted with the samples as no suitable reference materials were available for use in the biogeochemical analysis. The laboratory standards were relied upon and the implications of this are discussed in this section and in the conclusion of this research.

Reference materials

By laboratory and material

Repeat analysis of Au in reference materials used by the analytical laboratories during the analysis of plant and regolith samples are listed in Table 3.5. Expected variability of Au measurements in the range 0.2 – 10 ppb of standards (V14 & V16) is between 81 – 130% but achieved precision is considerably better and is between 47 – 75%. Precision is also generally better than expected for Au measurements in calcrete (Table 3.5). The expected and measured concentrations of the full analytical suite of elements in the V14 and V16 reference materials used during biogeochemical analysis are presented in Appendix A.

Table 3.5: Expected and measured Au in reference materials during biogeochemical and geochemical analysis.

Reference material [# of analyses]	Analytical Laboratory	Sample Type	Expected Au (ppb)	Mean measured Au (ppb) ± 1SD (RSD%)	RSD% range min-max
V14 [52]	Acme	Vegetation	8.6 ± 7^ (81%)	9.1 ± 4.3 (47%)	± 45-290%
V16 [52]	Acme	Vegetation	0.9 ± 1.17^ (130%)	1.2 ± 0.9 (75%)	± 16-420%
BSL9	Genalysis	Calcrete	4.986 ± 2.89* (58%)	N/A	-
CMM-07	Genalysis	Calcrete	42.103 ± 6.12* (14%)	N/A	-
NGL-21	Genalysis	Calcrete	19.3 ± 1.93* (10%)	N/A	-
OxA71 [6]	ALS	Calcrete	0.077 ± 0.013 (17%)	0.081 ± 0.0042 (5%)	± 2-7%
ST-345 [2]	ALS	Calcrete	0.055 ± 0.009 (16%)	0.058 ± 0.0042 (7%)	± 5%
G2000 [6]	ALS	Calcrete	0.3 ± 0.1 (33%)	0.3 ± 0 (0%)	± 0%
GBM999-5 [3]	ALS	Calcrete	0.55 ± 0.25 (45%)	0.73 ± 0.32 (44%)	± 18-50%
GEOMS-03 [3]	ALS	Calcrete	0.3 ± 0.1 (33%)	0.36 ± 0.057 (16%)	± 9-18%

Vegetation by batch

The 1628 biogeochemical data discussed in this study are extracted from analytical reports that included approximately 2370 individual analyses. Gold measurements from 52 analyses of V14 and V16 reference materials throughout the biogeochemical analysis of approximately 2370 vegetation samples are presented in Table 3.6. Precision of Au (RSD%) measurements of reference materials has some variation between analytical batches. Precision data for the full analytical suite of elements measured for reference materials are included in Appendix A.

Table 3.6: Reproducibility of Au measurements in vegetation standards from 7 batches over 4 years (Acme Analytical Laboratories, Vancouver). Values are mean ± standard deviation and the relative standard deviation (RSD) as a percentage of the mean in parentheses.

Batch No.	Date	Number of repeats	Standard V14 Mean±1SD (ppb) (RSD)	Standard V16 Mean±1SD (ppb) (RSD)
1	Jul-09	11	9.2 ± 7.0 (76.1%)	0.7 ± 0.5 (71.4%)
2	Apr-11	16	9.0 ± 1.8 (20.0%)	1.4 ± 1.1 (78.6%)
3	Nov-11	7	10.3 ± 6.8 (66.0%)	1.5 ± 1.4 (93.3%)
4	Nov-11	8	8.6 ± 1.9 (22.1%)	1.4 ± 0.5 (35.7%)
5	Nov-11	6	9.3 ± 3.8 (40.9%)	1.4 ± 1.0 (71.4%)
6	May-12	2	7.7 ± 0.3 (3.9%)	1 ± 0.2 (20.0%)
7	May-12	2	8.3 ± 2.3 (27.7%)	0.5 ± 0.4 (80.0%)

Precision of Au measurements of the reference materials for the data used in this study is poor: RSD ranges from 22 to 76% for V14 (expected 8.6 ± 7 ppb), and 36 to 93% for V16 (expected 0.9 ± 1.17 ppb) in batches where more than two repeat analyses of the reference materials were conducted. For poor reproducibility of results, it is suggested by Dunn (2007, p.254), that pathfinder elements of Au are used to substantiate elevated Au results.

The precision of Au measurements of reference materials used during the analysis of vegetation is much lower than the precision associated with the reference materials used during the analysis of geochemical materials (e.g., Table 3.5). Dunn (2007, p.254) presents the precision and accuracy of Au measurements of reference material, V6 and NIST 1575a (Table 3.7). For these materials, the relative standard deviation is 37% and 64% respectively. Such a high RSD is of particular concern for low concentrations of Au (e.g., < 1 ppb) and these results should be treated with caution.

Table 3.7: Precision and accuracy of Au in standards from Dunn (2007, p.254)

	V6	NIST 1575a
Target	0.73	(0.25-2.6)
# of analyses	30	19
Mean	0.7	0.42
Std. Dev.	0.26	0.27
RSD %	37	64

3.6.2. Sample duplicates

Data compiled for this study are from various laboratories, and samples have been prepared and submitted to the labs by several researchers using various systems. Analysis of sample duplicates in this compilation of data are of two types: repeat of digested sample (pulp duplicate); and, two sub-samples of the bulk sample.

Sample duplicates in biogeochemical studies with small sample population (e.g., < 200, Hopkinson 2009) were produced by pulverising the plant material using a stainless steel rotating blade mill and collecting sub-samples of the homogenised product. Duplicate calcrete samples from Tomahawk (Klingberg 2009) are multiple specimens from the same location (rather than an homogenised sample). Approximately one sample out of ten was submitted to the analytical laboratory as a blind duplicate in both studies. For larger batches (e.g., > 300), typical of surveys conducted as part of the regional module, samples were submitted to the analytical lab for pulverisation and in this case, no sample splits were performed.

Repeatability (or difference) of element concentration measurements between sub-sample splits (or duplicates) for each material can be represented as a '% difference error', from Reid *et al.* (2010):

$$\%\ \text{difference error} = \left(\frac{\text{abs}(\text{assay1} - \text{assay 2})}{\max(\text{assay1 or assay 2})}\right) \times 100$$

The average variability (as used in *Section 5.2*) is the average of multiple % difference error calculations ± the standard error of the mean:

$$\text{Average \% variability} = \left(\frac{\Sigma\left(\frac{\text{abs(assay1}-\text{assay 2)}}{\text{max(assay1 or assay 2)}}\times 100\right)}{n}\right) \pm \left(\frac{\sigma}{\sqrt{n}}\right)$$

Pulp duplicates (internal)

'Pulp duplicates' are an internal control where the laboratory conducts a repeat analysis on the digested sample (solution). This has been done for 41 samples from 7 batches of biogeochemical analyses. The % difference error for each pair of biogeochemical analyses has been calculated for the full analytical suite of elements. The range and mean % difference error for each element in included in Table 3.8. The difference of Au measurements from pulp duplicates of biogeochemical samples is as high as 80%. Higher % difference errors (> 20%) are evident for As, Au, Co, Ge, Hf, Hg, Re, and Sc. Error data cannot be calculated for In, Pt, U, and W as the concentrations are below the analytical detection limit for all sample pairs.

Table 3.8: Summary of repeat biogeochemical analysis of 41 pulp duplicates presented as % difference error (%DE), and Mean %DE ± Standard error of mean (SEM).

Element	Range %DE	Mean %DE ± SEM	Element	Range %DE	Mean %DE ± SEM
Ag	0 - 57	12 ± 2.4	**Na**	0 - 41	2.9 ± 0.35
Al	0 - 50	7.1 ± 2.2	**Nb**	0 - 50	5.7 ± 2.4
As	0 - 80	20 ± 4.2	**Ni**	0 - 50	14 ± 2.1
Au	0 - 80	28 ± 4.3	**P**	0 - 41	2.9 ± 0.37
B	0 - 41	4.8 ± 0.58	**Pb**	0 - 55	12 ± 2.2
Ba	0 - 41	5.4 ± 0.68	**Pd**	0 - 80	9.9 ± 3.2
Be	0 - 50	1.2 ± 1.2	**Pt**	0 - 41	
Bi	0 - 50	2 ± 1.4	**Rb**	0 - 41	3.4 ± 0.56
Ca	0 - 41	3 ± 0.32	**Re**	0 - 80	27 ± 3.8
Cd	0 - 80	11 ± 2.8	**S**	0 - 41	5.8 ± 0.97
Ce	0 - 41	8.3 ± 1.2	**Sb**	0 - 43	9.8 ± 2.1
Co	0 - 75	23 ± 3.3	**Sc**	0 - 67	23 ± 3.6
Cr	0 - 41	7.9 ± 1.2	**Se**	0 - 67	17 ± 2.6
Cs	0 - 41	8.9 ± 1.3	**Sn**	0 - 60	14 ± 2.7
Cu	0.27 - 41	3 ± 0.42	**Sr**	0 - 41	2.5 ± 0.3
Fe	0 - 41	8.9 ± 1.5	**Ta**	0 - 50	2.4 ± 1.7
Ga	0 - 50	3.7 ± 2	**Te**	0 - 67	4.5 ± 2.3
Ge	0 - 86	30 ± 4.7	**Th**	0 - 50	7.8 ± 2.4
Hf	0 - 80	29 ± 3.8	**Ti**	0 - 50	4.7 ± 1.6
Hg	0 - 86	20 ± 2.9	**Tl**	0 - 41	0.81 ± 0.8
In	0 - 41		**U**	0 - 41	
K	0 - 41	2.4 ± 0.35	**V**	0 - 41	0.7 ± 0.69
La	0 - 41	9 ± 1.6	**W**	0 - 41	
Li	0 - 86	18 ± 2.3	**Y**	0 - 41	9.4 ± 1.3
Mg	0 - 41	3 ± 0.46	**Zn**	0 - 41	4.7 ± 0.63
Mn	0 - 41	3.4 ± 0.54	**Zr**	0 - 50	15 ± 2.6
Mo	0 - 41	8.4 ± 1.4			

Seasonal repeats

Variation in the biogeochemistry of individual plants from 10s to 100s of percent can be expected between seasons (Cohen *et al.* 1987, Stednick *et al.* 1987, Dunn 2007) as a result of changes in climate or resource availability (e.g., water and nutrients). A more significant control on the seasonal differences in individual plant biogeochemistry is the use of destructive analytical techniques and the inability to collect and reanalyse the same sample material. The heterogeneous element distribution within the plant organs means that biogeochemical variation would be apparent within season and between seasons.

Collection of multiple samples from the same plant within the same season was conducted at the Glenmarkie Au deposit in the Glenloth goldfield. Four samples were collected from each quadrant (N, E, S, and W) of two pearl bluebush plants: GLX1 (508020 mE 6559984 mN, GDA94 zone 53); and GLX2 (508023 mE 6559986 mN, GDA94 zone 53). Eight samples in total were collected and submitted to the laboratory for separate biogeochemical analysis. The percentage difference between the highest and lowest concentration measured for each element in GLX1 and GLX2 are presented in Table 3.9. Higher % difference errors (≥ 50%) are evident for As, Au, Cd, Ge, Hf, Hg, Pb, Sb, Sc, Sn, Ta, Th, and Zn. Some of these elements have a high % difference error determined from the repeat analysis of pulp duplicates (from Table 3.8) and may compound the error caused by the heterogeneous distribution of elements within the plant.

Table 3.9: Percentage difference errors between the lowest and highest concentration measured in four samples collected from two individual pearl bluebush plants.

	GLX1	GLX2
Ag	29	50
Al	BDL	BDL
As	58	67
Au	67	83
B	11	13
Ba	33	33
Be	BDL	BDL
Bi	BDL	BDL
Ca	25	26
Cd	25	63
Ce	30	23
Co	41	27
Cr	6.3	44
Cs	43	49
Cu	18	23
Fe	22	17
Ga	BDL	BDL
Ge	BDL	67
Hf	67	75
Hg	38	69
In	BDL	BDL
K	11	20
La	29	20
Li	9.4	19
Mg	24	24
Mn	19	36
Mo	21	47

	GLX1	GLX2
Na	14	10
Nb	BDL	BDL
Ni	20	40
P	20	17
Pb	33	61
Pd	69	73
Pt	BDL	BDL
Rb	28	47
Re	50	50
S	16	21
Sb	50	50
Sc	BDL	67
Se	22	14
Sn	40	60
Sr	23	28
Ta	50	BDL
Te	BDL	BDL
Th	33	50
Ti	20	33
Tl	33	33
U	BDL	BDL
V	BDL	BDL
W	BDL	BDL
Y	43	27
Zn	18	55
Zr	28	31

3.6.3. Detrital contamination of biogeochemical samples

There are many physical and chemical effects that dust can have on vegetation: dust can effect photosynthesis, respiration and transpiration (Farmer 1993), which can ultimately have an effect on the productivity of the plant and the plant chemistry. Furthermore, the physical addition of detrital material to the surface of plant organs can have a direct influence on the chemistry of the sample, with particular implications for plant biogeochemistry when used as a method of mineral exploration.

Research on the use of biogeochemistry in the northern hemisphere acknowledges the potential for detrital contamination of samples proximal to roads (e.g., < 100 m; Dunn *et al.* 1995, Dunn 2007). These areas are typically well-vegetated and have stabilised soils (particularly away from roads), which is of significant contrast to Australian conditions. A major challenge for biogeochemistry in Australia is the susceptibility to detrital contamination from readily transported soil as a result of vast aridity and sparse vegetation.

Contamination is a result of aeolian and/or alluvial entrained detritus (Hill 2004, Hulme 2010). The proportion of detrital input through each process depends on plant macro-morphology (e.g., canopy height) and the micro-morphology (e.g., foliage shape and surface texture). Plants with a low canopy height (e.g., chenopods: pearl bluebush) are most at risk of aeolian contamination and from alluvial processes such as soil splash on low branches during light rainfall events or periodic flooding as a result of intense rainfall events.

Detrital contamination can adversely influence the biogeochemical results in two ways: 1. non-mineralised aeolian particles adhere to the surface of the sample material, potentially diluting any expression of mineralisation (Hulme 2010, p.26); and/or, 2. aeolian detritus derived from proximal mineralisation producing a false positive anomaly. It is therefore important to examine the results (especially those with high concentrations of economic elements) for signs of detrital inputs.

Indicators of detrital contamination are Fe and Al, which constitute the oxyhydroxides and clay particles in the soil: it is probable that trace metal cations, as contaminants, will be adsorbed onto or into these particles (Hill 2004, p.75). Furthermore, elements commonly contained in resistate minerals (e.g., cassiterite, ilmenite, spinel, zircon, chromite; Eggleton 2001, p.103), high field-strength elements (e.g., Ti, Hf, Nb, Th, and Zr: Dunn 2007, p.108), and elements not known to hyper accumulate in plants (e.g., Ti, Cr, Sc, Si, and Zr: Brooks *et al.* 1998, Reid 2008), can be useful tracers of detrital input.

This section (3.6.3) compares recognised detrital contaminant elements between different species sampled in the Tunkillia and regional central Gawler Craton surveys, and also compares these data with data from biogeochemical surveys throughout various South Australian settings, with a particular focus on studies from the Middleback Ranges.

Contamination of biogeochemical samples

Central Gawler Craton (this study)

Central Gawler Craton biogeochemical results show a positive relationship between Zr and Fe for 1628 samples belonging to 5 different species (Figure 3.3). Higher Zr and Fe results are characteristic of pearl bluebush, which have a canopy height < 50 cm and form the open chenopod shrub land on the sheet wash regolith types. Lower Zr and Fe results are from species with a canopy greater than one metre from the ground (e.g., mulga, black oak and Victoria Desert mallee). These larger species form dense woodland in areas within aeolian dunes.

Dunn *et al*. (1995, Ch.2) present average element abundance in plants, compiled from various sources. Zirconium and Fe have a suggested average of 0.1 ppm and 150 ppm (0.015%) respectively and potentially includes dust-contaminated samples. These data have a bias towards the northern hemisphere. A total 65% of samples in this study have Zr and Fe concentrations less than or equal to the averages (inside the dotted box, Figure 3.3). The remaining samples that exceed the average concentrations are predominantly pearl bluebush and black oak (Figure 3.3).

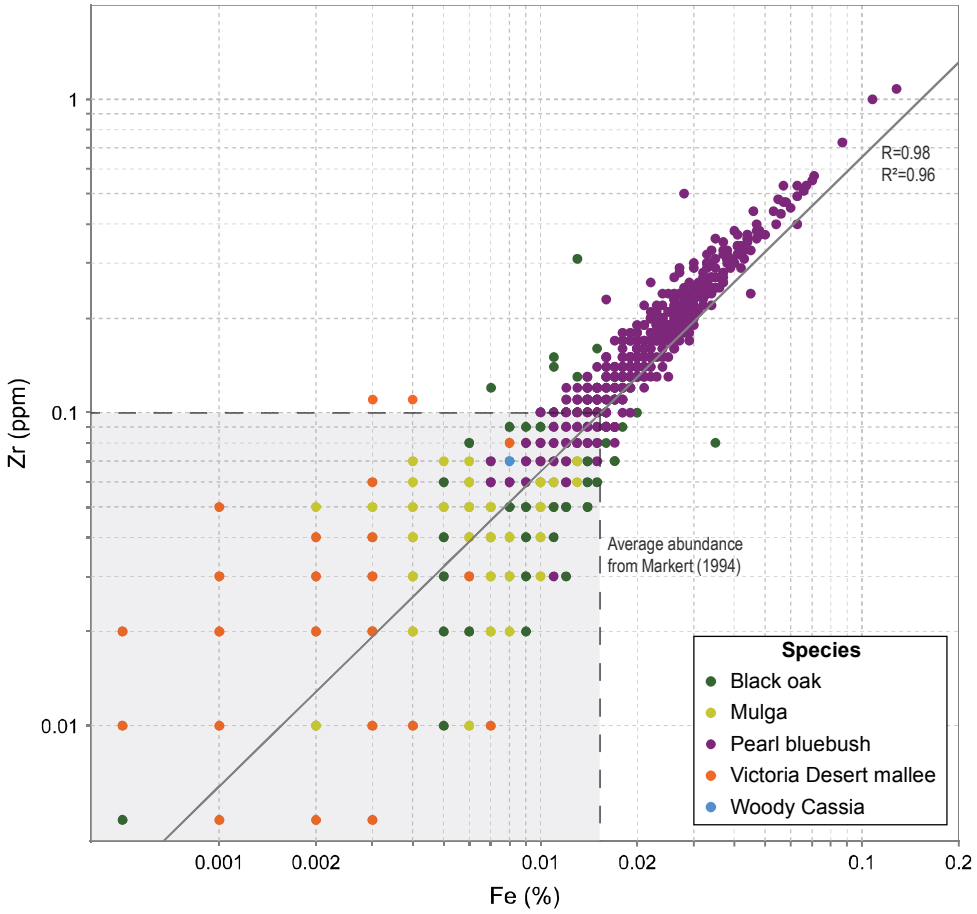

Figure 3.3 - Gawler Craton biogeochemistry of indicator elements for detrital contamination. Shaded area represents concentrations below average from Markert (1994).

A regional perspective

Pearl bluebush leaves and/or twigs have been sampled in independent biogeochemical studies in South Australia (Lintern *et al.* 2006b, Hicks 2010, Mitchell 2010, Tanti 2011, Thomas 2011), and the Broken Hill region (Knight 2010). The biogeochemical study at the Boomerang Au Prospect involved washing of combined leaf and twig samples to remove detritus (Lintern *et al.* 2006b). Unfortunately, Zr was not reported in the analytical suite of elements so the effect of washing could not be monitored.

For the Middleback Ranges on the Eyre Peninsula, Tanti (2011) ashed samples prior to acid digestion and analysis. Element concentrations are typically higher in ashed samples: particularly elements contained in resistate minerals and not readily volatilised (e.g., Dunn 2007, p.108). The Zr results were up to 2.7 ppm with an average of 0.3 ppm (Tanti 2011).

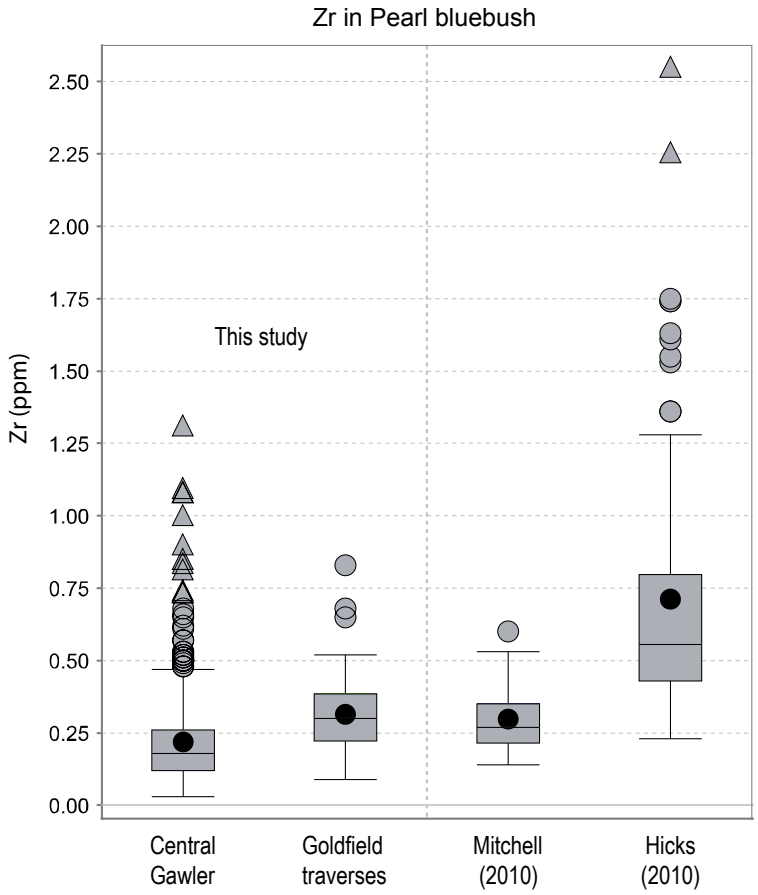

Figure 3.4 – Tukey box plots with outlier (O) and far outlier (Δ) of pearl bluebush Zr data compiled for this study, historic Glenloth and Earea Dam goldfields, and from independent studies in the Middleback Ranges on the NE Eyre Peninsula, SA.

Mitchell (2010) and Hicks (2010) sampled pearl bluebush leaves and used analytical methods comparable to the methods I used for the collection of data in central Gawler Craton surveys. Zirconium concentration in pearl bluebush is highest in the study by Hicks (2010), where samples were collected from an open chenopod shrub land, whereas samples collected by Mitchell (2010) were from medium-density woodland. In contrast, samples from the central Gawler Craton (Tunkillia) and the goldfield traverses (this

study) have low Zr concentrations (Figure 3.4). Some far outliers (Figure 3.4) are acknowledged as proximal (< 100 m) to a frequently used track.

Samples from the Middleback Ranges have a direct correlation between Zr and Fe albiet with a higher spread (lower correlation coefficient) than the central Gawler data. This indicates that there is a varying abundance of Zr and Fe-oxide minerals (e.g., hematite vs goethite).

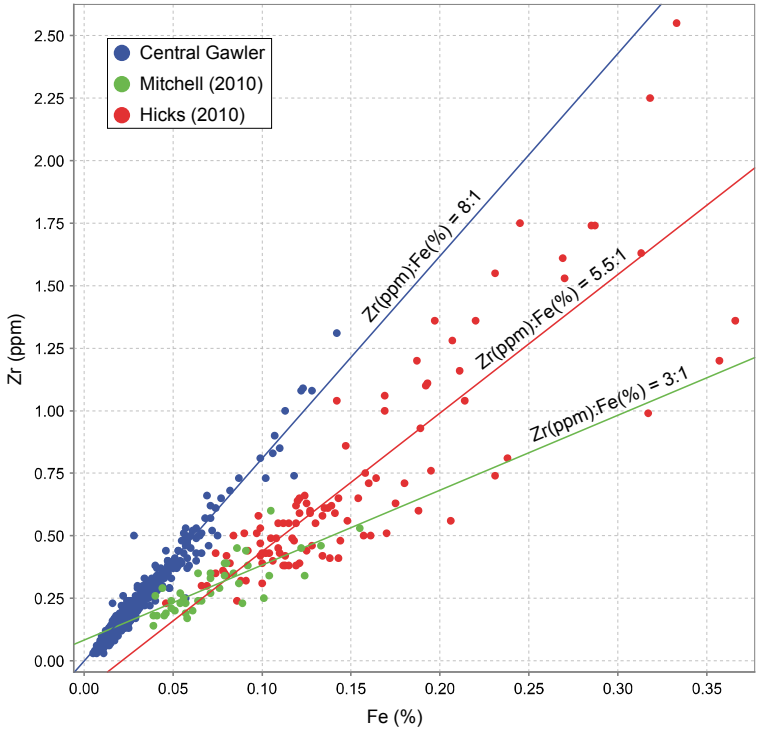

Figure 3.5 - Detrital contamination indicators (Zr and Fe) in pearl bluebush from the central Gawler Craton (this study) and from the Middleback Ranges (Hicks 2010; Mitchell 2010). Trend line slope ratios are Zr(ppm):Fe(%).

Microscopic imaging

The microscopic physiology of South Australian plant material has been investigated for the detrital adhesions on the epidermis, and for distribution of Ca crystal and metal inclusions within the internal tissues (Lowrey 2007, Hulme 2010, Tanti 2011, Thomas 2011). These studies have been brief, in which Tanti (2011) presents an SEM micrograph a pearl bluebush twig cross section with mention of Fe-oxide particles, and Lowrey (2007, pp. 15 & 114) presents images of Ca crystals contained in black oak branchlets, and reports Fe-oxide particles without supporting images. Hulme (2010) investigated the metal distribution within the internal leaf structure of river red gum (*Eucalyptus camaldulensis*) using reflected light micrographs, and multi-element chemistry using LA-ICP-MS.

Reflected light microscope imaging of pearl bluebush material highlights the surface texture difference between leaf and twig material (Figure 3.6). Leaves have a sponge-like appearance and contain visible detrital grains of predominately quartz sand typically 100 µm in size (Figure 3.6: Images B & C). Twig material has a less porous surface than the

leaves, however the topography in the surface is host to fine grain platy particles (Figure 3.6: Image D), which are predominantly Fe-oxides (Tanti 2011).

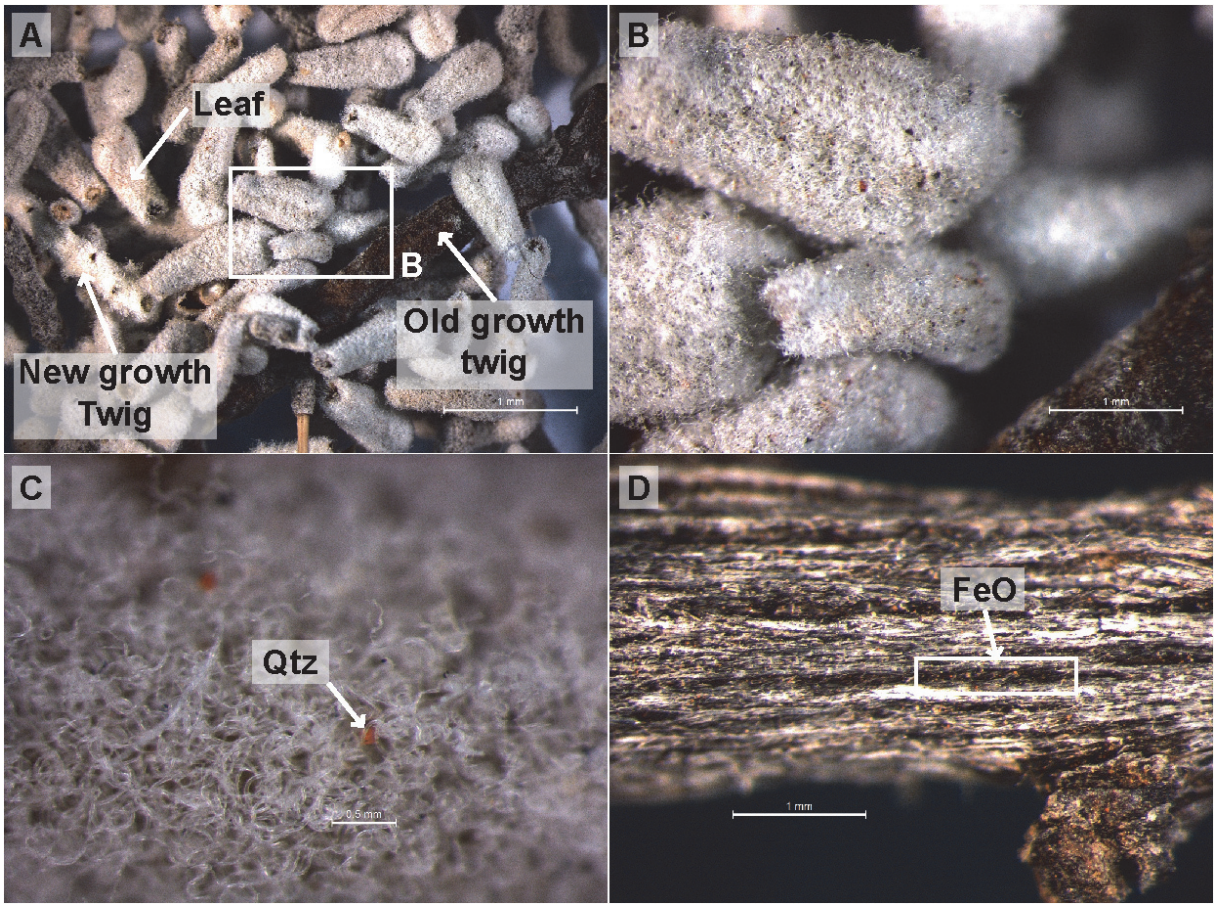

Figure 3.6 - Reflected light micrographs of pearl bluebush foliage (A-C) and twig (D).

Summary of potential contamination

The magnitude of detrital contamination of biogeochemical samples based on Zr and Fe follows the order: pearl bluebush >> black oak > Victoria Desert mallee. Detrital contamination is a physical addition of material to the samples rather than elements taken up by the roots. Therefore the detrital contaminants are not a direct response to the substrate, underlying geology and/or mineralisation. This could have one of the following effects:

1. Dilute the biogeochemical response of the plant (from element uptake via roots) to the substrate, geology, and/or mineralisation; or,
2. Produce a result that is influenced by material of transported origin (local or distal source).

A discussion of these results is contained within *Chapter 7*.

TUNKILLIA AREA

4. Tunkillia background

Foreword

The Tunkillia Au prospect has a history of exploration and research that spans two decades. This chapter provides an enclosed and coherent background of the Tunkillia Au Prospect. This chapter also introduces the regolith studies that have been conducted at the Tunkillia Au Prospect. I have used data provided by Minotaur Exploration and Honours theses (Hopkinson 2009, Klingberg 2009). Data from these diverse sources is synthesised. Chapter 5 then incorporates these data with new data collected as part of this study to reinterpret the landscape processes relevant to mineral exploration at Tunkillia.

4.1. Introduction

Gold mineralisation at the Tunkillia Au Prospect was discovered in 1996 by Helix Resources Ltd. through anomalous Au-in-calcrete concentrations (Martin 1997, Ferris & Wilson 2004). Follow-up geochemical sampling of calcrete, from 1996 to 1998, further defined a 50 km^2 area contained within regional northward drainage, with Au concentrations commonly > 10 ppb (Figure 4.1 & Figure 4.2). Extensive exploration since 1998, through various joint venture agreements[2], with thousands of geochemical samples from more than 200,000 m of drilling (Minotaur Exploration Ltd., pers. comm. 2011), has defined a resource of 878,000 oz. of Au, and 2.5 Moz. of Ag at Area-223 (Mungana Goldmines Ltd. 2012). The Tunkillia Au Prospect is presently one of the largest undeveloped Au projects in South Australia (Mungana Goldmines Ltd. 2011).

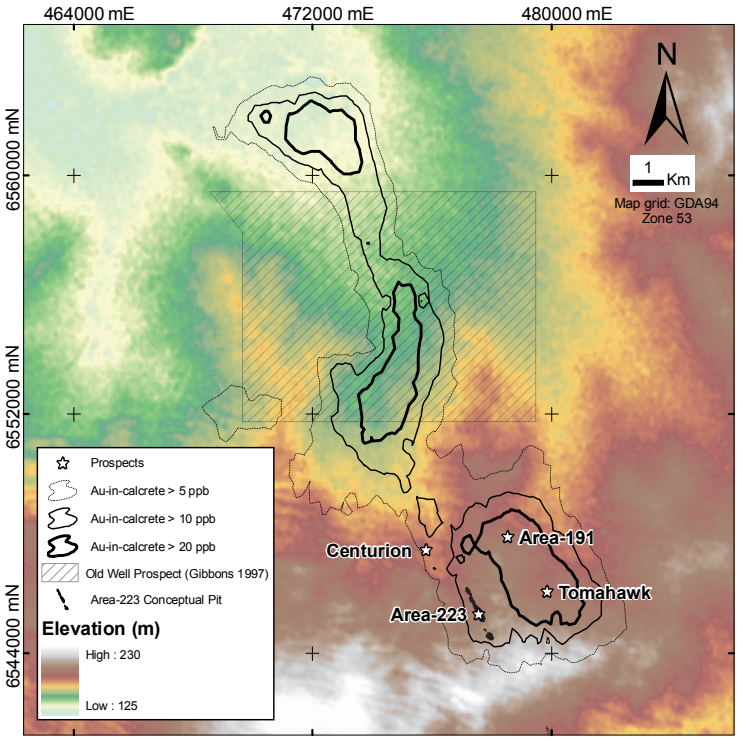

Figure 4.1: Regional Au-in-calcrete data (SARIG 2012) on the 1-second (30 m) SRTM Digital Elevation Model (DEM) and the Tunkillia Au Prospect.

[2] Minotaur Exploration Ltd. earning 51% interest 2005-2012 (Helix Resources Ltd. diluting), and Mungana Goldmines Ltd. earning and 70% interest from July 2012 (Helix Resources Ltd. diluting).

Collaborative projects between Minotaur Exploration Ltd. and the University of Adelaide from 2006 to 2011 investigated the expression of mineralisation at Tunkillia by sampling various surficial regolith materials and vegetation. Most notably was the biogeochemical study by Lowrey (2007), in which the chemistry of black oak samples collected along a traverse could be used to delineate mineralisation (see Belperio 2009a). Further collaborative ventures ensued with the application of biogeochemical methods at various exploration targets (Hopkinson 2009, Vasey 2009) alongside a regolith geochemical sampling material (Klingberg 2009, Risely 2009).

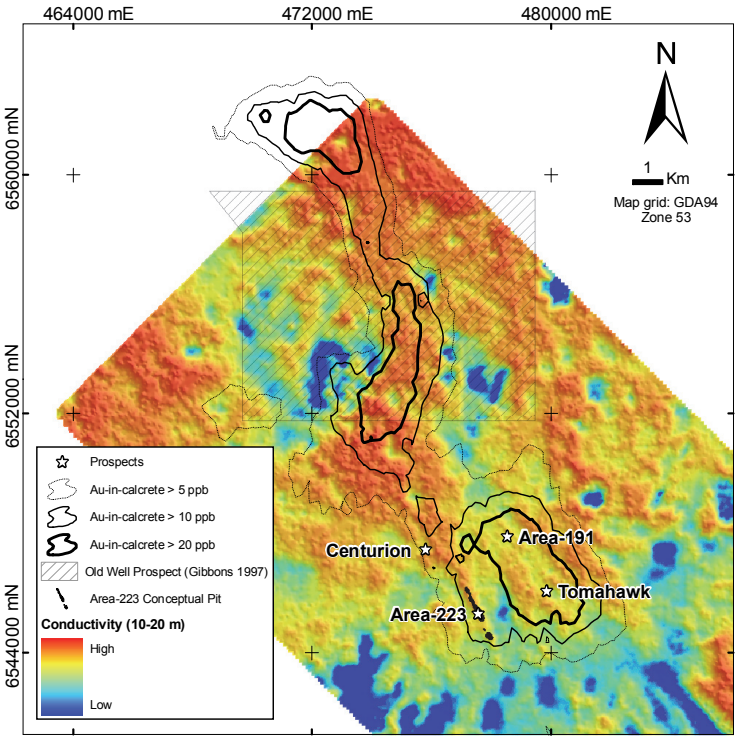

Figure 4.2: Regional Au-in-calcrete data (SARIG 2012) on the airborne electromagnetic survey 10-20 m depth slice (from Minotaur Exploration Ltd.) and the Tunkillia Au Prospect.

Other regolith studies investigated the source of Ca associated with the high concentrations of Au in calcrete (Dart *et al.* 2007), partial digest geochemistry of soils (Fabris 2010, Fabris & Keeling 2010), and palaeo-geomorphological controls on contemporary regolith geochemistry (Dart 2009, Klingberg 2010), with implications for understanding the high concentrations of Au in calcrete down-slope of Tunkillia (e.g., Gibbons 1997; Figure 5.2).

Studies with a deeper focus investigated the hydrogeochemistry of groundwater extracted from drill holes (detailed in Section 5.6; Gray & Pirlo 2005), and the mineralogy of diamond-drill core (from depth > 80 m) in what was an early application of the Hylogger™ hyper-spectral logging tool (Thomas *et al.* 2006). Deposit-scale modelling reported fluid flow, strain, and alteration across the Yarlbrinda Shear Zone proximal and distal to the Tunkillia mineralisation (Potma & Skirrow 2006, Robinson & Potma 2007).

4.2. Location

The Tunkillia Au Prospect is approximately 550 km NW of Adelaide, 200 km directly west of Woomera, and 5 km outside the eastern boundary of the Yellabinna Regional Reserve (Figure 1.1). The Prospect is in the SW corner of the Wilgena pastoral lease. Access to the Prospect is via the Yerda homestead track from the non-sealed Glendambo-Tarcoola road out of Kingoonya.

4.3. Geology

The Tunkillia Au Prospect is hosted by the foliated Palaeoproterozoic Tunkillia Suite (U-Pb age of ca. 1680 Ma; Ferris 2001). The Suite consists of medium- to coarse-grained granites that have been intensely sheared and brecciated with a dominant foliation associated with the Yarlbrinda Shear Zone (Ferris & Wilson 2004). This 120-km-long Shear Zone is has a low magnetic response up to several kilometres wide – a result of the alteration of primary magnetite to ilmenite (Chalmers *et al.* 2007). It is expected that the zone of low magnetic response should be much wider than the zone of visible alteration (i.e., quartz-carbonate-muscovite-rutile; Potma & Skirrow 2006). Sericite alteration (from plagioclase) is widespread throughout the Tunkillia region, and suggested to be coeval with mineralisation (Ferris & Wilson 2004, Fraser *et al.* 2007). Fresh to slightly weathered bedrock exposure is sparse and associated with subtle, isolated, low-relief exposures to the west and south of the project area. At the prospect scale, the geology has been interpreted from close-interval drilling at Area-223 to have zones of variably foliated and sheared granite, with weakly foliated mafic dykes and undeformed felsic dykes (Figure 4.3; Fraser *et al.* 2007).

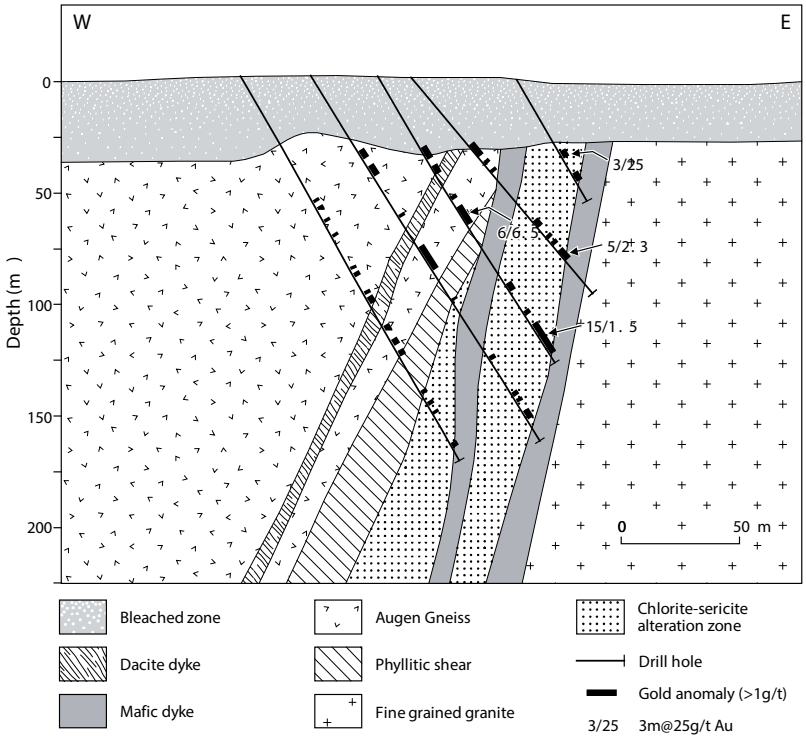

Figure 4.3: Area-223 cross section 111350 mN (6545091 mN, GDA94 zone 53), (Fraser *et al.* 2007)

4.4. Mineralisation

The Tunkillia Au Prospect is the product of a large hydrothermal system associated with the Yarlbrinda Shear Zone (Ferris & Wilson 2004). Modelling by Robinson & Potma (2007) suggests that the western margin of the Shear Zone has been subjected to more localised strain, and that the inside of the 'bend' in the Shear Zone was likely a long-lived fluid conduit, increasing mineralisation potential in this region (i.e., Area-223). Area-223 is the main zone of mineralisation within the Tunkillia Prospect. Primary Au and Ag mineralisation is hosted within narrow, steeply dipping quartz and sulphide (dominantly pyrite and minor galena) veins in association with intense sericite alteration (Figure 4.3). Mineralisation at Area-223 is contained within an envelope approximately 3.5 km long by 200 m wide and to a depth of at least 300 m from the surface (Belperio 2009b). The resource is estimated to be 26.3 Mt at 1.04 ppm Au for 878,000 oz. and 3.0 ppm Ag for 2.5 Moz. (Mungana Goldmines Ltd. 2012). Geochemical pathfinders for primary mineralisation at Tunkillia reportedly include Ag, Pb, and As (Ferris & Wilson 2004).

A flat-lying oxide zone within highly weathered bedrock is present from a depth typically greater than 40 m (Figure 4.3; Belperio 2007). The coherent oxide mineralisation forms a capping to primary mineralisation and constitutes approximately one-quarter of the estimated resource as of 2009 (Belperio 2009b). Higher grade Au intersections (> 1.0 ppm) in the oxide zone are typically associated with highly weathered mafic dykes (Belperio 2007).

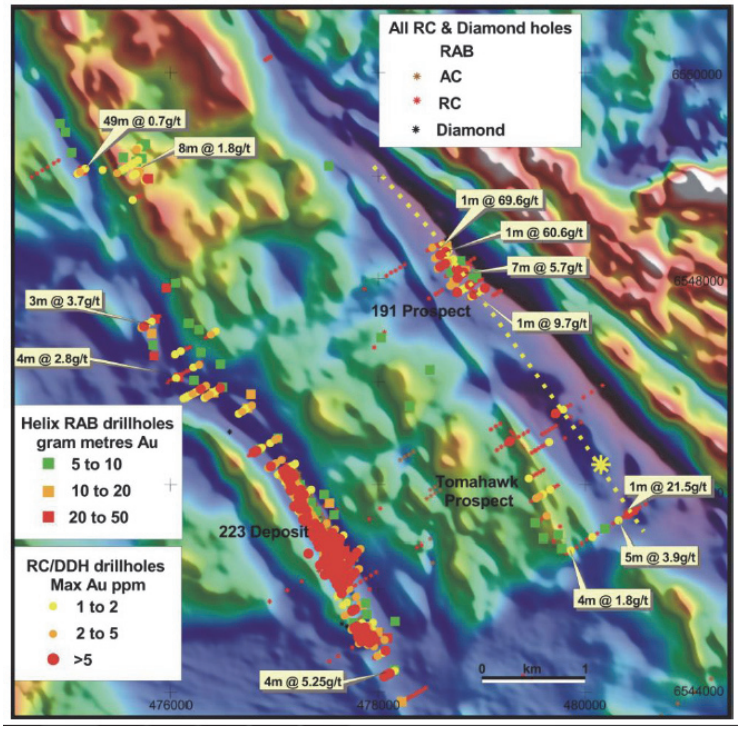

Figure 4.4: Aero-magnetic image of the Tunkillia Au Prospect with significant drilling results at Area-223 deposit, Tomahawk and Area-191 prospects, and other discreet occurrences of Au mineralisation. Round markers represent maximum grade Au intersections (e.g., red is > 5 ppm Au). Square markers represent the grade and extent of the Au intersection (e.g., grams x metres). From Belperio (2009a).

Drill testing of 5 – 300 ppb Au-in-calcrete results at a 50 by 500 m spacing has identified additional discrete occurrences of mineralisation, such as the Area-191 Prospect on the eastern extent of the Yarlbrinda Shear Zone (Figure 4.4; DMITRE 2006a). However, exploration targets such as Tomahawk (south of Area-191; Figure 4.1) remain enigmatic because limited Au mineralisation within narrow sericite-altered zones has been found underlying this surface geochemical expression (Hill 2006). In contrast to Area-223, Tomahawk has minor Au distributed throughout the saprolite, and primary mineralisation is typically low grade (≪ 5 ppm Au) in fresh bedrock at depths greater than 50 m (Flint 2009, p.10). Drill testing of biogeochemical targets identified from the work by Hopkinson (2009) at Tomahawk revealed two intervals of Au mineralisation: 4 m @ 1.0 ppm Au from depths 72 to 76 m, and 4 m @ 2.6 ppm Au from depths 100 to 104 m (Belperio 2010).

The Centurion exploration target is the NW extension of the central alteration zone that hosts Au and Ag mineralisation at Area-223. Drill-testing has revealed limited mineralisation with grades > 2 ppm Au (Figure 4.4). Centurion has also been tested using biogeochemical methods, which found anomalous Au and Ag in plants (Ames 2010).

4.5. Regolith

The regolith at the Tunkillia Au Prospect can be classified into two broad groups: transported and residual. Transported regolith includes indurated and unconsolidated material that has been laterally transported, whereas residual regolith represents the *in-situ* weathered bedrock (e.g., saprolith).

Transported regolith

Quaternary aeolian and alluvial sands associated with ESE-orientated, longitudinal dunes of the Great Victoria Desert dominate the landscape at Tunkillia. Aeolian dunes in the region have a suggested (core) age of 100 ka (Rhodes *et al.* 2005), although younger dune phases have also been dated in the region (c. 25 ka; Sheard *et al.* 2006, Lintern 2007). At Tunkillia, aeolian dunes form a 1 – 10 m thick blanket of mostly siliciclastic sediment that is dominated by quartz with minor clay and iron oxides. Regolith carbonate development in the older dunes is limited to occasional friable and powdery mottles and rhizomorphs. Three dune phases have been differentiated by age (based on spatial relationships and pedogenesis) and plant communities (Figure 4.5; Lowrey 2007). A larger variation in soil type and plant communities is observed between the dune crests and the swales. Swales typically consist of clay rich soils with cryptogam cover that host a variable abundance of indurated regolith (calcrete and silcrete lag). This is suggested to be exposures of a palaeo-sheet wash landform with palaeo-drainage (Dart 2009, Klingberg 2009) and is depicted by *CHep* in Figure 4.5.

Dunes overlie and continue to encroach over (e.g., near Area-191) a sheet wash plain (CHep) with broad, shallow drainage depressions (Aed; Figure 4.5). Calcrete is well developed across this sheet wash plain where, in the dune swales, it is either exposed at the land surface (CHep), or buried by less than 50 cm of aeolian sediments (ISps; Figure

4.5). Calcrete profiles are typically tens of cm to > 2 m thick (Chen 2002a, Alonso-Zarza & Wright 2010), but locally are up to 1 m thick. Calcrete profiles (exposed in drilling sump pits), typically consist of (in descending order) sediment-supported well-rounded nodules; hardpan morphologies; and, rhizomorphic and irregularly shaped nodules (e.g., Figure 2.7). Sheet wash landforms contain angular pebbles to small boulders of silcrete fragments, and angular to well-rounded sand to pebbles of quartz and vein-quartz composition. Pebbles appear to have been sourced from the basal parts of transported regolith and from erosion of the underlying silcrete.

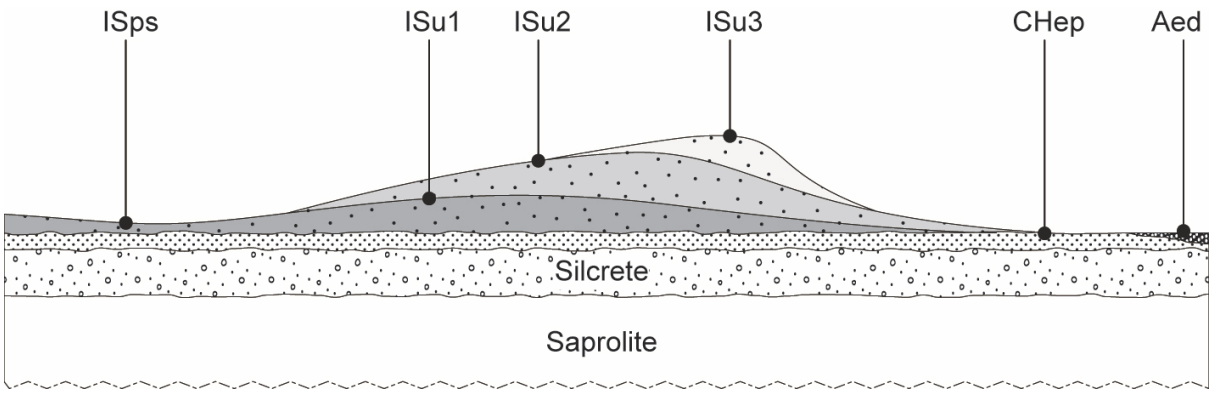

Figure 4.5: Simplified relationship of major regolith types at Tunkillia: sand plain (ISps), phases of dune development (oldest to youngest: ISu1, ISu2, ISu3), erosional surface underlying dunes (CHep), and alluvial drainage (Aed). Regolith types are from the regolith-landform map by Klingberg (2010). Dune phases are adapted from Lowrey (2007).

Residual regolith

Well-rounded pebbles from the base of transported regolith are preserved by siliceous cement that also overprints the underlying (largely) kaolinitic upper saprolite. Angular stock-work quartz veins from the saprolite are also incorporated by the silcrete. The saprolite is derived from the weathering of felsic and mafic Proterozoic crystalline basement. An example of the regolith relationships is exposed in the mesa landscape around Glenloth, 30 km NE from Tunkillia (Figure 4.6). Depth of silcrete ranges from exposed to up to 10 m. The age of the silcrete and its host sediments (e.g., gravels and pebbles) are poorly constrained, but regionally this material is thought to have formed in the Late-Tertiary (Wopfner 1978, Callen 1983) and related to the hinterland of the Cainozoic Eucla Basin.

Saprolite at Tunkillia is typically white and kaolinitic with localised areas of slightly ferruginised saprolite often occurring above the weathering front (Lowrey 2007). Most of the saprolite is derived from granite and besides kaolinite also include vein quartz, muscovite and phengite (Thomas *et al.* 2006). The upper 50 m of regolith (transported and residual) is discussed in detail in *Section 5.1*.

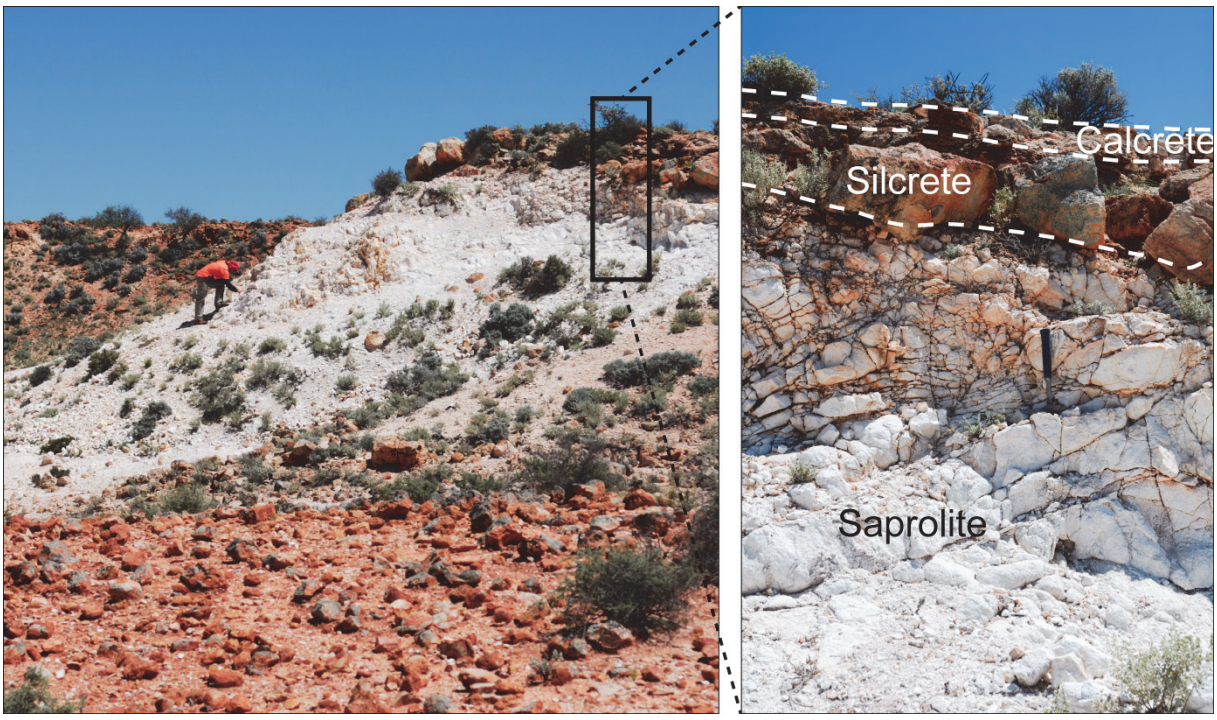

Figure 4.6: Breakaway near Glenloth goldfield, and *Glenloth North* survey area exposing silcrete and the underlying highly weathered crystalline bedrock (Glenloth Granite). (508480 mE 6562700 mN GDA94 zone 53).

4.6. Groundwater

A hydrogeochemical study of groundwater at Tunkillia by Gray and Pirlo (2005) found the groundwater to be dominantly saline and neutral to acidic (pH 3 – 7). Tunkillia groundwater is uniformly saline (average 2.9% total dissolved salt) suggesting low flow rates, and contains high concentrations of dissolved base metals (Mn, Cu, Zn) and REE. Groundwater collected from 94 drill holes across Tunkillia had 0.012 ± 0.3 µg/L (± 1 SD of mean) dissolved Au with the highest concentration at Area-191 (2.53 µg/L). Variation in groundwater Au concentrations across the study area is suggested to be a result of differing sulphide and accessory mineral assemblages between the main occurrences of mineralisation. Tunkillia groundwater was also found to be Ca- enriched and K-depleted, which Gray and Pirlo (2005) thought to reflect the hydrolysis of Ca-rich feldspar.

4.7. Vegetation

Vegetation changes at Tunkillia are closely correlated with landform setting, particularly phases of dune development and swales (Figure 4.5). Dune slopes and crests are colonised mostly by woodland or shrubland dominated by mulga (*Acacia aneura*), horse mulga (*Acacia ramulosa*), red mallee (*Eucalyptus socialis*), spinifex (*Triodia spp.*) and tussock grasses.

Dune swales are an open woodland colonised by Victoria Desert mallee (*Eucalyptus concinna*), horse mulga (*Acacia ramulosa*), and umbrella wattle (*Acacia ligulata*) with occasional pearl bluebush (*Maireana sedifolia*), daisy bluebush (*Cratystylis conocephala*) and Walker's pea (*Bossiaea walkeri*). Exposures of the underlying palaeo-surface within dune swales are dominated by black oak (*Casuarina pauper*), pearl bluebush (*Maireana*

sedifolia), and, low bluebush (*Maireana astrotricha*). This vegetation community is similar to that occupying the plains flanking the dune field, with the addition of saltbush (*Atriplex spp.*).

Species sampled at Tunkillia for chemical analysis are: black oak and Victoria Desert mallee.

5. Tunkillia case studies

Foreword

This chapter encompasses the cases studies at the Tunkillia Au Prospect. The first part is a detailed analysis of the regolith profile at Tunkillia and builds on the background geological information presented in Chapter 4. The relationship between different sampling materials (plants and calcrete) is discussed using data from previous University of Adelaide Honours' research at the Tomahawk Prospect (within Tunkillia) which is integrated with drill-hole and topographic data. This work has been published in *Geochemistry: Exploration, Environment, Analysis* (van der Hoek *et al.* 2012). The landscape processes at Tomahawk are discussed in a broader landscape and geological context with new biogeochemical data that surround Tomahawk in the eastern part of the Tunkillia Au Prospect. The Centurion target was the focus of another University of Adelaide study in 2010 and the data are discussed in this chapter using data sets such as topography, drill hole, airborne electromagnetic data, and calcrete geochemistry, which were not discussed by previous researchers. This chapter concludes with a micro-scale analysis of how the gold is included within the calcrete and the implications this has for calcrete and biogeochemical exploration within the Tunkillia Au Prospect. The next chapter provides case studies in the region surrounding Tunkillia. These case studies provide a broader spatial context of biogeochemical sampling by focussing on small Au mineralisation occurrences and areas where mineralisation is unknown.

The Tunkillia case studies chapter provides a discussion of components of the regolith and biogeochemistry throughout the Tunkillia Au Prospect in five parts:

- *Section 5.1* Regolith mineralogy and geochemistry at the profile-scale (depth: 0 – 50 m);
- *Section 5.2* Plant biogeochemistry and calcrete geochemistry comparison at Tomahawk;
- *Section 5.3* Plant biogeochemistry of the eastern part of the Tunkillia Au Prospect (Area-191 to Tomahawk);
- *Section 5.4* Plant biogeochemistry of the Centurion target (1.5 km north of Area-223 mineralisation); and,
- *Section 5.5* Internal calcrete morphology and geochemistry at the microscopic-scale.

This chapter includes new data in *Sections 5.1, 5.3, and 5.5*, and existing data from independent University of Adelaide Honours' studies in *Sections 5.2 – 5.4*. The existing biogeochemical and calcrete geochemistry data are compiled and reinvestigated alongside new biogeochemical data and with an improved understanding of the area. Dataset locations and their respective sources are presented in Figure 5.1.

The Tunkillia Au Prospect was chosen for this study because it is a good example of a challenging exploration setting in which transported cover overlies a deep (but not too deep) gold mineral system. Previous exploration by various companies (i.e., Minotaur Exploration Ltd. and Mungana Goldmines Ltd.) and research conducted by University of Adelaide Honours' students provided a foundation for this research. Drill-hole data, samples, and airborne electromagnetic surveys were made available to provide constraints on the surface geochemistry and biogeochemistry.

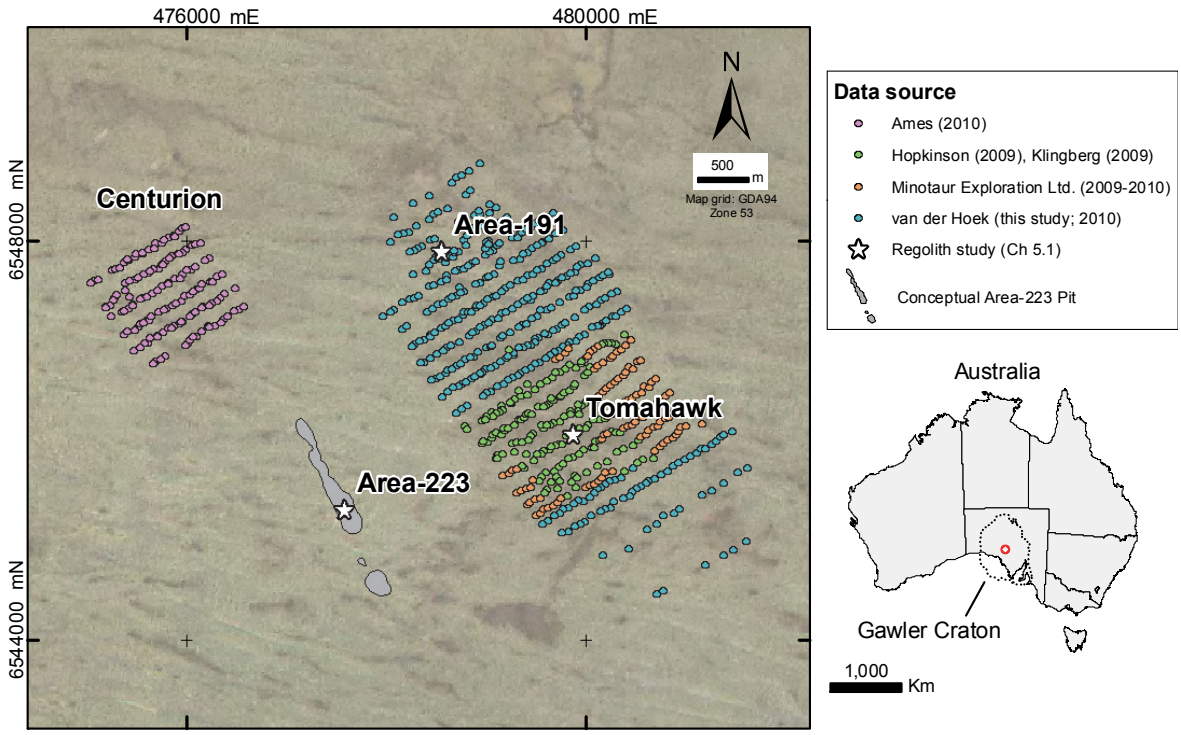

Figure 5.1: Tunkillia Au Prospect within the central Gawler Craton, South Australia (inset), Area-223 conceptual pit, regolith profile locations, and biogeochemical sample locations coloured by sampling program (or study) on the Landsat TM image.

5.1. Regolith profiles

Early exploration at the Tunkillia Au Prospect used inexpensive air-core drilling methods to explore beneath the large Au-in-calcrete anomaly. Drill cuttings were visually logged and geochemical analyses, typically consisting of Au only, used single samples from the bottom of the hole. Since the discovery of the Au/Ag resource at Area-223 (Figure 4.4), more petrological and geochemical data have become available, revealing the mineral assemblage and geochemical pathfinder elements associated with the mineralised zone in fresh rock (Ferris & Wilson 2004). The challenge with exploration targeting at Tunkillia is the thick sequence of regolith that overlies mineralisation. Regolith at Tunkillia consists of transported dune sands underlain by kaolinised basement (or pallid zone) to a depth of 50 m. The most pronounced feature of the regolith profile at Tunkillia is the marked colour change at the interface between transported and residual regolith (e.g., Figure 4.6). Features in the saprolite are difficult to identify due to uniform colour, particularly when samples are pulverised while drilling. This often leads to poorly defined or subjective classifications of deep weathering profiles and inconsistencies in regolith logging (Anand & Butt 2010). Infrared spectroscopic devices such as PIMA (Portable Infrared Mineral Analyser) and Hylogger™ can assist with regolith logging through rapid data acquisition and objective logging of mineral species (Eggleton 2009, Anand & Butt 2010). Infrared spectroscopic analysis becomes even more powerful when integrated with geochemical data (Merry *et al.* 1998). Previous applications of Hylogger™ at Area-223 focused on hydrothermal alteration of fresh basement rocks and found abundant muscovite and phengite (Thomas *et al.* 2006). There have been no multi-element studies of the upper regolith to determine element dispersion from mineralisation through the weathering profile at the Tunkillia Au Prospect. This is of particular concern as many of the drill holes start and finish in the regolith, and recent multi-element analysis of plants and calcrete have been used to target underlying mineralisation (e.g., Tomahawk and Centurion; Hopkinson 2009, Ames 2010).

Geochemistry and mineralogy of the regolith profile to a depth of 50 m is investigated using Hylogger™, X-Ray diffraction, and Self-Organising Maps analysis of whole-rock geochemistry. Samples are 1 m composite powders from air core drilling from three sites (Figure 5.1):

- Area-223, the main Au and Ag resource;
- Area-191, a discrete occurrence of Au mineralisation; and,
- Tomahawk, an area with 5 – 200 ppb Au-in-calcrete results.

5.1.1. Geochemistry and mineralogy results

Spectral analysis

Three reflectance spectra were measured for each 1 m composite rock sample from air-core drilling. Identical curves indicate homogeneity of samples. Sample spectra were matched to mineral spectra in a training library through an automated process using The Spectral Assistant (TSA; Berman *et al.* 1999, CSIRO 2010a). The dominant minerals

assigned through this process have a low error (good match) and are presented, with abundance in Table 5.1. Figures 5.2 – 5.4 are the compiled logs for Area-191, Tomahawk and Area-223 and include data from the Hylogger™: visible wavelength image (line scan); reflectance spectra (red is maximum absorption); and TSA-assigned minerals.

Table 5.1: Major minerals by profile, exported from The Spectral Geologist software. WX=well crystalline, PX=poorly crystalline (disordered).

Mineral (%)	Area-223	Area-191	Tomahawk
Kaolinite PX	6	2	1
Kaolinite WX	31	85	94
Montmorillonite	3	10	2
Phengite	43		
Phengitic Illite	16		

Clay group minerals

Kaolinite accounts for > 80% of the identified minerals in the regolith at Area-191 and Tomahawk (Table 5.1). Well-crystalline kaolinite (WX) is typically distinguished by a deeper AlOH absorption feature at c. 2200 nm whereas disordered, or poorly-crystalline kaolinite (PX) has a diminished absorption feature (e.g., Pontual 2007). These two end members of kaolinite crystallinity are identified in the regolith at Tunkillia. The disordered kaolinite is dominant in the transported regolith units whereas the well-crystalline kaolinite occurs within the residual regolith.

High kaolinite crystallinity (as indicated by a well-defined AlOH absorption feature) is most pronounced at Tomahawk. Moderately-crystalline kaolinite (WX) is present in the saprolite at Area-191 to a depth of 47 m. The lower part (44 – 50 m) of Area-191 profile contains smectite minerals (Figure 5.2). Montmorillonite is typically present as a minor component in the uppermost regolith (0 – 8 m) of each profile (Figures 5.2 – 5.4).

Mica group minerals

Phengitic white mica (phengite) is the dominant mineral in the saprolite at Area-223 (Figure 5.4; Table 5.1). Phengite is also identified in one interval from Tomahawk at depth 19 m (Figure 5.3). Phengite and phengitic illite are identified as the dominant minerals from a depth of 4 m corroborating previous results from Hylogger™ analysis in the area (Thomas *et al.* 2006). At the depths of 15 – 24 m, WX predominates with a lower abundance of phengite. Gold concentration is highest in this interval (340 ppb).

Fe-oxide minerals

Broad IR absorption features at 410 – 520 nm and 900 nm are typical of Fe-oxides. These features are evident in Figures 5.2 – 5.4 (blue column) and generally correspond with darker intervals on the line scan. The strongest absorption features are measured from the transported regolith (0 – 4 m), a two-metre interval Area-223 with a prominent colour change at depth from 31 metres (Figure 5.4), and in the lower profile of Area-191 (Figure 5.2).

XRD analysis

Transported regolith is characterised by quartz, calcite, dolomite ± gypsum and kaolinite. The saprolite is dominated by quartz, K-feldspar (microcline) and plagioclase feldspar (albitic) at Area-191 and Tomahawk, and dominated by muscovite and/or phengite at Area-223 (Figures 6.2 – 6.4). Plagioclase co-exists with K-feldspar at the base of each profile but the signal is diminished or absent in the upper profile. Only K-feldspar is present at a depth of 16 m at Area-191 and Tomahawk (Figures 5.2 – 5.3). Tomahawk samples at 16 and 50 m have a weak muscovite response from XRD analysis.

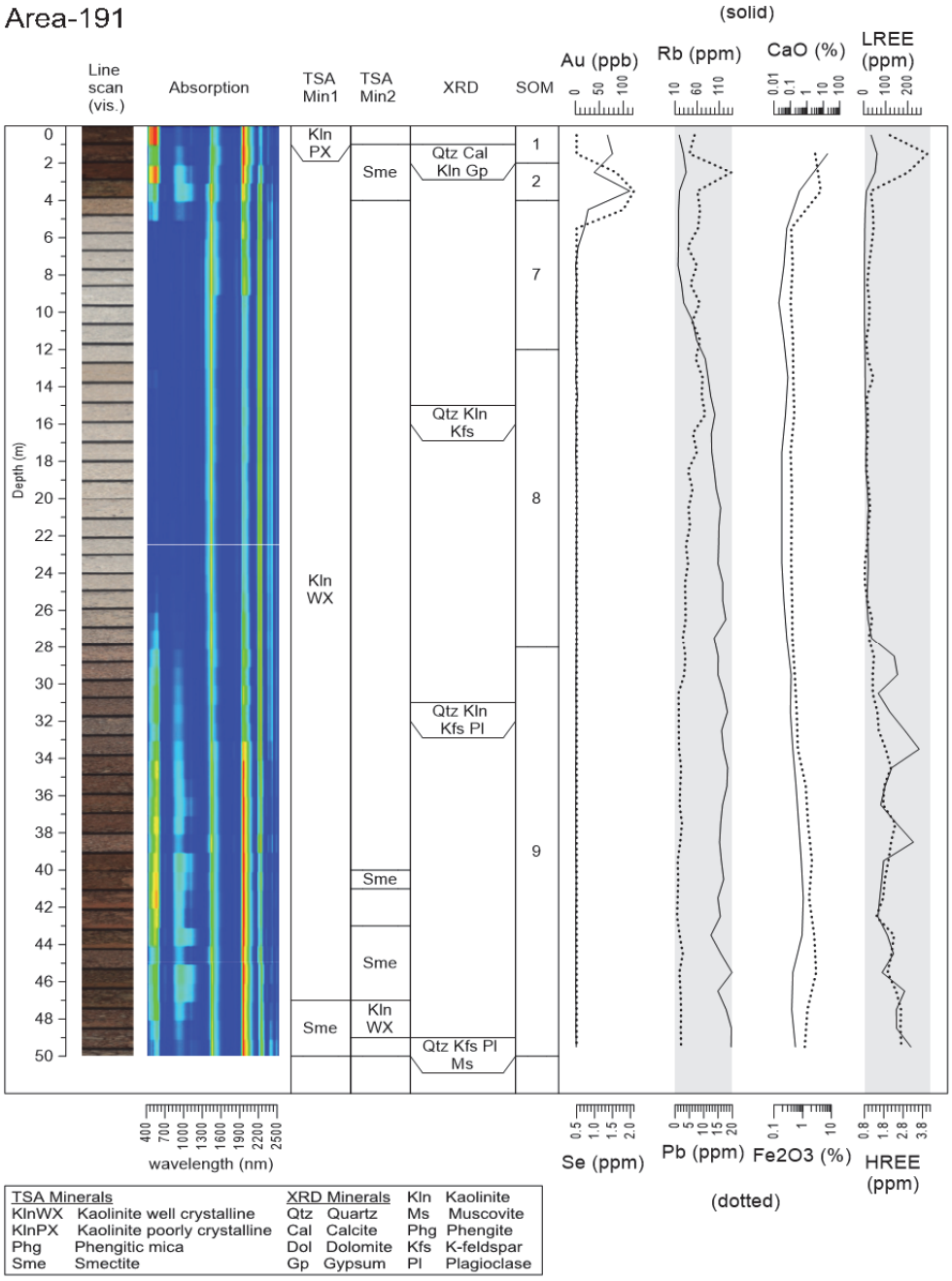

Figure 5.2: Log of Area-191 regolith (0-50 m): visible wavelength line scan and Hylogger™ absorption features (red=higher absorption); TSA-assigned mineralogy (Min1 & Min2); XRD mineralogy, K-means clusters from SOM analysis of whole-rock geochemistry (see Appendix A for geochemistry), and selected down-hole geochemistry. Lower axis are for the dotted series. Blanks represent no second mineral in TSA column; and, no data in XRD column. LREE is the sum of La, Ce, Pr, Nd, and HREE is the sum of Ho, Er, Tm and Yb.

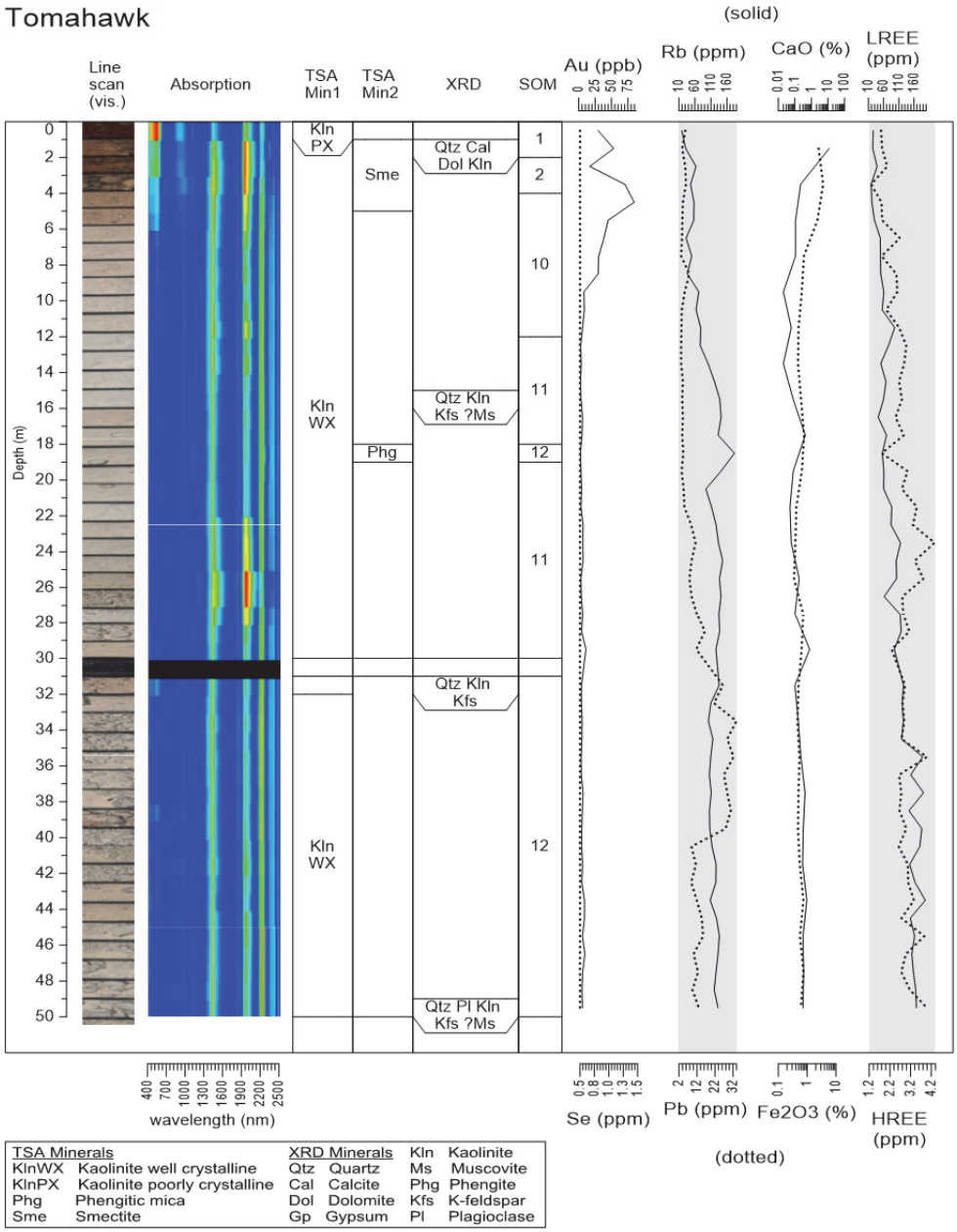

Figure 5.3: Log of Tomahawk regolith (0-50 m): visible wavelength line scan and Hylogger™ absorption features (red=higher absorption); TSA-assigned mineralogy (Min1 & Min2); XRD mineralogy, K-means clusters from SOM analysis of whole-rock geochemistry (see Appendix A for geochemistry), and selected down-hole geochemistry. Lower axis are for the dotted series. Blanks represent no second mineral in TSA column; and, no data in XRD column. No sample collected at 31 m. LREE is the sum of La, Ce, Pr, Nd, and HREE is the sum of Ho, Er, Tm and Yb.

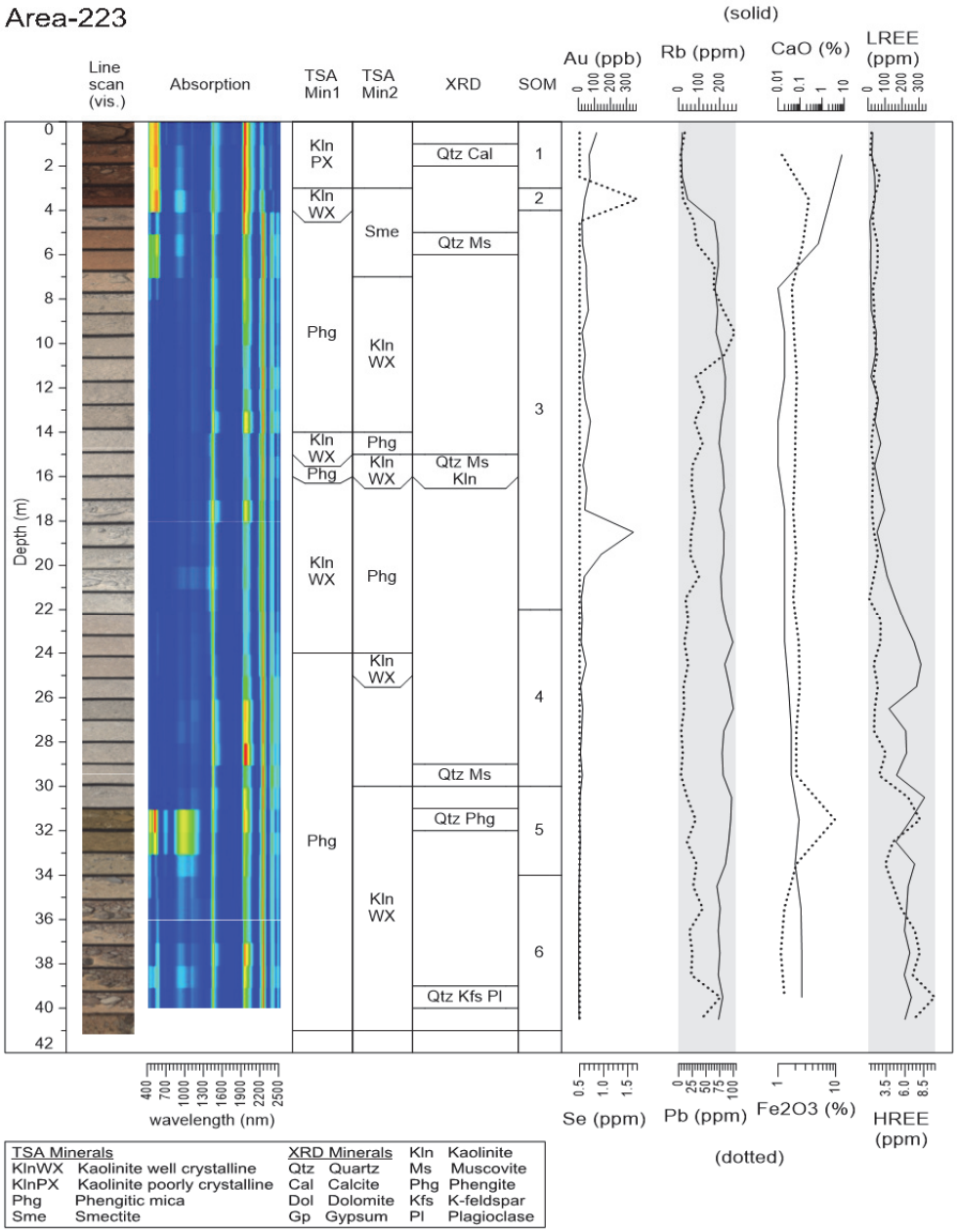

Figure 5.4: Log of Area-223 regolith (0-41 m): visible wavelength line scan and Hylogger™ absorption features (red=higher absorption); TSA-assigned mineralogy (Min1 & Min2); XRD mineralogy, K-means clusters from SOM analysis of whole-rock geochemistry (see Appendix A for geochemistry), and selected down-hole geochemistry. Lower axis are for the dotted series. Blanks represent no second mineral in TSA column; and, no data in XRD column. LREE is the sum of La, Ce, Pr, Nd, and HREE is the sum of Ho, Er, Tm and Yb.

Geochemistry

Self-Organising Maps (SOM) and k-means cluster analysis

Twelve clusters of samples are derived using SOM analysis and a k-means[3] clustering approach of 57-element geochemical data within SiroSOM. The minimum, maximum and average values of each cluster for the full suite of elements are included in Appendix B. A summary of selected elements are included in Table 5.2. Labels are assigned to each cluster (e.g., Sand, upper, middle lower etc.) post analysis and are based on site, depth, physical characteristics, and major element geochemistry.

Table 5.2: Average concentration of major elements (wt. %), Au (ppb) and Au-associated elements (ppm) by cluster. Quantization error (q-error) is a cluster average.

	Clusters											
	1	2	3	4	5	6	7	8	9	10	11	12
	Si-Ca sand	Fe-ind. sediment	Area-223 Upper	Area-223 Middle	Area-223 Oxide	Area-223 Lower	Area-191 Upper	Area-191 Middle	Area-191 Lower	Tomahawk Upper	Tomahawk Middle	Tomahawk Lower
q-error	6.8	4.7	2.9	2.8	6.6	2.7	2.8	1.9	2.2	2.2	2.3	2.2
Depths (m)	0-2	2-3	4-21	22-29	30-33	34-41	4-11	12-27	28-50	4-11	12-29	18-50
SiO_2	56	67	71	72	66	73	68	68	72	65	70	69
Al_2O_3	7.2	16	16	15	15	14	21	19	15	21	17	19
Fe_2O_3	2.1	3.8	2	2.2	5.9	1.2	0.42	0.43	1.5	1	0.56	0.57
CaO	13	0.99	0.09	0.033	0.075	0.12	0.04	0.043	0.27	0.075	0.2	0.3
MgO	2.7	0.66	0.8	0.9	0.71	0.17	0.12	0.12	0.22	0.38	0.29	0.18
Na_2O	0.32	0.4	0.51	0.4	1.2	3.1	0.6	1	3.8	0.59	0.76	1.5
K_2O	0.56	0.77	4.3	5.1	5.2	5.5	0.99	3.8	4.2	1.4	3.8	4.2
MnO	0.013	0.01	0.02	0.02	0.03	0.01	0.01	0.01	0.012	0.01	0.01	0.01
TiO_2	0.27	0.41	0.35	0.35	0.47	0.1	0.29	0.23	0.18	0.27	0.16	0.22
P_2O_5	0.013	0.013	0.018	0.068	0.15	0.07	0.01	0.011	0.071	0.01	0.014	0.025
TOT/C	3.5	0.37	0.063	0.083	0.06	0.17	0.038	0.023	0.02	0.12	0.17	0.088
TOT/S	0.083	0.043	0.066	0.12	0.075	0.02	0.045	0.043	0.058	0.05	0.07	0.022
LOI	17	9.8	4.6	3.5	4.1	1.8	8.6	6.4	2.8	9.1	6.3	5
Ag	0.1	0.1	0.19	0.26	0.25	0.79	0.1	0.1	0.1	0.1	0.1	0.1
As	1.9	5.6	0.78	0.5	1.8	0.54	0.53	0.5	0.5	0.74	0.5	0.5
Au	69	56	63	23	9.6	2.8	7.1	2	1.1	31	4.8	5.4
Bi	0.1	0.12	0.15	0.11	0.2	0.1	0.1	0.1	0.1	0.1	0.1	0.1
Cd	0.14	0.1	0.1	0.1	0.1	0.1	0.1	0.1	0.1	0.1	0.1	0.1
Cu	8.4	9.9	1.8	2	38	5.3	1.4	1.9	11	3.5	1.9	2.3
Mo	0.31	0.32	0.34	0.15	3.7	0.5	0.16	0.11	0.19	0.14	0.41	1.1
Ni	5.9	5.7	1	0.81	3.9	1.9	1.3	1.2	2.4	1.1	1.4	1
Pb	5.9	9.4	43	10	24	36	7.2	5.8	1.8	4.4	7.1	19
Sb	0.1	0.1	0.1	0.1	0.13	0.1	0.1	0.1	0.1	0.1	0.1	0.1
Se	0.5	1.3	0.5	0.5	0.5	0.5	0.66	0.5	0.5	0.5	0.5	0.5
W	0.87	1.8	5.2	9.5	6.2	1.8	1.9	1.3	1.8	1.6	0.88	2.3
Zn	28	13	4.7	18	37	26	1.4	2.1	23	2.3	3.2	2.9
Ba	590	930	1100	1400	1000	910	440	1500	1500	480	1000	1300
Rb	21	42	200	240	250	200	29	100	120	56	130	120
Sr	490	160	75	300	530	350	40	180	570	52	140	280

Figure 5.5 contains the 'component-plane maps' for Au, Ag, Ca, Fe, K, Mg, Se, and Si. These maps are a graphical representation of the geochemical data. Each node (hexagon) that contains a white marker represents one or more sample(s). Warm-coloured nodes represent samples with higher concentrations of a particular element: for example, samples in cluster 6 have the highest concentrations of Ag. Figure 5.5 also illustrates the sample and cluster relationships: nodes at diagonally opposite corners of the map represent the most dissimilar samples – all 57 elements considered. Component plane maps for the remaining elements are included in Appendix B. Division of the profile by clusters is illustrated in Figures 5.2 – 5.4.

The quantization error (q-error) is a measure of the distance a sample is from the node vector. High q-error values indicate outliers or boundaries within a dataset (Fraser & Dickson 2007). The highest q-errors are associated with transported regolith (clusters 1-2)

[3] A method of cluster analysis that aims to partition *n* observations into *k* clusters. The number of clusters is determined by when the variance within the clusters is minimised.

and the Area-223 oxide zone (cluster 5). Both units form a contrast against adjacent regolith in one or more elements (e.g., Si, Fe, Ca, K; Table 5.2).

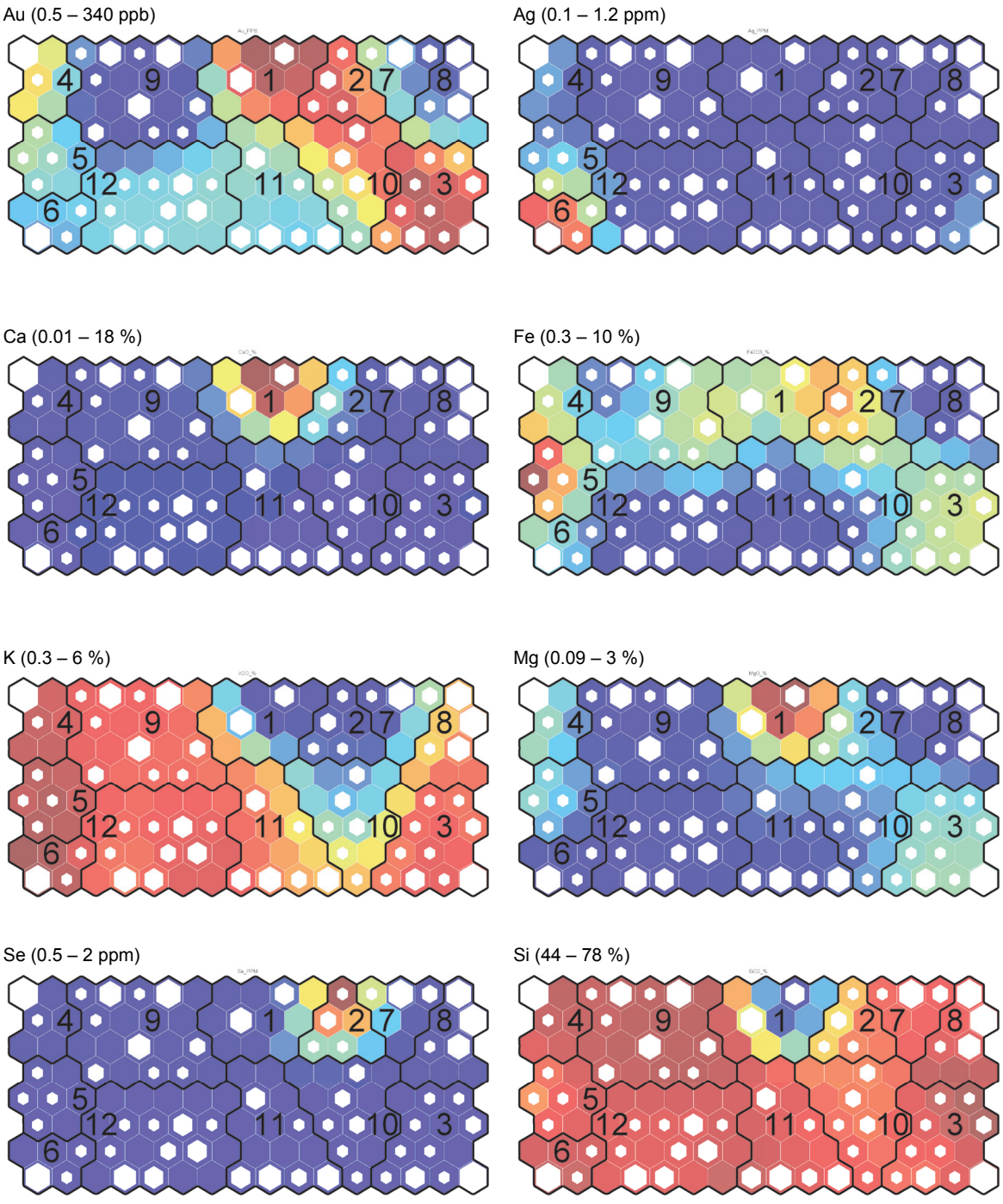

Figure 5.5: Component-plane plots, with clusters (1-12). Colours represent element concentration: red = high, blue = low. E.g., samples in cluster 6 have high concentrations of Ag. Size of white hexagons denotes the number of samples represented by a particular cell. No white hexagon = no samples. Clusters: Aeolian sand (1), indurated sediment (2), Area-223 (3-6), Area-191 (7-9). And Tomahawk (10-12).

Major elements

Two clusters represent the transported regolith and are common to the top of each profile: (1) Ca and Mg-rich samples represent aeolian sands and calcrete, and (2) Fe-rich samples represent indurated sediments and/or clay hardpan (Table 5.2). The abundance of Ca, Mg and Fe in clusters 1-2 is illustrated by the red hexagons in Figure 5.5. Silica concentrations in the transported regolith are as low as 44 % in samples in these clusters. The ten remaining clusters represent various zones of each profile. There is no commonality of clusters between profiles.

Magnesium follows two trends as indicated by the two broad groups of aqua/red-coloured hexagons on the Mg component-plane plot in Figure 5.5. Magnesium in clusters 1-2 is associated with Ca, whereas in clusters 3-5 Mg is associated with K and Fe. The higher concentrations of K and Mg in the clusters 3-5 represent the abundant phengite and phengitic illite in the residual regolith at Area-223 (Table 5.2). Total Al in the saprolite throughout Tunkillia (Table 5.2) follows a trend similar to the proportion of kaolinite WX (Table 5.1).

Trace elements

Concentrations of REE are presented in Figures 5.2 – 5.4 as the sum of light elements (La, Ce, Pr, Nd) and the sum of heavy elements (Ho, Er, Tm, Yb). Rare earth element concentrations increase with depth gradually at Tomahawk (Figure 5.3) and abruptly in the middle–lower saprolite at Area-191 and Area-223 (Figures 5.2 & 5.4). Figure 5.6 highlights a distinct group of samples at Area-223 with higher La:Ce ratios and that comprise cluster 3 in the SOM analysis. This trend is also evident in Figure 5.4 where there is an offset between light and heavy REE depletion. Cluster 3 samples have a good correlation with P and S ($R > 0.9$). Rare earth element concentrations are largely responsible for the horizontal distribution of nodes on the map: nodes (and samples) on the left side of the map have higher concentrations of REE (see Appendix B for all component-plane plots).

Rubidium concentrations are highest in the saprolite at Area-223 (175 – 250 ppm) and one sample at Tomahawk (180 ppm), and concentrations are markedly lower in the saprolite of the other two profiles (Figure 5.7). High Rb results are associated with phengitic samples as indicated by a phengitic sample from Tomahawk plotting with the Area-223 samples (Figure 5.7). Rubidium concentrations appear uniform throughout the Area-223 saprolite (Figure 5.4). At Area-191 and Tomahawk, Rb concentrations diminish gradually in the upper saprolite. Transported sediments contain < 50 ppm Rb.

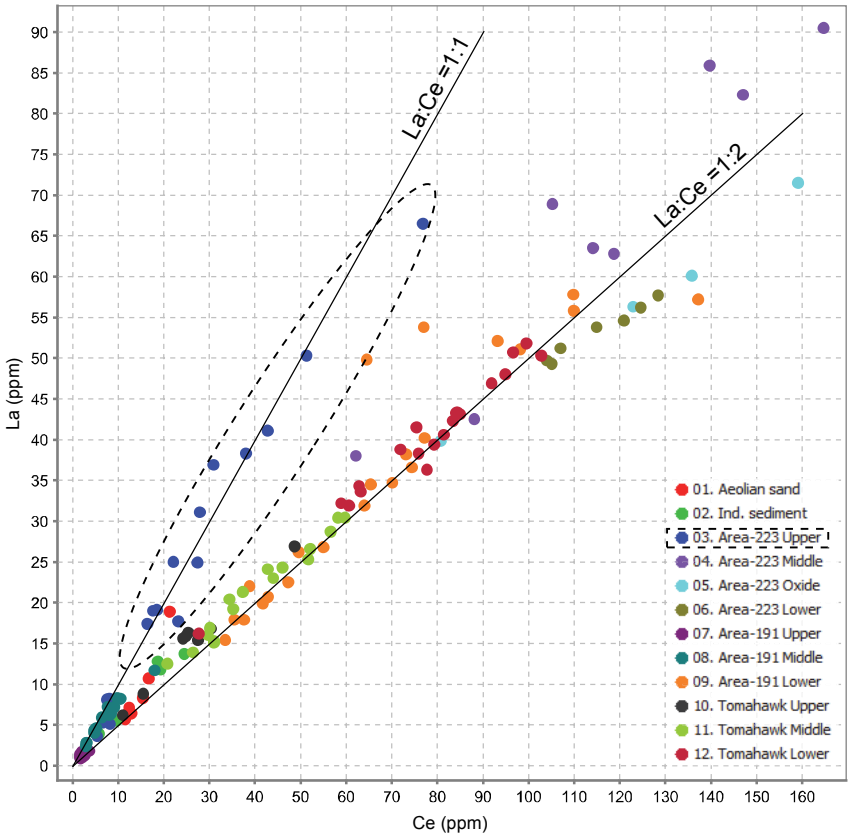

Figure 5.6: La vs. Ce scatterplot. Coloured by cluster (derived from SOM and K-means analysis)

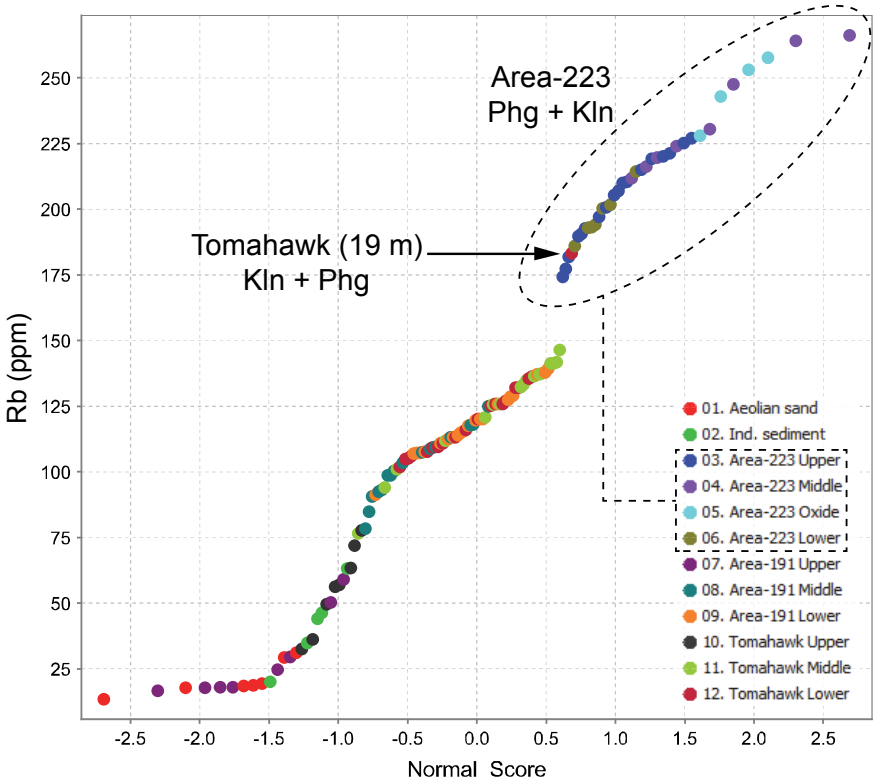

Figure 5.7: Rb cumulative distribution plot. Coloured by cluster (derived from SOM and K-means analysis).

Mineralisation-associated elements

Gold is most abundant in the transported regolith of each profile (30 – 120 ppb; clusters 1-2) and in the upper saprolite of Area-223 (18 – 340 ppb; cluster 3) and Tomahawk (6 – 85 ppb; cluster 10). Samples with the lowest concentrations of Au are from the saprolite at Area-191 (< 26 ppb; clusters 8-9). Figure 5.5 shows the higher concentrations of Au to be associated with the Mg and Fe in the transported regolith at all profiles and with phengitic saprolite at Area-223. Gold concentrations up to 85 ppb occur in the saprolite at Tomahawk in spite of the lack of phengite and Mg and Fe. Average Au concentrations of each regolith domain are in Table 5.2. The Au component-plane plot (Figure 5.5) shows some horizontal separation of elevated Au results. This is primarily due to REE element concentrations (see Appendix B for component-plane plots). Detectable Ag (> 0.1 ppm) occurs exclusively at Area-223 (Figure 5.5). Silver:gold is 460:1 at the bottom of profile compared to < 1:1 at the surface (Table 5.2).

Indurated sediments have between 3 – 5 % Fe (cluster 2; Figure 5.5). An Fe-rich interval in the saprolite at Area-223 (31-33 m; cluster 5) has high concentrations of As, Bi, Cu, Mn, Ti and Zn (Table 5.2). Sediments at Area-191 and Area-223 have detectable concentrations of Se (0.5 – 2.1 ppm; Figure 5.5). Selenium is below detection limit (> 0.5 ppm) in all other samples (Figure 5.5). Gold concentrations in the Se-rich samples are lower than the upper saprolite. Tungsten is associated with Au in the saprolite and is most abundant at Area-223 (Table 5.2). Lead is up to 100 ppm in the upper saprolite at Area-223 (Figure 5.4; Table 5.2). Total S has minimal association with Au, Ag or Pb.

5.1.2. Discussion

Infrared spectroscopic analysis

Kaolinite is a major component of the regolith and forms from the weathering of alumino-silicate primary minerals such as feldspars and muscovite (Nesbitt & Young 1989, Eggleton 2001, McQueen 2006b, Eggleton 2009). Well-ordered kaolinite is abundant in the saprolite at Tunkillia and is typical of authigenic formation in residual regolith (Eggleton 2009, Pontual 2009). A nearby exposed weathering profile (30 km NE of the Tunkillia Prospect; Figure 4.6), which has preserved stock-work quartz veins within the saprolite, demonstrates that authigenic kaolinite formed from the weathering of granitic parent material.

Area-223 is characterised by phengitic mica that likely formed during the hydrothermal alteration associated with movement along the Yarlbrinda Shear Zone (Potma & Skirrow 2006). White mica is very stable during weathering processes (McQueen 2009), and is difficult to visually identify in the pallid zone. This is evident in the line scan images (Figures 5.2 – 5.4). Kaolinite and mica are in near-equal proportions for most of the Area-223 profile. Samples from between 26 – 30 m are purely phengitic indicating minimal feldspar in the parent material (Figure 5.4).

X-ray diffraction

The stability of major minerals during weathering approximates the crystallisation sequence of Bowen's reaction series: Ca-rich plagioclase < Na-rich plagioclase < K-rich feldspar < muscovite (McQueen 2009). That is, plagioclase is altered during the early stages of weathering and muscovite is altered during the advanced stages of weathering. Plagioclase and K-feldspar are present at the base of all three profiles. Area-223 saprolite at depths < 32 m contains quartz, muscovite and kaolinite. Muscovite has likely formed at the expense of feldspar during hydrothermal alteration (Alderton *et al.* 1980). Progressive alteration of feldspars indicates the depth and intensity of weathering. K-feldspar is retained in the saprolite from depths between 16 – 50 m at Area-191 and Tomahawk indicating the K-feldspar weathering front is between 4 – 16 m. The weathering front of plagioclase is between 16 – 32 m at Area-191 (Figure 5.2). Tomahawk is more deeply weathered than the other profiles as indicated by the visibly deeper pallid zone (line scan; Figure 5.3). Deeper weathering at Tomahawk is also evident from the plagioclase weathering front loosely constrained to between 32 – 50 m deep.

Geochemistry

REE distribution

Plagioclase has a higher affinity for REE than K-feldspar during the formation of primary minerals (e.g., Rollinson 1993). As plagioclase is altered before K-feldspar in the initial stages of weathering (McQueen 2009), then REE are also mobilised early in the weathering process. Plagioclase is completely altered in the upper saprolite at Area-191 and Tomahawk (depths < 16 m), resulting in REE depletion compared with the base of the profiles (Figures 5.2 – 5.4). The advanced weathering of the upper saprolite is possibly the cause for high concentrations of REE and Ca in groundwater at the Tunkillia Au Prospect (e.g., Gray & Pirlo 2005).

White mica and kaolinite are the dominant minerals in the regolith at Area-223 (Figure 5.4). The kaolinite is likely to have formed from the alteration of plagioclase (e.g., Nesbitt & Young 1989). The higher concentrations of REE in the saprolite Area-223 are likely retained in the white mica (originally in feldspars) that is preserved during weathering (e.g, McQueen 2009).

Fractionation of the light REE is most evident immediately above the Fe-rich oxide zone at Area-223 (Figure 5.4). Samples that are enriched in the light REE also have higher concentrations of S and P. Although it is possible that the REE and P could represent monazite, the greater abundance of labile minerals (plagioclase and K-feldspar) verses more stable minerals (white mica) is probably a more dominant control on REE fractionation (e.g., Nesbitt 1979). The Fe-rich oxide zone is likely a reflection of the higher abundance of sulphide minerals at Area-223. Enriched S, P and REE above the oxide zone are possibly a result of vertical migration through capillary action.

Rubidium

Saprolite that contains phengitic white mica, in addition to kaolinite, has higher concentrations of Rb than the kaolinitic saprolite without the white mica (Figure 5.7). During hydrothermal alteration of plagioclase to white mica, the Rb has a higher affinity to the mica phase (e.g., Fleet *et al.* 2003). White mica has a high stability during the weathering process (McQueen 2009), therefore the Rb is retained in the profile within the mica as the labile minerals such as plagioclase are weathered. This immobility of Rb during weathering has been used as a proxy for porphyry Cu mineralisation (Armbrust *et al.* 1977)

SOM analysis of geochemistry

A SOM analysis and K-means approach considers all 57 elements for an independent and objective classification within and between profiles. This process assigns places samples in groups and these groups are then interpreted based on visual inspection, infrared spectroscopic analysis, and geochemistry. SOM analysis and K-means clustering shows that the transported regolith in each profile fit into two geochemically similar groups (1 and 2; Table 5.2). Geochemistry of the samples in these clusters (i.e., transported regolith) is significantly different from the underlying saprolite. The high concentrations of Ca, Mg, and Fe relative to the saprolite (clusters 3-12) displace the total Si as shown by the Si component-plane plot (Figure 5.5). Clusters 1 – 2 have a high average q-error which indicates higher geochemical heterogeneity of samples within these groups. In spite of the high q-error and high geochemical variation, the samples are not different enough to be assigned to a neighbouring node on the SOM. Nodes that represent the saprolite samples generally have a low q-error thus indicating that samples represented by these nodes are more geochemically homogenous (Table 5.2).

Saprolite cluster assignment broadly represents mineralogy, in particular the alteration of plagioclase and K-feldspar to kaolinite. Plagioclase is altered during the early stages of weathering hence this boundary is the lowest in the profiles. K-feldspar is weathered during later stages of weathering hence the weathering front higher in the profile. Area-191 saprolite consists of three clusters (Figure 5.2). Division of clusters 8-9 represents the upper extent of plagioclase and is marked by REE depletion at depths < 28 m. Division of clusters 7-8 represents the upper extent of K-feldspar and is marked by the depletion of K and Rb at depths < 16 m.

Tomahawk saprolite consists of three clusters (Figure 5.3). Division 10-11 represents the upper extent of K-feldspar marked by the depletion of K and Rb. Clusters 11 and 12 are intertwined possibly due to the gradual REE depletion and irregular distribution of white mica. Cluster 12 probably represents zones of increase white mica content.

Area-223 saprolite consists of four sequential clusters with three divisions. Cluster 6 at the base of the profile is Ag-rich (1.2 ppm). Plagioclase and K-feldspar are present at 40 m, but do not feature further up the profile probably due to alteration to muscovite (hydrothermal) and kaolinite (weathering). Cluster 5 is distinguished by Fe-oxides and enrichment in As, Bi, Cu, Mn Ti, and Zn. Division of clusters 3-4 approximately marks REE depletion and higher concentrations of Au and Pb at depths < 22 m (Figure 5.4).

Implications for exploration

The high concentration of Ca and Au in the transported component of the regolith profile represents the Au-in-calcrete anomaly, but this alone does not distinguish the Area-223 Au/Ag deposit from the Area-191 or Tomahawk exploration targets. There were no other mineralogical or geochemical features of the transported regolith that distinguished Area-223 mineralisation from the other sites. This is probably due to a large Si dilution and all three profiles contained within the broad Au-in-calcrete anomaly over the Tunkillia Au Prospect. Residual regolith or saprolite (depths > 4 m) at Area-223 contains indicators of underlying mineralisation measureable using geochemical and mineralogical analysis. Area-223 saprolite is distinguished from the Area-191 and Tomahawk targets by the presence of phengitic white mica, and high concentrations of Rb, Au, Ag, and Pb.

The abundance of phengitic white mica using Hylogger™ at Area-223 is expressed by Rb concentrations > 175 ppm (Figure 5.7). The upper saprolite at Area-223 has high concentrations of Pb (10 – 100 ppm), Au (up to 340 ppb) and detectable concentrations of Ag (0.1 – 1.2 ppm). Rubidium and Pb concentrations are well above the limits of detection of 5 ppm for handheld portable X-ray Fluorescence (pXRF) instruments (Olympus Innov-X 2011). Rubidium could be used as a surrogate for mica (Figure 5.8) in samples from the pallid zone, and Pb as an indicator of sulphides using pXRF devices at Tunkillia. Gold and Ag concentrations in the saprolite are, as expected, below the detection limit (5 ppm; Olympus Innov-X 2011) for measurement by pXRF and would require laboratory-based analytical methods.

XRD analysis reaffirms the major mineral assemblage from Hylogger™ analysis. The real value of XRD analysis in this study has been the identification of remnants of primary minerals (K-feldspar, plagioclase and muscovite) that have been altered during intense weathering. These weathered minerals were not identified by infrared spectroscopic analysis but are important for the interpretation of multi-element geochemical analysis, particularly for REE. Infrared spectroscopic devices are capable of rapid data acquisition (compared with many weeks for laboratory geochemical analysis) that can be used to assess mineralisation potential whilst exploring in the Tunkillia area.

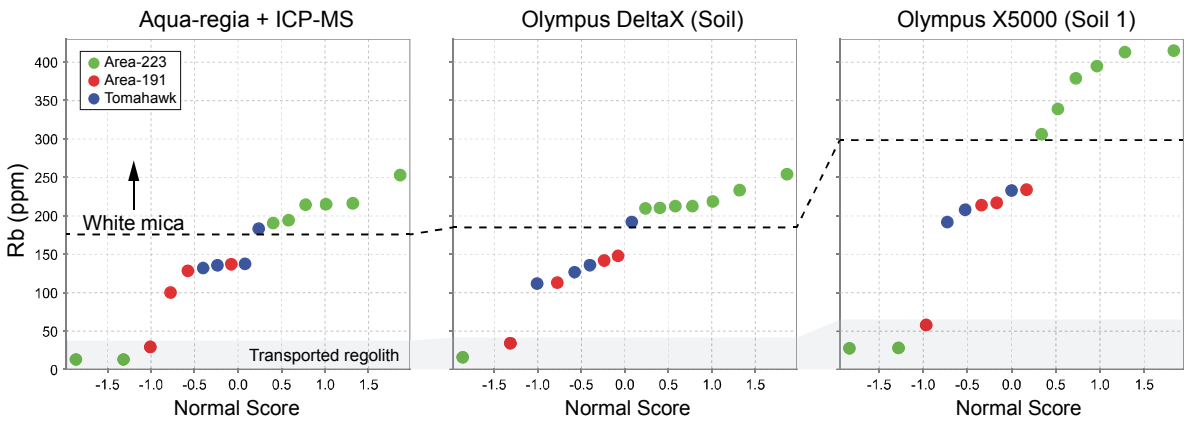

Figure 5.8: Rb in the same regolith samples measured by ICP-MS (left) and Olympus pXRF (middle & right). pXRF analysis was conducted on powders that were used for XRD analysis. Samples are transported regolith (shaded) and residual regolith.

Hylogger™ and XRD techniques provide constraints on major element geochemistry, weathering processes, and parent material. Geochemical analysis of the regolith for a wider suite of elements than Au only would complement the mineralogy and be of value for SOM analysis. SOM analysis provides an objective and quantitative comparison of samples within and between profiles based on a full suite of elements. New data can be uploaded to the existing SOM as it is collected and compared with the existing classifications. Geochemical data measured using portable instruments could be analysed using SOM although the measurement of trace elements such as Au and Ag would still require lab-based techniques due to such low concentrations.

Rubidium and Pb could be used as a proxy for hydrothermal alteration and mineralisation where no mineralogical data are available by measuring the saprolite using pXRF. This method could be used to assess new and archived drill cuttings for alteration and mineralisation at the Tunkillia Au Prospect, particularly in areas where previous exploration has assayed for Au only.

5.2. Plant and calcrete inter-relationships at Tomahawk

This section is published in Geochemistry: Exploration, Environment, Analysis (van der Hoek et al. 2012) following the presentation of the abstract at the International Applied Geochemistry Symposium (van der Hoek et al. 2011). The published typeset is included in Appendix C.

The Tomahawk Au-in-calcrete anomaly is the subject of two independent studies investigating the surface expression of mineralisation through multi-element analysis of plant and calcrete surveys (Hopkinson 2009, Klingberg 2009). Sample locations are denoted by the green markers in Figure 5.1. Results from these independent studies have not been compared or discussed previously. This section discusses plant and calcrete chemistry from previous studies in conjunction with drill hole data that was not used in the earlier studies. Targets developed from biogeochemical sampling in this area are claimed to have led to the intersection of deep mineralisation by drilling (Belperio 2010).

5.2.1. Results

Table 5.3 lists summary data for Au, Ca and Mg concentrations measured in each sample media (calcrete, Victoria Desert mallee, and black oak), and the average observed variation of Au concentration between sub-sample splits. The average % variability for the plant samples includes both species. Suggested geochemical backgrounds are the commonly used 50th percentile (Matschullat *et al.* 2000, McQueen 2005a), and 90th percentile of the undisturbed data distribution.

Table 5.3: Summary of Au, Ca, and Mg in calcrete and plant samples (average in parentheses)

Material	Au (ppb)	Percentile Au threshold (ppb)	Au Avg. variability (%)	Ca (%)	Mg (%)
Calcrete [n=98]	< 1.0-194.0 (36.8 ± 3.14)	50th: 24 90th: 79	32.0 ± 9.0 [n=10]	0.78-27.06 (19.76 ± 0.46)	0.08-3.5 (0.74 ± 0.07)
Plant [n=164]	< 0.2-10.1 (0.77 ± 0.084)	50th: 0.5 90th: 1.6	35.7 ± 11.4 [n=19]	-	-
Victoria Desert mallee [n=28]	< 0.2-6.4 (1.0 ± 0.26)	-	-	0.33-1.45 (0.78 ± 0.05)	0.093-0.26 (0.19 ± 0.007)
Black oak [n=136]	<0.2 - 10.1 (0.72 ± 0.087)	-	-	0.42-1.56 (1.04 ± 0.02)	0.171-0.464 (0.31 ± 0.005)

Calcrete geochemistry

All calcrete samples are indurated nodular or hardpan morphologies (Klingberg 2009). Calcium is the dominant cation in the carbonate, with a minimal dolomite (Mg) component (Table 5.3). For most elements, concentrations are well above analytical detection limits. Elements in the analytical suite consistently below analytical detection limits are: Pd and Pt (99.07%); and Re, Se, and Ta (100%).

Au and associated elements

Gold concentrations are between 1 – 194 ppb and form a somewhat contiguous area of elevated results > 20 ppb over mineralisation (Figure 5.9). Data collected by Klingberg (2009) supports the results from the 2 sets of company calcrete data from Tomahawk: 200 by 500 m spacing assaying for Au, Ca, Pb and Zn in 1996; and, 25 m by 100 m spacing assaying only for Au in 1998. Variation in Au concentration between duplicate samples ranges from 12 to 70%.

Drill cutting geochemical data at Tomahawk are limited to Au only, however, elements included in the analytical suite across other parts of Tunkillia, and found to be associated with mineralisation are: Ag, Pb, As, Au, S, and Zn. In addition to the pathfinder elements identified by Klingberg (2009; Au, Pb, Zn and Fe), As and Ga exhibit a minor similarity in distribution to Au in calcrete, but any direct relationship with these elements and mineralisation is negligible.

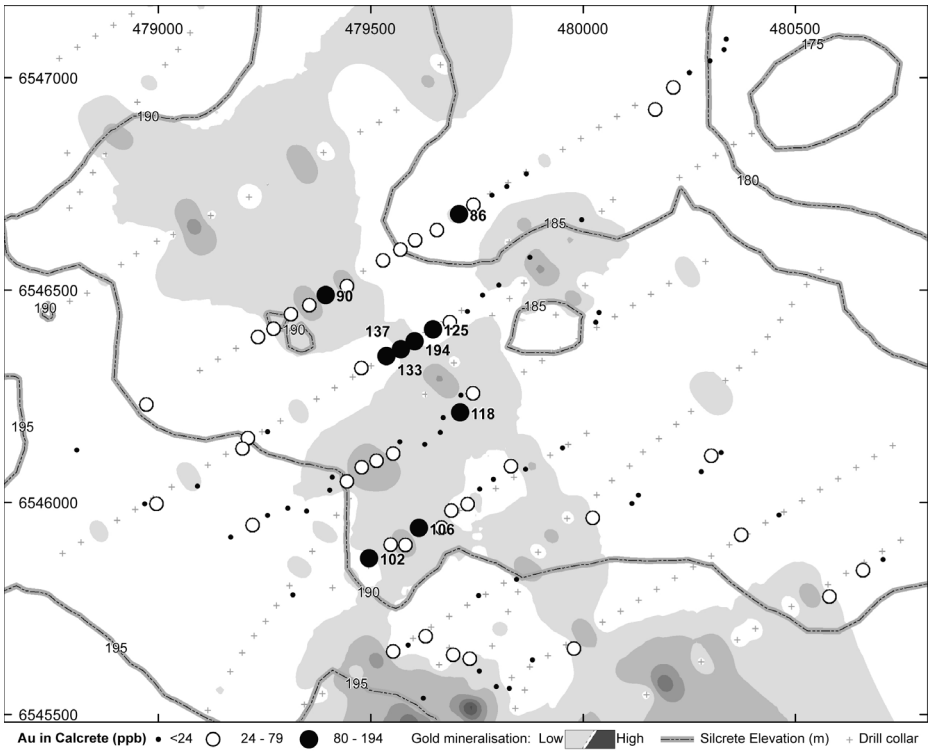

Figure 5.9: Mineralisation at Tomahawk represented by the summation of Au assays, silcrete topography from drill logs, and Au-in-calcrete results (from Klingberg 2009).

Aluminium has a strong positive relationship with Ga and a positive relationship with Pb. Analysis of calcrete cross-sections using SEM and LA-ICP MS revealed bulk samples with high Au concentrations (c. 100 ppb) to have coarse-grained detrital inclusions: pore spaces contained a combination of clay (Al, Fe) and Ca-based crystals determined from energy dispersion spectra. Low Au-containing samples (< 40 ppb) exhibited a more micritic, crystalline (with zoning) internal morphology and a minimal detrital sand component.

Au distribution

More than half (59) of the calcrete samples were collected from sheet wash erosional plains (CHep in Klingberg 2009) demonstrating regolith-landform-controlled calcrete distribution. Calcrete with elevated Au concentrations (e.g., > 50 ppb) are largely from both colluvial sheet wash plain and aeolian sand plain (mapped as Chep and ISps in Klingberg 2009) regolith types (Figure 5.10).

Samples with moderately elevated Au in calcrete (50th percentile, or ≥ 24 ppb) are widespread (Figure 5.9). Some of these samples overlie mineralisation, while others have either been collected away from drilling lines, or have no supporting data from drilling (Figure 5.9). Irregular sample spacing on the eastern and western flanks of the survey has resulted in a few isolated clusters of samples with elevated Au that either has no underlying mineralisation, or data from drilling. These elevated results do not appear to be associated with underlying known mineralisation (Figure 5.9).

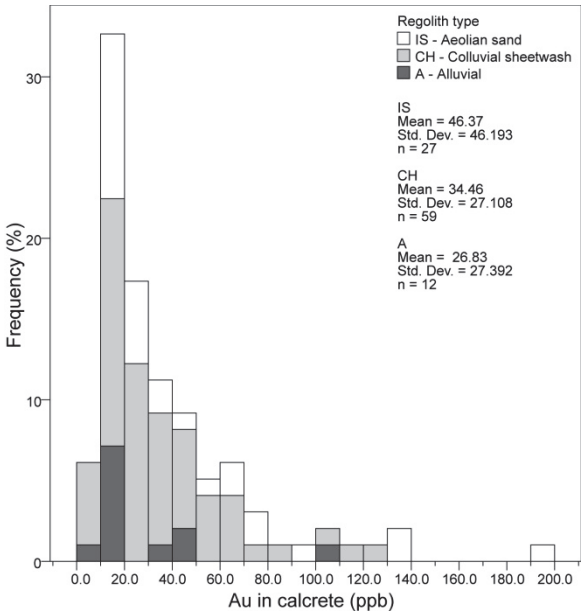

Figure 5.10: Au in calcrete distribution across the dominant regolith types at Tomahawk (10 ppb bins)

Calcrete with highly elevated Au concentrations (90th percentile, or ≥ 80 ppb) are constrained to an area with underlying mineralisation and a minor axis of depression in the topography of the silcrete surface (Figure 5.9). Maximum levels of mineralisation in the Tomahawk area lie to the south, up-slope of the depression; however there is no significant Au in calcrete result recorded from overlying this site.

Plant biogeochemistry

Element concentrations in plant material are typically lower than calcrete, with trace elements typically near analytical detection limits. This causes poor precision (Dunn 2007, pp. 229-230), and also makes investigating element associations challenging. Elements with concentrations below analytical detection limit in plant material at Tomahawk are: Be, Ga, In, Nb, Pd, Pt, Ta, Tl, V and W.

Calcium is the most abundant element from the analytical suite. Black oak typically hosts a higher concentration of Ca and Mg than the Victoria Desert mallee (Table 5.3), which corroborates with a greater abundance of Ca crystals within black oak plant tissues compared to Victoria Desert mallee tissues, observed via SEM imaging of sections (Figure 5.11). Black oak appears to be more susceptible to dust contamination with a greater abundance of detrital mineral particles (Al, Fe Ti and Zr) entrapped in the rough epidermal layer of branchlets (Figure 5.11, A). Victoria Desert mallee typically contains higher concentrations of U, Mn, Li, and Re in plant tissues than black oak.

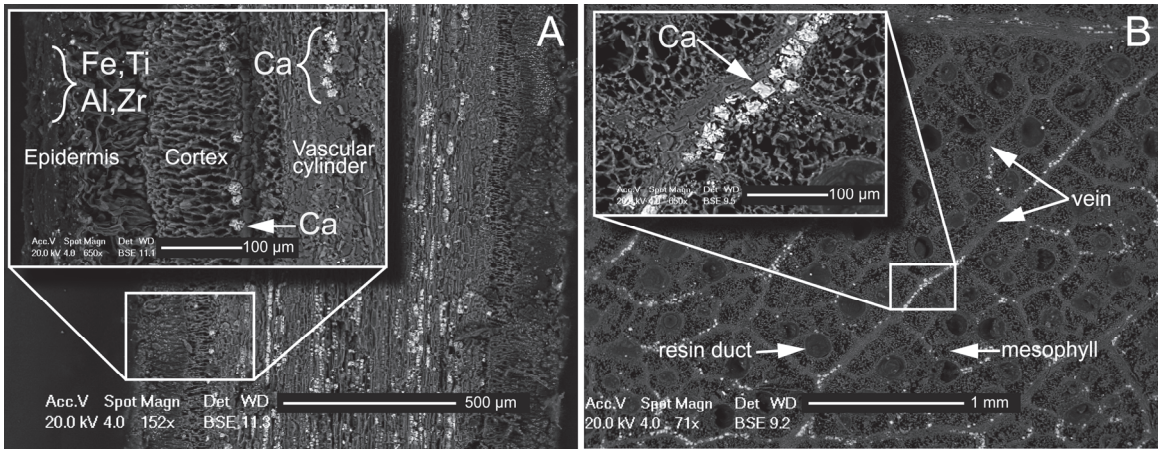

Figure 5.11: SEM backscatter micrographs of long sections of black oak branchlet (A) and Victoria Desert mallee leaf (B) samples with a high Ca content.

Au and associated elements

Occurrences of highest Au concentrations are independent of the plant species (Table 5.3). Gold in plant foliage is typically low, and ranges between < 0.2 – 10.1 ppb. In total, 30% of the samples register ≤ 0.2 ppb, which is the analytical detection limit for Au, and limits the significance of element correlations. Elevated Au in plants weakly corresponds to the elevated abundance of LREEs (Y, La and Ce) and Hg. The difference of Au concentration in duplicate samples ranges from 0 to 75%.

Au distribution

Variation in plant chemical composition, between and within regolith-landform units, occurs for many elements (e.g., REE, Fe, Mg, Na, P, S, Sc, and Se). Landform has minimal influence on the distribution of plant samples with elevated Au content (Figure 5.12). The two highest Au concentrations are a black oak sample (10.1 ppb) from an aeolian sand (IS) regolith type, and Victoria Desert mallee sample (6.4 ppb) from a sheet wash (CH) regolith type.

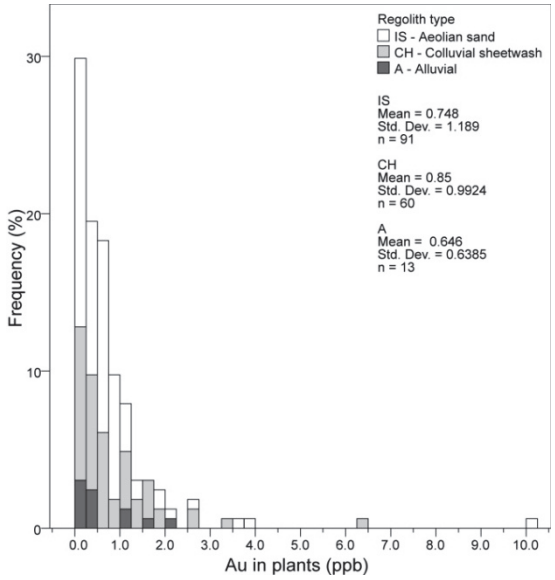

Figure 5.12: Au in plant distribution across the dominant regolith types at Tomahawk (0.25 ppb bins)

Plant samples with moderately elevated Au (50th percentile, or ≥0.5 ppb) are widespread, extending the full width of the survey (Figure 5.13). A large number of these samples are collected away from drilling lines and do not have supporting drill cutting data. Gold concentration in plant data is highly variable at a 50 m sample interval and this threshold is not definitive of the underlying mineralisation. Plant samples with highly elevated Au (90th percentile, or ≥1.5 ppb) are from both species, and have a sporadic distribution across aeolian sand (IS) and sheet wash (CH) regolith types. These elevated results are typically supported by, or are proximal to the margins of, underlying mineralisation. A number of plant samples with elevated Au (e.g., 3.8 and 1.6 ppb in Figure 5.13) do not have drill data available.

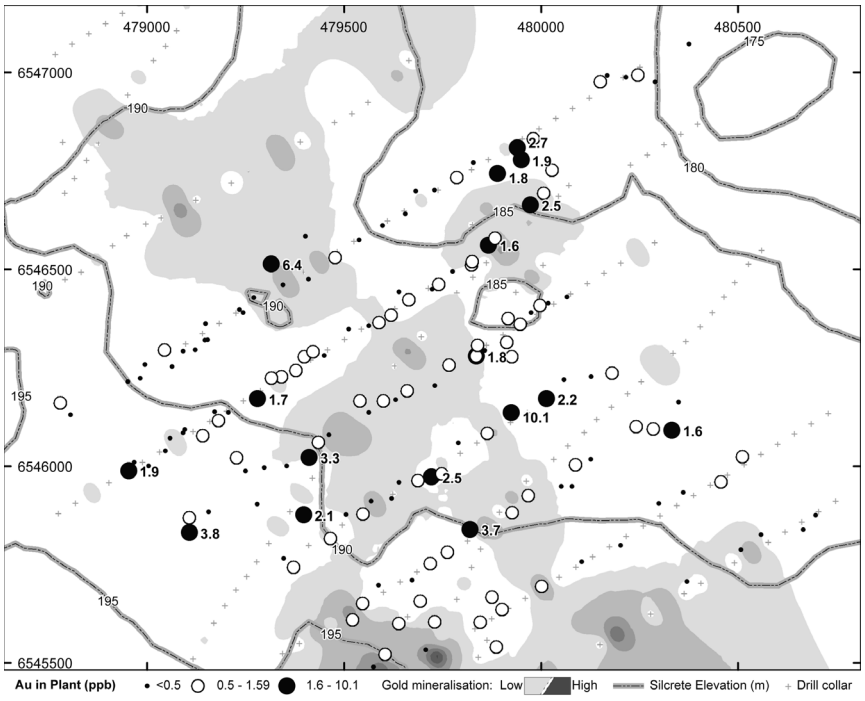

Figure 5.13: Mineralisation at Tomahawk represented by the summation of Au assays, silcrete topography from drill logs, and Au-in-plant results (from Hopkinson 2009).

Au relationship: calcrete and plants

Gold concentration in calcrete is up to 20 times higher than in plants, and has a coherent central zone of highly elevated Au (≥ 80 ppb) results, which is associated with underlying mineralisation. The average Au concentration of 37 ppb in calcrete covers a broad area, in contrast to a much lower average Au concentration in plants (0.77 ppb) and a typically more sporadic distribution of elevated results. There is no apparent spatial association between maximum Au concentration in each material or with regolith type.

Analysis of 98 pairs of calcrete and plant chemistry data (< 65 m apart) does not reveal major-, or trace-element associations between the two materials, or with underlying mineralisation and lithology. Gold concentration in plants is highest in areas where calcrete has about 20 ppb, which is typically on the margin of the central zone of elevated Au in calcrete results (Figures 5.9 & 5.13).

5.2.2. Discussion

Palaeo and contemporary landscape controls

Alluvial channel gravels have been consistently recorded in drill logs throughout Tunkillia. A prominent channel sloping north from Area-223 is evident from the digital elevation model (DEM) and aerial imagery (Dart 2009), and is further supported by drill logs. This also complies with the palaeo-channel postulated by Gibbons (1997) at the Old Well prospect to the north of Tunkillia. Comparable channel sediments are less common at Tomahawk and the silicified-sediment (silcrete) topographic surface indicates a subtle NEE drainage vector (c. 0.7% slope gradient; Figure 5.9).

The availability of calcrete and plant species for sampling at Tomahawk is largely controlled by Quaternary geomorphology associated with sand dunes. While calcrete is typically confined to dune swales where aeolian cover is thin, the distribution is likely more widespread but at greater depth (e.g., Lintern 2007; Figure 4.5). Similarly, the occurrences of angular vein quartz surface lag has been interpreted as *in situ* and only exposed in dune swales (Klingberg 2009, 2010). Subsequent field observations, from Tomahawk and the silcrete breakaways near Glenloth (c. 30 km to the NE; Figure 4.6) have revealed this lag to be a product of saprolite and silcrete erosion locally concentrating the residual quartz vein fragments. Stock-work quartz veins (and potentially metals) preserved at the saprolite interface and well-rounded gravel to pebble-sized quartz fragments enclosed in the silicification have been later relinquished during erosion.

Tomahawk is centrally positioned in a broad, relatively flat-lying embayment on a larger north sloping palaeo-drainage channel parallel to Area-223. Lateral dispersion of the regional elevated Au-in-calcrete results, when filtered to > 10 ppb, is particularly evident northward from Area-223, with some minor dispersion NNE from Area-191. There is negligible deviation of Au-in calcrete > 10 ppb contour down slope of Tomahawk (Figure 4.1)

Models

Primary mineralisation at Tomahawk is broadly distributed rather than within a confined high-grade occurrence, and a direct relationship between Au in calcrete and plants with underlying mineralisation is therefore indiscrete and ambiguous. The elevated calcrete Au results at Tomahawk align with a broad topographic low (Figures 5.90 & 5.13) on the silcrete-sediment interface. Tomahawk appears to be isolated from inputs from Area-223 (to the west) and Area-191 (down palaeo-slope) due to palaeo and contemporary topography constraints (Figure 4.1). This sheltered topographic setting has evidently retained Au for the generation of an elevated Au in calcrete expression despite the limited underlying low grade mineralisation.

Ca cycling

Calcium and Sr in regolith carbonate on the Gawler Craton have a predominantly atmospheric source (rain and dust; Lintern *et al.* 2006a, Dart *et al.* 2007). Calcium-rich dust accumulated on the surface is translocated down the profile in rainwater solution eventually precipitating at the depth of seasonal wetting and subsequent drying (Wright & Tucker 1991, p.8) which is typically less than 1 metre on the sheet wash landforms at Tunkillia. Calcium crystals (e.g., Ca-oxalate) are common in plant tissues and serve a variety of functions (Nakata 2003). Decomposition of litter and crystal dissolution contributes Ca to the surface (Wright & Tucker 1991, Alonso-Zarza & Wright 2010) which can be up to 1.56 wt. % of dry leaf/branchlet material at Tomahawk as shown by the biogeochemical data (Table 5.3) and SEM micrographs (Figure 5.11).

Plants have a pivotal role in the Ca and hydrological cycle in the regolith. Water losses from soils through evapotranspiration and/or direct evaporation are suggested to be the main mechanisms of carbonate precipitation (Cerling 1984, Wright & Tucker 1991). Plants extracting water from the regolith induces the precipitation of Ca (and similarly, complexed-Au) from soil solutions forming calcareous rhizomorphs and calcrete (Cerling 1984, Lintern 2007). Plants also contribute water and solutes to the near-surface horizons via the roots through a process known as hydraulic-lift (or hydraulic redistribution; Richards & Caldwell 1987). At Tomahawk, this could facilitate the transport of Ca (and Au) containing solutions from deep, wetter regions in the profile, to sub-aerial plant organs or to drier near-surface horizons.

Au cycling

Plants at Tomahawk have accumulated Au in leaves at concentrations up to 10 ppb from various possible sources: calcrete, soil or silcrete; or directly from the saprolite and groundwater via deep roots. Hydraulic redistribution of Au from the aforementioned sources and into the soil horizons, is a suggested mechanism for the generation of elevated surface Au contents over mineralisation (Lintern 2007), and is a plausible mechanism for the area of elevated Au in calcrete at Tomahawk.

Capillary rise of saline groundwater with low concentrations of dissolved Au (Gray & Pirlo 2005) could be up to tens of meters in the kaolinitic saprolite (Wright & Tucker

1991, Keeling 2004) at Tomahawk. A groundwater depth of approximately 34 m coupled with capillary rise has the potential to translocate nutrients to within the reach of deep roots of plants accessing the capillary fringe. The salt tolerance of black oak (Niknam & McComb 2000) suggests this species could source nutrients from the capillary fringe and facilitate the ascent and accumulation of Au at the surface through a combination of hydraulic redistribution of the pore-water and litter fall and decay.

Evapotranspiration induces the precipitation of Ca from soil waters and Au can co-precipitate with Ca in the process. Subsequently, host sediments are cemented along with any residing Au, producing calcrete with a coarse-grained internal morphology. Specimens from Tomahawk support this co-precipitation mechanism, as detritus-rich calcrete samples are typically host to a higher Au content. Up to 80% of Au contained in calcrete has been reported to be water soluble (Gray & Lintern 1998, Lintern *et al.* 2001) and is an equitable local source of Au for plant uptake.

Expression of mineralisation

In calcrete and plants, Au concentration best expresses Au mineralisation at Tomahawk, although the % difference error for Au between sub-sample splits of these materials is high. Plants express Au mineralisation at Tomahawk as sporadic, high contrast elevated Au concentrations that have a sharp transition falling to below background levels (< 0.5 ppb). By comparison, Au in calcrete concentrations are more levelled and gradational and are typically > 20 ppb across Tomahawk.

Possible geochemical pathfinder elements for Au, as outlined by Dunn (2007, p. 254), and associated with mineralisation across other areas of Tunkillia include: Ag, Pb and As, Hg, Sb, and Bi. However, the abundance of these elements in calcrete and plants appear to have negligible association with underlying Au mineralisation at Tomahawk. Elements that correlate with elevated Au in calcrete and plant samples are Pb, and Y, La, Ce, Hg respectively. The associations of these elements with Au are weak in both materials, but are particularly supportive for the subtle Au responses in biogeochemical data. In this situation, a full multi-element geochemical analysis of calcrete appears to have no advantage over the conventional Au and base metal element suite used by mineral explorers.

Drill testing of an exploration target identified by a plant sample with a high Au content (10 ppb) revealed primary mineralisation at depths greater than 72 m (Belperio 2010). Detailed data from drilling at this particular location are not available for the compilation of the map in Figures 5.90 and 5.13. However, Au at such a great depth, and in unweathered basement, is unlikely to have significantly contributed to the elevated surface result. This requires further testing, and could include further drilling at several other sample points (calcrete and plants) that have elevated Au in calcrete and plant samples (e.g., 3.8 and 1.6 ppb in Figure 5.13). Based on the previous reported biogeochemical success (Belperio 2010), these sample points would be highly-ranked drilling targets.

Regular 50 m sample spacing is achievable for black oak and Victoria Desert mallee at Tomahawk and provides a homogenous data distribution in comparison to the more irregularly available calcrete in dune swales. Biogeochemical data at this spacing are highly variable for low concentrations of Au but have been useful for defining exploration targets (Belperio 2010). A wider sampling interval (e.g., 100 – 200 m) would be suitable for regional exploration to detect elevated Au in plants (≥ 0.5 ppb) but would likely miss the sporadic high Au results that overlie mineralisation (Figure 5.13). Calcrete data have a heterogeneous distribution when compared to plants, and sample collection by hand at regular 50 m intervals is typically not achievable due to burial by transported regolith materials. To maintain a 50 m calcrete sample spacing at Tomahawk, a different method of sample collection (e.g., auger) is required. The distribution of elevated Au in calcrete, despite irregular sample spacing, is more levelled than that of plants.

5.2.3. Conclusion

Surface dispersion of regolith material and geochemistry at Tomahawk is significant but more limited than previously thought (e.g., Dart 2009, Klingberg 2009, 2010). A sheltered palaeo-landscape setting with limited through flow, and vertical redistribution of Au from depth has generated an area of elevated Au in calcrete. Calcrete and plant sampling programs have successfully expressed Au at depth regardless of the local regolith-landform mapping unit, but elevated Au concentrations are not a certainty of underlying mineralisation. Calcrete sampling has proven to be a successful first pass exploration technique and is attributable to the discovery of mineralisation at Tunkillia (Martin 1997). Calcrete can with, minimal pre-analysis sample preparation, define a broad target (Au > 20 ppb) for further exploration. Plant sampling and biogeochemical analysis, which requires some level of systematic species sampling, is suitable as a first-pass regional Au exploration tool, and is able to produce targets over Au mineralisation at significant depth (> 40 m). Both sample materials have strengths and weaknesses such as widespread sample availability (plants) and broad elevated Au results (calcrete). These individual weaknesses can be overcome by integrating calcrete and plant sampling in exploration programs and can result in the identification of prospective areas and produce valid follow-up drill targets.

5.3. Biogeochemistry of the eastern Tunkillia Au Prospect

5.3.1. Geological and landscape setting

The eastern part of the Tunkillia Au Prospect contains Area-191 and Tomahawk prospects. These prospects were identified through geochemical sampling of calcrete. The area is characterised by 8 km² of > 10 ppb, and up to 200 ppb, Au-in-calcrete concentrations (Figure 5.14). Area-191 geology and mineralisation are well constrained. High grades of Au and sericite and chlorite alteration are reported in the area (Figure 5.4; DMITRE 2006a). Mineralisation at Tomahawk is generally low with narrow zones of high Au grades (DMITRE 2006b). The area of Au-in-calcrete concentrations > 10 ppb at Tomahawk are contained within a broad area of drainage towards the NNE (1% gradient; Figure 5.14) and was the subject of a calcrete reanalysis study by Klingberg (2009, 2010).

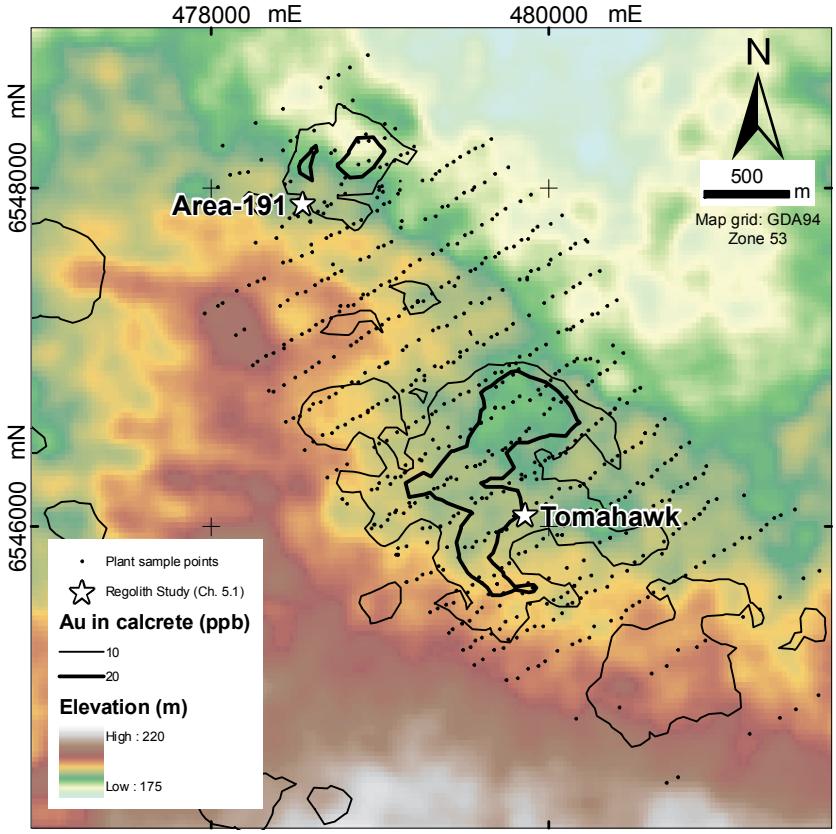

Figure 5.14: Biogeochemical sample points at the eastern part of the Tunkillia Prospect, calcrete geochemistry (25 by 100 m sample spacing), overlain on 1-second (30 m) SRTM digital elevation model (Slater *et al.* 2006). Calcrete contours produced from geochemical data (Minotaur Exploration Ltd.)

Previous work

A regional-scale drainage model proposed by Dart (2009)[4] highlights the topographic controls on the northward dispersion of auriferous sediment from the Area-223 deposit (Figure 4.1) whereas at Tomahawk the northward transport of auriferous sediments is

[4] Regional drainage model is derived from the 3-second (90 m) digital elevation model displayed with 10 m elevation intervals, Landsat TM imagery, and regional calcrete geochemistry.

more constricted. Klingberg (2009) geochemically analysed 98 calcrete samples and discussed the results in the context of local regolith-landform setting (e.g., Klingberg 2010), and Dart's (2009) regional drainage model. The DEM with 10 m elevation intervals has poor resolution at the scale of Tomahawk. Contoured calcrete geochemical data (25 by 100 m intervals) are well-aligned with drainage depressions on the 1-second (30 m) SRTM digital elevation model (Figure 5.14) meaning that there may have been some sampling bias. It is evident from the airborne electromagnetic surveys that palaeo-drainage are poorly defined in the eastern part of the Tunkillia Au Prospect (Figure 5.15). Results from the initial plant biogeochemical and calcrete geochemical studies from the Tomahawk prospect and their inter-relationships are discussed in Section 5.2.

Tunkillia study: Area-191 and Tomahawk

In-fill biogeochemical sampling with a spacing of 50 m by 200 m has been conducted over the eastern part of Tunkillia Au Prospect at Area-191 and surrounding the initial Tomahawk survey (Figure 5.1). Biogeochemical data from a total of 662 samples consisting of two dominant species are discussed in this section: branchlets from 455 black oak, and leaves from 207 Victoria Desert mallee. Biogeochemical data were measured from samples collected from Area-191 and Tomahawk prospects in alignment with existing drill traverses and provide a wider spatial context for the initial Tomahawk biogeochemical data (Figure 5.1). Calcrete geochemical data (Au only) discussed in this section are from Minotaur Exploration Ltd. (collected from between 1996 – 1998).

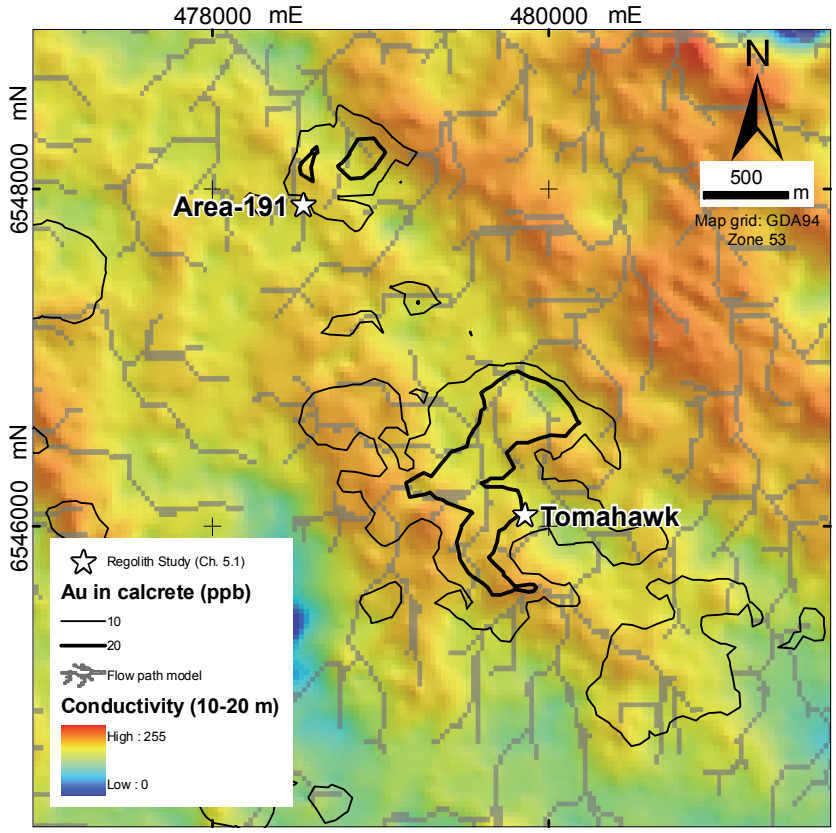

Figure 5.15: Au-in-calcrete anomaly of the eastern part of the Tunkillia Prospect. Flow paths modelled from the 1-second DEM are overlain on the 10-20 m depth slice of the airborne electromagnetic (AEM) data. Calcrete and AEM data are from Minotaur Exploration Ltd.

5.3.2. Biogeochemistry

Black oak branchlet and Victoria Desert mallee leaf samples contain similar concentrations of Au (Figure 5.16). Black oak samples generally have higher concentrations of Ca, Pb, Rb and Te.

Gold distribution

Plant samples have between 0.2 – 10 ppb Au but typically have < 1.6 ppb Au (95 percentile; Figure 5.16). Higher Au results align with the elevated Au in calcrete (> 10 ppb Au; Figure 5.17). Samples with 0.41 – 1.2 ppb Au are generally adjacent to higher Au in plant results (e.g., 1.3 – 2.8 ppb), but also form isolated occurrences, particularly to the south of Area-191 and on the NE margin of the survey area where Au concentrations are < 0.2 – 0.4 ppb (Figure 5.17). The highest Au concentrations are from Tomahawk (10 and 6.4 ppb; Section 5.2) and around Area-191 (up to 4.3 ppb). The elevated Au concentrations are from both plant species: Victoria Desert mallee leaves, however, on average contain slightly higher concentrations of Au than black oak (Figure 5.16).

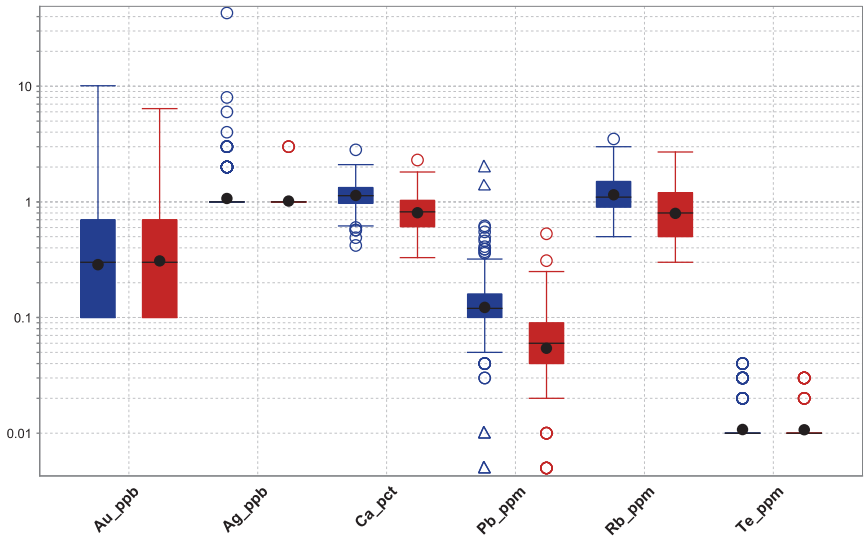

Figure 5.16: Box plot split by black oak (blue) and Victoria Desert mallee (red). Outliers represented by circles and triangles that are more than 1.5*(Q_3-Q_1) and 3.0*(Q_3-Q_1) from the box.

Other elements

Elements that are geochemically characteristic of mineralisation and alteration at Area-223 are Au, Ag, Pb and Rb. Lead is weakly correlated with Au (R=0.3) in Victoria Desert mallee leaves and Zr and light REEs (R=0.2) in black oak branchlets. Lead results have minimal relationship with lithology. Rubidium has a good correlation with K (R > 0.7), an essential plant nutrient. Rubidium and K concentrations are slightly higher in black oak (Figure 5.16) that typically colonise dune swales. There is no relationship between Rb or K with the lithology or drainage trends.

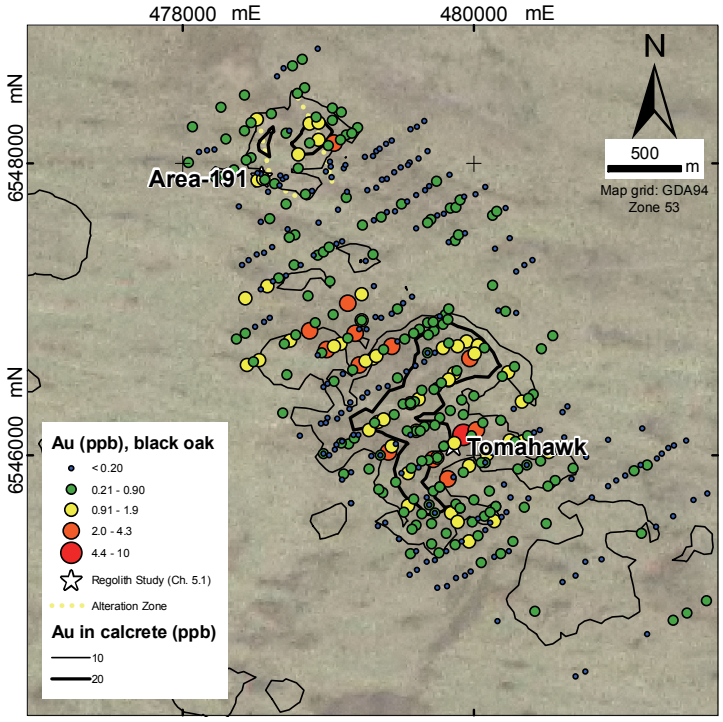

Figure 5.17: Au in black oak branchlets over the eastern part of the Tunkillia Prospect on Landsat TM image.

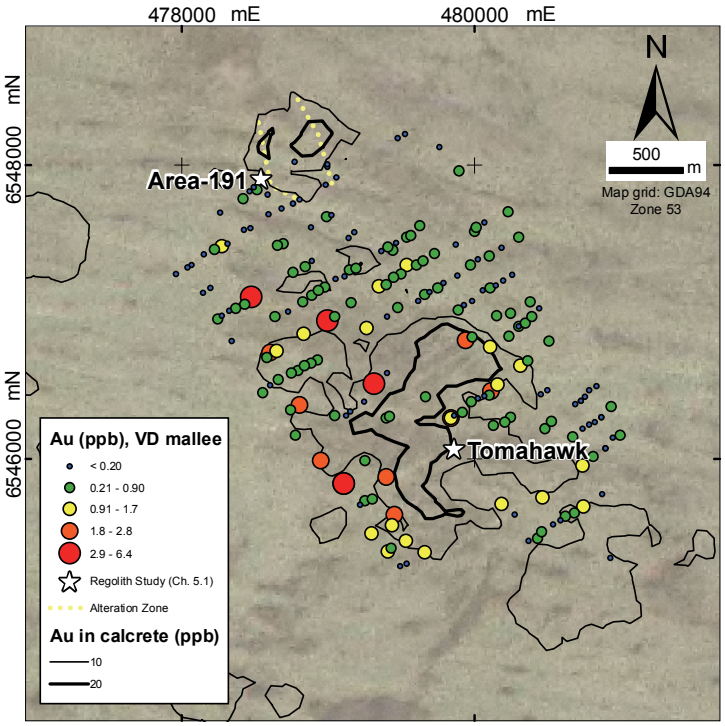

Figure 5.18: Au in Victoria Desert (VD) mallee leaves over the eastern part of the Tunkillia Prospect on Landsat TM image.

Silver concentrations in branchlets and leaves are between 1 – 43 ppb but are typically < 2 ppb (95 percentile; Figure 5.19). A total of 37 samples have ≥ 2 ppb Ag. Of these samples, 34 are black oak. Silver concentrations are between 2 – 4 ppb at Area-191 and 2 – 43 ppb at Tomahawk (Figure 5.19). The highest Ag result is from a depositional area at Tomahawk with Au-in-calcrete concentrations > 150 ppb Au (arrow in Figure 5.19). A group of samples with Ag between 2 – 4 ppb are from the southern tip of the Au-in-calcrete anomaly (Figure 5.19). Some low grade mineralisation (< 0.5 ppm Au) is known

to exist 200 m to the SE. These results are near the southern extent of the biogeochemical survey area and exploration drilling.

Tellurium concentrations in plants are below the analytical detection limit (< 0.02 ppm) in 93% of samples. A group of black oak samples to the south of Tomahawk contain up to 0.04 ppm Te (Figure 5.20). Central alteration zone and mafic dykes have been interpreted from drilling in this area to be as shallow as 20 m and 30 m. There is little relationship of Te results to lithology or other elements.

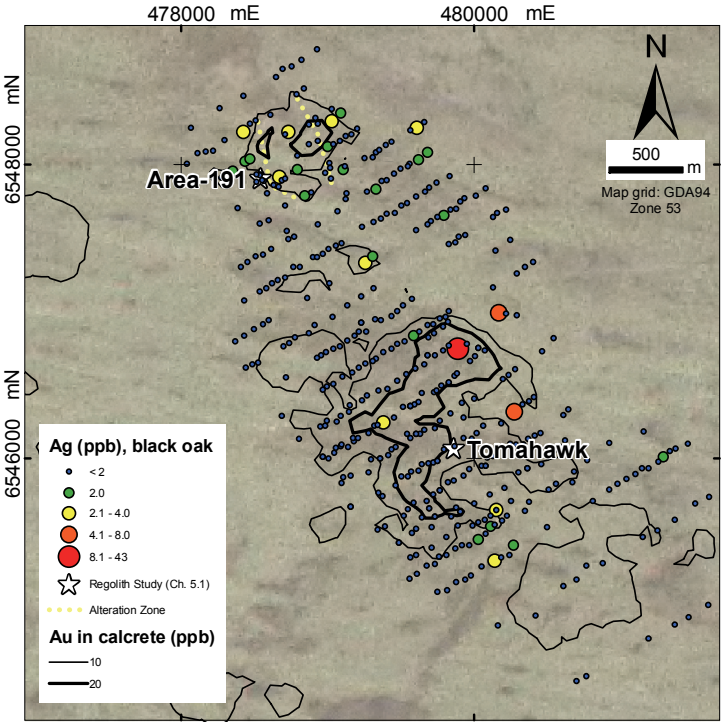

Figure 5.19: Ag in black oak branchlets over the eastern part of the Tunkillia Prospect on Landsat TM image.

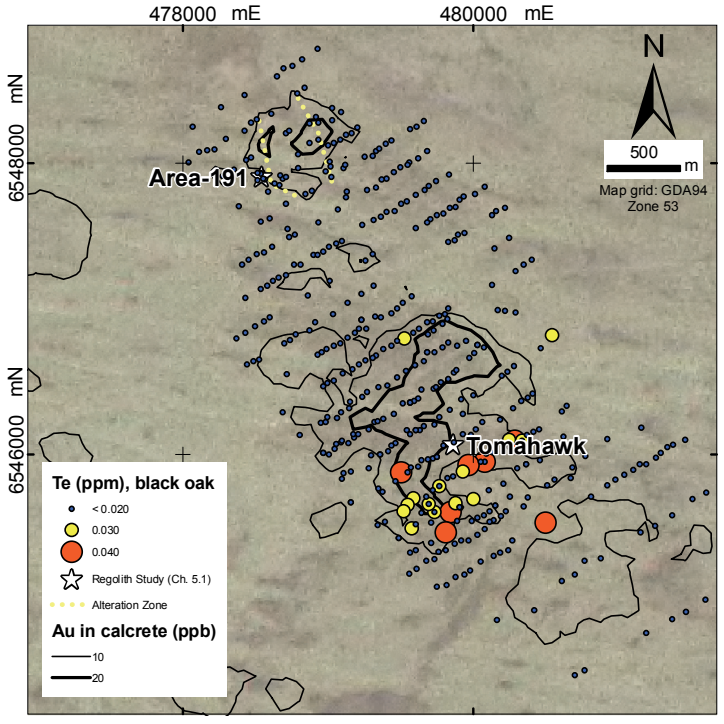

Figure 5.20: Te in black oak branchlets over the eastern part of the Tunkillia Prospect on Landsat TM image.

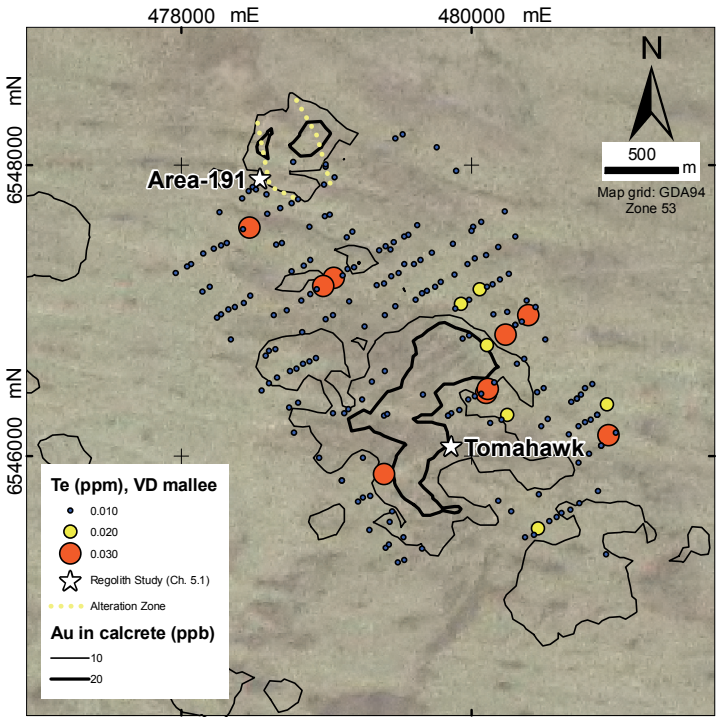

Figure 5.21: Te in Victoria Desert (VD) mallee leaves over the eastern part of the Tunkillia Prospect on Landsat TM image.

5.3.3. Discussion

Rubidium and Pb are geochemical pathfinders for alteration and sulphide mineralisation in the saprolite at the Tunkillia Au Prospect. Rubidium and Pb concentrations are well above analytical detection limits in biogeochemical samples. High concentrations appear erratic and are not indicative of known mineralisation or lithology. White mica is resistant during weathering (McQueen 2009). The higher concentrations of Rb associated with Area-223 are retained in mica whereas Rb in feldspar at Area-191 and Tomahawk is mobilised during early stages of weathering. Rubidium has a good correlation with K in the biogeochemical data. Potassium is an essential plant nutrient and it is therefore likely that the Rb is following this pathway. Lead is also present in feldspar (Scott 2009) and can be relinquished during weathering. Trace quantities of Pb occur naturally in plants (Broyer *et al.* 1972, Dunn 2007).

Area-191

Landscape controls

Area-191 is at the headwaters of the modelled drainage (Figure 5.15) and contained within several broad dune swales. Lateral transport of auriferous sediment into and out of the area has been restricted as indicated by localised high concentrations of Au in calcrete and, Au and Ag in plants (Figure 5.17 & Figure 5.19). Silver is generally mobile in the regolith (e.g., Kabata-Pendias & Pendias 2001, Lintern 2004b, Lintern *et al.* 2011), but the lateral extent of the expression of Area-191 by Ag is smaller than the expression by Au. High concentrations of Au in plants and calcrete are spatially related. Gold in plants > 0.2 ppb provide a wider footprint of Area-191 than that represented by the Au in calcrete. Calcrete sampling is limited to areas of surface exposure or development. It is

therefore possible that the Au-in-calcrete contours are influenced by sampling bias rather than Au from underlying mineralisation.

Transported regolith at Area-191 has up to 120 ppb Au whereas the underlying saprolite typically contains < 5 ppb Au (*Section 5.1*). This suggests that unconsolidated and auriferous regolith has been transported and emplaced over saprolite that has a low Au content. It is possible that plants are sourcing Au from the transported regolith even in areas with low concentrations of Au in calcrete. It is also possible that there has been some lateral transport of auriferous material within the swale corridors to increase the surficial expression of Area-191 mineralisation.

Tomahawk

Landscape controls

High concentrations of Au in calcrete at Tomahawk are constrained within alluvial depressions with headwaters towards the south (Figure 5.15). High Au-in-plant results are generally widespread; however the highest results are associated with locally elevated concentrations of Au in calcrete (Figure 5.17 & Figure 5.18).

High Te concentrations in black oak branchlets are restricted to the southern part of the > 20 ppb Au-in-calcrete anomaly near an area of elevated concentrations of Ag in plants (Figure 5.20). Chlorite and sericite alteration, and mafic dykes have been interpreted in this area as shallow as 20 m. These lithologies are typically deep (> 100 m) and the Te and Ag in plants results are inconsistent and therefore not reliable indicators. Leaf samples from nine Victoria Desert mallee plants contain detectable concentrations of Te, and are irregularly distributed. Standards used during biogeochemical analysis contain < 0.02 ppm Te (detection limit). It is unlikely the Victoria Desert mallee Te results are caused by analytical tailing but instead, could be an analytical artefact (Figure 6.8; Dunn 2007, p.308), or some natural other control.

Silver is recognised as a relatively mobile element in the regolith environment (e.g., Kabata-Pendias & Pendias 2001, Lintern 2004b, Lintern *et al.* 2011). Silver concentrations are below the analytical detection limit (100 ppb) in the transported regolith at Tunkillia (Klingberg 2009; Section 5.1). Lower Ag detection limits in biogeochemical material (2 ppb) allow for greater detection. Silver results > 2 ppb are typically from black oak branchlets collected from dune swales. The highest concentration of Ag in plants at Tomahawk (43 ppb) is from the most down-slope part of the central > 20 ppb Au-in-calcrete anomaly. Gold in calcrete at this point is also amongst the highest at the Tunkillia Au Prospect. There is minimal known underlying mineralisation at Tomahawk. It is possible that the plants are providing a response to Ag that has been laterally transported by hydromorphic processes or mechanically within sediments. Mobile elements such as K and Zn that are typically geochemically associated with alluvial landforms, do not show any discernible trends in the plant biogeochemistry, probably due to their status as essential plant nutrients and the species distribution (e.g., black oak colonise alluvial landforms).

Exploration

Exploration drilling to the south of Area-191 is focussed on the zone of > 20 ppb Au in calcrete at Tomahawk. Geochemical data is typically from the base of weathering (40 m). Gold concentrations are generally low grade although there are some high-grade intersections (DMITRE 2006b). Gold concentrations are up to 90 ppb (or 200 ppb Au-in-calcrete; Klingberg 2009) in the transported regolith and < 10 ppb in the underlying saprolite. Silver is below detection limit (< 100 ppb) throughout the regolith profile (0 – 50 m; *Section 5.1*) and calcrete (Klingberg 2009).

Implications for exploration

Geology and mineralisation at Area-191 is reasonably constrained. The mineralised zone is approximately 150 by 400 m (DMITRE 2006a), and is characterised by high concentrations of Au and Ag in plants and Au in calcrete. Digital elevation models indicate the transport vectors from Area-191 are to the NE but regional calcrete geochemistry indicates lateral dispersion is minimal (Figure 5.15). Plant biogeochemistry at Area-191 corroborates the findings from the initial biogeochemical study by Lowrey (2007), but also provide a broader spatial context. Biogeochemical sampling at Area-191 reiterates the calcrete geochemistry, both of which provide a response derived from underlying mineralisation.

Tomahawk is interpreted as being the SE continuation of alteration and mineralisation zone from Area-191 (DMITRE 2006a). Some narrow mineralised veins have been discovered at depth at Tomahawk. Geochemical data for the upper saprolite is seldom measured, although the available data indicates that Au concentrations are typically low. A shallow source of Au for inclusion into calcrete is yet to be determined. The Au-in-calcrete anomaly is contained within a NE drainage depression yet the area up-slope to the south is largely underexplored by drilling and regolith methods. Digital elevation models and biogeochemical sampling results (particularly Ag) are suggestive of mineralisation to the south. Encouragingly, sericite and/or chlorite alteration and low grade mineralisation (< 0.5 ppb Au) feature in some of the southern-most drill logs. The logs are non-specific and use ‘pallid zone’ and ‘weathered basement’ to describe the regolith. It is recommended that area to the south of Tomahawk is re-evaluated beginning with mineralogical and geochemical analysis of existing drill cuttings using methods described in *Section 5.1*.

5.4. Biogeochemistry of the Centurion target (north of Area-223)

5.4.1. Landscape and geological setting

The Centurion exploration target is 1.5 km NW of Area-223 and was the subject of a biogeochemical study by Ames (2010; Figure 5.1). Centurion is contained within regional palaeo-drainage that is attributable to the northward transport of auriferous sediment from Area-223 (Figure 4.1) and it is probable that some of the auriferous calcrete at Centurion is derived from mineralisation at Area-223. Drilling at Centurion prior to the biogeochemical study has defined a zone of sericite and chlorite alteration that is interpreted to be the continuation of the central alteration zone at Area-223 (Figure 5.22). Aeromagnetic imagery reveals the structural complexity in the basement geology at Centurion (Figure 5.22). Gold mineralisation has been defined from drilling but is generally low grade (< 0.1 ppm Au) although narrow zones grade above 1 ppm and even 10 ppm at depths greater than 50 m (Belperio 2009a; Figure 4.4). Drilling in this area has been more limited, particularly to the west of the central alteration zone and outside the regional Au-in-calcrete anomaly.

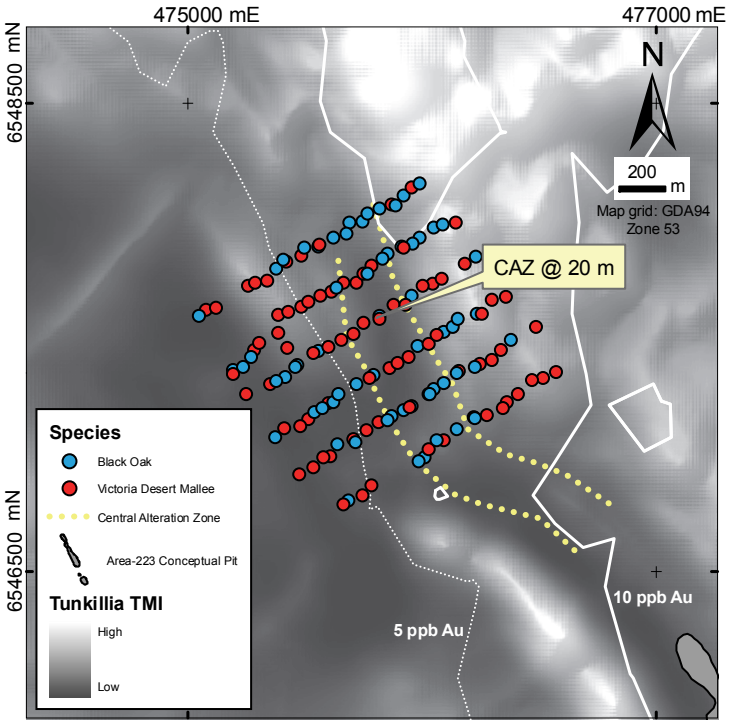

Figure 5.22: Centurion biogeochemical survey area marked on the local aeromagnetic image (geophysical data are from Minotaur Exploration Ltd.).

Previous work

Biogeochemical sampling over Centurion was conducted by Ames (2010). The results and discussion were focussed on Au, Ag, As, B, Ca, Ce, Cu, Fe, Hg Mo, Pb, Se, and Zn and were interpreted in the context of a regolith landform unit (RLU) map derived from field observations and Google Earth™ imagery (Ames 2010). The study makes no use of existing regional datasets (calcrete geochemistry and SRTM digital elevation model), or relevant literature (e.g., Gibbons 1997, Dart 2009, Klingberg 2009) and therefore does not

acknowledge that Centurion is contained within the northward palaeo-drainage from Area-223 or that there is some underlying mineralisation (e.g., Belperio 2009a).

Centurion study

The biogeochemical data from Ames (2010) are re-evaluated with an improved understanding of the regolith geochemistry at the Tunkillia Au Prospect (*Sections 5.1 – 5.3*). This section uses regional and local datasets that were either not utilised or not available prior to this study. Biogeochemical data from two dominant species are discussed in this section: 65 black oak branchlets, and 80 Victoria Desert mallee leaves. These species are identical to the species discussed from the eastern part of the Tunkillia Au Prospect (*Section 5.3*). Data for elements associated with mineralisation at the eastern part of the prospect are used for discussion in this section. Calcrete data are from the regional dataset (South Australian Resources Information Geo-server 2012).

5.4.2. Biogeochemical results

Black oak branchlet and Victoria Desert mallee leaf samples contain similar concentrations of Au, As, and Zn (Figure 5.23). Black oak samples have higher concentrations (on average) of Pb, Ca, Fe, La and Ce, although Ce and La have a higher range of concentrations in Victoria Desert mallee samples (Figure 5.23). Nickel concentrations are slightly higher in Victoria Desert mallee samples, although both species have a similar range of concentrations.

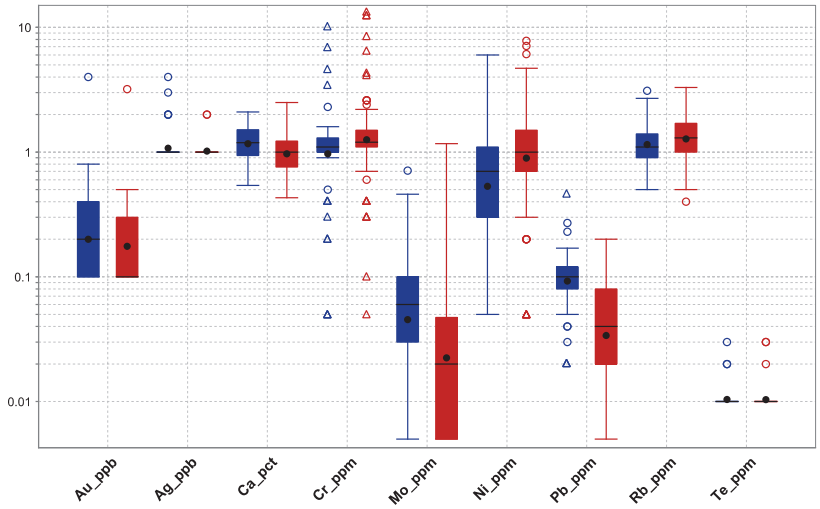

Figure 5.23: Box plot split by black oak (blue) and Victoria Desert mallee (red) at Centurion. Outliers are represented by circles and triangles that are more than 1.5*(Q_3-Q_1) and 3.0*(Q_3-Q_1) from the box. The highest 190 ppb Ag result (black oak) is removed to de-skew the Y-axis.

Gold and gold-associated elements

Plant samples have between 0.2 – 0.8 ppb Au with two outliers of 3.2 ppb Au in Victoria Desert mallee leaves and 4 ppb Au in black oak branchlets (Figure 5.23), which are within the area of > 10 ppb Au in calcrete (NE corner, Figure 5.24). Plant samples from the Au-in-calcrete anomaly (> 5 ppb) generally contain > 0.2 ppb Au (detection limit; Figure 5.24). A group of samples with 0.2 – 0.5 ppb Au lie outside the 5 ppb Au-in-calcrete contour in an area not explored by drilling (black ellipse, Figure 5.24).

Detectable concentrations of Ag (> 0.2 ppb) are measured in six black oak and two Victoria Desert mallee samples. The highest Ag concentration (190 ppb) is a black oak sample from the same area as the high Au-in-plant and Au-in-calcrete results (Figures 5.24 & 5.25). Plant samples that have high concentrations of Au or Ag are from within the regional Au-in-calcrete anomaly (> 5 ppb; Figures 5.24 & 5.25).

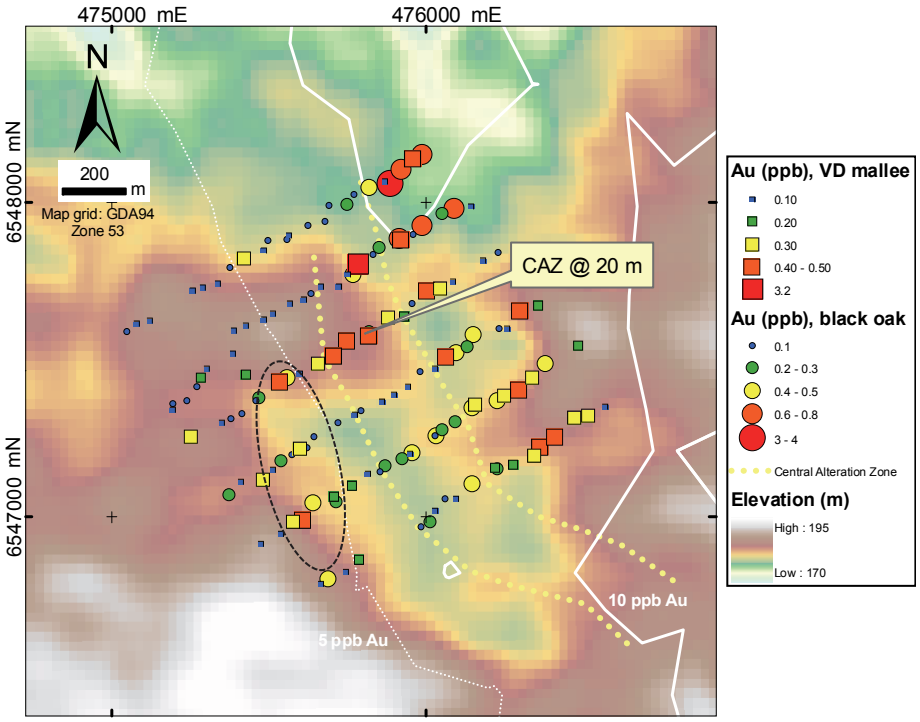

Figure 5.24: Au in plants at Centurion, and Au-in-calcrete data (SARIG) on the 1-second digital elevation model. Shallowest occurrence of the central alteration zone (CAZ) is marked.

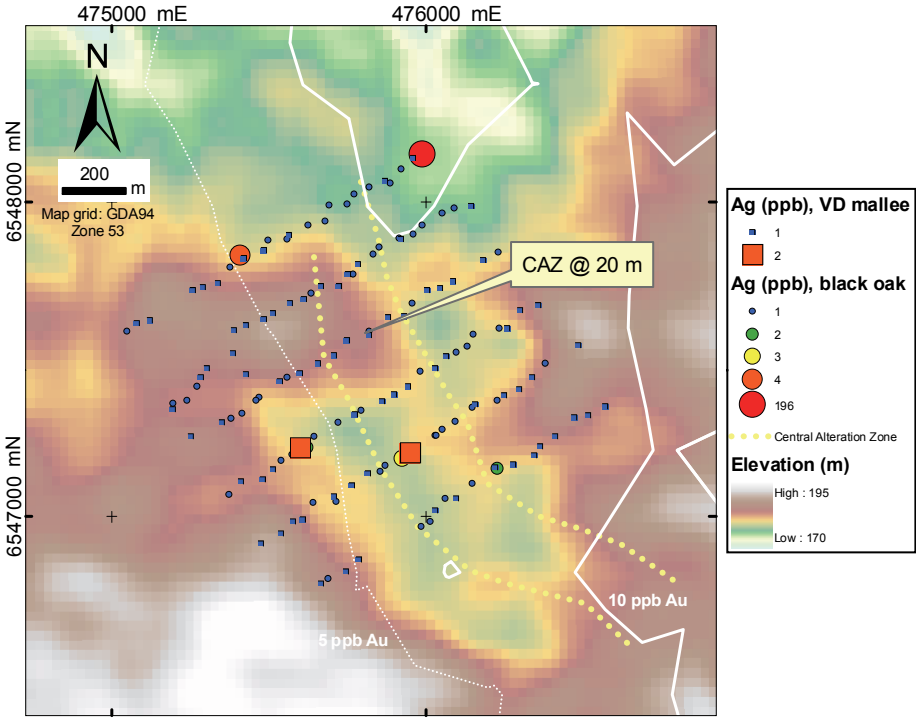

Figure 5.25: Ag in plants at Centurion, and Au-in-calcrete data (SARIG) on the 1-second digital elevation model. Shallowest occurrence of the central alteration zone (CAZ) is marked.

Other elements

Nickel has a strong positive correlation with Cr (R=0.9) and Mo (R=0.85). High Mo and Ni results have a similar distribution (Figures 5.26 & 5.27). High Ni concentrations in plants are best aligned with the central alteration zone where it is closest to the surface (from drill logs; Figures 5.27), whereas Mo provides a broader expression (Figure 5.26). North and south of this locally shallow alteration zone, the depth of the pallid zone increases and the central alteration zone is recorded at a greater depth. Figure 5.26 shows elevated concentrations of Mo over the alteration zone along a structural zone that is represented by low magnetic response in the basement. Molybdenum concentrations immediately drop to background concentrations away from the zones of alteration and low magnetic response. Tellurium concentrations are generally < 0.02 ppm (detection limit). Six samples (not in sequence) contain 0.02 – 0.03 ppm Te (Figure 5.28). The elevated Te results more closely follow drainage from the south.

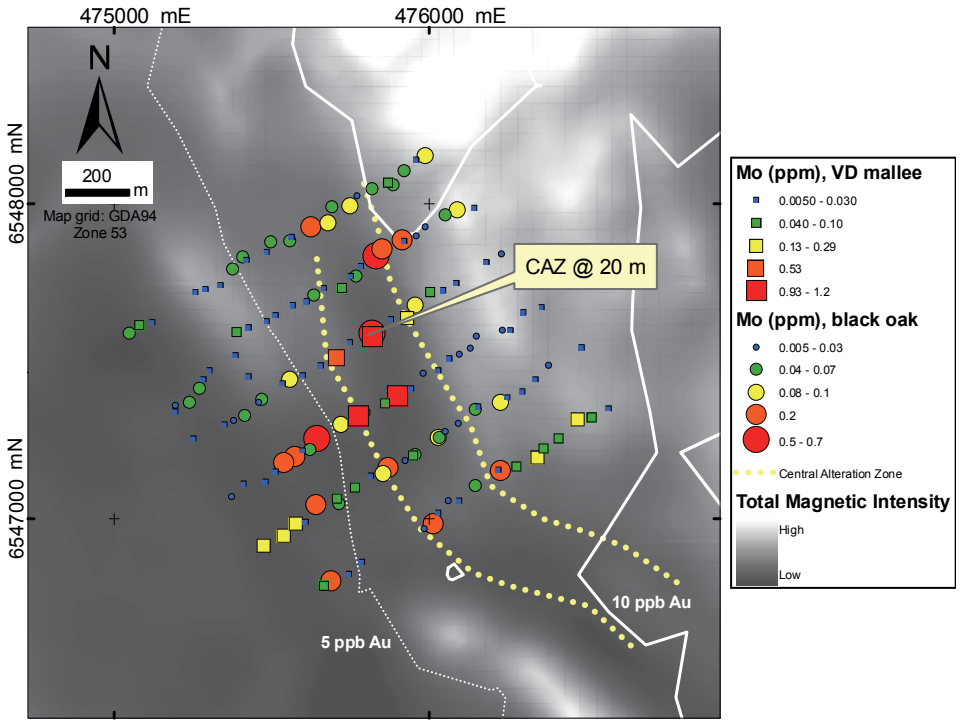

Figure 5.26: Mo in plants at Centurion, Au-in-calcrete data (SARIG). Magnetic data are from Minotaur Exploration Ltd. Shallowest occurrence of the central alteration zone (CAZ) is marked.

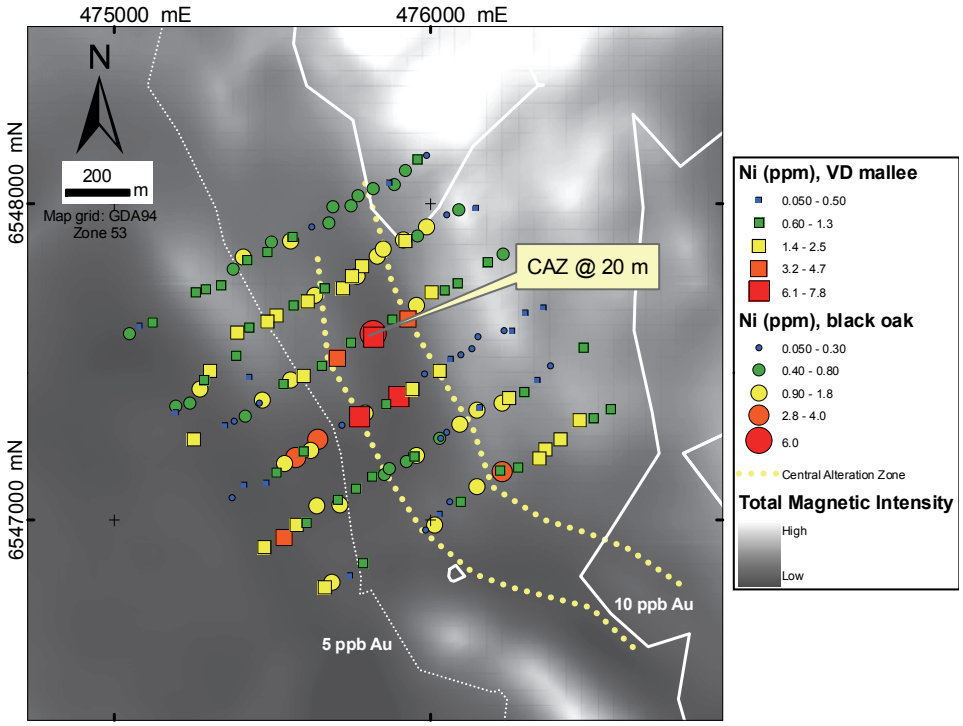

Figure 5.27: Ni in plants at Centurion, and Au-in-calcrete data (SARIG). Magnetic data are from Minotaur Exploration Ltd. Shallowest occurrence of the central alteration zone (CAZ) is marked.

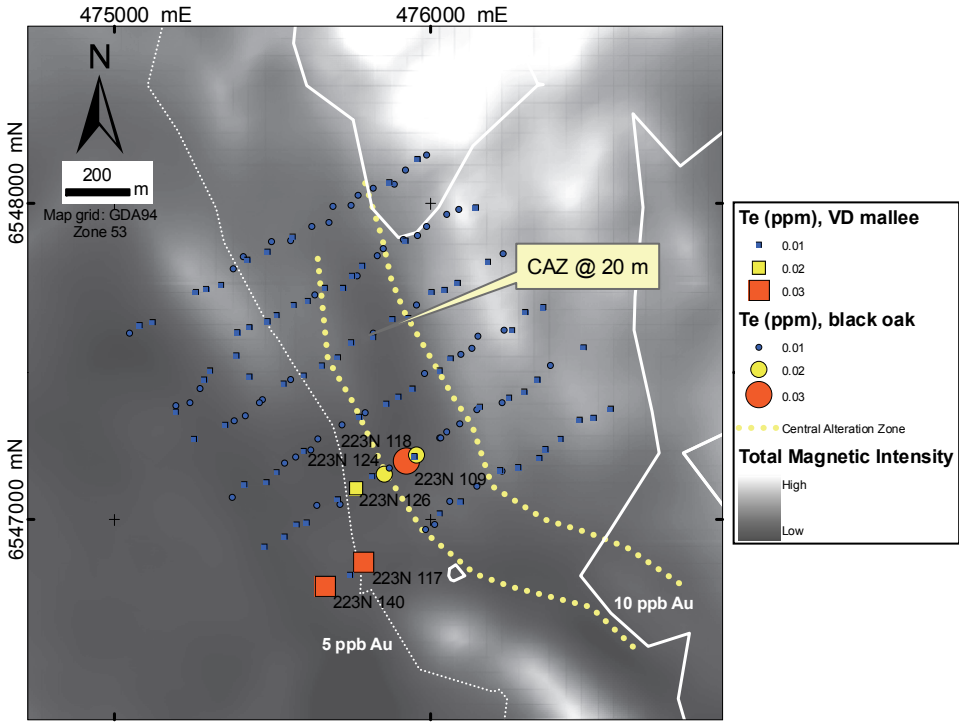

Figure 5.28: Te in plants at Centurion, Au-in-calcrete data (SARIG). Magnetic data are from Minotaur Exploration Ltd. Shallowest occurrence of the central alteration zone (CAZ) is marked.

5.4.3. Discussion

Landscape controls

The Centurion biogeochemical survey is along strike, and down-slope of Area-223 mineralisation (Figure 4.2) within the NW palaeo-channel that is host to transported auriferous sediments (Figure 6.2; Gibbons 1997, Dart 2009). Gold-in-plant results are

highest down-slope within the zone of > 10 ppb Au-in-calcrete, and are generally above analytical detection limit (0.2 ppb) from the zone of > 5 ppb Au-in-calcrete (Figure 5.24). The position of Centurion down-slope of Area-223 mineralisation and alignment of high concentrations of Au in plants and calcrete is strongly suggestive that the plants are expressing Au from a transported source. This is further supported by Ag, an element that is readily mobilised in the regolith (Lintern 2004b, Lintern *et al.* 2011). Although Ag concentrations are generally close to detection limit, the highest Ag and Au results are aligned (Figure 5.25).

Detectable concentrations of Te clustered at the south of survey are not in numbered sequence (Figure 5.28), suggesting this is not a case of analytical tailing following the analysis of a standard. The samples are from within local drainage towards the north – a similar pattern of detectable Te in the headwaters is seen at Tomahawk. At Tomahawk however, the Te is associated with Ag and Au, and is suggestive of mineralisation upslope. Figure 5.29 indicates, by conductive sediments, that there is a possibility of physical and/or hydromorphic Te transport into Centurion from the south. This line of drainage, however, cannot be linked to a source of mineralisation.

Nickel and Cr concentrations are higher in the transported regolith than in the residual regolith, although Mo concentrations are similar (*Section 5.1*). There is no obvious topographic control (including regolith conductivity) on the distribution of samples with higher concentrations of Ni, Cr and Mo.

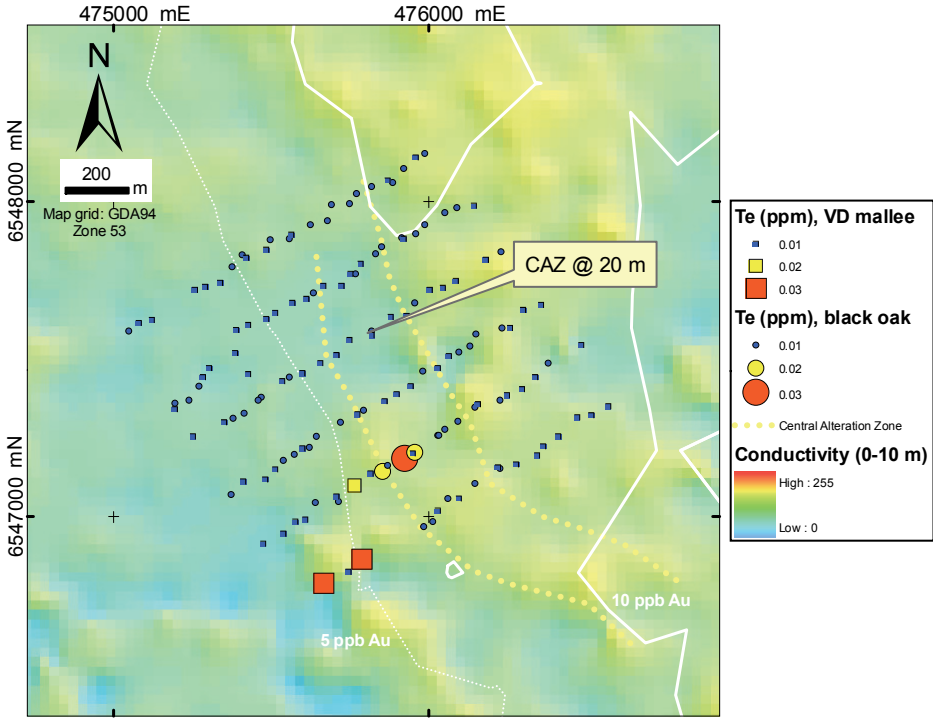

Figure 5.29: Tellurium in plants at Centurion, Au-in-calcrete data (SARIG), overlain on the airborne electromagnetic survey 0-10 m depth slice (from Minotaur Exploration Ltd.). Shallowest occurrence of the central alteration zone (CAZ) is marked.

Lithological controls

Nickel, Cr, and Mo have a good correlation and are all in highest concentrations where the central alteration zone is most shallow. The elevated concentrations appear to follow a region of basement with a low magnetic response. Drilling to the west of the central alteration zone at Centurion is limited and the geology or mineralisation is poorly constrained. Significant Te results are probably too few and too close to the analytical detection limit to fully interpret, although they suggest that the highest mineralisation potential is in the southern part of Centurion toward Area-223. Tellurium results may also be related to lithology but they more closely follow drainage. The AEM data is consistent with transport from the south. Interpretation is limited by the low concentrations of Te and the edge of the survey.

5.4.4. Conclusion

A review of the regional calcrete and elevation data, and drill logs indicates the regolith at Centurion is transported from the south. Gold and Ag in biogeochemical samples reiterate the zone of high Au-in-calcrete results (> 10 ppb). Nickel, Cr, and Mo, do not follow the same lateral physical or hydromorphic dispersion as Au or Ag. Instead, elevated Ni, Cr, and Mo results highlight shallow occurrence of the central alteration zone and follow basement structure. Elevated Ni, Cr, Mo, and Te results to the west of the central alteration zone are in an area not explored by drilling (see Appendix B for drilling pattern) and would suit further investigation.

5.5. Tomahawk calcrete at the microscopic scale

5.5.1. Rationale

Section 5.3 discusses the landscape control on sediment transport pathways into the Tomahawk area from the south, and illustrates how the high Au concentrations in calcrete are distributed within the landscape. This is supported by the minimal mineralisation that has been discovered underlying this anomalous Au-in-calcrete zone. Biogeochemical sampling results (*Section 5.3*) further support the notion that the surface geochemical expression of mineralisation has been laterally transported (e.g., Klingberg 2009). The physical relationship of Au within the calcrete at the microscopic scale, and what this means for the mode of Au transport in the landscape is investigated.

5.5.2. Samples

Polished sections were constructed from two calcrete samples collected as part of a study by Klingberg (2009) from locations identified as having high concentrations of Au in calcrete up to 194 ppb Au (Figure 5.30). Sample THKLK033 is from a sand plain (479600 mE, 6546380 mN, GDA94 zone 53) with a recorded 194 ppb Au, whereas sample THKLK075 is from a drainage depression (480300 mE, 6546110 mN, GDA94 zone 53) with a recorded 43 ppb Au (Figures 5.30 – 5.31). Element spot analyses (80 µm spot size) along a transect with approximately 500 µm spacing, and element maps were completed using LA-ICP-MS (see *Section 3.4.1* for methods) on the polished calcrete sections to determine Au location and association with morphology and chemistry.

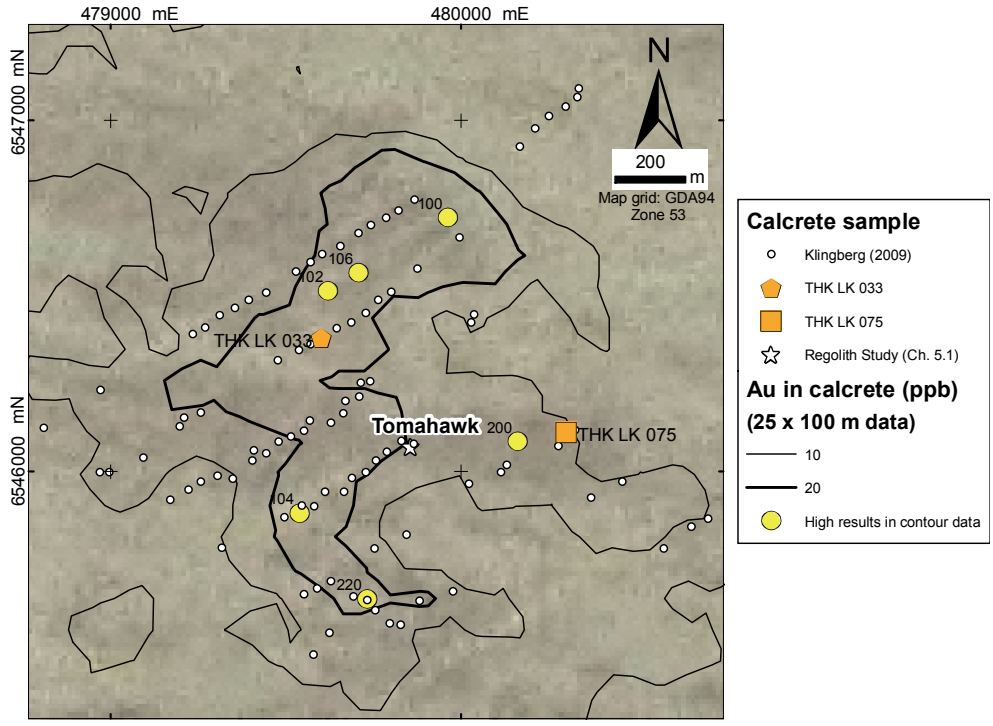

Figure 5.30: Tomahawk indicated by contours of Au-in-calcrete concentrations from samples collected at 25 by 100 m intervals and Au results > 100 ppb (yellow; data are from Minotaur Exploration Ltd.); and THKLK033, THKLK075, and other calcrete sample locations from Klingberg (2009). Background image is Landsat TM.

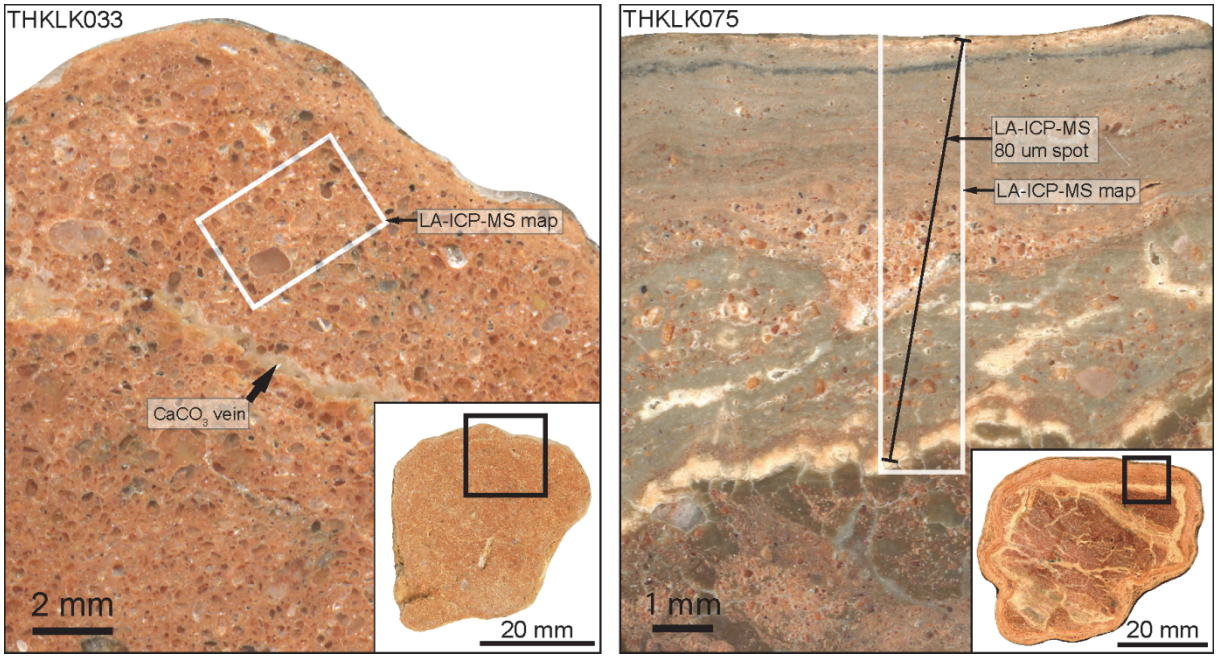

Figure 5.31: 25 mm mounted section of calcrete sample THKLK033 and THKLK075 from the Tomahawk area of elevated Au-in-calcrete. White box shows the area analysed by LA-ICP-MS. The arrow points to a calcite vein that divides the sample.

5.5.3. Laser mapping

Sample THKLK033

Sample THKLK033 consists of matrix-supported, poorly sorted, angular to rounded siliceous sand (Figure 5.31). Veins of pure Ca-carbonate, typically of multiple phases, are present along fractures within the matrix. The matrix is mainly composed of Ca with clay (Al, Fe, K; Figure 5.32). Gold is generally constrained to within the matrix albeit at low concentrations with some higher Au concentrations (> 4X higher) at sand grain boundaries (Figure 5.33). Occasional isolated Au particles appear within mineral grains (arrow, Figure 5.33).

Sample THKLK075

Sample THKLK075 contains three geochemically and visibly different zones: (1) microcrystalline Ca-rich interior with minor lithic fragments, (2) a lens of matrix-supported siliceous sand, similar to that described for THKLK033 above, and (3) exterior laminations of Ca-carbonate and clay minerals (Figures 5.31, 5.34, and 5.35). The sand lens mid-traverse contains the highest concentrations of Au (1.2 – 2.3 ppm), Si (60%) and Cu (48 ppm). Uranium, Ni and Zn are also particularly high in the sand lens (Figure 5.34). In contrast, the microcrystalline interior adjacent to the sand lens is particularly Mg-rich (up to 2%), REE-depleted (compared with the exterior laminations), and contains < 0.1 ppm Au. The exterior laminations contain higher concentrations of Al, Fe, K and REE. A dark band on the sample's periphery has elevated Co (20 ppm), Mn (980 ppm), and Ni (25 ppm; Figure 5.35). LA-ICP-MS mapping along a swath that includes the spot analyses reiterates the findings that the sand lens hosts the highest Au concentrations, and the genetic zones are distinguished by the Mg, REE and clay content (Figure 5.35).

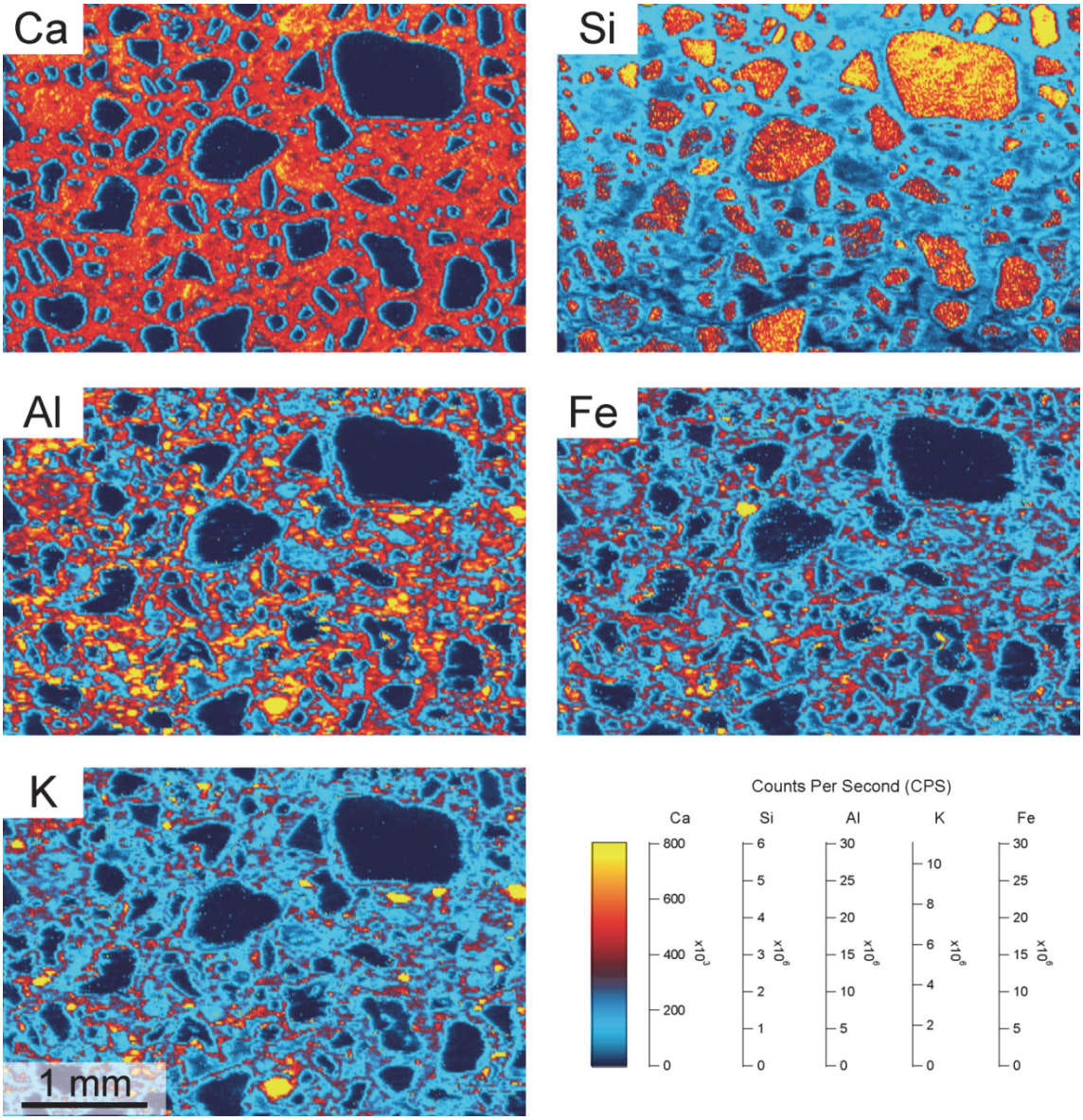

Figure 5.32: Element laser maps of sample THKLK033 from Tomahawk

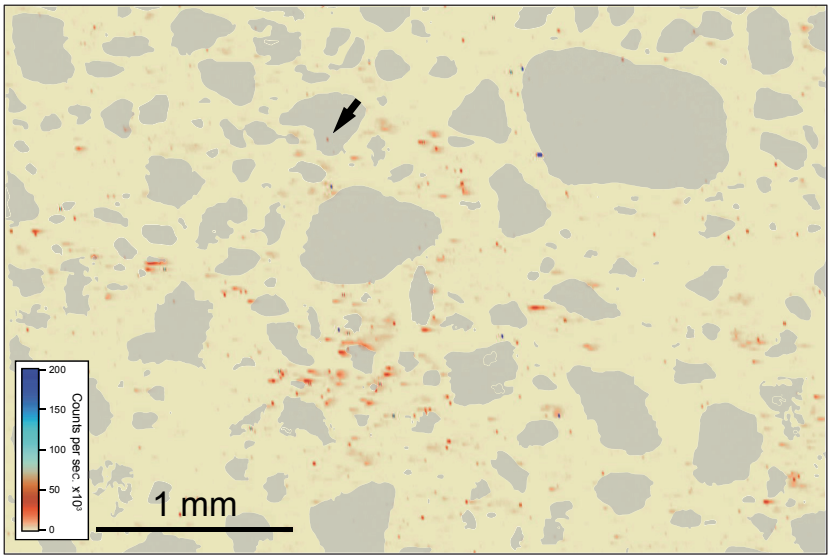

Figure 5.33: Laser map of Au distribution in sample THKLK033 from Tomahawk. A grey underlay highlights the position of sand grains. The arrow indicates elevated Au that appears within a mineral grain.

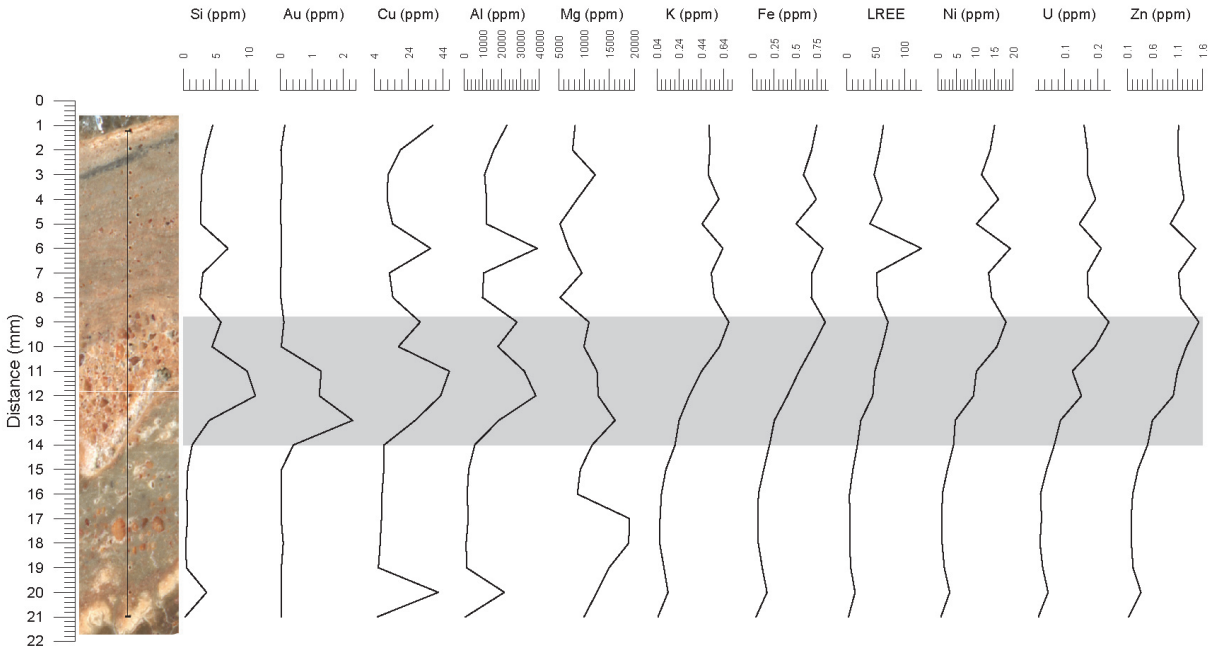

Figure 5.34: Element LA-ICP-MS spot analysis (80 µm) along a traverse at 500 µm-spacing from outer lamination (top) toward core (bottom) of sample THKLK075. Sand lens is indicated in grey.

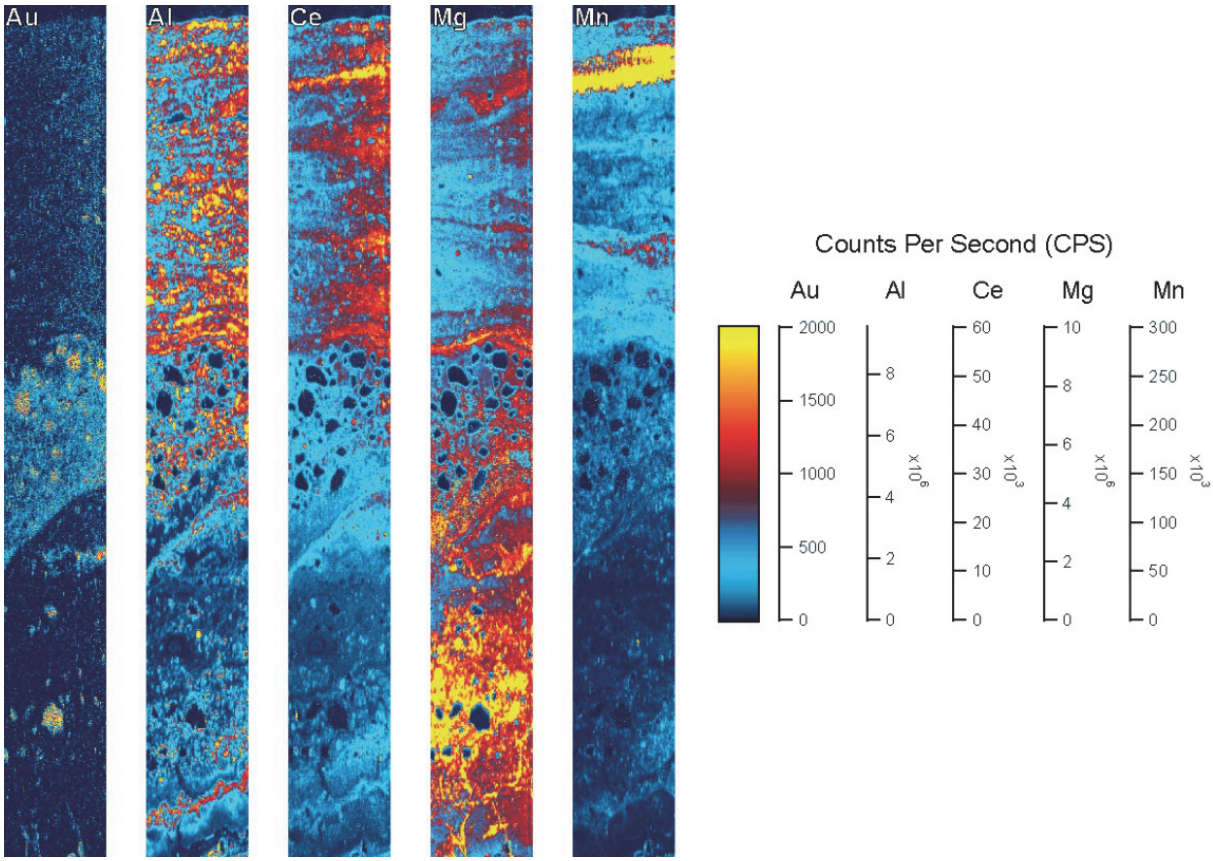

Figure 5.35: Element laser map of sample THKLK075 showing elevated Au in the sand lens, elevated concentrations of Al and Ce in the outer clay-rich laminations, Mg-rich interior, and the band of elevated concentrations of Mn.

5.5.4. Discussion

Model of calcrete formation

The nodular calcrete at Tomahawk has likely formed from two different processes: *in-situ* precipitation of micritic carbonate and/or the breakdown of a more massive calcrete. Sample THKLK075 has variable internal structure that shows authigenic Ca-carbonate cementation is a multi-cyclical process. The nodule has three texturally and geochemically different facies that represent different formation environments, possibly from a change in position within the soil profile. Similar morphologies and mechanisms of formation are reported by Wright and Tucker (1991); Chen (2002b); and, Chen and Roach (2002a). Elevated concentrations of Al, Fe, K, and REE in the outer laminations of TKLK075 possibly represent clay and clay-bound cations derived from the weathering of local granite (see *Section 5.1*). Sample THKLK033 consists of poorly sorted sand that is homogenously distributed throughout the Ca-carbonate matrix. Gold is constrained to the carbonate-clay matrix between sand grains in both samples. Figure 5.33 shows Au as inclusions within mineral grains (indicated by arrow), however, this is possibly material that is translocated from the matrix to the polished mineral grain during sample preparation.

Gold transport model

Gold is associated with the carbonate-clay cement within detrital sand layers in both calcrete samples (Figures 5.33 & 5.35). Gold concentrations are lower in the carbonate-clay matrix that does not contain sand grains (Figure 5.35). The affinity of Au for the coarse sediments suggests that Au is either in particulate form within the sediments and subsequently indurated with Ca-carbonate, or is in solution and is emplaced in the pore space between sand grains during illuviation (or a combination of the two; e.g., Lintern *et al.* 2009).

Three scenarios in producing the Tomahawk Au-in-calcrete anomaly are proposed:

1. Sediments (without Au) are transported north within the drainage system and Au (possibly ionic) that has vertically migrated to the surface from low grade mineralisation (< 0.2 ppm) is accumulated within the sediments and subsequently indurated by Ca-carbonate;
2. Sediments with Au (particulate) are transported north within the drainage system with Au from an up-stream source of mineralisation and are subsequently indurated by Ca-carbonate; and,
3. Calcrete with Au (ionic and/or particulate origin) is transported north within the drainage system with Au from an up-stream source of mineralisation.

At Area-223, for example, there is a prominent palaeo-drainage system controlling the dispersion of auriferous sediments to the north (Figure 6.2; Gibbons 1997, Dart 2009). Gold was incorporated into these sediments and calcrete at the source (Area-223, Centurion and immediately surrounding area) and transported along a well-defined path

as indicated by the digital elevation model and the airborne electromagnetic (AEM) data (Figures 4.1 & 4.2): this follows Scenario 2 and/or 3.

Digital elevation and flow-direction models at Tomahawk indicate local alluvial sediment transport directions are from the south (Figure 5.36): deep palaeo-drainage is not evident from the AEM in the immediate area, although it does become increasingly obvious downstream (Figure 4.2). A lack of significant mineralisation underlying the Tomahawk Au-in-calcrete anomaly suggests scenario 1 is not a dominant mechanism. This is further supported by sample THKLK075 having Au-rich Ca-carbonate matrix supporting coarse sediments with outer laminations containing low Au concentrations, suggesting a change in environment during calcrete formation. Therefore I suggest that Scenario 3 is the dominant mechanism at Tomahawk.

Sources

Figure 5.36 illustrates the possible transport directions from the south. Source C is a possible transport direction due to drainage from Area-223 mineralisation but does not account for Au-in-calcrete results near A or B. High density calcrete data are not available for the area between Area-223 and Tomahawk (along path C; Appendix B). Source A is the most favourable due to higher concentrations further up the headwaters. Source B is also favourable due to a broad area of calcrete with Au concentrations > 10 ppb in the headwaters that are contiguous with the main anomaly. The source of auriferous sediments could therefore be from A and/or B.

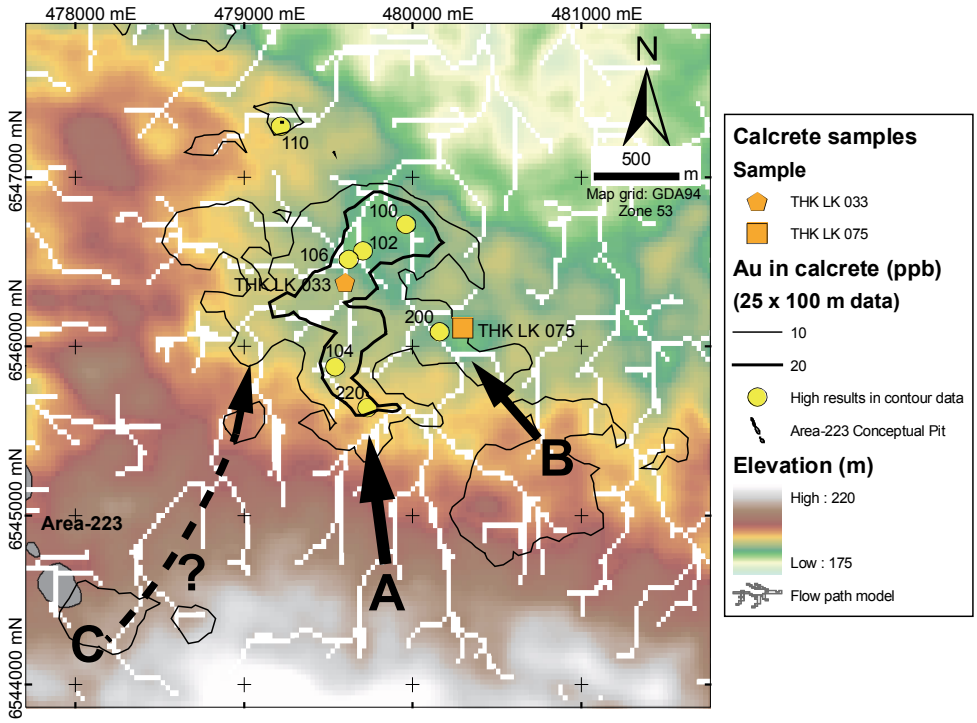

Figure 5.36: Drainage direction (white) at Tomahawk modelled from the 1-second SRTM digital elevation model (background image). Dominant transport directions into Tomahawk are indicted by arrows.

5.5.5. Conclusion

The Tomahawk Au-in-calcrete anomaly has been a challenging exploration target with minimal underlying mineralisation. Calcrete nodules have variable internal morphologies that represent different stages of Ca-carbonate precipitation. Calcium-carbonate cemented sand represents one of these stages and is host to higher concentrations of Au in both samples. Gold in the detrital phase indicates that particulate Au has been transported with the sediments and/or within calcrete nodules into areas that have minimal known underlying mineralisation. This juxtaposition of auriferous sediments over Au-poor saprolite occurs at Area-191 and Tomahawk (*Section 5.1*). Sediment transport at Area-191 is limited. Sediment transport into Tomahawk is predominantly from the south along drainage lines that contain high concentrations of Au in calcrete up into the headwaters. Gold and particularly Ag and Te results from biogeochemical sampling support the notion of a potential source to the south of Tomahawk. The headwaters at the south have had little exploration by drilling or regolith methods (see Appendix B).

5.6. Summary of the Tunkillia case studies

The Tunkillia chapter provides a detailed geochemical and mineralogical analysis of the regolith profile (transported and *in situ*) that is widespread in the area. It also provides a detailed comparison and discussion of the relationships between calcrete and plant chemistry, with data from drilling and the digital elevation model in the eastern part of the Tunkillia Au Prospect around Area-191 and Tomahawk. It also describes Au within calcrete and the implications this has on the transport of Au within the landscape. The key findings in this chapter are:

- Transported regolith is geochemically and mineralogically similar at each of the three sites within the Prospect. This indicates that there has been significant redistribution of regolith and that the transported cover is not useful to distinguish the site of mineralisation from the exploration targets within the Prospect.
- *In situ* regolith (saprolite) at Area-223 contains remnant white mica and kaolinite whereas the saprolite at the exploration targets is kaolinitic. The regolith study showed that whilst the transported material has confused exploration with surface geochemistry, there are indicators in the in the saprolite that have not been transported. These indicators could be expressed by plants, or the archived saprolite samples from drilling could be re-assessed.
- Plant and calcrete studies show that there some relationship between the Au in calcrete and plants although the plant results are more erratic. This is probably due to the lower concentrations of Au within plants compared with the calcrete. As the geochemical indicators of mineralisation in the saprolite are retained throughout the intense weathering, they are not available for uptake by the plants. However, a suite of elements were identified in the calcrete and plants (some commonality) that are correlated with Au.

Chapter 6 builds on this chapter by providing regional case studies in a range of landscape and mineralised settings. It provides a broader context to the Tunkillia case studies in areas where the scale of known mineralisation and associated dispersion of elements within the landscape is smaller.

REGIONAL AREA

6. Regional case studies

Foreword

This chapter encompasses four case studies using biogeochemical sampling methods for mineral exploration in the Yellabinna – Lake Harris region. This chapter presents all new biogeochemical data from these four sites. It also includes new data for calcrete and partial extraction soil geochemistry. The sites were chosen to provide a breadth of landscape processes and mineralisation scales in the region in order to compare with the focussed Tunkillia study. Study sites were chosen at the Glenloth and Earea Dam goldfields and the surrounding area to investigate the biogeochemical response and limitations in delineating narrow Au mineralisation. The Yellabinna case study is an area that has had limited mineral exploration and was chosen for its equivalent landscape setting to the Tunkillia Au Prospect – both are situated in the dunes of the Great Victoria Desert. Chapter 7 will provide a discussion of mineral exploration using biogeochemistry in the Tunkillia and regional case studies.

Four case studies were chosen to provide a breadth of landscape processes and mineralisation scales in the central Gawler Craton in order to compare with the focussed Tunkillia study. The locations of the four case studies are shown in Figure 6.1 and include discussions in the following sections:

- *Section 6.1* Biogeochemical expression of narrow (< 1 m) mineralisation at the historic Glenloth and Earea Dam goldfields;
- *Section 6.2* Biogeochemical expression of the Harris Greenstone;
- *Section 6.3* Biogeochemical and calcrete geochemical targeting mineralisation on the western Lake Harris plains; and,
- *Section 6.4* Biogeochemical and soil partial extraction surveys in the Yellabinna Regional Reserve.

Regional case studies are approximately 550 km NW of Adelaide, and > 10 km west of Kingoonya (Figure 6.1). Access is via the non-sealed Glendambo-Tarcoola road (adjacent to the trans-Australian railway) and established tracks. Individual survey areas are within the Wilgena pastoral lease with the exception of the samples that were collected from within Yellabinna Regional Reserve (by permit).

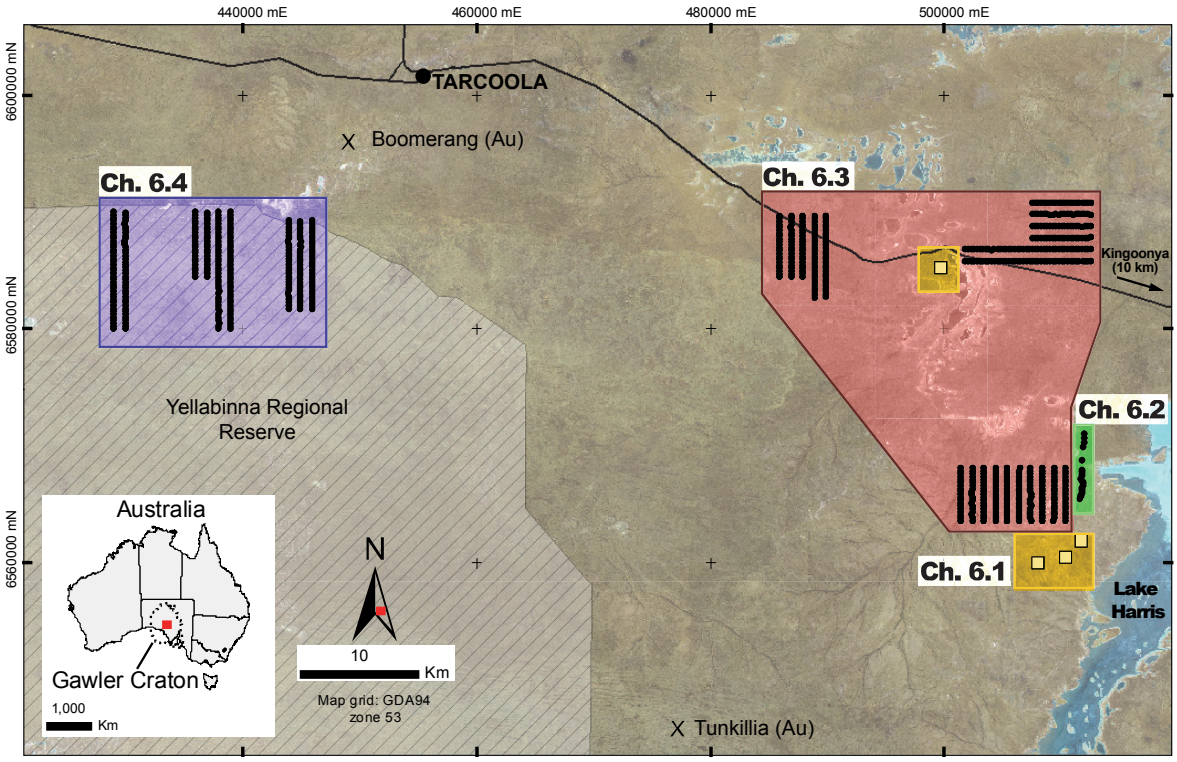

Figure 6.1: Regional case study locations on the Landsat TM.

6.1. Introduction

The Gawler Craton is prospective for a wide range of commodities hosted within Archean and Proterozoic bedrock. Commodities include Cu, Au, Ni, Ag, Pb, Zn, U, Pt, Pd, REEs, Sn, Cr, and Fe (banded Fe formation; Schwarz *et al.* 2010). An arc of Proterozoic Au mineralisation was recognised in the central Gawler Craton during the period of major exploration and geoscience activity of the early 1990s. The region has since been referred to as the Central Gawler Au Province (CGGP; Drown 2002, Drown 2003, Schmidt Mumm *et al.* 2006). The Central Gawler Au Province is broadly defined by Hiltaba-associated intrusive igneous rocks and includes the Tarcoola, Glenloth, Earea Dam, Tunkillia, and Barns mineralisation (Figure 6.2).

Ferris *et al*. (2003) conducted a mineral prospectivity assessment of the Yellabinna region (northern CGGP) and identified prospective mineralisation styles as Archean Ni-Cu-PGE-Au-Co extrusive komatiites and volcanic-hosted massive sulphide (VHMS) Zn-Cu-Au associated with the Harris Greenstone. Much of the Yellabinna region has been underexplored, particularly for VHMS mineralisation. This is due to widespread sedimentary cover and a poor geological understanding of the region (Ferris *et al.* 2003, p.27). Transported regolith on the western Lake Harris plains, and the pervasive sand dunes of the Great Victoria Desert have been an impediment to mineral exploration. Exploration in the area has been hindered by the lack of consistent surface geochemical sampling material as exemplified by patchy coverage of regional calcrete geochemical data (Figure 2.9). The irregular distribution of calcrete data points indicate that either calcrete development is not uniform across the Gawler Craton, particularly in areas

proximal to dune fields, saline lakes, and ephemeral drainage, or; geochemical sampling of calcrete is not applied by all mineral explorers in all exploration tenements.

6.1.1. Geology

The Gawler Craton underlies a large area of South Australia (Figure 6.2) and has been defined as Archean to Mesoproterozoic crystalline basement that has had minimal deformation since 1450 Ma (Schwarz *et al.* 2010). In the north-eastern Gawler Craton, and particularly around the eastern case studies near Glenloth are long sub-parallel linear features with a positive magnetic response identified as the Neoproterozoic Gairdner Dyke Swarm (Cowley & Flint 1993).

The Central Gawler Au Province covers many geological domains, although only a few are associated with the case studies: the Harris Greenstone, Nuyts, and Gawler Range Volcanics are associated with the case studies. The Archean Harris Greenstone consists of ultramafic (komatiite) and mafic volcanics, aluminous metasediments, felsic extrusives and/or intrusives and syntectonic acid intrusives (Daly & Fanning 1993). A few detailed studies have investigated the geochemistry of the komatiite (Coppens 1997), and the associated regolith (Sheard & Robertson 2004) in the context of mineral exploration.

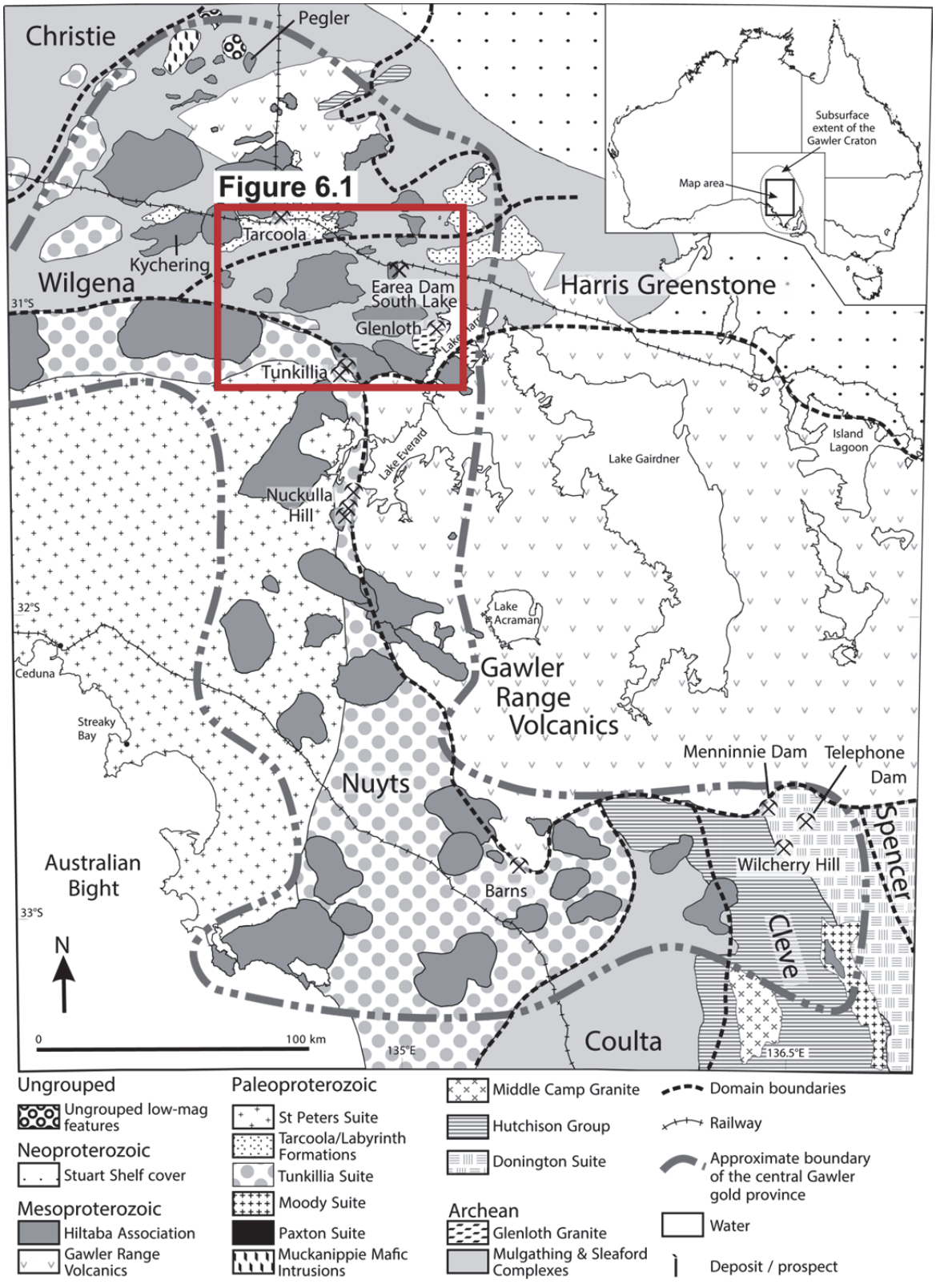

Figure 6.2 - Summary geology and interpreted domain boundaries of the central Gawler Craton, marked with gold mineralisation occurrences within the Central Gawler Gold Province. Extent of Figure 6.1 is shown. From Budd & Skirrow (2007).

6.1.2. Landscape

A province-scale (see Table 3.1) regolith-landform map (60 x 100 km) is included in Appendix B. At this scale, the dominant landforms are the longitudinal dunes of the Great Victoria Desert, Lake Harris, and the Kingoonya palaeo-channel system. At the regional-to-local scale (< 100 km²), the landscape can be further resolved into contemporary lakes, palaeo-drainage and associated gypsiferous aeolian sediments, silcrete-capped mesas with kaolinised-basement scarps, and sporadic exposures of non-weathered crystalline basement, and vein quartz and pegmatites. Transported sediments typically form dunes, or sheet wash and alluvial landforms. Detailed landscape and regolith descriptions for each survey area are included in their respective sections.

6.1.3. Vegetation

Yellabinna Regional Reserve

The vegetation community within the Yellabinna Regional Reserve is similar to that at Tunkillia (also within the Great Victoria Desert). Vegetation is closely associated with landform setting, particularly phases of dune development and swales (Figure 4.5). Dune slopes and dune crests are colonised mostly by woodland or shrubland dominated by mulga (*Acacia aneura*), horse mulga (*Acacia ramulosa*), red mallee (*Eucalyptus socialis*), and Victoria Desert mallee (*Eucalyptus concinna*). Spinifex (*Triodia spp.*) colonise some dune slopes but more frequently colonise vast, open sand plains with tussock grasses.

Dune swales are typically open sand plains (ISps; Figure 4.5) with woodlands colonised by Victoria Desert mallee (*Eucalyptus concinna*), horse mulga (*A. ramulosa*), and umbrella wattle (*Acacia ligulata*). Pearl bluebush (*Maireana sedifolia*) inhabit the dune swales where the sand cover is thin. Stands of black oak (*Casuarina pauper*) typically colonise dune swales, particularly in areas with thin aeolian cover and proximal to the saline lake sequence – likely due to the pooling of water and the *Casuarina sp.'s* recognised tolerance of saline conditions (e.g., Niknam & McComb 2000). Woody (or silver-leaf) cassia (*Senna artemisioides*) typically colonise sandy soils up-slope of sheet wash landforms and near drainage depressions, or areas with thin aeolian cover.

Western plains of Lake Harris

Pearl bluebush (*Maireana sedifolia*), low bluebush (*Maireana astrotricha*), and black bluebush (*Maireana pyramidata*) are widespread and abundant on the sheet wash plains and are a good indicator for the presence of indurated regolith carbonate at shallow depth (< 50 cm; Wotton 1992). Salt bush (*Atriplex spp.*) is also widespread and abundant on the sheet wash landforms, although generally does not coexist with the bluebush varieties. Woody cassia (*S. artemisioides*) typically colonise sandy soils up-slope of sheet wash landforms and near drainage depressions or areas with thin aeolian cover.

Species biogeochemically sampled in the regional case studies are: black bluebush, black oak, low bluebush, mulga, pearl bluebush, and Victoria Desert mallee.

6.2. Biogeochemical expression of narrow mineralisation (historic goldfields)

6.2.1. History of local prospecting

Alluvial Au was discovered at Glenloth in 1893, followed by the discovery of vein Au in 1901, and 10 operating mines by 1902. At about the same time (c. 1899) alluvial Au had led explorers to the discovery of mineralisation at Earea Dam. The Glenloth and Earea Dam goldfields were worked until c. 1915, and have since had intermittent activity (Drew 1992, p.27). Mineralisation in the goldfields is contained in sub-cropping, narrow quartz veins (< 1 m) that host disseminated Au and Sn: a mineralisation style typical of much of the western plains of Lake Harris.

The Glenloth goldfield is less than 3 km NW of Lake Harris in a landscape dominated by sheet wash regolith incised by alluvial drainage depressions (Figure 6.3). The plains are colonised by bluebush and saltbush, whereas the drainage depressions host mulga and black oak. Observed mineralisation occurrences in this goldfield are typically constrained to local depressions where erosion has exploited altered and incompetent bedrock. Locally elevated topography consist of granite tors or low mesas capped by Tertiary silcrete (Wopfner 1978).

The Earea Dam goldfield is 25 km NNW of the Glenloth goldfield and consists of multiple workings along a mineralised lode for a length of 600 m. Lintern (2004) investigated the multi-element geochemistry of the regolith at a costean in the Earea Dam goldfield (Figure 6.4). The study concluded that: the depth of weathering is shallow (< 4 m) with no distinct supergene zone; elements associated with mineralisation are Ag, Bi, Cu, Sn, Te, U, and W; and, only Ag has been mobilised from the site of mineralisation within the regolith for a distance of < 200 m into a depositional area.

Geochemical exploration in the Glenloth-Earea Dam region during the 1970s mostly used stream-sediment and calcrete geochemistry. Small quantities of cassiterite (Sn) occur in the region with vein quartz up to 1 m thick (e.g., Mt Mitchell Sn mine) and disseminated within the kaolinitic saprolite (Whitten *et al.* 1976). Early reports noted anomalous Mo, although repeat observations are unsupportive. Regional geochemical sampling of calcrete found Au concentrations between 1 – 8 ppb over Earea Dam (400 by 400 m sample spacing) and < 10 ppb over Glenloth (200 by 500 m sample spacing; SARIG 2012). At Glenmarkie, a mining operation in the Glenloth goldfield, laminar calcrete contains up to 270 ppb Au (opportunistic sample): this result is comparable to Au-in-calcrete results from the Challenger Au deposit (296 ppb; Edgecombe 1997) and the Tunkillia Au Prospect (c. 200 ppb; Belperio 2009a, Klingberg 2009).

Biogeochemical sampling has been conducted at many parts of the Tunkillia deposit (Thomas 2004, Lowrey 2007, Hopkinson 2009, Vasey 2009, Ames 2010), Boomerang (Lintern *et al.* 2006b), and Barns (Lintern 2005, Lintern 2007). These studies report elevated Au results proximal to mineralisation compared to background. In these settings, however, biogeochemistry does not reliably delineate known mineralised structures,

probably due to broad distribution of auriferous surface regolith and mineralisation being disseminated over a large area.

Goldfields study

For this study I investigated the biogeochemical expression of known mineralisation in western Lake Harris region by sampling pearl bluebush at 25 m spacing over four zones of mineralisation in the historic Glenloth and Earea Dam goldfields. A total of 65 samples were collected.

6.2.2. Mineralisation and survey configuration

Traverse locations in the Glenloth goldfield (Figure 6.3) were selected based on the historic production of the operations (Table 6.1; Fradd 1988, Hill & Crooks 1991, Drew 1992). The Earea Dam traverse was positioned in an area of dense vegetation (pearl bluebush) coverage between the Warburton and Wilgena Enterprise operations (Figure 6.4). Traverse orientations are perpendicular to the strike of the mineralised structures as reported by Hill & Crooks (1991), and Lintern (2004b; Table 6.1). Pearl bluebush terminals (leaves and twigs) were biogeochemically sampled at 25 m spacing for a distance of approximately 250 m on the foot- and hanging-wall side of the mineralised structure.

Table 6.1: Historic Au mining operations. Coordinates are UTM GDA94 zone 53.

Site	East (m)	North (m)	Orientation (dip/dip direction)	Au Production (oz.)	Traverse length (m)
Fabians No.3	511730	6561850	75/249	2500	410
Jay Jay	510380	6560450	28/255	900	430
Glenmarkie (William's)	508000	6559980	60/046	500	540
Earea Dam	499670	6585240	25-40/110	2000	390

Glenloth goldfield

Mineralisation consists of disseminated Au- and Sn-bearing quartz veins, typically less than one metre wide and up to a few hundred metres in strike, and is hosted in sheared and fractured Glenloth Granite (Daly & Fanning 1993, p.45). A narrow dolerite dyke of the regional Gairdner Dyke Swarm strikes NW through Glenloth and is parallel to the strike of mineralisation: an association typical of many Au deposits in the central Gawler Craton (Budd & Skirrow 2007). More than 25 mining operations (primarily underground; Figure 6.3) extracted approximately 10,000 oz. of Au (Drew 1992, p.27), 2500 oz. of which came from the Fabians No.3 operation (Hill & Crooks 1991, p.31).

Mineralisation is concealed by transported quartzose sands and gravels (CHep) that are typically less than a few metres thick and colonised by pearl bluebush. Alluvial regolith types (Aap and Aed) are associated with the three sites in the Glenloth goldfield. Exposures of non-altered Glenloth granite and Kenella Gneiss typically form the crests of broad rises.

Fabians No.3 and Glenmarkie (William's) are underground operations. Glenmarkie was one of the largest Au producers (PIRSA 2006) and a small ore crushing and processing

facility remains on site. Piles of waste material surround open-cut and underground workings at Jay Jay.

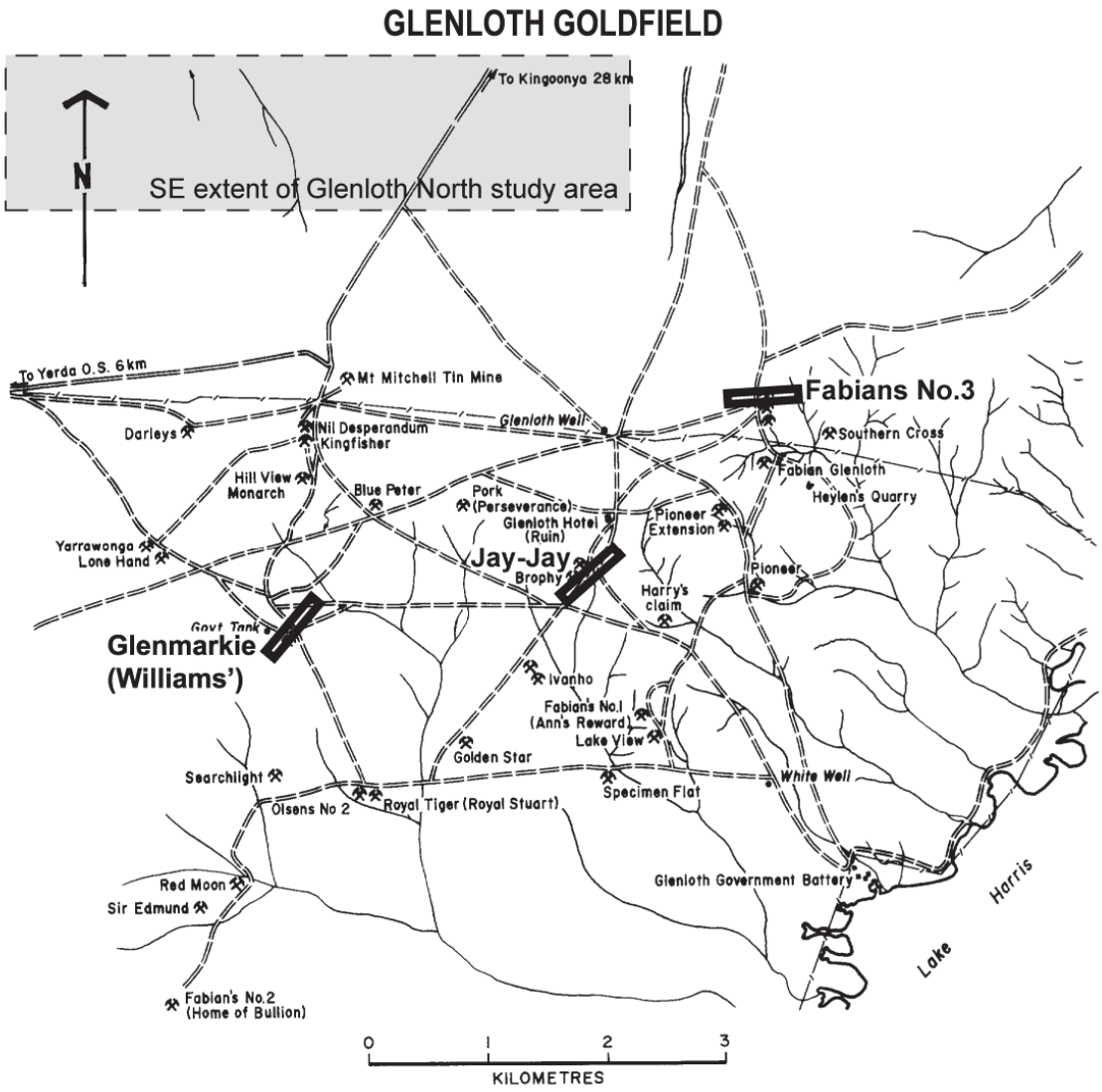

Figure 6.3: Biogeochemical traverses at the historic Glenloth goldfield and Glenloth North study area that is discussed in *Section 6.3*. Map adapted from Drew (1992). Key: double dashed lines are unsealed roads, and the single dashed line is the railway.

Earea Dam goldfield

Earea Dam goldfield is a series of open shafts on narrow Au-bearing quartz-hematite veins for a length of 600 m. This low production goldfield (2000 oz.) is just off the Glendambo-Tarcoola road (Figure 6.4). Sparse pearl bluebush colonisation over Ian's Mine prevented this site being used for a biogeochemical traverse. A suitable site was found crossing mineralisation immediately to the north (Figure 6.4).

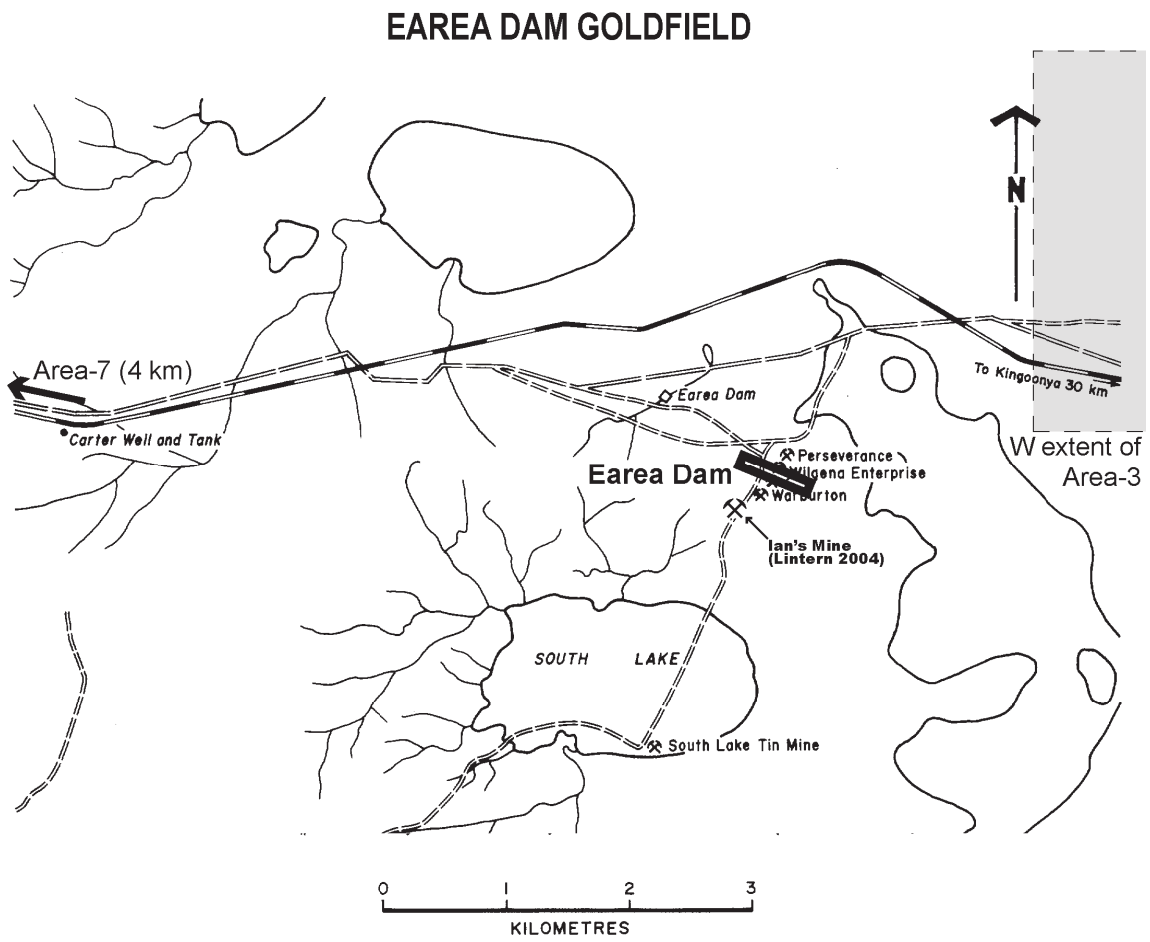

Figure 6.4: Biogeochemical traverse at the historic Earea Dam goldfield (dark rectangle), and location of the adjacent Area-3 and Area-7 surveys. Map adapted from Drew (1992). Key: double dashed lines are unsealed roads, and the alternating black and white line is the railway.

6.2.3. Results

Full results are included in Appendix A. The elements discussed in this section are selected based on the known geochemical association with mineralisation at Earea Dam (e.g., Lintern 2004b) and elements that have elevated concentrations overlying mineralisation for at least one of the mineralised sites.

Glenloth goldfield

Jay Jay

Mineralisation is expressed in plant samples with Au concentration between 0.8 ppb – 1.9 ppb for a width of 125 m (Figure 6.5). Samples directly overlying mineralisation have the highest concentrations of Ag (8 ppb), Cu (7.2 ppm), Sn (0.08 ppm), and U (0.02 ppm). A second zone of high Au results (2.2 ppb; higher than over the vein) is 125 m away from the mine pit and also has high concentrations of Bi (0.8 ppm), Sn (0.08 ppm), and U (0.02 ppm).

Fabians No.3

Mineralisation is expressed in plant samples with Au concentrations between 4 – 27 ppb for up to 200 m from mineralisation (Figure 6.6). High concentrations of Ag (5 – 14 ppb), Bi (0.05 ppm), Cu (5.3 ppm) and U (0.01 – 0.04 ppm) also align with mineralisation. Sample F302 with 27 ppb Au also has Zr and Fe (indicators of detrital contamination) at concentrations of 0.4 ppm and 0.06% respectively.

Glenmarkie (William's)

Mineralisation is expressed by samples with Au up to 4.3 ppb Au, and high concentrations of Bi (0.04 ppm) and Sn (0.06 ppm). Samples 65 m down-slope of the workings have high concentrations of Ag (11 ppb) and Cu (7 ppm; **Figure 6.7**). Samples peripheral to mineralisation have elevated Co and Mn. Uranium and Te results are less than or equal to the analytical detection limits (0.01 ppm and 0.02 ppm respectively).

Earea Dam goldfield

Earea Dam has the largest elevation difference (13 m) across the traverse from the goldfield traverses (Figure 6.8). Samples have Au concentrations between 0.2 – 1.3 ppb with the higher concentrations up to 150 m down-slope of mineralisation in alluvial regolith types (Aap and Aed; Figure 6.8). A sample with 0.7 ppb Au overlies mineralisation. Silver and Cu concentrations are also slightly elevated down slope from mineralisation. Highest Sn results are from the top of a low rise of that exposes slightly weathered intermediate igneous bedrock (SSer; Figure 6.8).

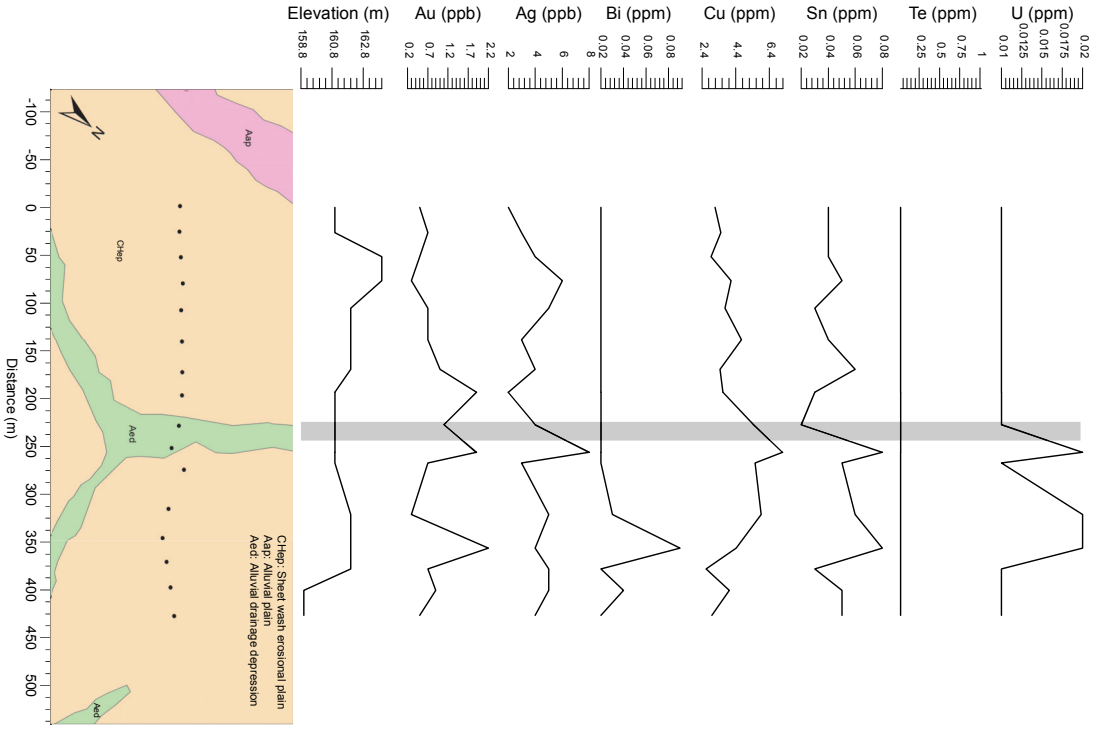

Figure 6.5: Jay Jay biogeochemical traverse (pearl bluebush twigs and leaves). Mineralisation is denoted by the grey strip.

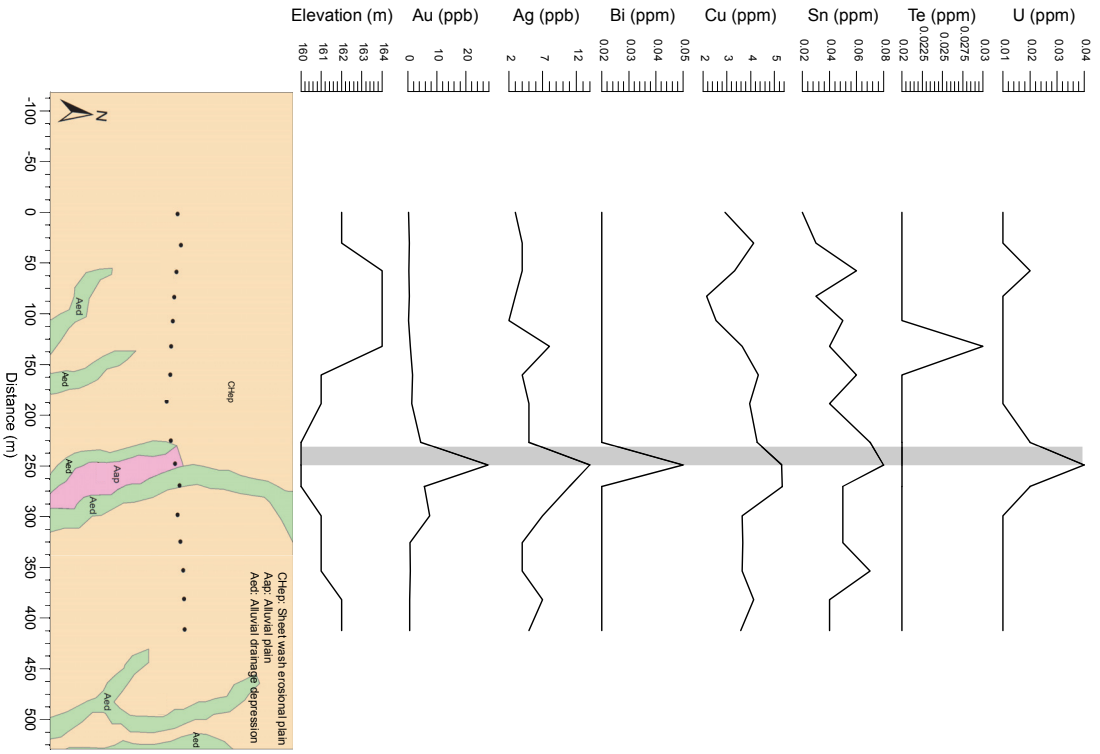

Figure 6.6: Fabians No.3 biogeochemical traverse (pearl bluebush twigs and leaves). Mineralisation is denoted by the grey strip.

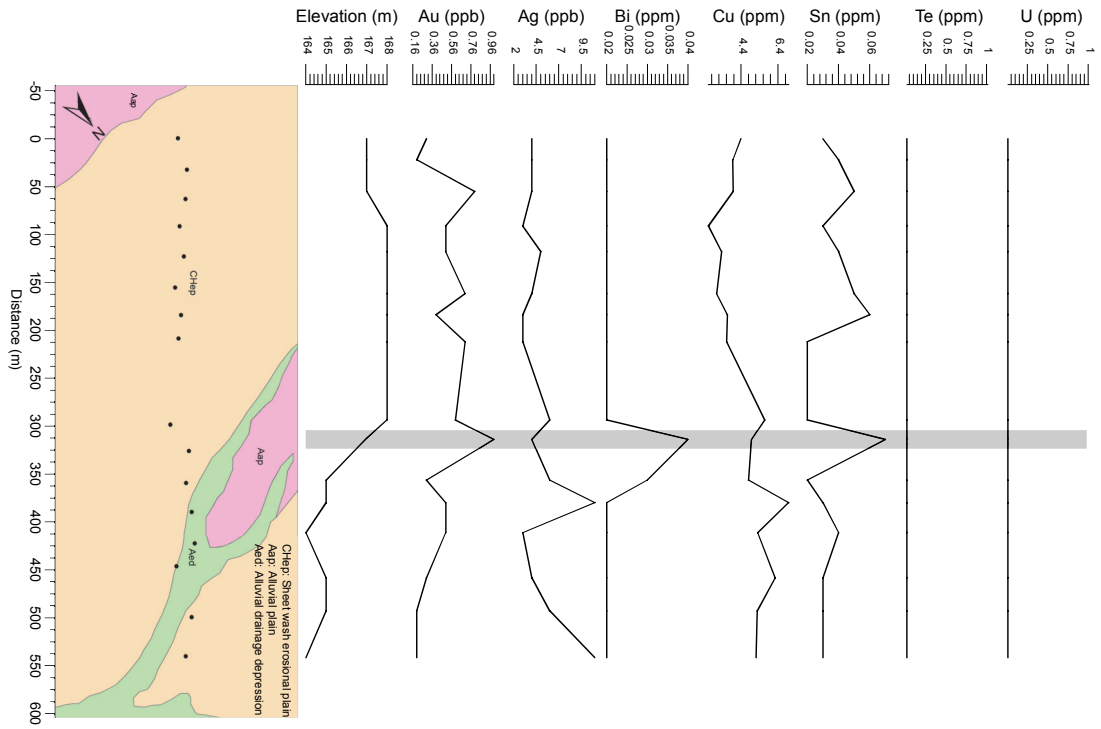

Figure 6.7: Glenmarkie (William's) biogeochemical traverse (pearl bluebush twigs and leaves). Mineralisation is denoted by the grey strip.

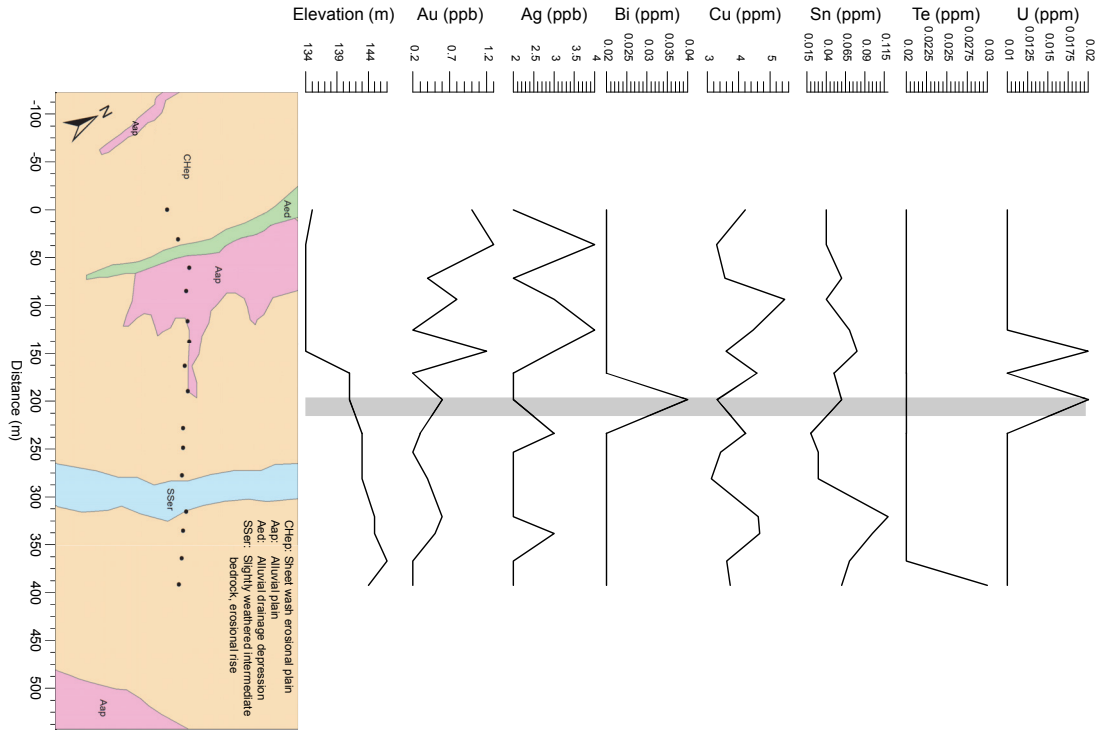

Figure 6.8: Earea Dam biogeochemical traverse (pearl bluebush twigs and leaves). Mineralisation is denoted by the grey strip.

6.2.4. Discussion

Biogeochemical expression

Landscape controls

Mineralisation in the Glenloth goldfield is exposed within drainage depressions (Figures 6.5 – 6.7). Drainage has exploited the altered bedrock that hosts mineralisation whereas unaltered bedrock (e.g., granite and granite tors) comprise areas of higher topography.

In contrast Earea Dam mineralisation strikes along the side of a hill rather than in a drainage depression. Upslope of mineralisation at Earea Dam is competent bedrock forming a local topographic high (Figure 6.8). The local topography is responsible for the physical (and probably hydromorphic) dispersion of elements away from mineralisation in the goldfields (e.g., Ag in the regolith at Earea Dam; Lintern 2004b). High Au and Ag biogeochemical results are offset down-slope of Earea Dam mineralisation and are providing a laterally transported expression of mineralisation.

The biogeochemical expression of mineralisation in the Glenloth goldfield has less lateral offset indicated by the Au, Ag, Bi, Sn, and U peaks that are situated over mineralisation. This is due to the regolith being constrained to broad drainage depressions.

Silver and Cu results at Glenmarkie are offset down-slope within the alluvial channel (**Figure 6.7**). Gold, Bi, and U concentrations are elevated in samples overlying Jay Jay mineralisation and a second peak adjacent to mineralisation (Figure 6.5). The low topographic gradient and minimal offset of the biogeochemical expression of the main site of mineralisation suggests that the second peak could represent parallel mineralisation.

Trace elements

Gold concentrations in pearl bluebush are generally < 1 ppb. High Au results align with the surface projection of mineralisation at Glenloth and are substantiated by elevated concentrations of Bi and U. Distal to mineralisation Bi and U concentrations are in the majority of samples less than or equal to detection limit. Bismuth and U concentrations are 2-3 times the analytical detection limit directly overlying the mineralisation at Fabians No.3 and Earea Dam (Figure 6.6 & Figure 6.8). At Jay Jay the peak concentrations of Bi and U are offset from the expected surface extension of the workings (Figure 6.5). This could be due to aeolian contamination of samples from abundant waste piles at this site, laterally transported regolith (although not prevalent control according to the RLU map), or a mineralised structure parallel to the narrow structure that was mined through open-pit and some underground working.

Detrital contamination

A total of 57% of the pearl bluebush samples have Zr concentrations defined as Tukey 'far-outliers' (>3*(Q3-Q1)) of the entire regional biogeochemical dataset (0.31 ppm; *Section 3.6.3*). The sample with the highest Au concentration (27 ppb at Fabians No.3)

contains 0.4 ppm Zr, which is potentially a result of detrital contamination by the addition of nano-particulate Au.

6.2.5. Conclusion

Biogeochemical sampling at a 25-m interval can express narrow mineralisation at the Earea Dam and Glenloth goldfields by elevated Bi and U. These elevated results are juxtaposed against samples with Bi and U concentrations less than the analytical detection limit. Gold concentrations are also elevated directly over the mineralised structure. Regolith-landform setting appears to control the distribution of Ag and Cu. The low concentrations and/or lateral transport in some traverses mean that the sporadic 'background' concentrations are equal to the concentrations from overlying mineralisation.

6.3. Biogeochemical expression of the Harris Greenstone

6.3.1. Geology and landscape setting

Bedrock of the Harris Greenstone Belt consists of greenstone, metakomatiite, and serpentinite lithologies bounded by Glenloth Granite to the south and the lower Gawler Range Volcanics to the north (Figure 6.9). Lithology and geochemistry studies of the regolith over the Lake Harris Greenstone by Sheard and Robertson (2004) showed that the base of transported cover (aeolian sands, alluvial clays to gravels, and colluvium) is typically at a depth of 14 m (Figure 6.9), and the soil geochemistry of the upper (10 – 200 mm) and lower (200 – 250 mm) horizons have different expressions of the underlying greenstone (Sheard & Robertson 2004). Komatiite indicator elements (Mg, Cr, Ni, As, Co, Fe, Mn and V) are elevated in soil over exposed and weathered greenstones. Mineralisation indicator-elements (Au, Bi, Cu, Pb, and W) also have locally elevated concentrations.

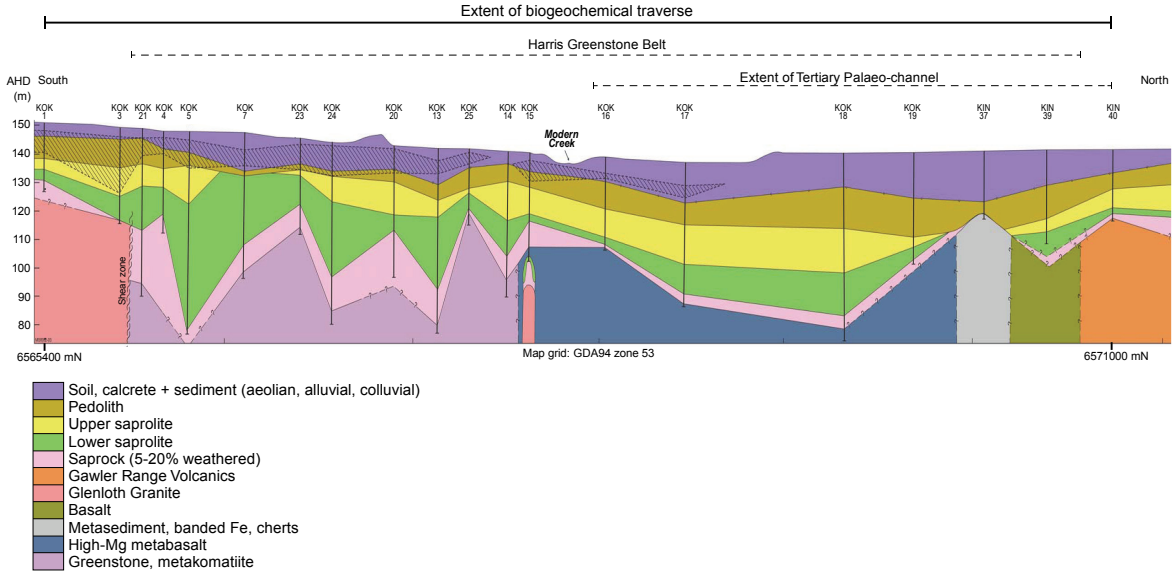

Figure 6.9: Cross section of the Lake Harris Greenstone (15 times vertical exaggeration). Adapted from (Sheard & Robertson 2004) PIRSA 2001 and 2002 drill sites (see Davies 2003).

Regolith

Figure 6.10 shows the biogeochemical samples and approximate drill-hole locations. The elevation drops 10 m over a distance of 5.6 km and drains from the Glenloth Granite towards the palaeo-channel to the north. Regional calcrete sampling from between 1996 and 1998 generally has < 10 ppb Au (SARIG 2012). Some sample locations have multiple Au measurements with significant variation (e.g., 1 – 16 ppb Au).

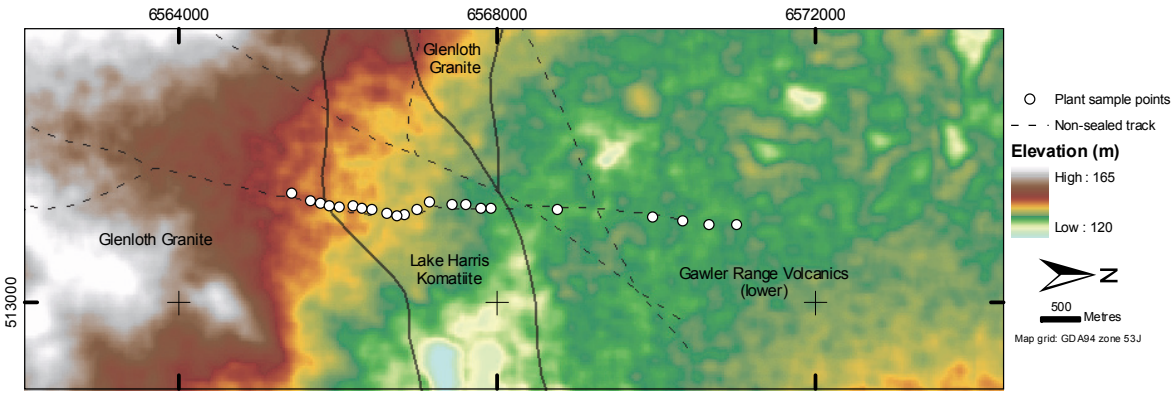

Figure 6.10: Pearl bluebush sample points that are collected from drill hole locations, overlain on the 1-arc second DEM. Geology polygons are from SARIG (2012).

Greenstone study

This aim of this study is to ascertain the biogeochemical expression of the greenstone and provide a reference (with open-file drill data) for the Glenloth North grid survey 1.5 km to the west (Figure 6.1). Plant samples were collected along the drill line in February 2012. Glenloth North samples were collected in February 2011. Pearl bluebush samples (leaf and twig) were collected at 22 drill holes: (from south to north) KOK1, KOK2, KOK3, KOK21, KOKDD4, KOK5, KOK22, KOK6, KOK8, KOK23, KOK9, KOK10, KOK11, KOKDD13, KOK25, KOKDD15, KOK14, KOK17, KOK19, KIN37, KIN39, KIN40 (Figure 6.9).

6.3.2. Greenstone biogeochemistry

Greenstone indicators

Higher concentrations of indicator elements (Mg, Cr, Ni, As, Co, Fe, Mn and V), are from the southern part of the traverse (Figure 6.14). Northern samples have comparatively lower concentrations of indicator elements and overly a high-Mg metabasalt (GRV). Copper and Ni have a similar distribution. The highest Cu result overlies the GRV.

Mineralisation indicators (Au, Bi, Cu, Pb, and W)

Bismuth is below the analytical detection limit (0.2 ppm) for all samples except one at 0.8 ppm. This sample also contains higher concentrations of Au (0.9 ppb), Sn (0.1 ppm), Hg (17 ppb), and Zr (0.8 ppm). Adjacent samples contain 0.8 and 1.4 ppb Au to the north and south (Figure 6.15). High Au results (0.6 – 0.9 ppb) and Ni results (1.1 ppm) overlie a metasediment bedrock lithology. Zirconium concentrations in this sample are between 0.33 – 0.38 ppm (Figure 6.13). Lead concentrations are highest from overlying the Glenloth Granite and decrease towards the north (Figure 6.16). A sample from over the GRV in the north contains up to 1.5 ppm Pb.

Other elements

Zirconium and Fe concentrations are amongst the highest from the central Gawler Craton dataset (Figure 6.11). All samples contain concentrations of Zr considered as Tukey 'far outliers' (3*(Q3-Q1)) of the entire regional dataset (> 0.31 ppm; *Section 3.6.3*). Samples are from a sheet wash plain adjacent to a frequently-used non-sealed track. Higher concentrations of Zr (1.3 ppm) and Fe (0.14 %) are from the alluvial sheet wash plain at the southern part of the traverse (Figure 6.13).

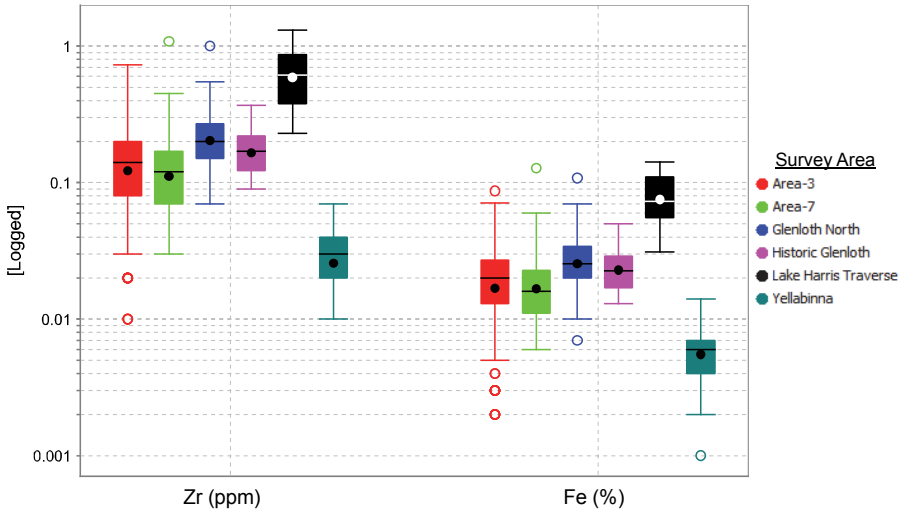

Figure 6.11: Zr and Fe concentrations in biogeochemical samples (all species) coloured by area.

Phosphorous is the only element that is consistently higher in the northern part of the traverse overlying the GRV (Figure 6.17). As Zr is lowest in this area, P has an inverse relationship with Zr (Figure 6.12), Al, Cs, Fe, Th and REE.

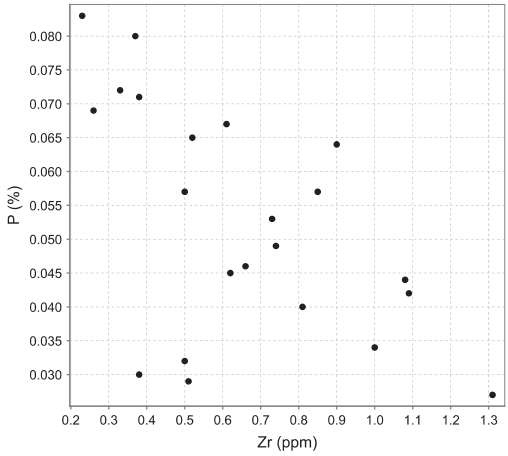

Figure 6.12: P vs. Zr in pearl bluebush

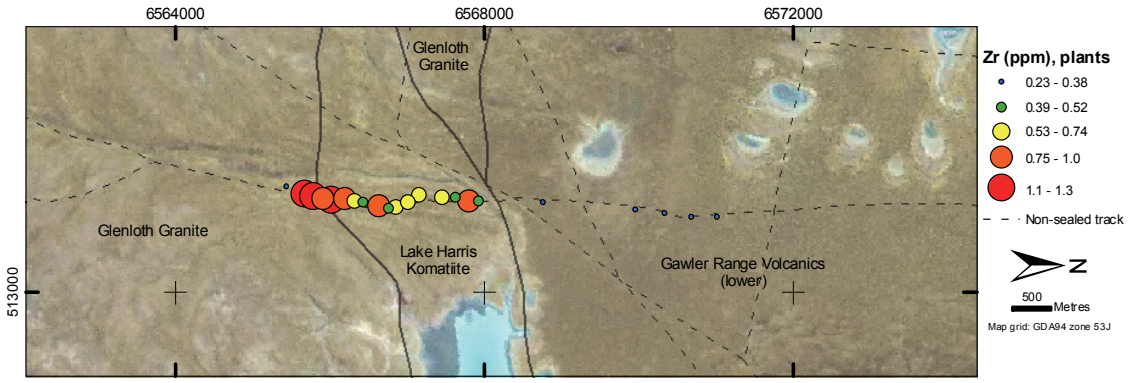

Figure 6.13: Zr in pearl bluebush on Landsat TM image. Geology polygons are from SARIG (2012).

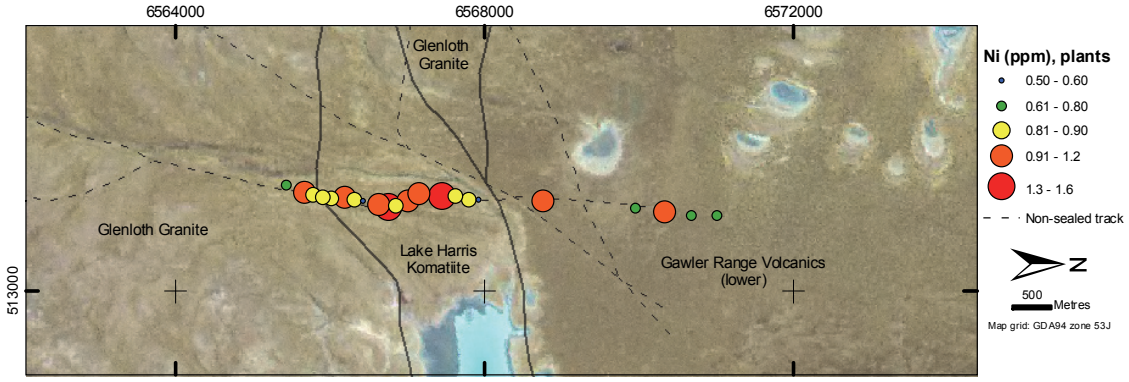

Figure 6.14: Ni in pearl bluebush on Landsat TM image. Geology polygons are from SARIG (2012).

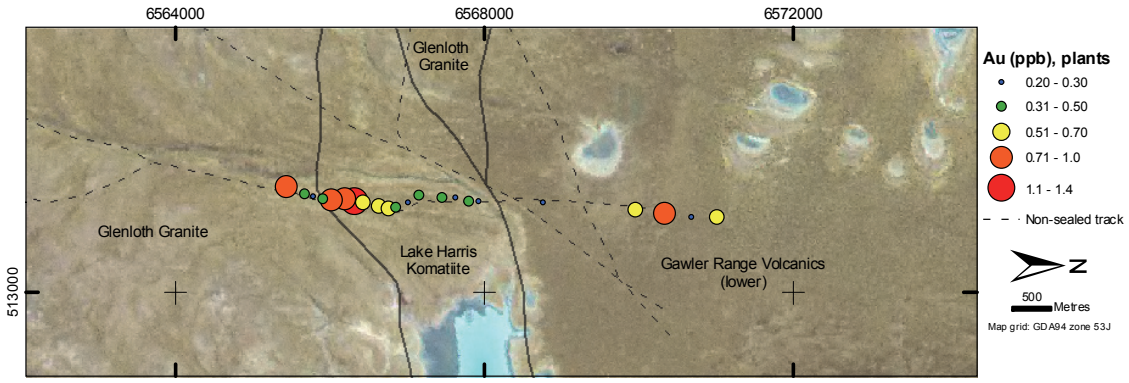

Figure 6.15: Au in pearl bluebush on Landsat TM image. Geology polygons are from SARIG (2012).

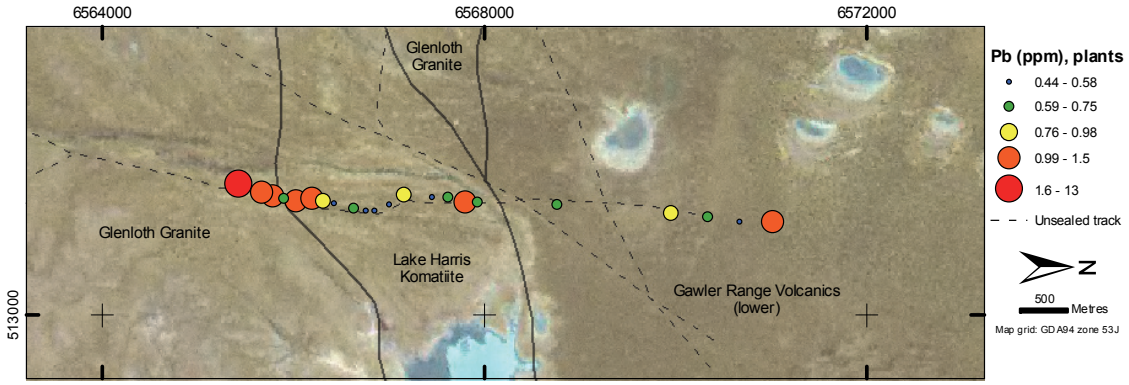

Figure 6.16: Pb in pearl bluebush on Landsat TM image. Geology polygons are from SARIG (2012).

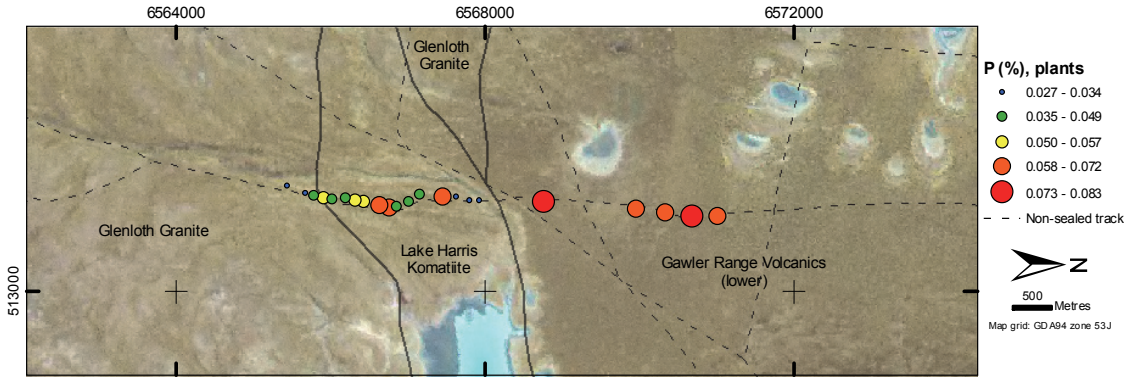

Figure 6.17: P in pearl bluebush on Landsat TM image. Geology polygons are from SARIG (2012).

6.3.3. Discussion

Contamination

Pearl bluebush are the most susceptible to detrital contamination in biogeochemical sampling (*Section 3.6.3*) and this is evident in the biogeochemical study of the Lake Harris greenstone sequence. Aeolian contamination is particularly high along this traverse as indicated by some of the highest Zr and Fe concentrations from the central Gawler Craton biogeochemical data (Figure 6.11). Sparse vegetation on the plain (tens of metres between plants) provides minimal stabilisation of surface material, increasing the potential for aeolian transport of detritus. The plain was subject to a minor dust storm at time of sample collection.

The relationship between Zr and P is an example of how detrital contamination can influence biogeochemical results. Phosphorous is essential plant nutrient and is between 0.03 – 0.08 % in pearl bluebush along this traverse. There is a noticeable inversion of Zr and P results from S-N at a lithological and regolith landform boundary. Phosphorous is immobile in alkaline regolith and mobilised in acidic weathering (Scott 2009). The regolith in the region is dominated by calcareous soils as indicated by the intimate pearl bluebush association. A sudden change in regolith alkalinity at this boundary is unlikely and therefore a sudden change in the availability of P in the regolith is unlikely. Zirconium concentrations are highest, and P concentrations are lowest in samples from the alluvial regolith landforms overlying the Glenloth Granite and Lake Harris Komatiite. It is possible that the addition of detrital material (Zr and Fe) has diluted the P concentration in these samples.

Landscape controls

Plant samples are from a broad area of colluvial and alluvial regolith that has been transported from the Glenloth Granite northwards. Higher plant Pb results are from the south and are underlain by Glenloth Granite. Lead concentrations in soil are also highest at this part of the traverse (Sheard & Robertson 2004). The northern most samples are collected from over the regional Kingoonya palaeo-channel (Figure 6.10) where sediments are typically 14 m deep (Sheard & Robertson 2004). Lead–in-plant results are associated with the Glenloth Granite and sediments derived from this area. The northern

most sample contains elevated Pb and is underlain by Gawler Range Volcanics (GRV). A similar expression of the GRV by Pb in pearl bluebush occurs in Area-3 (see *Section 6.4*).

Samples from the southern part of the traverse generally contain a higher concentration of metals (e.g., Au, Ni, and Pb). This is likely to be a result of either: the uptake of elements that have been transported by physical and/or hydromorphic processes northward from the Glenloth Granite and Lake Harris Komatiite and/or the physical addition of aeolian material to sub-aerial plant organs.

6.3.4. Conclusion

Plant biogeochemistry in this area is complicated by the thick sequence of transported cover, different regolith landforms, and a high level of detrital contamination. Aeolian detrital contamination has had an adverse effect on the biogeochemistry, as indicated by Zr and P results, and the level of this contamination changes with landform. The regolith landform boundary (approximately E-W) of predominantly alluvial sediments to colluvial and alluvial sediments coincides with an underlying lithology boundary. The biogeochemical expression of the greenstone is ambiguous. The biogeochemical expression is likely to be of the transported alluvial sediments derived from Glenloth Granite and Lake Harris Komatiite (10 – 25 m thick), and a variable detrital input.

6.4. Regional plant and calcrete surveys (25 km²)

6.4.1. Introduction

The region to the west of Lake Harris contains known occurrences of Au mineralisation at the Earea Dam and Glenloth goldfields, and Sn mineralisation (cassiterite) at Mt Mitchell (Glenloth goldfield) and South Lake (Figure 6.18; Whitten *et al.* 1976). The goldfields were discovered around 1900 through the presence of alluvial Au (Drew 1992). Regional geochemical sampling of calcrete (Au only) has since been conducted in the area from between 1996 – 1998 at a typical spacing of 400 m (Figure 6.18; SARIG 2012). Previous calcrete results are inconclusive of underlying Au mineralisation. Calcrete data on the western plains of Lake Harris is irregularly spaced and are not measured in large areas. The case studies in this section focus on a few areas that lack calcrete data from previous exploration (Area-3, Area-7, and Glenloth North; Figure 6.18). The case studies provide a discussion of new biogeochemistry and regolith geochemistry data in the context of landscape processes and mineralisation potential.

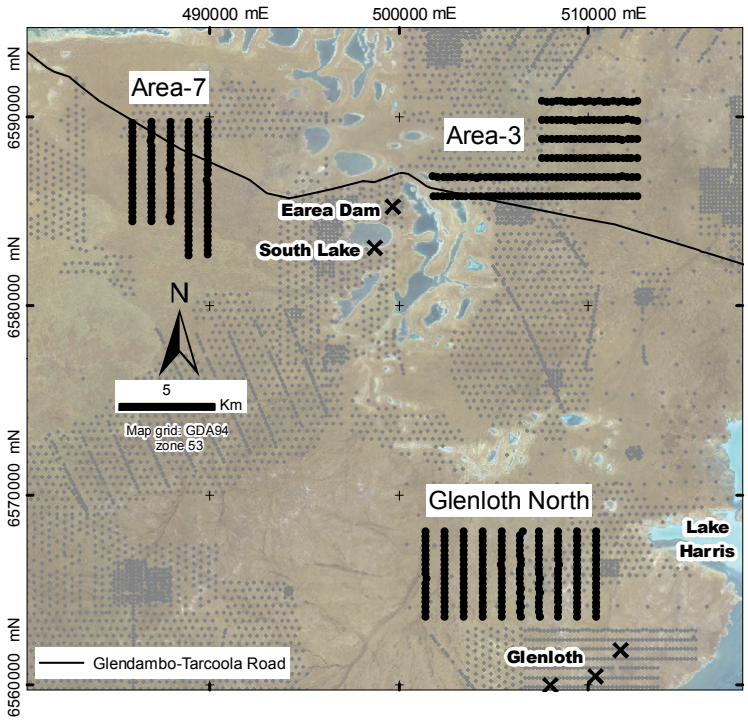

Figure 6.18: Sample points in Area-3, Area-7 and Glenloth North surveys (black), and existing calcrete data (grey; SARIG 2012).

Geology of the western Lake Harris area

Figure 6.19 illustrates the underlying bedrock and the associated aeromagnetic response for the three survey areas. The Lake Harris Komatiite is geophysically characterised by a strong positive response on the aeromagnetic image, and is present within the Glenloth North survey area. Gairdner Dolerite Dykes feature in the eastern part of the map. These sub-parallel NNW-trending linear features have a marked positive response on the aeromagnetic imagery (Cowley & Flint 1993). The dolerite dykes are associated with Au mineralisation at the Glenloth goldfield and are interpreted from aeromagnetic imagery to continue into the Glenloth North survey area.

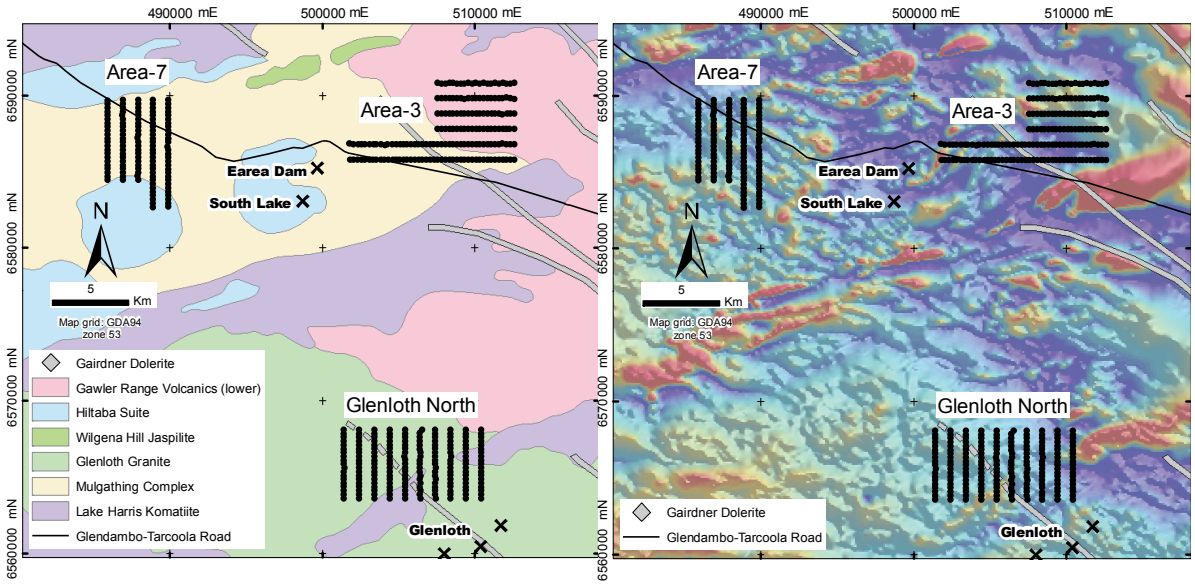

Figure 6.19: 1:2M-scale bedrock geology (left) and aeromagnetic response (right) associated with Area-3, Area-7 and Glenloth North surveys. Geology and aeromagnetic data are from SARIG (2012).

Previous work

Studies in the region (Figure 6.19) with a regolith focus include multi-element characterisation of Earea Dam Au mineralisation (Lintern 2004b) and the Lake Harris greenstone (1 km E of Glenloth North; Sheard & Robertson 2004), and broad geochemical mapping of stream sediments (Whitten *et al.* 1976). The biogeochemical expression of four narrow mineralised veins is discussed in *Section 6.1.2*. Mineralisation at the goldfields is characterised by increased concentrations of Au, Ag, Bi, Cu, Sn, and U in biogeochemical samples. The biogeochemical expression of the Lake Harris Greenstone was investigated and discussed in *Section 6.3*.

Regional studies

For this study I conducted plant biogeochemical and regolith geochemical sampling in three regional exploration surveys west of Lake Harris, each covering ~25 km². Biogeochemical samples were collected at a spacing of 250 by 1000 m and regolith samples were collected at a spacing of 500 by 1000 m. ‘Samples described in this section include a range of calcrete morphologies from powdery regolith carbonate, to highly indurated nodules and hardpan calcrete. I conducted this study to determine if biogeochemical sampling could be used to identify mineralisation in area that is underexplored using calcrete geochemistry, and to determine broad scale lithology and landscape processes.

6.4.2. Summary of results

A summary of regolith geochemistry

Regolith samples from Area-3 (A3), Area-7 (A7) and Glenloth North (GLN) have up to 25% Ca with < 3% Al, Fe, Mg, and K (Table 6.2). It is evident from the low Ca concentrations that some samples are not calcrete or calcareous soil, despite some effervescence with cold 10% w/v HCl at the time of collection. Calcium is most strongly

correlated with Sr, Cd, Au, and Se. Samples with low Ca concentrations generally have higher concentrations of Bi, Fe, Mn, Pb, Th, and W.

Table 6.2: Summary of regolith chemistry. Concentrations are in % unless indicated otherwise.

		Minimum	Maximum	Mean	Std. Dev.
Depth (m)	A3	0.4	2.8	0.91	0.58
	A7	0.3	3.5	1.1	0.68
	GL	0	3.2	1.2	0.65
Au (ppb)	A3	1	6	2.6	1.2
	A7	1	6	2.5	1.3
	GL	1	11	2.3	1.7
Ca	A3	0	25	13	7.4
	A7	1.5	23	13	5.8
	GL	0	25	8.9	5.8
Fe	A3	0.76	2.9	1.5	0.49
	A7	0.7	2.4	1.4	0.41
	GL	0.4	2.7	1.8	0.48
Mg	A3	0.2	1.2	0.62	0.22
	A7	0.22	1.2	0.56	0.23
	GL	0.36	2.8	0.87	0.41
K	A3	0.2	0.75	0.33	0.11
	A7	0.14	0.52	0.3	0.074
	GL	0.14	0.92	0.45	0.17

Regolith samples are from depths between 0 – 3.5 m (Table 6.2) and consist of a range of morphologies. Hardpan and nodular calcrete samples are typically from depths of < 1.3 m on erosional plains or silcrete-capped rises. Samples from > 1.3 m are more ferruginous and potassic (and Ca-poor) representing hardpan clays and poor calcrete development, typical of alluvial landforms. Pearl bluebush in the region are spatially correlated with hardpan calcrete at shallow depth. The affinity of pearl bluebush for hardpan calcrete in semi-arid South Australia is also reported by Wotton (1992). Wombat burrows are more abundant in areas with hardpan calcrete horizons.

Gold has a good correlation with Ca (0.67) and Sr (0.76) for 191 samples from the three survey areas. The best element correlation with Au within a study area is Se (0.76) at Glenloth North. Gold concentrations are between 1 – 11 ppb and are higher in samples collected from shallower depth (Figure 6.20). Calcium and Au concentrations are generally higher in samples collected at shallower depth (Figure 6.20). Calcium-poor samples collected from shallow depth are from areas where silcrete has prevented penetration of the auger.

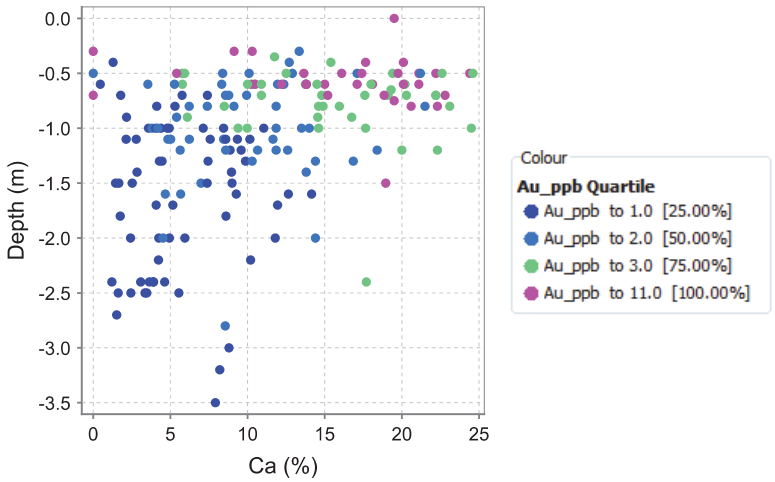

Figure 6.20: Depth plotted against Ca in regolith samples, coloured by Au concentration.

Regional biogeochemical surveys

Biogeochemical results in this section are presented by survey area. Each survey area is colonised by a different plant community (Table 6.3). Elements selected for discussion are known to be geochemically associated with mineralisation (e.g., Lintern 2004b), or form contiguous anomalism interpreted to be controlled by landscape and/or geology (Zn, Pb etc.). The full biogeochemical results are included in Appendix A.

Table 6.3: Species collected in each survey. Number of samples is in parenthesis.

Survey	Target species
Area-3	Pearl bluebush (145), woody cassia (26)
Area-7	Pearl bluebush (109), mulga (9), black oak (4)
Glenloth North	Pearl bluebush (190)

6.4.3. Area-3

Area-3 biogeochemical and regolith geochemical surveys were conducted during two seasons: February 14-24 2011; and, June 14-28 2011 (Figure 6.21). Biogeochemical analysis was conducted by Acme Analytical Laboratories for both seasons using the same analytical methods. Regolith geochemical surveys were collected using a hand auger in February 2011 and a mechanical auger in June 2011. Regolith samples were not collected along the three northern lines in June 2011 due to time constraints. Depth of sample was not recorded, however most samples were collected from depths < 1.5 m. Geochemical analysis of regolith samples was conducted by different analytical laboratories: Genalysis in February 2011, and ALS in June 2011. Each laboratory has a slightly different suite of elements included in the analysis and there is some difference in the lower analytical detection limits (see *Section 3.3*). The data could not be normalised because standards were not submitted to each laboratory with the samples. These datasets are combined and the difference in background concentrations can be seen in the results section.

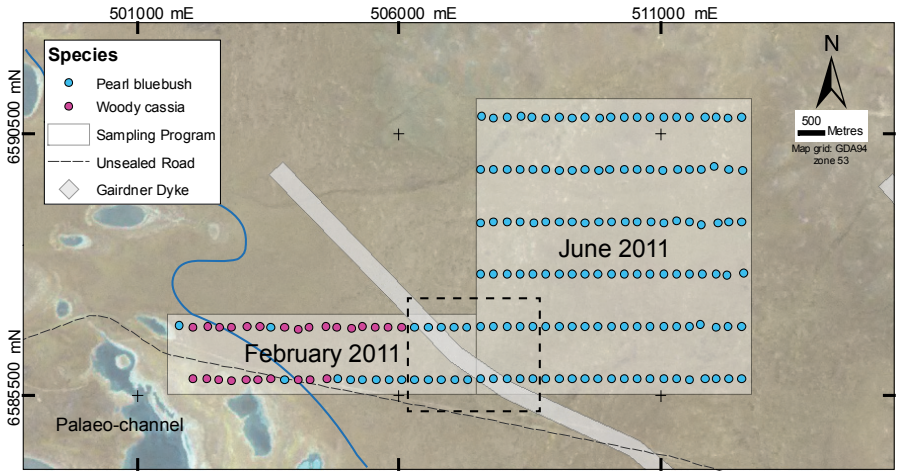

Figure 6.21: Biogeochemical sample points at Area-3 coloured by species. Approximate extent of the palaeo-channel is marked by the blue line. Dotted rectangle denotes an area of resampling for seasonal variation analysis.

Area-3 regolith geochemistry results

Regolith samples from near the palaeo-channel are Ca-poor (< 5%; Figure 6.22) and Na-rich (up to 0.4 %; Figure 6.23). Calcium-rich regolith samples (20 to 30 %) represent

well-developed calcrete. Calcareous regolith towards the east is also marked by the presence of pearl bluebush (e.g., Figure 6.21). Silver, Sn, and U concentrations are higher in samples from near the salt lakes (e.g., Ag, Figure 6.24) although there is minimal association with these elements and Na. Regolith samples from the east are underlain by Gawler Range Volcanics and have higher concentrations of Pb (up to 9 ppm; Figure 6.25).

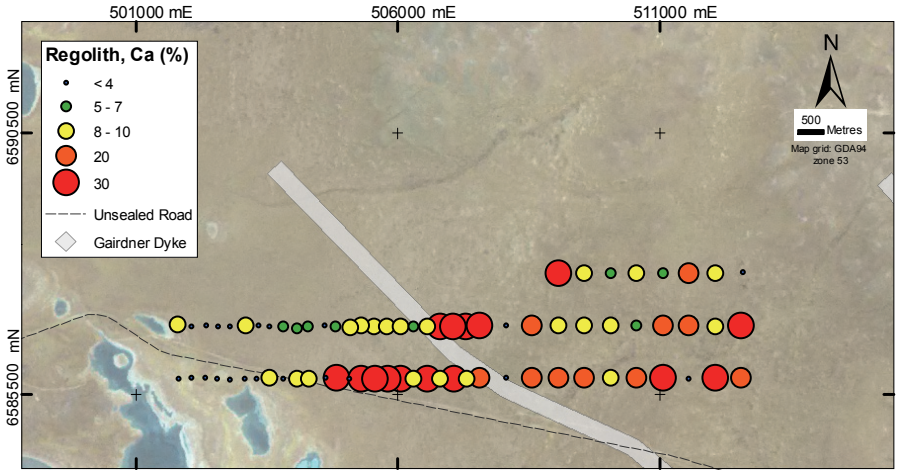

Figure 6.22: Ca in regolith samples on the Landsat TM.

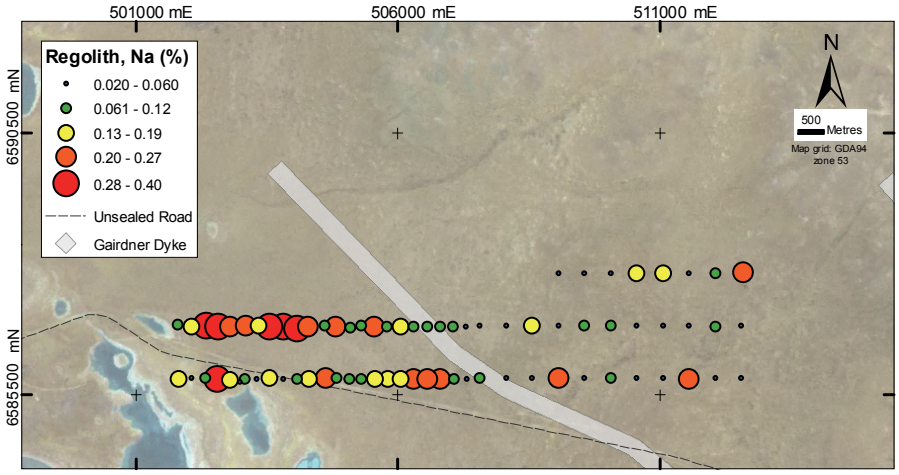

Figure 6.23: Na in regolith samples on the Landsat TM.

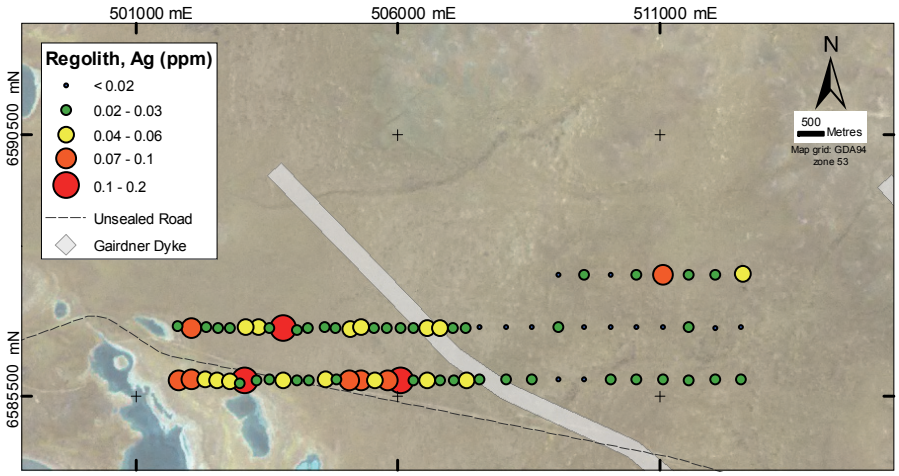

Figure 6.24: Ag in regolith samples on the Landsat TM.

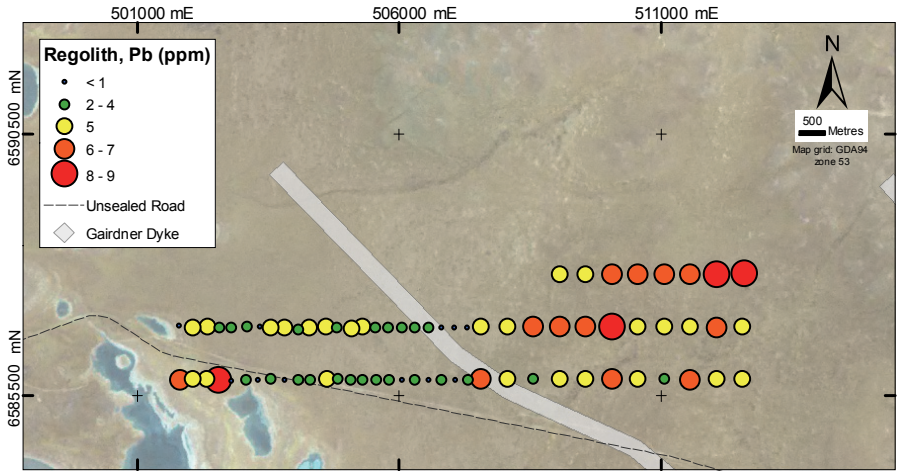

Figure 6.25: Pb in regolith samples on the Landsat TM.

Gold and gold-associated elements

Gold-in-regolith results from this study (Figure 6.26) corroborate results from previous calcrete sampling programs (Figure 6.27): the highest Au concentrations are from near the unsealed road at the 506,000 mE grid reference. Gold has a positive correlation with Ca, Cu, and Te. Copper and Te are biogeochemical indicators of mineralisation in the Glenloth and Earea Dam Goldfields (*Section 6.2*). Samples from the western part of the survey have Te concentrations equal to or less than the analytical detection limit (0.05 ppm). Samples from the eastern part of the survey (June 2011; Figure 6.21) were geochemically analysed by a different laboratory with a lower limit of detection for Te (0.01 ppm). Gold has a negative correlation with Bi and Sn. Bismuth and Sn are associated with Al and Fe.

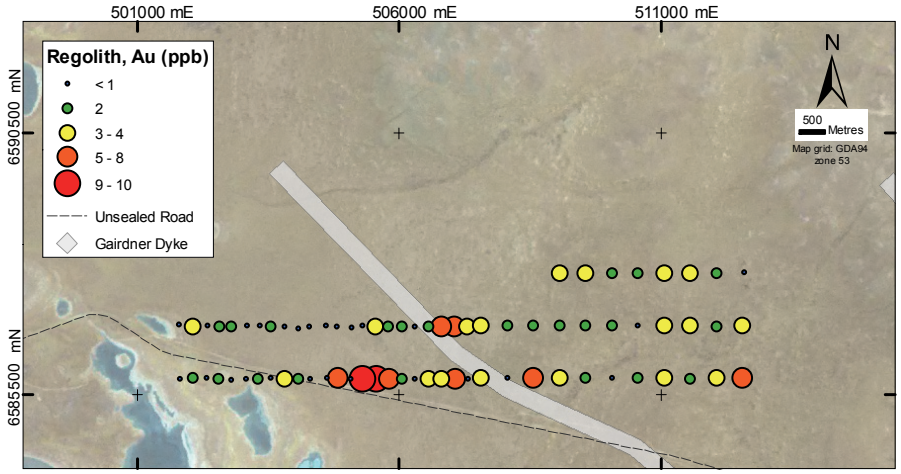

Figure 6.26: Au in regolith samples on Landsat TM.

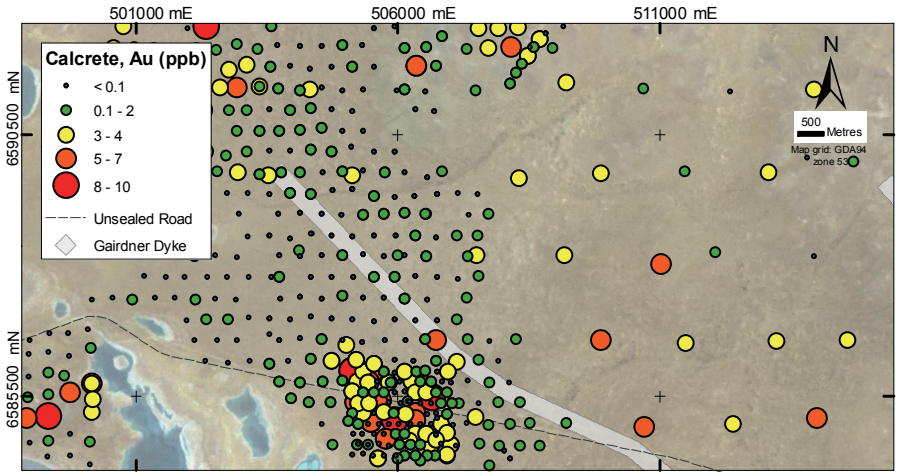

Figure 6.27: Au in calcrete. Data are from SARIG (2012)

Area-3 biogeochemistry results

The biogeochemical results of the first five pearl bluebush samples either side of the season 'boundary' were compared by resampling the same plants in different seasons (dotted rectangle in Figure 6.21**)**. Elements that have a mean concentration from one season that is within the interquartile range of the other season are considered to have similar background concentrations: Al, Ba, Bi, Ca, Cd, Co, Cs, Fe, Ga, Ge, Hf, Hg, In, K, La, Li, Mn, Nb, Ni, Pt, Rb, S, Te, Ti, U, V, W, and Y. Elements that have significantly higher concentrations in February 2011 are: Au, Ce, Cr, Cu, P, Sc, Se, Ta, Th, Tl, Zn, and Zr. In contrast, elements that have higher concentrations in June 2011 are As, B, Be, Mg, Mo, Na, Pb, Pd, Re, Sb, Sn, and Sr. Chromium has the largest background concentration difference with concentrations that are on average three times higher in samples collected during February 2011. Contamination from the mill could be the cause of the high Cr results (e.g., Dunn 2007), however Ni, which is also present in the steel components of the mill, is not elevated in these samples . The higher Cr results are correlated with Zr, REE, Pb ($R > 0.75$) which suggests detrital contamination. The variability of the Cr results is problematic for identifying potential ultramafic bedrock using biogeochemistry at Area-3.

Gold and gold-associated elements

Pearl bluebush samples (twigs and leaves) and woody cassia samples (leaves) have between 0.2 – 1.9 ppm Au but typically have < 1.2 ppb Au (95 percentile). The highest Au results are from pearl bluebush and woody cassia samples (1.9 ppb; Figure 6.28). The woody cassia sample was collected from less than 100 m from the unsealed Glendambo-Tarcoola road whereas the highest Au-in-pearl bluebush result is from an area overlying a dyke from the Gairder Dyke Swarm. Gold concentrations in calcrete are also highest in this area (Figures 6.26 & 6.27). Gold concentrations are > 1 ppb in samples from 1 km² in the western part of the survey but are generally lower in samples from the east (0.02 – 1.0 ppb; Figure 6.28). Silver concentrations reach 10 ppb adjacent to the dyke (Figure 6.29).

This research has shown that biogeochemical indicators for mineralisation at Earea Dam (2 km east) are Bi and U (*Section 6.2*). Uranium concentrations are above analytical

detection limit in only one sample that is 100 m from the Glendambo-Tarcoola road. Bismuth is below the analytical detection limit (0.02 ppm) for the majority of samples. High Bi concentrations (0.04 – 0.05 ppm) are immediately followed in ascending numerical order by a sample with slightly lower Bi concentration (0.03 ppm).

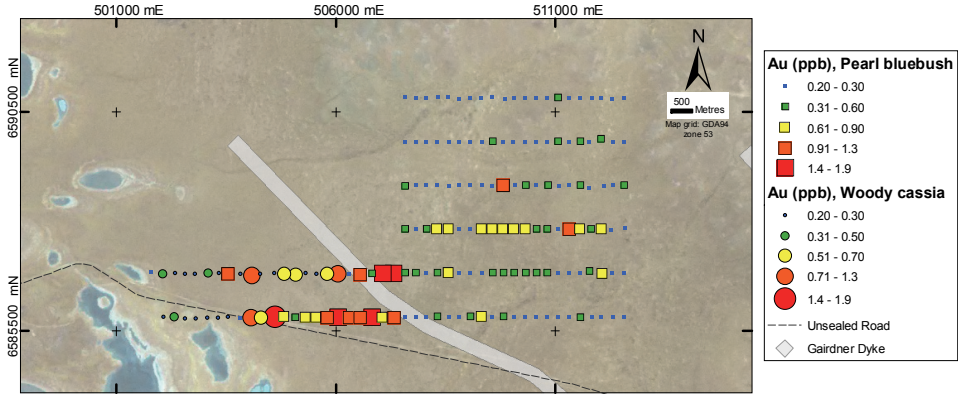

Figure 6.28: Au in vegetation at Area-3 on the Landsat TM image.

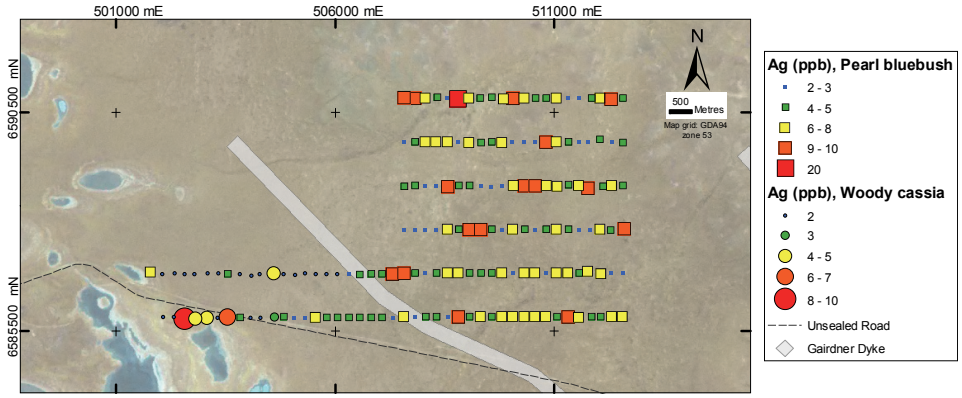

Figure 6.29: Ag in vegetation at Area-3 on the Landsat TM image.

Other elements

Detrital contamination indicator elements: Fe and Zr; are strongly correlated (0.97) and have a good correlation with REE, Co, Cs, Hf, and Th. Higher concentrations of Fe and Zr are measured in pearl bluebush samples and a total of 16 pearl bluebush samples from Area-3 have > 0.31 ppm Zr (the far outlier for the regional dataset; *Section* 3.6.3). The highest concentrations of Fe and Zr are measured in samples from immediately north of the unsealed road.

Lead concentrations are highest in plant samples from the NE corner (Figure 6.30), and are weakly correlated with Mn, Fe, and Co. The area of elevated Pb in plants in the NE is closely aligned with the positive response on the aeromagnetics and is underlain by Gawler Range Volcanics (Figure 6.31). Pearl bluebush samples contain up to ten times higher Pb than woody cassia samples (Figure 6.30). Higher Pb concentrations in woody cassia samples (up to 0.2 ppm) are adjacent to the unsealed road and the salt lakes (Figure 6.30).

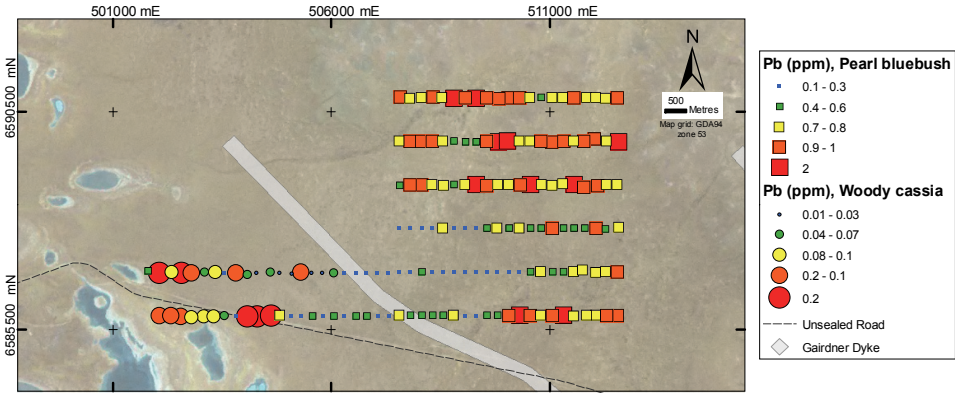

Figure 6.30: Pb in vegetation at Area-3 on the Landsat TM image.

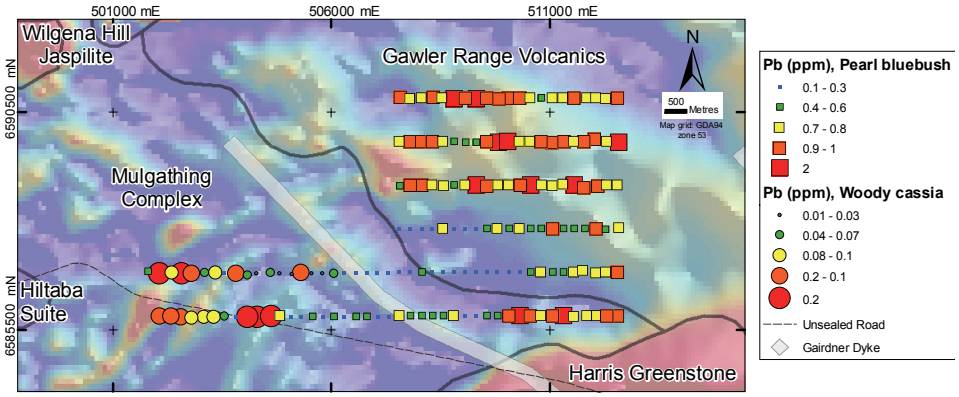

Figure 6.31: Pb in vegetation at Area-3 on the Aeromagnetic imagery. Total magnetic intensity on the background image is from high (red) to low (blue). Aeromagnetic data and geology polygons are from SARIG (2012).

Area-3 discussion

Landscape controls

The salt lakes and palaeo-channel are the main controls on regolith geochemistry and biogeochemistry at Area-3. Regolith samples collected from near the salt lakes and palaeo-channel inherently have higher Na concentrations and lower Ca concentrations. Gypsum is prevalent near the lakes and would be reflected by total S in the geochemistry, although S is not in the analytical suit for the western samples. The regolith sample type is inconsistent (e.g., not all calcrete) throughout Area-3.

Biogeochemical sampling in Area-3 is complicated by inconsistent species (sample) coverage. The contrast in biogeochemical background between pearl bluebush and woody cassia makes comparison of biogeochemical results difficult (e.g., summary of species, Appendix B). Woody cassia colonise sandy soils (e.g., Cunningham *et al.* 1981) and Na-rich regolith surrounding the lakes, whereas the pearl bluebush colonise Ca-rich soils of the eastern plains (Figure 6.21).

Higher Pb concentrations in woody cassia samples from adjacent to the unsealed road are probably a result of aeolian contamination from the road (Figure 6.30). Higher Pb concentrations in woody cassia near the saline lakes could be due the association with salts. The Gawler Range Volcanics are relatively undeformed (Allen *et al.* 2008) and the thick volcanic sequence masks the underlying deformed geology (Rajagopalan *et al.* 1993). The aeromagnetic signature associated with the high Pb in plant results from the

east is broad and positive, whereas high Pb in plant results from the west are underlain by deformed bedrock (e.g., complex aeromagnetic response). It is therefore unlikely that the area high Pb in plant results in the east are an expression of unmapped GRV.

Two seasons, two techniques

Conducting a survey over two seasons has implications for biogeochemical sampling due to climatic changes (rainfall and temperature) and the plants' response to these. The same analytical laboratory was used for biogeochemical analysis of samples collected in February and June of 2011. Major elements (Al, K, Ca, and Fe) do not differ significantly across the seasons. More significant variation in the biogeochemistry is caused by the Na/Ca potential from E-W (regolith geochemistry) and the change in plant species.

Regolith geochemical analysis was conducted by two different analytical laboratories. Laboratory selection in this case was at the discretion of the company geologist. This was not problematic for major elements (e.g., Al, K, Ca, and Fe) at Area-3 due to the high concentrations in the sampling material (measured as %; Appendix B), but is a problem for trace elements. Trace element geochemistry has a contrast over the season boundary caused by the lower analytical detection limits and the suite of elements that differ between the two laboratories. For example, Pb concentrations are slightly higher in the regolith samples from the east (June 2011) and contrast against lower concentrations of samples from the western sampling program (February 2011). Ideally the same laboratory should be used and the submission of standards with the unknowns (samples) is recommended to calculate calibration factors and adjust the data for each analytical batch.

Implications for exploration at Area-3

Angular fragments of Gawler Range Volcanics (GRV) are widespread in the NE corner of Area-3 suggesting that GRV is present at shallow depth, although not encountered in augering for calcrete. There are some isolated exposures of GRV. High concentrations of Pb in pearl bluebush delineate the GRV in Area-3 according to the positive response on the aeromagnetic image (Figure 6.30). The low Au concentrations in the sampling materials (up to 1.3 ppb in plants and 5 ppb in regolith samples; Figure 6.28) collected from overlying the GRV are inconclusive of underlying mineralisation or even laterally transported signatures of distal mineralisation. The potentially thick sequence of GRV (e.g., up to 1000 m; Allen *et al.* 2008) is thought to be impermeable and that the base of this sequence is a favourable interface for the concentration of mineralising fluid and the precipitation of Au (Potma & Zhang 2006). It is unlikely that mineralisation concealed beneath the GRV would be expressed geochemically in the regolith unless the mineralising fluids have permeated the GRV along fractures (e.g., Yarlbrinda Shear Zone). The use of surface geochemical methods in the NE of Area-3 (over GRV) has been inconclusive and is likely an ineffective exploration approach.

The highest Au concentrations in plant and calcrete samples (< 6 ppb) align with an area of previously defined high Au concentrations in calcrete (Dominion Mining Ltd., 1996) – there appear to be no reported drilling activity for this anomaly. This small area of anomalous Au concentration in regolith and plant samples is in a favourable structural

setting next to a dolerite dyke (Gairdner Dyke Swarm) for potential Au mineralisation even if it is sub-economic (e.g., Gairdner Dyke in the Glenloth goldfield).

6.4.4. Area-7

Sample locations and species distribution at Area-7 are illustrated in Figure 6.32. The geology of Area-7 is interpreted (at 1:2M scale) as Mulgathing Complex and Hiltaba Suite (Figure 6.32), although much of this is untested by drilling. There are some previous mineral exploration drill holes surrounding Area-7 (none within Area-7) from the 1980s that targeted Au and sedimentary U mineralisation. Drill holes that were targeting U intersected bedrock at 30 m (Figure 6.32; Styles 1980, pp.85, 95-96).

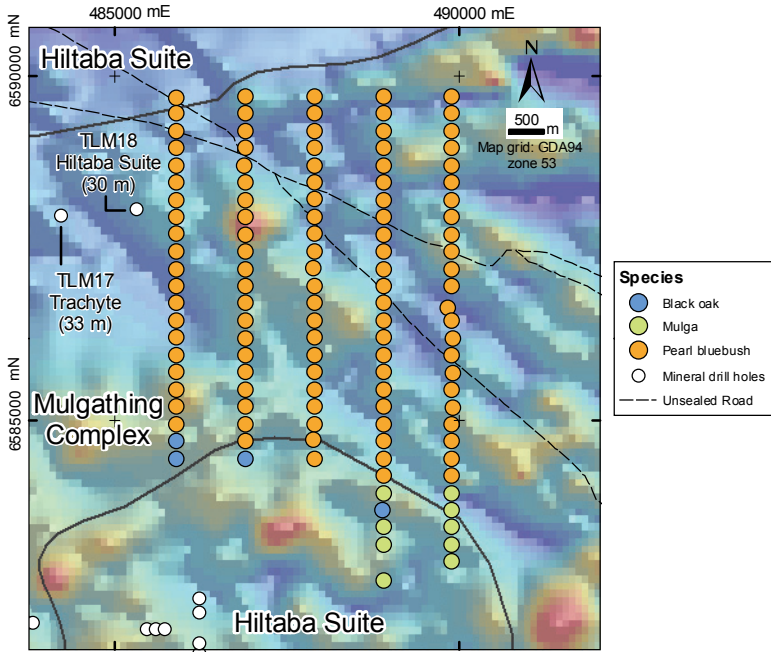

Figure 6.32: Sample locations in Area-7 coloured by species. 1:2M-scale geology, drill hole locations and aeromagnetic image are from SARIG (2012).

Area-7 regolith geochemistry

Road and railroad infrastructure in Area-7 restricted the access of the vehicle-mounted auger to sample locations and prevented the collection of some regolith samples on the regular grid pattern (e.g., Figure 6.33). Biogeochemical samples were collected at these locations. The longer two eastern traverses were conducted first and terminate at the south in the dunes at the edge of the Great Victoria Desert. Regolith samples from the dunes were collected at depths exceeding 2 m and the Ca concentrations for these samples is low (< 10%; Figure 6.33). Poor calcrete development and difficulty mobilising the auger within the dunes meant the subsequent western traverses terminate on the sheet wash plains.

Regolith samples contain between 1.5 – 23% Ca (typically > 21%; 95th percentile) and between 0.7 – 2.4% Fe (Figure 6.34). Calcium has a positive association with P, Cd, As, and Au, and has a negative association with Ce and La. Elements that are below analytical detection limits in all samples from Area-7 are Re (0.05 ppm) and Te (0.05 ppm).

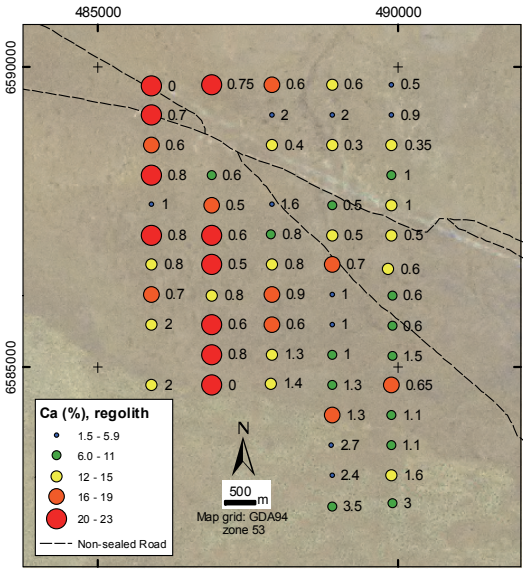

Figure 6.33: Ca in regolith at Area-7 labelled by depth of collection (m).

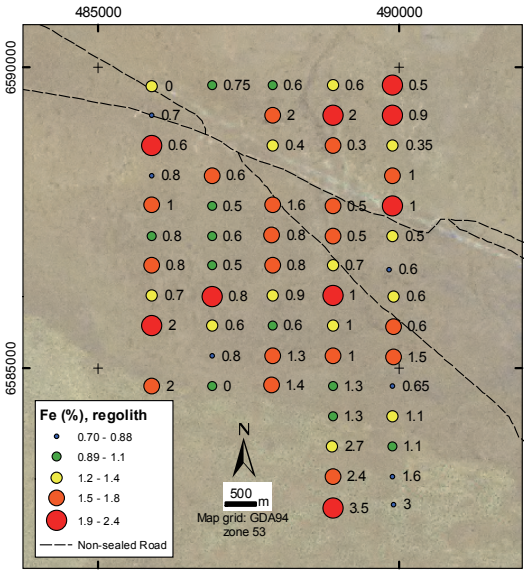

Figure 6.34: Fe in regolith at Area-7 labelled by depth of collection (m).

Gold and gold-associated elements

Regolith samples from Area-7 have between 1 – 6 ppb Au but typically have < 5 ppb Au (95 percentile; Figure 6.35). Samples with the highest Au concentrations are from the west and are underlain by bedrock interpreted broadly as Mulgathing Complex by Fairclough & Schwarz (2003). Gold in the regolith has a positive association with Ca, Cd, Co, Cu, P, Se, and Sr. The highest Ag concentrations in regolith samples from Area-7 align with the linear features on the aeromagnetic image and are generally higher the NE (Figure 6.36).

Elements associated with mineralisation at Glenloth and Earea Dam goldfields (Ag, Au, Bi, Cu, Sn, U) have a minimal association with Au in regolith samples from Area-7. Bismuth and Sn have a strong positive correlation (R=0.7) and there is a slight correlation between Au and Cu (R=0.5). Tellurium concentrations are below analytical detection limit (0.05 ppm) for all regolith samples.

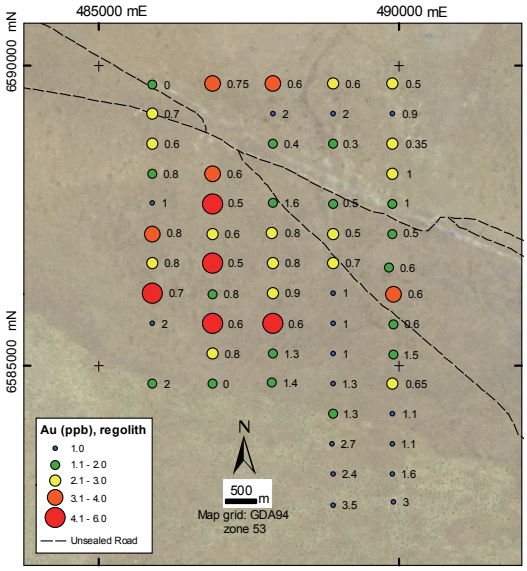

Figure 6.35: Au in regolith at Area-7 labelled by depth of collection (m).

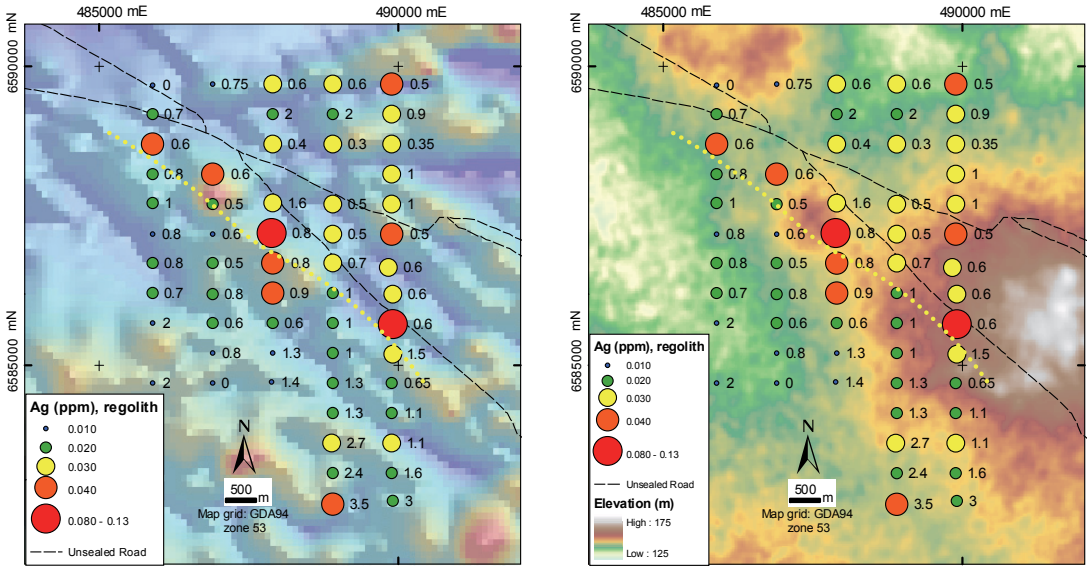

Figure 6.36: Ag in regolith samples at Area-7 on the state aeromagnetic image (left) and the 1-second DEM (right). Yellow dotted line indicates a region of high Ag in plant and regolith results that align with bedrock structure (indicated by the aeromagnetic image) and a local drainage divide (DEM).

Area-7 biogeochemistry

Gold and gold-associated elements

Gold concentrations in pearl bluebush, mulga, and black oak are between < 0.2 – 1.1 ppb but are typically < 0.8 ppb (95 percentile; Figure 6.35). Pearl bluebush have the highest concentrations of Au. The highest Au results occur in sequence for more than 20 samples on the eastern-most traverse (Figure 6.37). The sample that is lowest in the sequence is from the NE corner and the sample number inscrease towards the south (e.g., A7001 … A7028). Other high Au results in the four western traverses are irregularly distributed.

Silver concentrations in plants are between 2 – 11 ppb but are typically < 8.8 ppb (95 percentile; Figure 6.36). Pearl bluebush have higher Ag concentrations than black oak and mulga. High Ag concentrations (7 – 11 ppb) in adjacent samples are systematically 10 –

15 samples apart in the sequence (Figure 6.36). Higher Sn results occur in sequence for 2 – 5 samples and have a similar distribution to the Ag results. Bismuth, Sn, and Te have a poor relationship with Au. Samples with detectable concentrations of Te (0.02 – 0.06 ppm) are all from the SW of the drainage divide. Uranium is below the analytical detection limit (0.01 ppm) for all but one sample.

Other elements

Contamination indicator elements Fe and Zr have a strong correlation (0.95). The highest Fe and Zr results (0.13% and 1.1 ppm) are from a pearl bluebush sample < 2 m from an unsealed track. This sample contains 0.7 ppb Au, and 0.02 ppm U – the only sample to contain U at a concentration above the analytical detection limit (0.01 ppm). High Pb results are from the western part of Area-7 (up to 3 ppm; Figure 6.40).

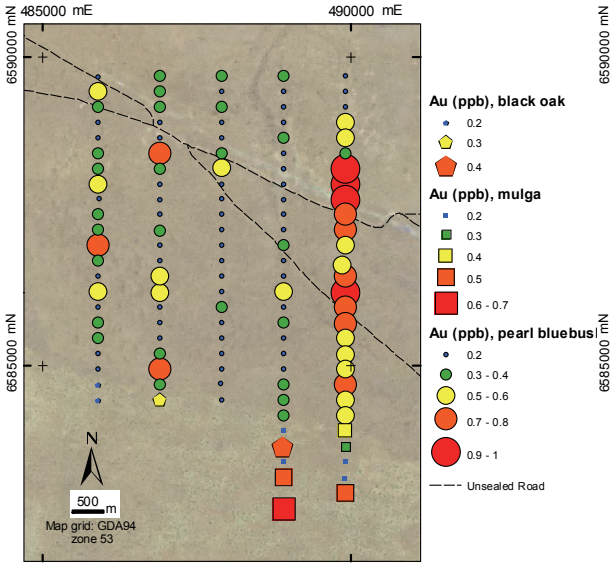

Figure 6.37: Au in plants at Area-7 on the Landsat TM.

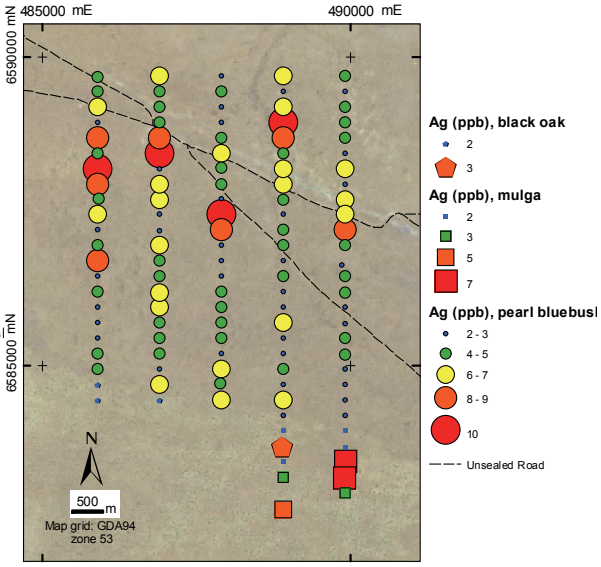

Figure 6.38: Ag in plants at Area-7 on the Landsat TM.

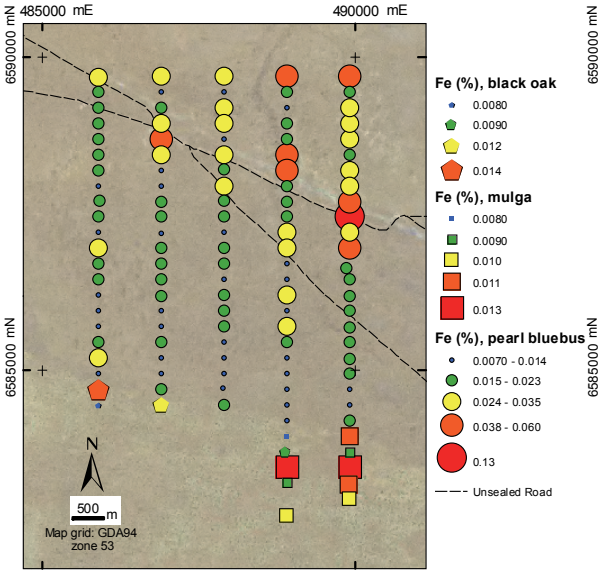

Figure 6.39: Fe in plants at Area-7 on the Landsat TM.

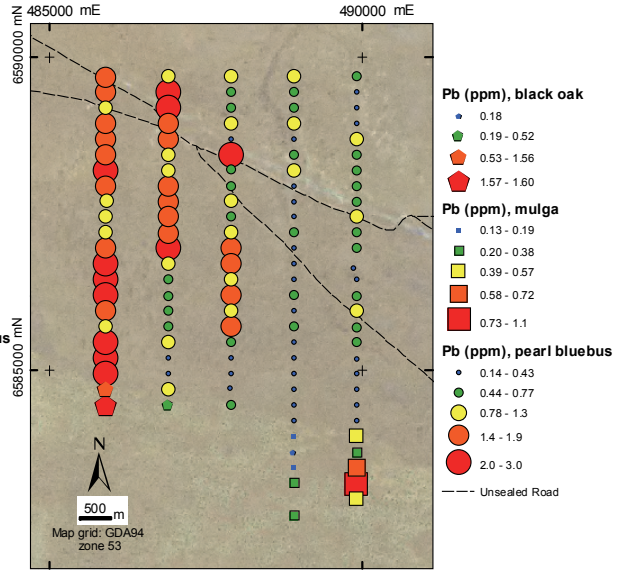

Figure 6.40: Pb in plants at Area-7 on the Landsat TM.

Area-7 discussion

Landscape controls

The geology of Area-7 is broadly defined as Mulgathing Complex and Hiltaba Suite (Figure 6.19). These lithologies are not expressed by regolith geochemistry or biogeochemistry. The geological map units are more geologically complex than what is represented by the 1:2M scale map polygons. A a close association with regolith geochemistry or biogeochemistry is therefore unlikely. High Pb-in-plant results in Area-3 are characteristic of the Gawler Range Volcanics (GRV; Figure 6.30) but this does not appear to be the cause of anomalous Pb at the western part of Area-7 (Figure 6.40). Gawler Range Volcanics are generally undeformed (e.g., Figure 6.31; Blissett *et al.* 1993, Allen *et al.* 2008) and have a positive magnetic response that can mask underlying

deformed geology (Rajagopalan *et al.* 1993) – the aeromagnetic response at Area-7 does not suggest GRV. It is possible that the Pb-in-plant results at Area-7 are an expression of concealed geology (as for Area-3) and are constrained to the SW catchment area (Figure 6.41). It is also possible that the high Pb results are instead caused by analyte carry over during analysis due to high Pb concentrations in the reference materials or samples (e.g., Rodushkin & Axelsson 2000).

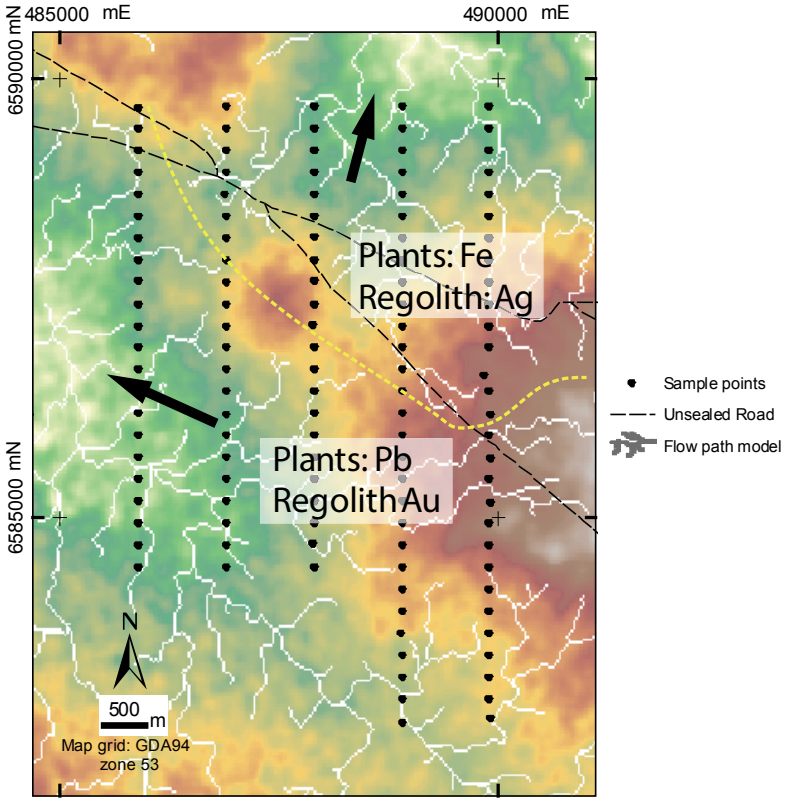

Figure 6.41: Sample points at Area-7 on the Digital Elevation Model and derived flow path model. Yellow line marks the local drainage divide and black arrows denote dominant transport vectors.

Regolith samples with high Ag (> 0.04 ppm) are collected from depths > 0.6 m along an area of elevated topography (dotted yellow line, Figure 6.36). Regolith and plant samples NE of the dotted line have higher concentrations of Ag and could be a result of a dominant physical or hydromorphic dispersion towards the NE. High Au-in-regolith results are constrained to SW catchment. Drainage into this catchment originates from along the drainage divide (dotted yellow line, Figure 6.41) and in the sand dunes to the south (outside the survey area; Figure 6.41).

Problems with biogeochemical data

Biogeochemical results from near the unsealed Glendamo-Tarcoola road show contamination by Fe, Zr, Co, and U. The highest concentrations of these elements are measured in samples near the intersection of the road and railway (eastern traverse; e.g., Figure 6.39) where vehicles braking and accelerating have generated dust. Gold concentrations are also slightly higher near the road. This could be attributed to detrital contamination but the long sequence of high results is suggestive of an analytical issue.

High Au concentrations in plants along the eastern-most traverse (Figure 6.37) indicate that there is an analytical issue for the Au biogeochemical data at Area-7. Higher Au results are from adjacent the unsealed road but the contiguity of the anomalism along the traverse in number sequence is possibly an error introduced during the analysis. It is possible that analyte carry-over within the ICP-MS instrument has occurred during sample analysis. Similar carry-over issues are discussed by Rodushkin & Axelsson (2000). High Ag concentrations are systematically 10-15 samples apart (Figure 6.38) in sequence. The highest Ag-in-plant result at Area-7 is 11 ppb whereas the reference materials (V14 and V16) used by the analytical laboratory during biogeochemical analysis contain 24 and 32 ppb Ag. The high Ag concentrations in reference materials could have been retained in the analytical cell and has carried over to the analysis of samples.

Implications for exploration at Area-7

The Au concentrations in regolith and plant samples at Area-7 are low compared with sites of known mineralisation (e.g., Tunkillia, and Glenloth and Earea Dam). Gold-in-regolith results up to 6 ppb are constrained to the SW catchment area but do not form a contiguous anomaly: regolith samples with low Au concentrations (2 – 3 ppb) occur between the high Au concentrations (Figure 6.35). Lateral variation at this sample spacing is possible. For example, calcrete samples collected over the Glenloth goldfield using 500 m spacing typically have < 6 ppb Au, but can exceed 10 ppb Au in spot samples (SARIG 2012). Biogeochemical sampling has some positive Bi, Sn, and Te anomalies (all associated with mineralisation at the Earea Dam and Glenloth goldfields; *Section 6.1.2*) but Au concentrations are low in these samples.

The SW catchment is in the head waters of a palaeo-channel that is locally up to 30 m deep (Styles 1980). It is possible that the Au in regolith is locally sourced from the drainage divide where the high Ag results occur, or is laterally transported from the dunes along drainage depressions (Figure 6.41). Calcrete development diminishes towards the south in the dunes (e.g., SE samples, Figure 6.33). Follow-up calcrete sampling towards the south would likely yield Ca-poor regolith samples. Furthermore, vehicle access to the dunes would be difficult and destructive.

6.4.5. Glenloth North

Glenloth North regolith geochemistry

Regolith was geochemically sampled on a 500 by 1000 m grid pattern except where exposed silcrete prevented auger penetration near areas of high local topography. In these locations, the soil profile is thin and calcrete development is typically limited to coatings on the silcrete. Calcium-rich regolith samples (> 10%) are from the slopes of the silcrete plateau (Figure 6.42) and collected from depths < 1.3 m. Regolith samples from the topographic lows have higher Fe concentrations (Figure 6.43) and represent samples collected from depths > 1.3 m. Deeper samples generally have higher concentrations of Bi, Hf, Mo, Th, V, and Zr.

Gold and gold-associated elements

Regolith samples have between 1 – 11 ppb Au (Figure 6.44). Samples with higher Au concentrations are more calcareous (Figure 6.20) and are from areas of higher topography (Figure 6.44). The highest Au concentration (11 ppb) is in sample GL153 from the southern margin of the survey area (Figure 6.44). Sample GL153 has 2 ppm Te. Tellurium results are higher (up to 7 ppm) in the SE corner of Glenloth North. High Ag results (up to 0.2 ppm) are from a drainage depression downslope to the north of the highest Au-in-regolith results (Figure 6.45).

Other elements

Regolith samples from Glenloth North have the highest concentrations of Ni (108 ppm), Cu (43 ppm), and Te (7.6 ppm). The Lake Harris Komatiite mapped in the eastern part of Glenloth North is distinguished by high concentrations of Cr and Ni (e.g., Figure 6.46). Other greenstone pathfinder elements (e.g., Mg, As, Co, Fe, and Mn) are sporadic and do not delineate the Lake Harris Komatiite. Copper results are also sporadic.

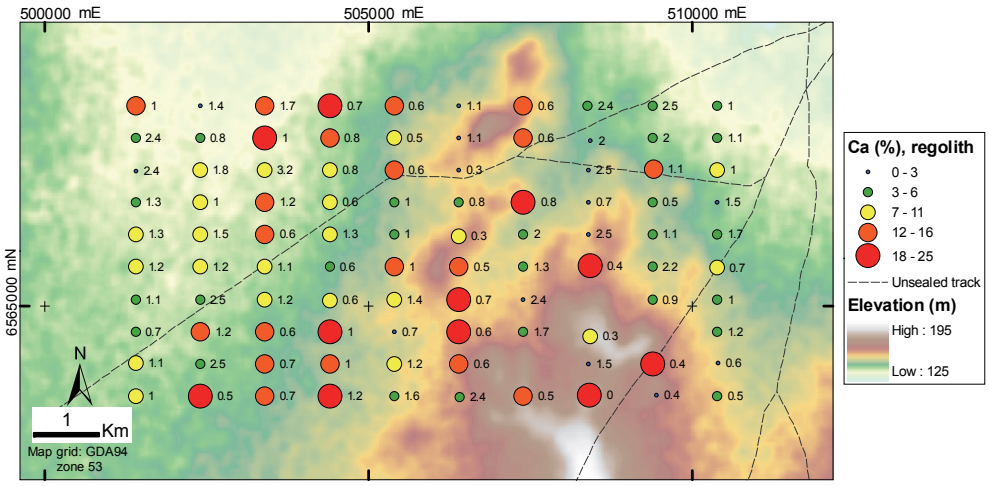

Figure 6.42: Ca in regolith samples from Glenloth North on the Digital Elevation Model (DEM). Points are labelled by depth of collection (m).

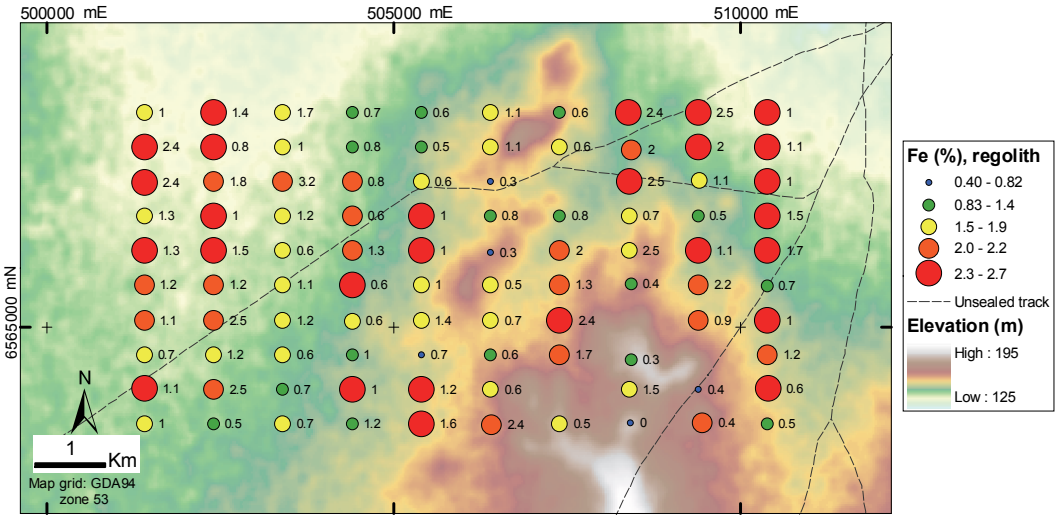

Figure 6.43: Fe in regolith samples from Glenloth North on the Digital Elevation Model (DEM). Points are labelled by depth of collection (m).

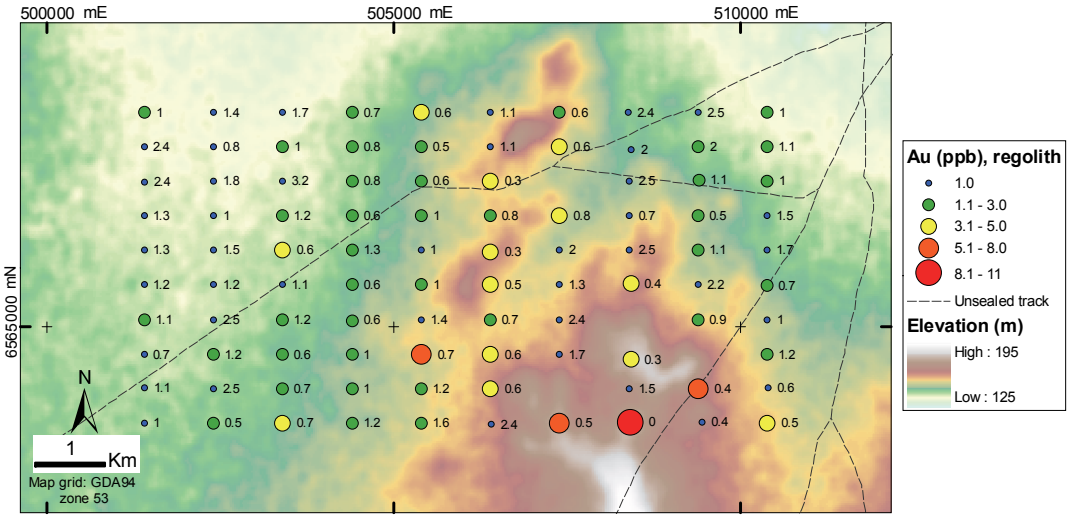

Figure 6.44: Au in regolith samples at Glenloth North on the Digital Elevation Model (DEM). Points are labelled by depth of collection (m).

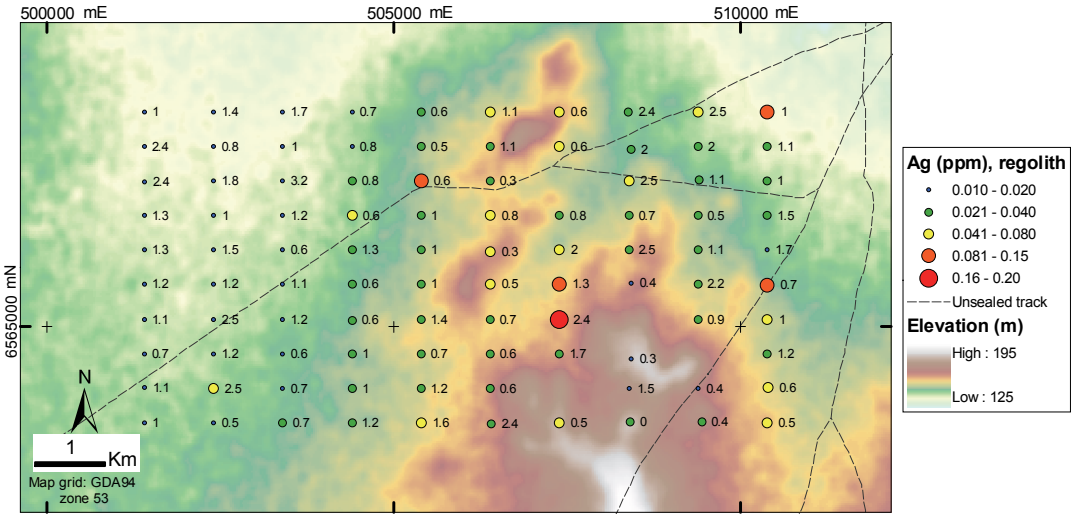

Figure 6.45: Ag in regolith samples at Glenloth North on the Digital Elevation Model (DEM). Points are labelled by depth of collection (m).

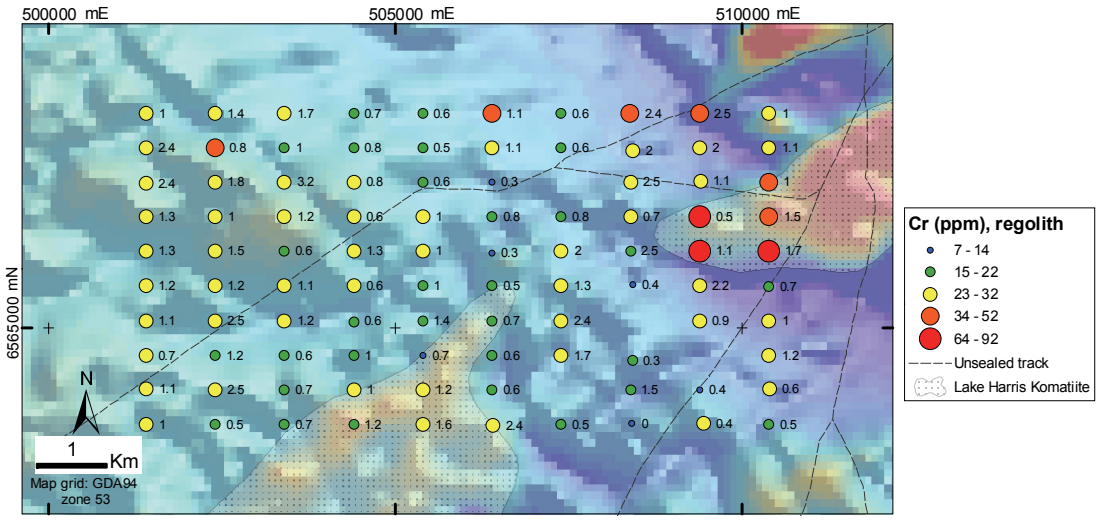

Figure 6.46: Cr in regolith samples at Glenloth North on the state aeromagnetic image. Points are labelled by depth of collection (m).

Glenloth North biogeochemistry

Gold and gold-associated elements

Pearl bluebush samples contain between 0.2 – 1.3 ppb Au, although concentrations are typically < 0.5 ppb (95 percentile; Figure 6.47). The highest Au result (1.3 ppb) aligns with a 5 ppb Au-in-calcrete result and is 500 m from an unsealed track (Figure 6.47). Bismuth and U (consistent biogeochemical indicators of mineralisation in the Glenloth goldfield, *Section 6.1.2*) concentrations are near or below the analytical detection limits at Glenloth North: 4 samples have detectable concentrations of Bi (0.03 – 0.05 ppm). Elements that have concentrations below the analytical detection limits for all samples are: Be (0.1 ppm), In (0.02 ppm), U (0.01 ppm), V (2 ppm), and W (0.1 ppm).

Samples from drainage depressions throughout Glenloth North area have markedly higher concentrations of P and Zn (Figure 6.48). Samples from the drainage depressions in the eastern part of the area have higher concentrations of Ag (14 – 250 ppb; Figure 6.49). Silver results ≤ 13 ppb are irregularly distributed across the area (Figure 6.49).

Other elements

Pearl bluebush samples with > 1.1 ppm Ni in the eastern-most traverse are characteristic of the Lake Harris Komatiite (Figure 6.50). This includes the sample marked by the black arrow (Figure 6.50) that is from an area with a positive aeromagnetic response that is similar and adjoining to the area mapped as Lake Harris Komatiite. Other isolated samples with > 1.1 ppm Ni are from areas that have a weaker aeromagnetic response and are from within broad drainage depressions (western lines) and near an unsealed track (SE corner).

Elements that are typically associated with detrital contamination (Al, Fe, Hf, Th, Zr) have a strong correlation (> 0.9) with REEs (La, Ce, and Y) and have higher concentrations in samples from the east (e.g., Fe; Figure 6.51).

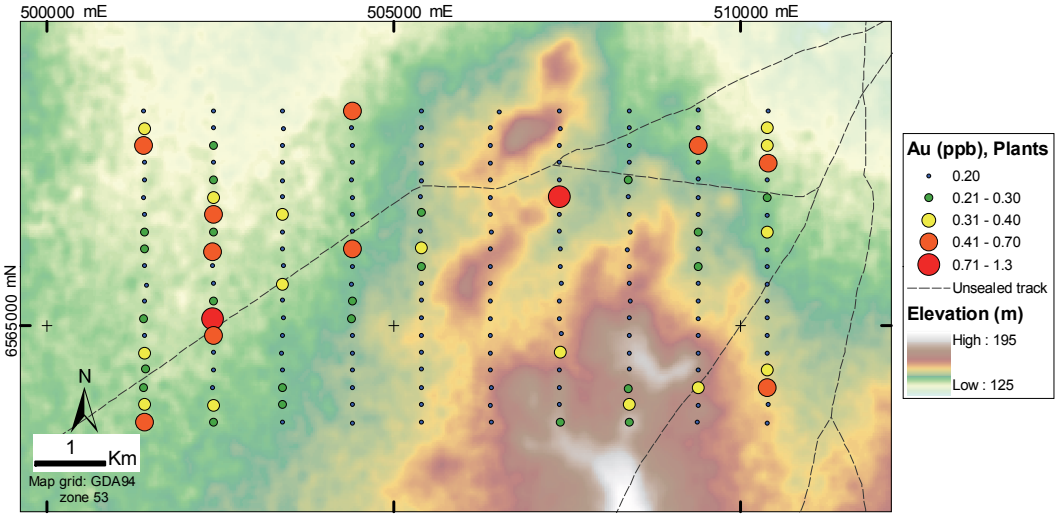

Figure 6.47: Au in pearl bluebush leaf/twig samples at Glenloth North on the Landsat TM.

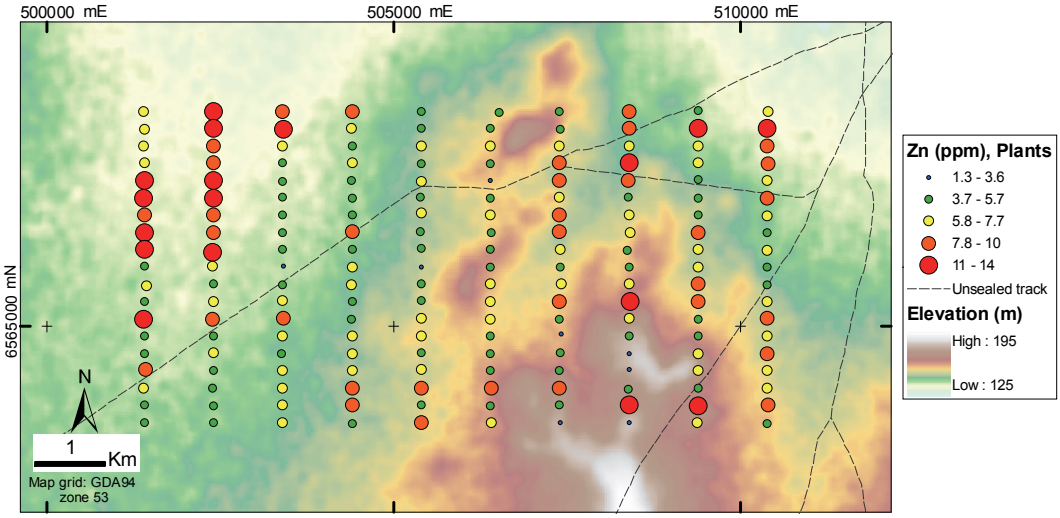

Figure 6.48: Zn in pearl bluebush leaf/twig samples at Glenloth North on the Landsat TM

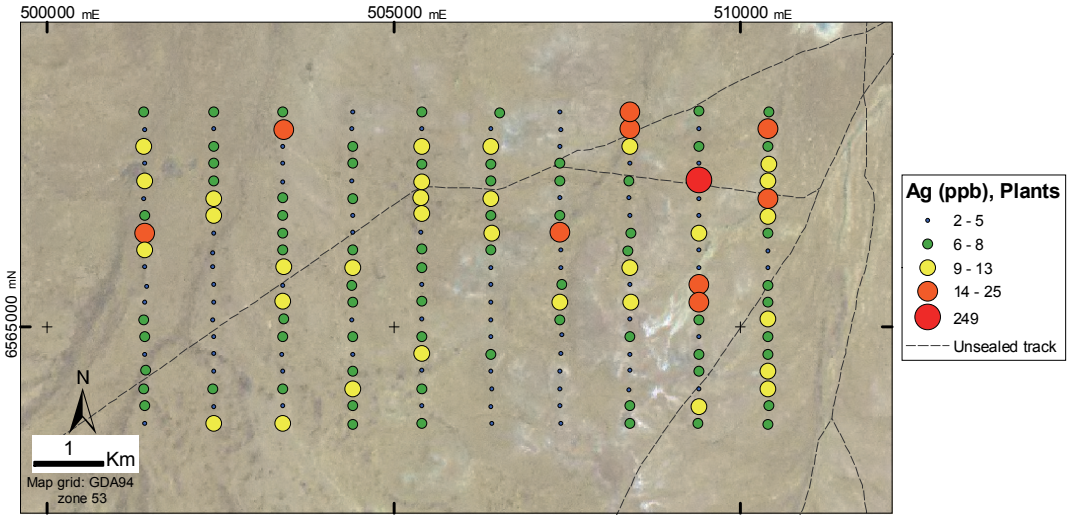

Figure 6.49: Ag in pearl bluebush samples at Glenloth North on the Landsat TM.

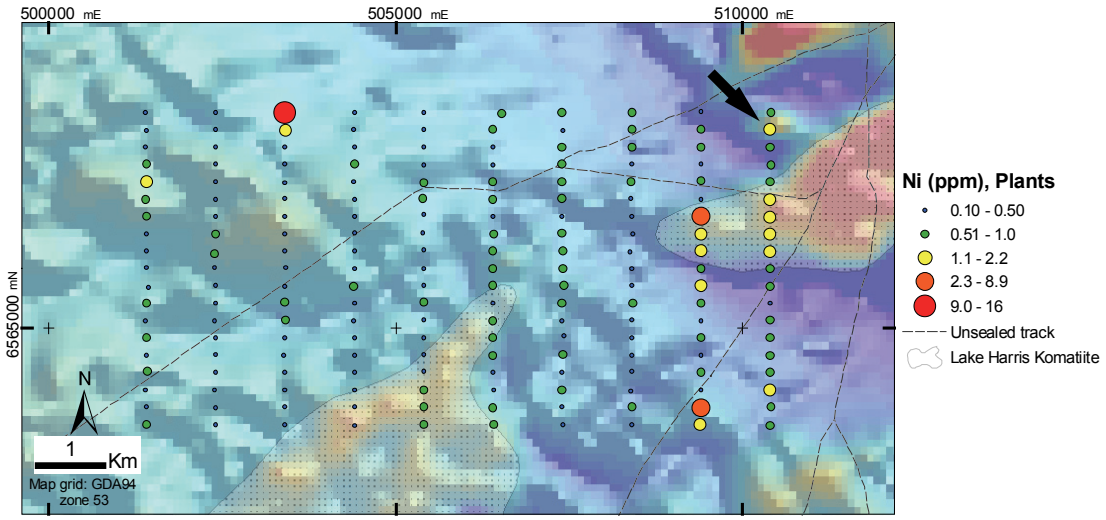

Figure 6.50: Ni in pearl bluebush samples at Glenloth North on the state aeromagnetic imagery.

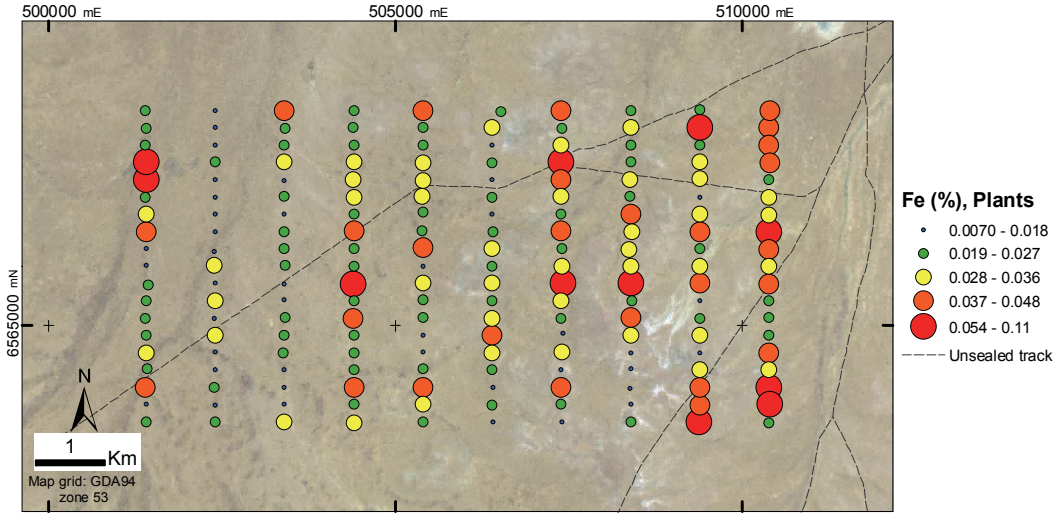

Figure 6.51: Fe in pearl bluebush leaf/twig samples at Glenloth North on the Landsat TM

Glenloth North discussion

Landscape controls

The silcrete plateau and exposed saprolite is the dominant landscape control on physical and hydromorphic dispersion in the Glenloth North survey area. Calcrete development is variable as indicated by the Ca-in-regolith results. Calcium-poor regolith samples are from the drainage depressions (Figure 6.33) and have higher concentrations of Fe, P, Zn, and Ag. Higher P and Zn in these samples probably represent the increased abundance of Fe-oxides. Some regolith samples collected from the silcrete plateau have low Ca and Fe. These samples are presumably Si-rich although Si is not included in the analytical suite.

The high Ag-in-regolith result is down-slope of the high Au-in-regolith results (Figure 6.52). Silver is readily mobilised in the regolith (Lintern 2004b, Lintern *et al.* 2011) and is possibly a laterally transported expression of Au results. It is likely that the Au in regolith is locally sourced as the samples are collected from the plateau.

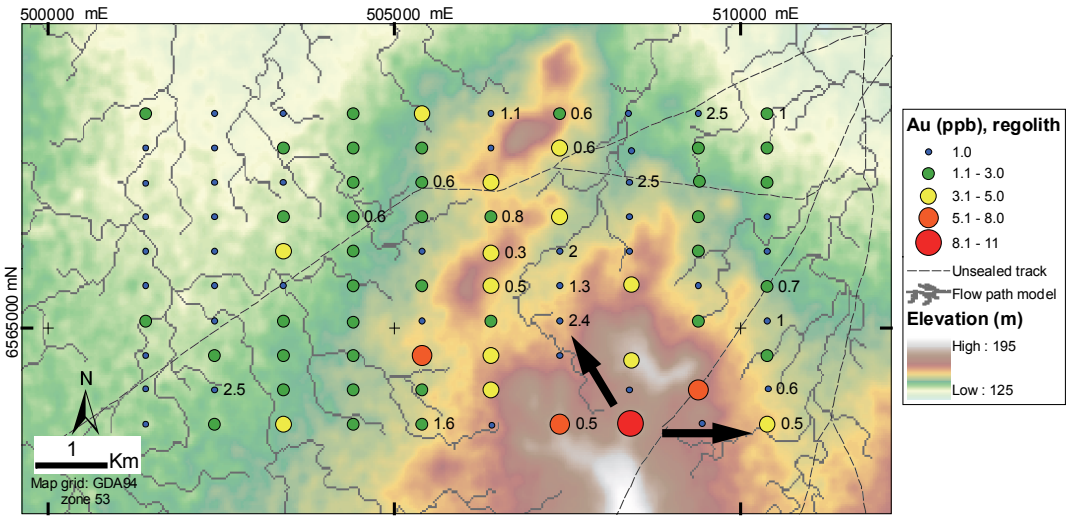

Figure 6.52: Au in pearl bluebush leaf/twig samples at Glenloth North on the Digital Elevation Model and derived flow path model. Samples are labelled by Ag concentration (ppm). Arrows indicate regolith transport direction.

Implications for exploration at Glenloth North

The Lake Harris Komatiite in the eastern part of Glenloth North is distinguished by high Cr and Ni concentrations in regolith, and high Ni concentrations in plants. The sedimentary cover in the area could be more than 10 m thick (Sheard & Robertson 2004) yet there is still a strong geochemical expression. The komatiite is also mapped in the central southern part of the survey area but has no surface biogeochemical or geochemical expression. The aeromagnetic response of this body is diminished, which could represent a subtle difference in lithology.

A hand sample of the saprolite exposed at Glenloth North (sample GL195a; 510430 mE, 6563780 mN, GDA94 zone 53) was tested for Rb using an Olympus DeltaX pXRF. Rubidium concentrations > 150 ppm in the saprolite were found to represent white mica at the Tunkillia Au Prospect (*Section 5.1*). The sample collected from Glenloth North had < 40 ppm Rb (< 10 ppm Rb in whole rock ICP-MS analysis) suggesting a low presence of white mica. White mica may not represent the alteration style associated with mineralisation in this area as it does at the Tunkillia Au Prospect.

6.4.6. Conclusion: Implications for mineral exploration

Targeting a consistent sampling material (geochemical and biogeochemical) in the plains to the west of Lake Harris is problematic, as demonstrated in Area-3, Area-7 and Glenloth North. Geochemical sampling of regolith at < 1 km spacing did not reveal any highly elevated Au results. Two areas warrant further investigation due to elevated Au-in-regolith results (5 – 10 ppb) at Area-7 contained within a catchment, and, Area-3 near the Tarcoola-Glendambo road. Biogeochemical sampling reiterates the Au-in-calcrete anomaly at Area-3 but is generally inconclusive of mineralisation. Biogeochemical sampling delineates geology at Area-3 and Glenloth North and possibly Area-7 but the biogeochemical data from Area-7 appears to have problems with detrital contamination, and contamination during ICP-MS analysis.

6.5. Greenfields exploration: Yellabinna Regional Reserve

6.5.1. Landscape and geological setting

Landscape

The Yellabinna Regional Reserve is dominated by longitudinal sand dunes of the Great Victoria Desert – a similar landscape setting to the Tunkillia Au Prospect 50 km NW. Deception Hill is the highest landmark (179 m) and is an irregular occurrence where bedrock is exposed (SARIG 2012; Figure 6.53). Dune swales are generally sand plains (e.g., ISps, Figure 4.5) except where massive silcrete is exposed in some swales of the west-most traverse (428970 mE, 6584330 mN, GDA94 zone 53). The dunes diminish to the north and east of the survey area. Surrounding Deception Hill is the prominent Kingoonya and Tolmer palaeo-channels (Figure 8.30; Hou & Alley 2003, Hou 2008). The Kingoonya palaeo-channel is locally characterised by evaporite-dominated sediments, and sequence of ephemeral saline lakes, whereas the Tolmer channel is more obvious to the south of the Yellabinna study area.

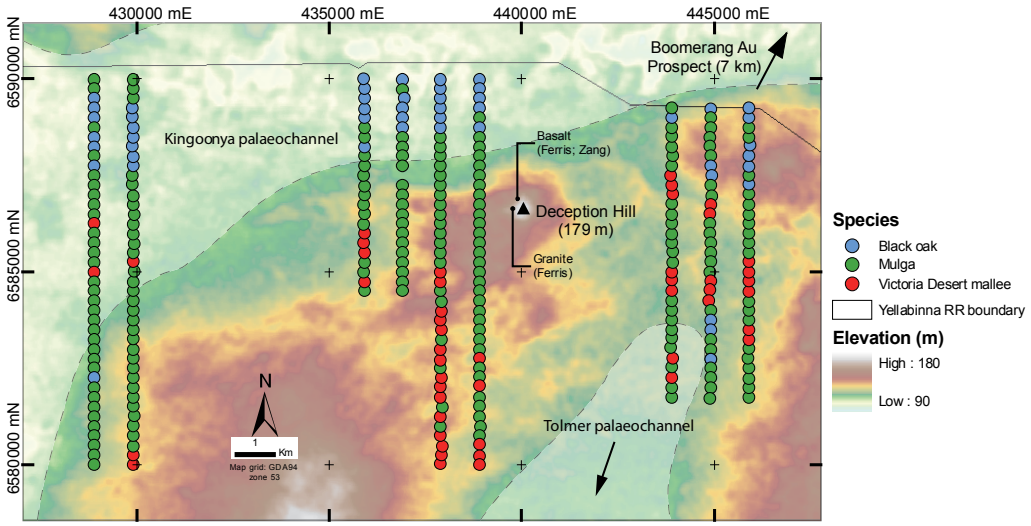

Figure 6.53: Palaeochannels associated with the Yellabinna study area (Hou & Alley 2003).

Geology

Granite and basalt lag have been identified 500 m from Deception Hill (Figure 6.54) and geology in the immediate area is interpreted as South Lake Gabbro of the Mulgathing Complex. Basement geology is concealed by regolith away from Deception Hill and has been interpreted as largely being the late Archean Mulgathing Complex. The Complex consists of the Christie Gneiss (host rock of Challenger Au deposit), Kenella Paragneiss, and mafic–ultramafic rocks of the Lake Harris Komatiite (Figure 6.54; Daly & Fanning 1993, Swain *et al.* 2005).

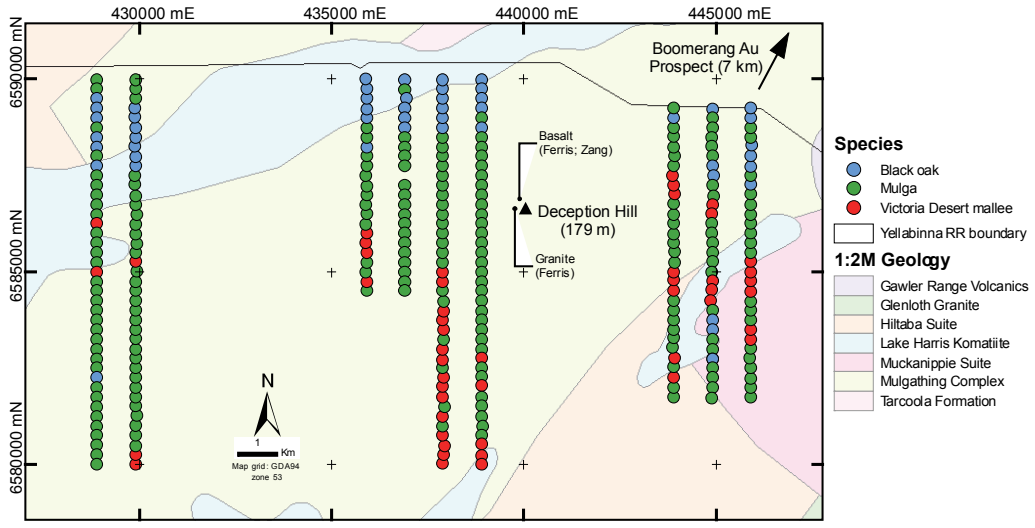

Figure 6.54: Sample locations, by species, in the Yellabinna Regional Reserve, and 1:2M-scale geology from South Australian Resources Information Geo-server.

Previous exploration

Calcrete sampling was conducted in the north-eastern Yellabinna Regional Reserve in the late 1990s at 800 by 3000 m spacing (McConachy 2001). Exploration efforts in the region have since been limited due to difficult access within the dunes, poor calcrete development, and, subsequently inconclusive geochemical results. The reconnaissance calcrete sampling program involved the collection (by hand auger) of 77 regolith samples that were geochemically analysed for Au, Ca, Mn, Fe, Co, Ni, Cu, Zn, As, Mo, Ag, Pb, Bi, and U (McConachy 2001). Calcium was typically low (≥ 10% in only 10 samples) corroborating with the sample morphology description (e.g., 'sand' or 'sandy'). Gold concentrations were also low (0 – 5 ppb), although higher Au concentrations were associated with higher Ca content (c. 20 %).

The Boomerang Au Prospect is 7 km NE of the Deception Hill survey (Figure 1.1). Drill testing at the Boomerang Au Prospect identified high concentrations of Au, Co, and Ni (Grenfel Resources NL 1997). Significant drilling results include several metres with concentrations of Au between 3 – 11 ppm (at depths 30 – 70 m), and up to 0.5% Zn and 0.35% Pb (Ferris *et al.* 2003). Biogeochemical sampling of pearl bluebush over the Boomerang Au Prospect was unable to delineate mineralisation (Lintern *et al.* 2006b). Gold concentrations in plant tissue were between 0.15 – 1.1 ppb but, surprisingly, Co is not included in the analytical suite for the biogeochemistry.

Yellabinna study

This section includes a discussion of plant biogeochemistry and partial extraction soil geochemistry of samples collected in the northern Yellabinna Regional Reserve near Deception Hill (Figure 6.53). A total of 303 samples of the most widespread and abundant species were collected at a 250 by 1000 m spacing for biogeochemical analysis: 205 mulga (*Acacia spp.*) phyllodes; 50 black oak (*Casuarina pauper*) branchlets; and, 48 Victoria Desert mallee (*Eucalyptus socialis*) leaves (Figure 6.53). Soil samples were collected from adjacent to every second biogeochemical sample with a resultant spacing

of 500 by 1000 m. A total of 141 soil samples were geochemically analysed for partial extraction geochemistry of weakly bound cations.

6.5.2. Results

Biogeochemistry

Elements that are below analytical detection limits for all samples are: Al (0.01%), Be (0.1 ppm), Ga (0.1 ppm), In (0.02 ppm), Nb (0.01 ppm), Pt (1 ppb), and V (2 ppm). Mulga are the most widespread species (Figure 6.53) and contain the highest concentrations of Au (1.1 ppb), Ag (12 ppb), Cu (22 ppm) and Re (550 ppb). Black oak branchlets and Victoria Desert mallee leaves contain Au at concentrations up to 0.8 ppb and 0.7 ppb (Figure 6.55). Samples have low concentrations of U (< 0.14 ppm), Te (< 0.07 ppm), Sn (< 0.12 ppm) and Bi (0.09 ppm). Tin and Bi do not exhibit any trends associated with topography or soil geochemistry. High concentrations of Sn and Bi occur periodically as groups in sequence.

Samples from around Deception Hill have elevated concentrations of Cu, Hg, Ni, Tl, and Zn. Copper forms an inner halo and Ni forms an outer halo around a Tl and Zn core with a diameter of approximately 2 km. Rhenium concentrations are between 1 – 550 ppb (Figure 6.56). Rhenium normally follows PGE, REE and Mo (Kabata-Pendias & Pendias 2001, Dunn 2007, Scott 2009) in rocks, but this relationship is not apparent in the biogeochemical data. Silver and Re results have a similar distribution near Deception Hill (Figures 6.56 & 6.57).

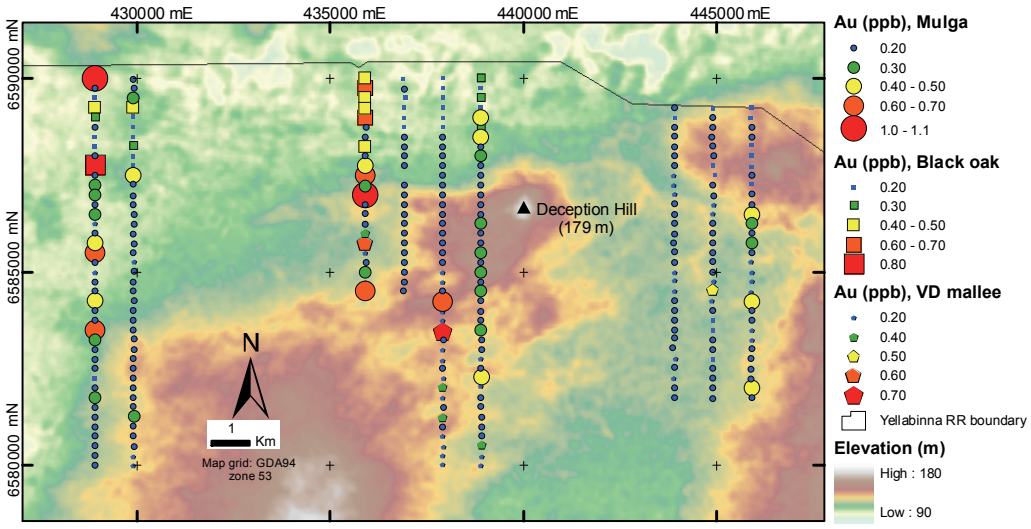

Figure 6.55: Au concentrations in plants within the Yellabinna Regional Reserve on the 1-second DEM.

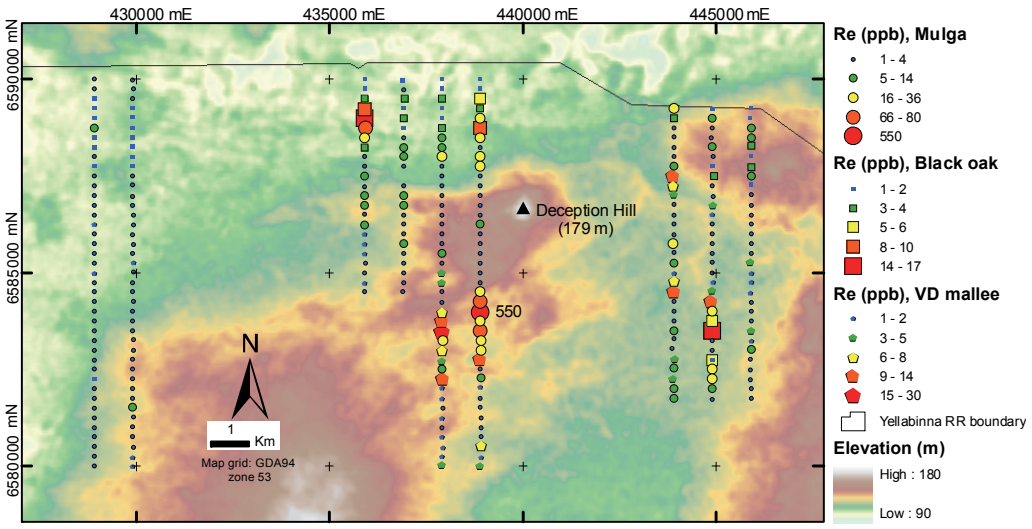

Figure 6.56: Re concentrations in plants within the Yellabinna Regional Reserve on the 1-second DEM.

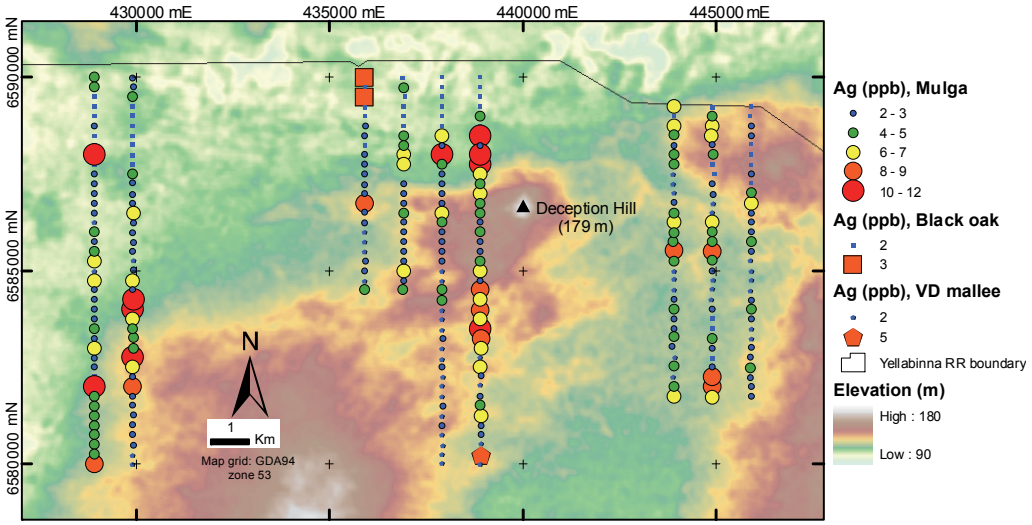

Figure 6.57: Ag concentrations in plants within the Yellabinna Regional Reserve on the 1-second DEM.

Plants: greenstone indicator elements

Geochemical indicators for mafic rock types (e.g., greenstone) include Mg, Cr, Ni, As, Co, Fe, and Mn. Magnesium is a macronutrient for plants and the samples have up to 0.47% Mg: there are no trends indicative of landscape or bedrock controls on Mg. Nickel, Mn and Co results exhibit similar spatial trends. The highest Ni results are from the NE corner of the survey and are associated with a local topographic high (Figure 6.58). Other high Ni results surround Deception Hill (lowest Ni result from nearest to Deception Hill), particularly to the SW and are coincident with the area of high concentrations of Re and Ag in plants (Figures 6.56 & 6.57).

Chromium concentrations are between 0.4 – 1.9 ppm – similar levels seen in the Cr data from the central Gawler Craton biogeochemical surveys (Appendix B). Higher Cr results (> 1 ppm) occur in groups of up to 20 sequential samples (Figure 6.59). High Cr concentrations fall to background levels gradationally along sample sequence (e.g., traverse 2 at 430,000 mE; Figure 6.59) and abruptly between adjacent traverses.

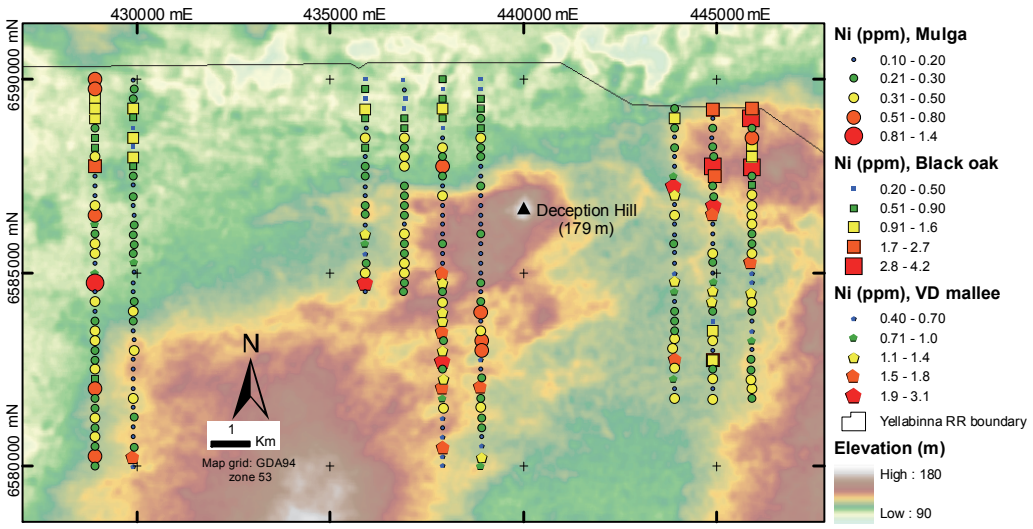

Figure 6.58: Ni concentrations in plants within the Yellabinna Regional Reserve on the 1-second DEM.

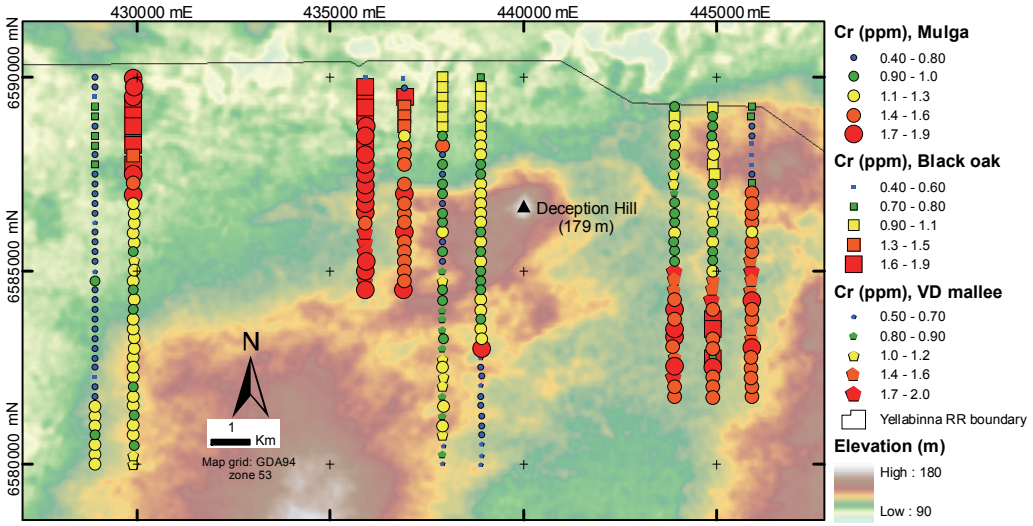

Figure 6.59: Cr concentrations in plants within the Yellabinna Regional Reserve on the 1-second DEM.

Soil geochemistry (partial extraction)

Elements that are below analytical detection limits (1 ppb) in all soil samples are: Bi, Pt, Sb, Sn, Te, and W.

Gold and gold-associated elements

Soil samples collected from the palaeo-channel have the highest concentrations of Au (0.4 ppb; Figure 6.60), Ag (7 ppb; Figure 6.61), Ca (400 – 1600 ppm), Sr (3 – 8 ppm), and S (580 ppm); and low concentrations of REE (Figure 6.62). Samples with higher concentrations of Au have higher concentrations of Ca, Sr, and S. Higher Ag results are generally from the palaeo-channel, whereas samples with Au concentrations between 0.01 – 0.2 ppb are more widespread (Figure 6.60).

Soil: greenstone indicator elements

Manganese concentrations are between 400 – 4000 ppb against an analytical detection limit of 5 ppb. The highest Mn results are from 10 km² immediately west of Deception Hill (Figure 6.63). Manganese, Cr, and As results exhibit similar trends. Elevated

concentrations of Zn (Figure 6.64), Cd, REE, Ni and As are measured in samples from the Mn anomaly but are not associated with Mn across the whole Yellabinna survey area. Manganese has a weak correlation with Cd, Fe, and V in all samples. Extractable Mn in soil corroborates results from previous calcrete sampling programs (e.g., McConachy 2001). Cobalt and Ni have similar trends and are elevated near the areas of highest topography (near Deception Hill and the NW corner (e.g., Ni, Figure 6.65). Magnesium concentrations are higher in samples from the palaeo-channels.

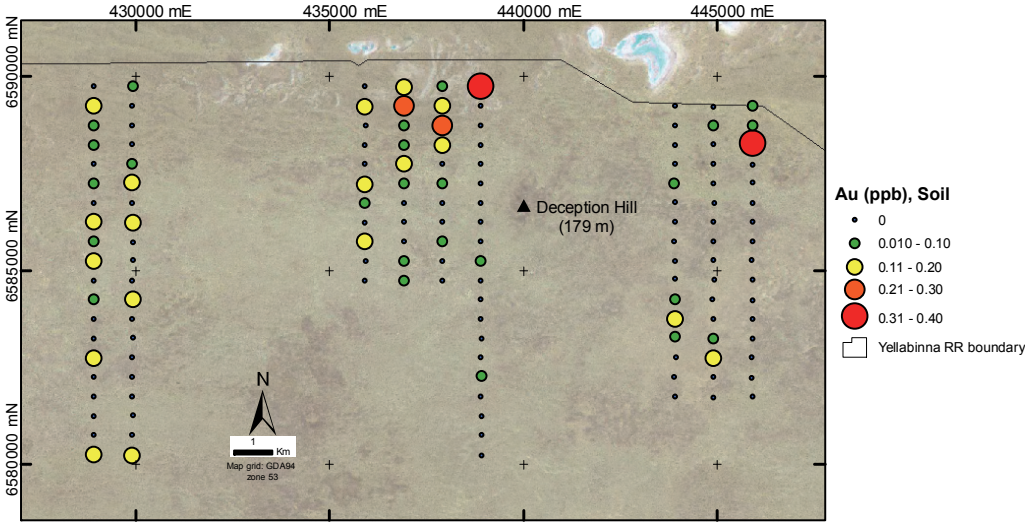

Figure 6.60: Au in soil, Yellabinna Regional Reserve on the Landsat TM image.

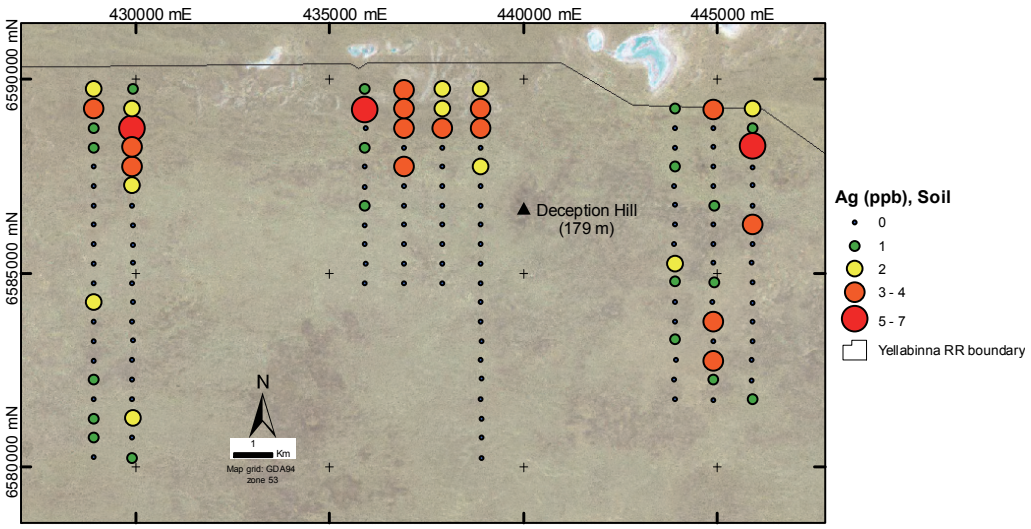

Figure 6.61: Ag in soil, Yellabinna Regional Reserve on the Landsat TM image.

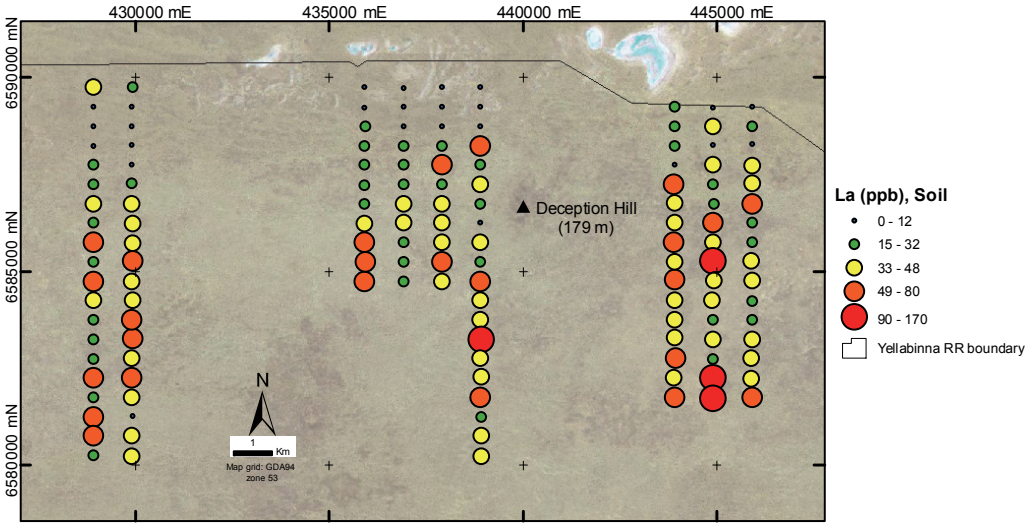

Figure 6.62: La in soil, Yellabinna Regional Reserve on the Landsat TM image.

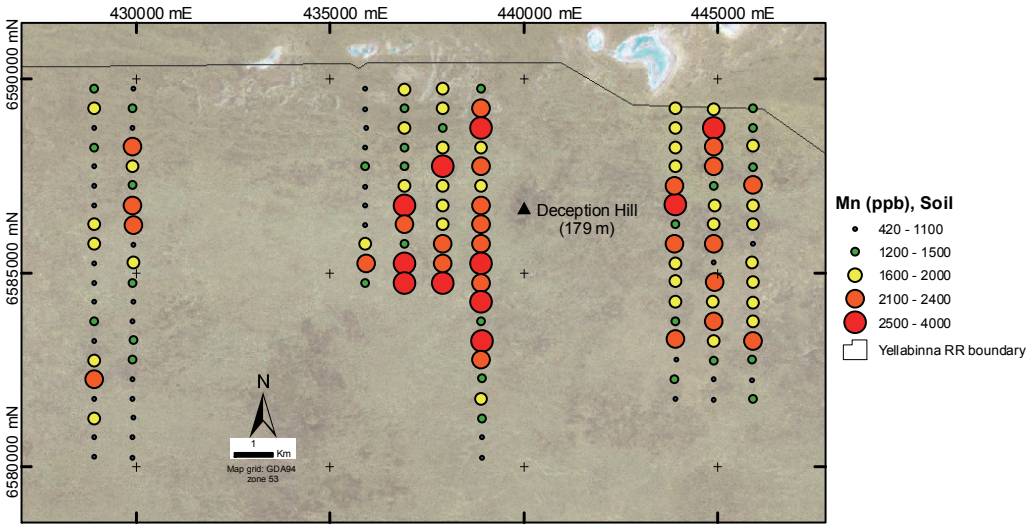

Figure 6.63: Mn in soil, Yellabinna Regional Reserve on the Landsat TM image.

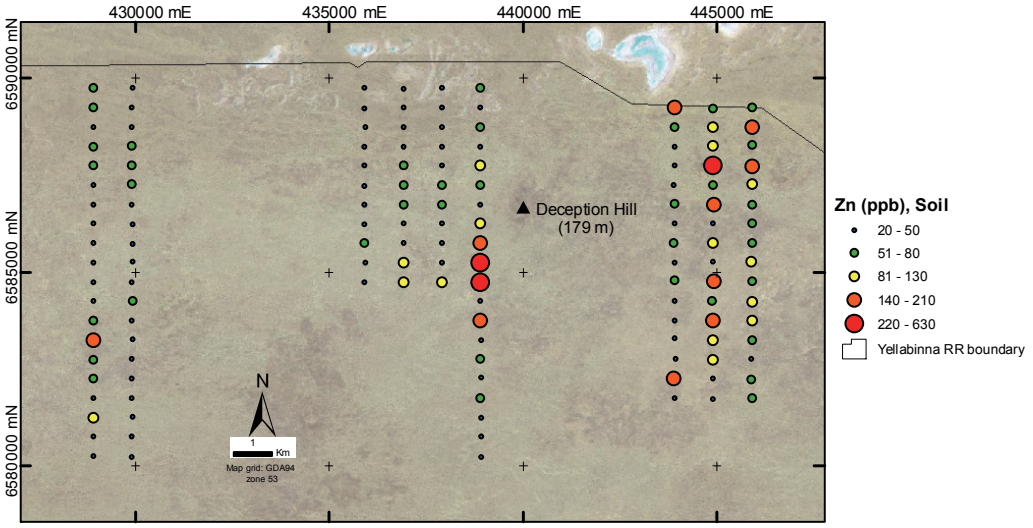

Figure 6.64: Zn in soil, Yellabinna Regional Reserve on the Landsat TM image.

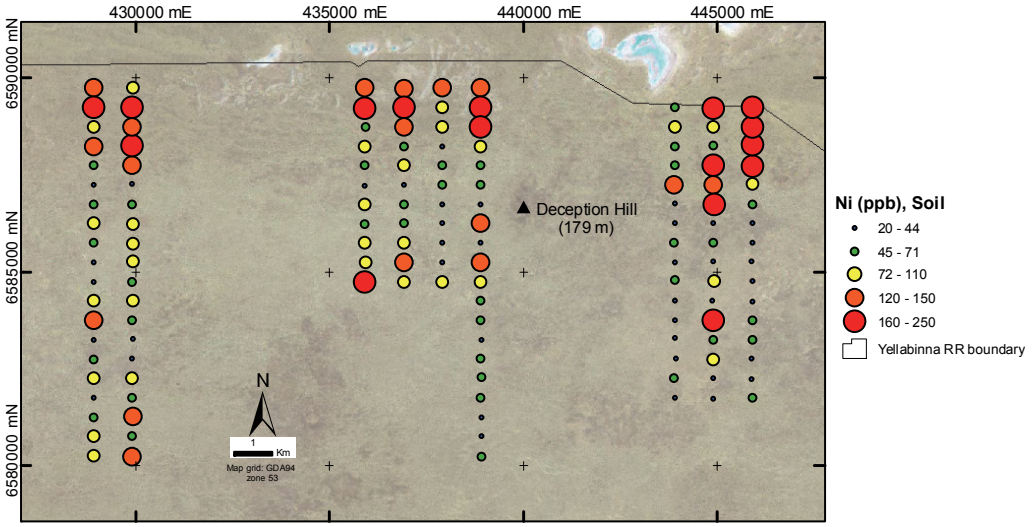

Figure 6.65: Ni in soil, Yellabinna Regional Reserve on the Landsat TM image.

6.5.3. Discussion

Landscape controls

Soil geochemistry varies between the quartzose sand-dominated sediments in the dunes and the evaporite-dominated sediments proximal to the lake sequence. Samples nearer to the palaeo-drainage have higher concentrations of extractable Ag, Au, Ca, Co, Cu, Rb, Ni, S, and Sr. The large contiguous Mn anomaly down-slope of Deception Hill probably represents ferromagnesian minerals such as pyroxene and olivine (e.g., Hoatson *et al.* 2005) and/or Fe- and Mn-oxide weathering products (e.g., Kabata-Pendias & Pendias 2001, Scott 2009) derived from locally exposed bedrock.

Biogeochemistry

Chromium

Plant samples from the Yellabinna survey area contain up to 1.9 ppb Cr, which is high relative to biogeochemical samples from the central Gawler Craton (this study) have average concentration < 2 ppm Cr (Appendix B). Figure 6.59 shows high Cr results in sequence and sharp contrast to background (< 0.8 ppm) suggesting contamination during processing or biogeochemical analysis by ICP-MS. Reference materials (V14 and V16) that are used during the biogeochemical analysis have between 1.2 – 320 ppm Cr. The high Cr content of the reference materials may have carried over to the analysis of the unknowns (samples). Another possible cause of Cr contamination is from mechanical wear of Cr-steel components in the equipment used for pulverising plant samples prior to *Aqua regia* digestion and analysis by ICP-MS.

Rhenium

In biogeochemical data world-wide, Re is typically below analytical detection limits (1 ppb; Dunn 2007). Rhenium results up to 500 ppb at Deception Hill are extremely anomalous in biogeochemical surveys in the Gawler Craton (Figure 6.66) and worldwide.

There are some cases reported in the scientific literature where Re concentrations in plants reach 40 ppm overlying Cu-Mo-Au and PGE-Ni-Cu mineralisation (Dunn 2007), and even as high as 300 ppm (Kabata-Pendias & Pendias 2001). Rhenium is associated with granites and pegmatites (Kabata-Pendias & Pendias 2001) but is generally associated with PGE in mafic–ultramafic rocks (Taylor & Eggleton 2001, Scott 2009); and, is a suggested pathfinder element for hydrothermal epigenetic mineralisation (McQueen 2005b). Rhenium typically has a close geochemical coherence with Mo due to similar ionic radii and electronegativity (Morris & Short 1969) but this association is not apparent in the biogeochemical data from the central Gawler Craton. Molybdenum is an essential micronutrient for enzyme production in plants (Dunn 2007). Lack of coherence of Re with Mo is possibly due to weathering and increasing fractionation moving away from the source (Morris & Short 1969). Both plant standards used during the analysis contain > 1 ppb Re, therefore rejecting the possibility of incomplete cell wash-out and analyte carry-over during analysis by ICP-MS. Biogeochemical samples in the Yellabinna generally have lower concentrations of Re than the other surveys (except Lake Harris and Tunkillia). This is possibly related to the increased thickness of transported regolith throughout Yellabinna, Lake Harris and Tunkillia. The unusually high Re results in the Yellabinna are near exposed mafic bedrock (e.g., Deception Hill) corroborating Mn-in-soil results, but are also from an area that is known to have ultra-mafic rock types that largely underlie sedimentary cover (Ferris *et al.* 2003).

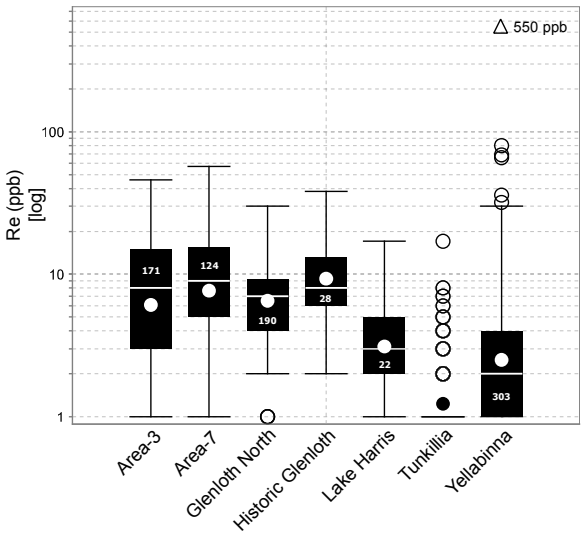

Figure 6.66: Re in biogeochemical samples from the central Gawler Craton coloured by survey area.

Exploration Implications

It is evident from field observations and previous reports (e.g., McConachy 2001) that calcrete sampling is an ineffective method of exploring in the Yellabinna Regional Reserve, primarily due to poor calcrete development. Vehicular access is limited by the soft terrain, dense vegetation, and Department of Environment, Water and Natural Resources (DEWNR) regulations. Pervasive aeolian sediment is well-drained, so calcrete horizons would be deep and the use of hand auger tools would be arduous.

Soil geochemistry

Partial extraction (MMI) geochemical analysis of soil showed low concentrations of Au, Ag, and other base metals throughout the Yellabinna survey area. Trace element dispersion from bedrock at Deception Hill is evident from the soil results. A study using partial extraction methods over mineralisation at the Tunkillia Au Prospect found that extractable Au was up to 49 ppb against a suggested background of < 9 ppb (Fabris 2010). Methods used in the study at the Tunkillia Au Prospect involved sieving soils samples prior to a partial extraction on a 75 and 200 μm size fraction.

Sieving was not implemented in the Yellabinna survey due to the scale of the survey (minimum 20 km per traverse by foot), the time required for sieving, and soil moisture content. Soil moisture content would have been the most significant impediment to sieving samples in the field, particularly for the < 75 μm size fraction. The alternative option of collecting a bulk sample for off-site drying and sieving is also not practical as it would require a sample mass 30 times greater due to the < 75 μm fraction comprising < 4% of a bulk sample (see Appendix B for particle size distribution analysis). Off-site sieving of soils samples could be implemented in more targeted follow-up sampling programs.

Biogeochemical sampling

Each 10 km traverse comprises 42 plant samples with a total weight of 4 kg (c. 100 g per sample). The low weight of plant material is an advantage for biogeochemical sampling in the Yellabinna as samples in this area are collected on foot. This makes biogeochemical sampling practical with a low environmental impact on the dunes. Future biogeochemical sampling in the Yellabinna Regional Reserve should sample mulga as it is the most widespread and abundant species. Victoria Desert mallee is also present in the dunes (although less abundant) and can be used as an alternative for mulga when mulga coverage is thin. Black oak colonise drainage landforms which are atypical in the Yellabinna Regional Reserve due to thick dune cover.

Multi-element dispersion is evident from bedrock at Deception Hill. The most compelling results are the extremely high concentrations of Re in plants over several square kilometres. Gold results are inconclusive of mineralisation. Vegetation may have some valid elevated concentrations of Au in the NW-most samples given the proximity to geological contacts, and also the presence of mineralisation (although sub-economic) in a comparable landscape setting at the Boomerang Au Prospect. Boomerang had a weak positive response in plant chemistry. Plant samples throughout the Tunkillia Au Prospect surveys have U concentrations up to 0.36 ppm. Biogeochemical surveys at Deception Hill have lower U results than Tunkillia and have been inconclusive of U mineralisation.

6.5.4. Conclusion

Soil geochemical and plant biogeochemical sampling is inconclusive for Au mineralisation using Au as a pathfinder. Geochemical pathfinder elements for Au (Bi, Sb, Sn, Te, and W) are below analytical detection limits in soils. This is possibly due to one or more of the following reasons: absence of significant Au mineralisation; inadequate sampling method (e.g., no pre-concentration of soil sample); and/or scale of geochemical mapping is not sufficiently dense to capture geochemical dispersion from mineralisation. The spacing of plant biogeochemistry and soil geochemistry collection points is sufficiently dense to map the laterally dispersed geochemical expression of bedrock at Deception Hill.

6.6. Summary of the Regional case studies

The regional chapter (*Chapter 6*) provides a series of case studies that discuss the results of biogeochemical and regolith geochemical surveys in various landscape settings. It provides a broader context to the Tunkillia case studies (*Chapter 5*). Chapter 6 begins with a case study investigating the biogeochemical response over known mineralisation in the Glenloth and Earea Dam goldfields using close sample spacing. The remaining case studies are conducted in areas that have been underexplored using calcrete geochemistry, and do not have any known sources of mineralisation. The key findings from this chapter are:

- Narrow mineralisation in the Glenloth and Earea Dam goldfields can be identified using biogeochemical sampling and Au, Ag, Bi, Cu, Sn, Te, Sn, and U;
- Lateral dispersion of sediments in the goldfields has increased the size of the surface geochemical (and biogeochemical) anomaly, but the anomaly has been broadly contained within a topographic low;
- Biogeochemical sampling over the Lake Harris Greenstone was unable to identify the changes in geology below 10 – 25 m of transported cover. Instead the biogeochemical samples showed a stronger response to the changes in regolith-landscape setting, and high levels of detrital contamination due to the open plains and sparse vegetation;
- Gridded biogeochemical (and regolith) sampling and analysis at 250 – 1000 m spacing was able to map kilometre-scale lateral dispersion in the Yellabinna Regional Reserve (e.g., Deception Hill). These were good results from a wide spaced survey in an underexplored area;
- Calcrete development was highly variable in the vicinity of regional drainage into Lake Harris (Area-3, Area-7, and Glenloth North); and,
- Biogeochemical sampling was able to identify changes in rock types in some areas, particularly higher Pb in plants over the Gawler Range Volcanics, and high Ni in plants and Cr in regolith over the Lake Harris Komatiite.

Chapter 7 follows with a discussion of the findings from the Tunkillia and Regional case studies and how the findings relate to the aims of the thesis.

7. Discussion

Foreword

This chapter provides a discussion of my results from the Tunkillia and Regional case studies and how these relate to the original thematic problems outlined at the beginning of the thesis. That is, to identify the indicators of mineralisation in surface materials (plants and calcrete) in the central Gawler Craton, and discuss the regolith processes that control their distribution in the landscape. Chapter 8 provides a conclusion of the methods used in this study and potential issues that should be considered for future applications of these methods for mineral exploration on the central Gawler Craton.

7.1. Best elements in varying media

7.1.1. Saprolite

Saprolite at Tunkillia is up to 50 m thick and can be characterised using a few key elements. The degree of weathering and saprolite development is best shown by the depleted light REE, K and Rb in the upper profile. These elements are hosted within feldspar and plagioclase that are minerals most susceptible to weathering. Minerals that are more resistant to weathering, such as mica, will preserve elements that are hosted within these minerals. The saprolite at Tunkillia's Area-223 contains phengitic white mica, in addition to kaolinite, and has higher concentrations of Rb than the kaolinitic saprolite without the white mica (Figure 5.7). This is because during hydrothermal alteration of plagioclase to white mica, the Rb has a higher affinity to the mica phase (e.g., Fleet *et al.* 2003). White mica has a high stability during the weathering process (McQueen 2009), therefore the Rb is retained in the profile within the mica as the labile minerals such as plagioclase are weathered. The Rb concentrations are high enough that they can be measured using portable XRF instruments. The implications for this are that the alteration can be mapped within the saprolite with shallow drilling depth.

7.1.2. Transported regolith

Elements associated with the Au anomalism in calcrete at Tunkillia were identified by Klingberg (2009) to be Au, Pb, Zn and Fe. Further investigation as part of my studies found there was also a slight correlation between Au and As, Ga, Cu, and calcrete morphologies with detrital composition (e.g., sand lenses). Whilst these elements are associated with Au in the calcrete, I found that there is minimal association with Au-in-calcrete with Au in drill holes. Micro-scale analysis of the calcrete (Section 5.5) showed that lenses of detritus within the calcrete were host to enriched Au, clay, and trace metals (e.g., Figures 5.32 & 5.34). A regolith study at Earea Dam by Lintern (2004b) found that these elements (Ag, Bi, Cu, Sn, Te, U, and W) were associated with Au mineralisation.

7.1.3. Plants

I found that the best elements for indicating Au mineralisation in plants are Au, Ag, and Bi and Te. The most consistent element for indicating Au mineralisation is Au. Copper, Sn, and U are useful indicators of narrow mineralisation although they were less consistent for narrow mineralisation in the goldfields (see *Section 6.2*). Tellurium could be a useful indicator of mineralisation at Tunkillia (south of Tomahawk). However, further drilling is required to test this association. The best indicator for the proximity to Au mineralisation is a multi-element suite consisting of Au, Ag, Bi, Cu, Sn, Te, and U.

Not all geochemical indicators of mineralisation can be used as biogeochemical pathfinder elements. For example, Rb in the saprolite represents a mineral phase that is resistant to weathering and is therefore not readily available for uptake by plants. Tungsten is not a useful biogeochemical indicator of mineralisation as it is below detection limit (0.1 ppm W) in all biogeochemical samples.

7.2. Effect of cover

Regolith at Tunkillia consists of deeply weathered bedrock (up to 50 m deep) and a shallow blanket of transported regolith (<10 m thick). Landscape processes have transported regolith (including calcrete) tens of kilometres down slope from the Tunkillia mineralisation and increased the size of the surface anomaly (e.g., Gibbons 1997). The lateral dispersion has been facilitated by physical transport of calcrete within broad palaeo-drainage (see *Chapter 4*). This was helpful in the discovery of the mineral system, but it has since provided a challenge for the use of surface geochemistry to constrain underlying mineralisation. Instead extensive drilling has been required to identify the zones of mineralisation ('Tunkillia Dataset', *Appendix B*). A detailed analysis of the regolith (e.g., *Chapter 5.1*) did not show any indicators of mineralisation in the transported cover. However, the *in situ* regolith contained mineralogical and geochemical indicators of alteration (e.g., white mica and Rb) that could be used to distinguish mineralisation from the less prospective exploration targets. Although sampling *in situ* regolith at Tunkillia requires a sample from drilling, there are many of the samples archived samples that would be suitable for a re-sampling/analysis program to map the alteration in the *in situ* regolith at shallow depth.

At a regional scale the landscape has a significant control on calcrete development (Goudie 1983, Wright & Tucker 1991) and the lateral dispersion of regolith. For example, calcrete is poorly developed in drainage depressions, areas with shallow/outcropping bedrock, and sand dunes. Areas with well-developed calcrete are shown by the high concentrations of Ca in regolith samples. Areas with good calcrete development (e.g., hardpan) are typically colonised by pearl bluebush, an association also acknowledged by Wotton (1992).

Dispersion of elements in the regional case studies is shown by regolith and plant chemistry. A particularly good example is the drainage depressions in the Glenloth North case study (Ag and Zn in plants) and the dispersion of elements from outcropping bedrock in the Yellabinna case study (Mn in soil, and Ni, Ag, and Re in plants). The masking effects of transported cover are particularly obvious in the Harris Greenstone biogeochemical study (*Section 6.3*). This traverse is from an area where 10 – 25 m of transported sediments overlie bedrock (Sheard & Robertson 2004). The biogeochemistry more closely maps the changes in the regolith landforms than the underlying bedrock in the Lake Harris Greenstone case study.

7.3. Recommended sampling strategy

7.3.1. Sampling pattern

Previous calcrete sampling programs have typically used a staggered grid (400 – 1600 m) to maintain equidistance between samples in all directions. Biogeochemical and regolith geochemical sampling patterns for this study were inspired by the uneven grid drilling pattern at the Tunkillia Au Prospect, where a 50 by 200 m grid was used. The short distance (50 m) is along a traverse perpendicular to strike of geological structure hosting mineralisation. This spacing is sufficient for the Tunkillia area due to the lateral dispersion of auriferous sediments increasing the size of the regolith expression of mineralisation.

Close-spaced biogeochemical sampling was conducted at Tunkillia (50 m) and in the historic goldfields (25 m). In the goldfields the Au anomaly overlying mineralisation is a two-point anomaly (2 samples) – see *Section 6.2*. A sampling grid up to 50 m could probably identify mineralisation in the goldfields because of the lateral dispersion within the broad landscape depression. The biogeochemical sampling at Tunkillia was conducted at 50 by 200 m and the elevated Au results broadly fit the Au-in-calcrete anomaly (see *Section 5.2*). However, the high concentrations of Au in plants do not always align with the high Au in calcrete point-for-point. Plants at Tunkillia contain Au at concentrations orders of magnitude lower than the calcrete (e.g., <10 ppb in plants compared with 10-300 ppb in calcrete). At Tomahawk, where drilling has not revealed significant mineralisation to date, the 50 m scale Au-in-plant results appear to be somewhat erratic and do not provide significant additional information to calcrete geochemical data as to the potential location of mineralisation. Other elements such as Te show a multi-point anomaly at the 50 x 100 m scale at Tomahawk. However, this potential target is yet to be drilled. Based on the length and width of the Au and pathfinder element anomaly in plants the Tunkillia prospect could have been discovered using regional biogeochemical sampling program with 200 m grid spacing.

Biogeochemical sampling in the regional programs was conducted at 250 by 1000 m and regolith geochemical sampling was conducted at 500 by 1000 m. Biogeochemical sampling has been conducted at the kilometre scale in Canada and has identified

mineralisation (Dunn *et al.* 2009). Collection of biogeochemical samples at 250 m spacing along a traverse is feasible for the size of the surveys in this study and is easily conducted on foot. The 250 m spacing would be sufficient to detect narrow Au mineralisation such as the Fabians No.3 deposit in the Glenloth goldfield, and close to the spacing suitable to identify mineralisation at the Tunkillia Au Prospect. Lateral dispersion of the regolith (and signatures of mineralisation) is a significant factor to consider when selecting suitable sample spacing. Spacing of biogeochemical samples > 250 m may be too large to detect mineralisation in the small regional survey areas (i.e., 25 km²) on the western plains of Lake Harris (*Section 6.4*). Where sampling is > 250 m is the results may be hit and miss for Au mineralisation (e.g., Fabians No.3 and Tunkillia) and is more dependent on the dispersion of elements within the landscape.

7.3.2. Continuity of sampling material

Inconsistent coverage of sampling material provides a challenge for selecting an optimal spacing and pattern for sampling. For example, calcrete development is highly variable in many areas of the Gawler Craton, particularly at Area-3, Area-7, and Glenloth North. Calcrete geochemistry data from previous exploration in the area surrounding the Kingoonya palaeo-channel is irregular (e.g., Figure 6.18). This is mainly due to previous mineral explorers having used generic soil sampling techniques, which did not focus on but may have included calcrete, or poor calcrete development. This study found that calcrete is poorly developed in areas where the soil profile is deep and poorly drained (e.g., alluvial landforms such as channels), or the soil profile is shallow (e.g., in areas with silcrete or Gawler Range Volcanics). It is important to have an understanding of the landscape process and be equipped with a regolith map of the area.

7.4. Contamination

7.4.1. Detrital contamination of biogeochemical samples

Sub-aerial plant organs are susceptible to contamination by aeolian-, or alluvial-sourced detritus. Contamination was assessed in this study using Fe and Zr concentrations. Pearl bluebush samples have the highest concentrations, on average, of Fe and Zr than the other species collected in this study and are therefore the species most ‘at risk’ of detrital contamination. This is due to the low canopy height and the rough surface textures that can accumulate foreign material. The sponge-like texture of the surface of black bluebush leaves is suggested by Dignam (2008) as a reason for targeting the twigs only for biogeochemical studies, yet the author provides only a reference to a personal communication with S.M. Hill in 2008. Biogeochemical sampling has been conducted by the exploration industry using pearl bluebush. Imaging of plant organs shows that the leaves attract the most detrital contamination (Figure 3.6) yet some sampling programs involve the removal of woody material and the chemical analysis of the leaves (Minotaur Exploration Ltd *et al.* 2010, p.17). The significance of detrital contamination in

biogeochemical surveys is not fully appreciated or acknowledged in the literature from Australian studies and it is an aspect of biogeochemistry in arid Australia that needs further attention.

Detrital contamination is intensified in samples collected from sparsely-vegetated landscapes, such as the Lake Harris Greenstone case study (*Section 6.3*), where surface soils are unstable (minimal moisture or vegetation etc.), or collected from near unsealed roads or tracks. This thesis acknowledges that detrital material is most abundant on the surface of pearl bluebush samples, and that the detritus are composed of, but not limited to, Fe-oxides, Zr, and quartzose sand. This study provides no quantitative data on the relative abundance of these detrital components, or the influence this input would have on enriching or diluting the trace element chemistry of the sample.

Central Gawler Craton

In the Gawler Craton case studies presented here there are two potential sources of contamination. One is derived from mining and exploration activities, and the other is through natural aeolian and alluvial processes.

The collection of plant samples from the Tunkillia Au Prospect and the Glenloth and Earea Dam goldfields post-dates the exploration and mining activity in these areas. It is possible that some contamination has been derived from anthropogenic surface material. As the contamination indicator elements (Fe and Zr) do not appear to be correlated with Au it is assumed that plant samples collected in the regional surveys are not contaminated from mineralisation-derived detritus.

The plains are a chenopod shrub-land colonised primarily by various bluebush species (*Maireana spp.*) These low-canopy shrubs are most at risk of contamination due the proximity of foliage to the ground, which can accumulate detrital material from aeolian and alluvial processes. Intense rainfall events can cause soil-splash contamination of low-hanging foliage (Hill 2004), or detritus entrained in flood waters (particularly along subtle drainage depressions) resulting in contamination of foliage up to 40 cm from the ground. Contamination from flood waters on bluebush is visually distinguished by discolouration of the pale foliage, and an accumulation of organic material banked up against the plant. The visual contamination was confirmed by high Fe and Zr in the biogeochemical results in the regional studies (*Section 6.4*). Cleaning of these materials after collection is ineffective and causes complications (Dunn 2007), and it is therefore up to the discretion of the sampler to avoid collecting such material. Black oak, Victoria Desert mallee, and mulga foliage have higher ground-clearance and are not exposed to the aeolian and alluvial contamination that affects the chenopods.

Summary of potential contamination

The magnitude of detrital contamination of biogeochemical samples based on Zr and Fe follows the order: pearl bluebush >> black oak > Victoria Desert mallee. Detrital input can:

1. Dilute the biogeochemical expression of substrate, underlying geology and/or mineralisation; or,
2. Produce an elevated result of transported origin (local or distal source).

Plant biogeochemistry is proposed as an additional method of mineral exploration to calcrete, which could be used in areas where calcrete is poorly developed (e.g., sand dunes). Pearl bluebush typically colonises the erosional plains in the presence of well-developed calcrete, an association also recognised by Wotton (1992). On these regolith types, plant sampling is an easy and cost-effective exploration method. However, there is a higher contamination potential. Plants in aeolian regolith types (e.g., dunes: Tunkillia, Yellabinna) have lower potential for contamination.

It is recommended that further biogeochemical studies, especially those using bluebush species (*Maireana spp.*), should investigate the effects of detrital contamination. This could be done by separating organs for individual biogeochemical and microscopic analysis, or by washing samples to remove detritus from the rough surface of the leaves and/or twigs. Washing samples could provide a quantitative assessment of the chemistry of the detritus retrieved after washing, the solutes removed during washing, and the enrichment or dilution effect of the biogeochemistry of the bulk sample.

7.5. Methods of sample analysis

Gold is well-known for being heterogeneously distributed within geochemical sample materials, or the 'nugget effect' (e.g., Smee & Stanley 1988, Anand *et al.* 2004), as demonstrated by the LA-ICP-MS mapping of polished calcrete sections from the Tunkillia Au Prospect. Repeat analysis of Au in geochemical reference materials generally varies < 40% (relative standard deviation) but is > 80% (and up to 420%) in biogeochemical reference materials. Repeatability of Au measurements in pulp duplicates and re-sampled plants is equally as poor. This is not reassuring for the submission of plant sub-sample duplicates, at an additional cost per sample, to monitor the quality of the Au results in the unknown samples. Low Au concentrations (e.g., 1 – 1.5 ppb) should be interpreted with caution. Gold concentrations higher than 1.5 ppb can be valid results, although it is recommended that pathfinders for Au are also investigated (i.e., Ag, Bi, Cu, Sn, U, and Te).

Ashing plant samples (prior to *Aqua regia* digest) is an alternative preparation method useful for measuring elements that are in very low concentration (Dunn 2007). This method is common in the literature from the northern hemisphere although it is acknowledged the ashing process may result in the loss of some volatile elements. This

method was not used in this study in order to maintain consistency with the methods used for the existing data at the Tunkillia Au Prospect, but may be worth investigating further for the application of biogeochemistry in Australia.

Reference materials for biogeochemical analysis

Analysis by solution ICP-MS can be sensitive to samples with high concentrations of a particular element. This can result in incomplete wash-out of the analytical cell between samples and carry-over effects to the measurement of subsequent samples (e.g., Rodushkin & Axelsson 2000). The reference materials (V14 and V16) that are used by Acme Analytical Laboratories during the biogeochemical analysis of samples typically have higher concentrations of most elements than the unknowns/samples (see Appendix B). The reference materials are generally inserted in the queue of unknowns at a regular interval (10 – 20 samples) to monitor the precision and accuracy of the instrument. Standards or samples that have a high concentration of a particular element have the potential to carry over to subsequent analyses (e.g., biogeochemical data for Au at Area-7). It is recommended that standards more closely matched to Australian plant species are considered for future biogeochemical analyses.

Why submit reference materials?

Analytical laboratories typically use 'in house' or internal reference materials. These are materials that have had many repeat analyses so that the laboratory feels that they are confident with the expected chemical composition. Internal reference materials become an issue when samples are submitted to different laboratories and there is no commonality of the reference materials. For example, regolith samples from Area-3 were submitted to two different analytical laboratories for geochemical analysis and there is a difference in measurement sensitivity for some elements (e.g., Pb). A correction factor could have been applied if a common Certified Reference Material (CRM) was submitted with the samples to the laboratories. It is recommended that user-supplied reference materials be submitted with the samples in future geochemical sampling programs.

Timing: from collection to results

Exploration programs using biogeochemical methods can potentially have a longer duration (from sample collection, to receiving the results from the laboratory) than a geochemical analysis of a regolith sample material. This is mainly due to the requirement for plant samples to be dried within several days of collection (or even less time in the case of succulent species) to impede decomposition. Plant samples require low-temperature drying (< 100 °C) for up to 48 hours. Gaining access to an oven of sufficient size to accommodate large batches of plant samples can be challenging. Even access to smaller ovens, such as that at the University of Adelaide can accommodate up to 40

samples per rotation. This becomes a time and energy (electricity) intensive process. Sorting and pulverisation of plant material (post drying) is a tedious process, with each sample taking 5 to 10 minutes. This throughput time includes cleaning of equipment between each sample. These post-drying procedures can be conducted by the commercial laboratories but incur additional fees.

Transit times for postage and analysis largely depend on the time of year, and the commercial laboratory conducting the analysis. Transit duration from Australia to the analytical laboratory in Canada is typically less than two weeks with the provision that the shipment is not delayed by customs. Time of year is a significant factor due to the exploration activity of the northern hemisphere. Results for this study were received between 2 – 4 months (depending on batch) after the date of dispatching samples from Australia. Delays were due to the maintenance of analytical equipment and a large influx of samples. The varying delay had no impact on the quality of the data and did not appear to introduce any bias. However, it is desirable to minimise sample turnaround for timely decision making in the exploration process.

Alternate Australian-based analytical laboratories could be used in future programs to improve turn-around times. The same analytical laboratory was used for the acquisition of biogeochemical data for this study to maintain consistency with existing datasets (e.g., Tunkillia) regarding the element suite, and the analytical detection limits. It should be noted that the ashing of biogeochemical samples is not available at all analytical laboratories and does incur additional fees.

Botanist or Field Assistant?

Semi-arid southern Australia typically has a low level of plant species diversity that is governed by the low rainfall and resource availability (Specht 1994). The advantage of low species diversity is that training field assistants for biogeochemical sampling programs can be conducted using an illustrated guide to assist in species identification. Sampling guides suggest selecting plants that are easily identifiable, dominant, and widespread (Hill 2002). It may not always be possible to satisfy these parameters without conducting an orientation study. In the case of the Yellabinna Regional Reserve biogeochemical survey, the ground was traversed on foot only once, and an assessment of the dominant species was made by the sampler ‘on the fly’. The dominant species were collected with the assumption that the species are widespread, and upon its absence, the next most dominant species is sampled.

Correct identification of the plant genus is crucial to interpreting biogeochemical data. Each plant species has different nutritional requirements and therefor the uptake and bioaccumulation of each element differs between species. For example, *Eucalyptus spp.* can accumulate elements such as Ce and La at higher concentrations than mulga or black oak in the same environments. The difference in background concentrations could be interpreted as anomalous without the identification of the plant species. Omissions or

incorrect species identification of plant samples can potentially be resolved by using the biogeochemical data and data analysis techniques such as Principle Components Analysis (PCA). The average biogeochemistry for the five species discussed in this study is included in Appendix B.

Cost per sample

Biogeochemical analysis of plant samples is typically higher than the geochemical analysis of regolith samples. For example, one biogeochemical analysis costs approximately AU$45 compared with a cost of between AU$30 – 35 for a geochemical analysis of regolith and approximately AU$45 for geochemical analysis of soil using partial extraction methods. This cost does not incorporate the cost of the machinery required to collect calcrete samples in semi-arid environments. Labour costs are similar, although a biogeochemical survey, depending on the scale could be conducted more effectively on foot, with minimal previous training.

7.6. Temporal effects

In this thesis I have included several temporal comparisons of biogeochemical sampling. Seasonal variability of biogeochemical samples is detailed in the quality control section (*Section 3.6*) and the regional case studies (*Section 6.4*). The most detailed example is included in *Section 3.6* where many repeats were collected from overlying mineralisation at Glenmarkie in the Glenloth Goldfield. A percentage difference of more than 50% was evident for 13 elements – Au being one of them. This level of variation is reported by other authors (e.g., Cohen *et al.* 1987, Stednick *et al.* 1987, Dunn 2007). Challenges that I found for repeat analysis of biogeochemical samples over multiple seasons are:

- No suitable biogeochemical reference materials to resubmit with the unknowns;
- Potential changes in the equipment used to prepare and analyse the samples (e.g., increased wear of the mill(s));
- ‘Re-sampling’ only samples the same plant and not the same material – there is known heterogeneity of element distribution within the plant; and,
- Plant health and nutrient requirements change in response to changes in climate.

It is recommended that the biogeochemical sampling is conducted over a short time period (several days where possible), and that the date of collection is noted so that if a significant delay between sampling occurs the seasonal difference can be properly acknowledged and interpreted.

7.7. Comparisons between plants

Different plant species have different nutritional requirements, and tolerances to climate and environment. The biogeochemistry and the biogeochemical expression of the landscape/geology will be different for each species. Factors influencing the distribution of calcrete in the landscape (e.g., salt lakes or exposed bedrock) also control the plant community. Plants tolerant of saline conditions (e.g., black oak; Niknam & McComb 2000) or sandy soils (e.g., woody cassia; Cunningham *et al.* 1981) have a different biogeochemical expression to plants that colonise calcareous soils (e.g., pearl bluebush; Wotton 1992). Appendix B contains tabulated data of the chemistry (average concentration ± standard deviation) of each species used for this thesis.

8. Conclusions

Foreword

The study begins with a detailed characterisation and discussion on the regolith processes at the Tunkillia Au Prospect in the central Gawler Craton. It then builds on these findings at Tunkillia through a series of regional case studies that provide a broader context in a range of landscape and mineralised settings. This chapter presents a brief outline of highlights and considerations found in this research.

This research has investigated the regolith processes in areas with known Au mineralisation using biogeochemistry and regolith geochemistry (calcrete and soil) in the central Gawler Craton, South Australia. The individual case studies cover a variety of scales, landscape and mineralisation settings.

Key findings from this research include:

- Hydrothermal alteration in saprolite at the Tunkillia Au Prospect can be determined geochemically using Rb content and is measurable using portable XRF;
- Gold in plants is the best indicator for Au mineralisation at the Tunkillia Au Prospect and the Glenloth and Earea Dam Goldfields but a better proxy for mineralisation is a multi-element suite that consists of Au, Ag, Bi, Cu, Sn, Sn, and U.
- Potential source of the transported Au-in-calcrete anomaly, as indicated by a drainage modelling and a coherent Te-in-plant anomaly, lies to the south of Tomahawk in an area yet to be drilled – A new drill target?;
- Gold in nodular calcrete is associated with the carbonate-clay cement within detrital sand layers indicating transport within sediments and within calcrete.
- In areas of deep cover (e.g., 10 -25 m) near Lake Harris palaeo-drainage the biogeochemistry more closely maps the changes in the regolith landforms than the underlying bedrock.
- Detrital contamination, as indicated by Zr and Fe concentration, is prevalent in pearl bluebush foliage, and most pronounced in samples collected from sparsely-vegetated areas;
- Standards used by the analytical laboratory, which contain elements at concentrations much higher than the unknowns (samples), may cause carry over issues during analysis – A demand for Australian biogeochemical standards;

Biogeochemical sampling and analysis has proved to be an effective technique for mapping surface geochemistry in regional surveys in the central Gawler Craton. It was the most effective technique in the underexplored Yellabinna Regional Reserve. This area is sensitive landscape with restricted exploration activity. Vehicle mobility within some

areas of the Yellabinna dune field would have been impossible due to steep dune slopes and soft sand. Traversing the dunes on foot was efficient and effective for biogeochemical and soil sampling, and vehicle access was not required. Widespread sample coverage was achieved and high sample numbers were possible due to the light weight of plant material.

Biogeochemical sampling and analysis was able to identify known mineralisation at the historic Glenloth and Earea Dam Goldfields, and Tunkillia Au Prospect. This research also identified a suite of possible pathfinder elements that could be used with biogeochemical sampling. In light of these biogeochemical pathfinders, the results suggest there are prospective areas within Tunkillia Au Prospect that would suit further exploration and potential drilling.

Challenges remain for the use of biogeochemistry for mineral exploration in the central Gawler Craton, and other semi-arid parts of Australia. These include standards used in the analytical process, and detrital contamination. Further work is required on the effect of detrital contamination, and the use of appropriate standards by the commercial laboratory (i.e., element concentrations similar to the unknown samples).

9. References

ALDERTON D. H. M., PEARCE J. A. & POTTS P. J. 1980. Rare earth element mobility during granite alteration: Evidence from southwest England. *Earth and Planetary Science Letters* **49**, 149-165.

ALLEN S. R., MCPHIE J., FERRIS G. & SIMPSON C. 2008. Evolution and architecture of a large felsic Igneous Province in western Laurentia: The 1.6 Ga Gawler Range Volcanics, South Australia. *Journal of Volcanology and Geothermal Research* **172**, 132-147.

ALONSO-ZARZA A. M. & WRIGHT V. P. 2010. Chapter 5 Calcretes. *In:* Alonso-Zarza A. M. & Tanner L. H. eds., *Developments in Sedimentology*, Vol. Volume 61, pp 225-267, Elsevier.

AMES T. W. 2010. Biogeochemical expression of the area NW of Area 223, Tunkillia, Gawler Craton, South Australia. Honours thesis, Geology and Geophysics, University of Adelaide, Adelaide (unpubl.).

ANALYTICAL SPECTRAL DEVICES 2011. TerraSpec Spectrometer <http://www.asdi.com/products/terraspec/terraspec-hi-res-mineral-spectrometer>. (retrieved 27/1/13).

ANAND R. R. & BUTT C. R. M. 2010. A guide for mineral exploration through the regolith in the Yilgarn Craton, Western Australia. *Australian Journal of Earth Sciences* **57**, 1015-1114.

ANAND R. R., HOUGH R., PHANG C., NORMAN M. & GLEUHER M. 2004. Regolith mineral hosts for gold and other base metals. *AMEC Minerals Exploration Seminar June 2004*, pp. 27-30. CRC LEME.

ANAND R. R. & PAINE M. 2002. Regolith geology of the Yilgarn Craton, Western Australia: implications for exploration. *Australian Journal of Earth Sciences* **49**, 3-162.

ANAND R. R., PHANG C., WILDMAN J. E. & LINTERN M. J. 1997. Genesis of some calcretes in the southern Yilgarn Craton, Western Australia: Implications for mineral exploration. *Australian Journal of Earth Sciences* **44**, 87-103.

ANDERSON J. 2011a. ASX Release: Another upgrade for IVR's Peterlumbo silver project in South Australia ahead of imminent drilling. *Investigator Resources Ltd.*

ANDERSON J. 2011b. ASX Release: Re: Presentation at Noosa Mining & Exploration Conference, 15 July 2011, entitled: High grade silver targets & excellent copper gold prospects in the southern Gawler Craton. *Investigator Resources Ltd.*

ANDERSON J. 2012. *High grade Paris silver discovery heads a new generation of targets in South Australia*. *RIU Explorers Conference, February 21st*, Fremantle.

ARMBRUST G. A., OYARZUN M. J. & ARIAS J. 1977. Rubidium as a guide to ore in Chilean porphyry copper deposits. *Economic Geology* **72**, 1086-1100.

ARNE D. C., STOTT J. E. & WALDRON H. M. 1999. Biogeochemistry of the Ballarat East goldfield, Victoria, Australia. *Journal of Geochemical Exploration* **67**, 1-14.

BARNETT C. T. & WILLIAMS P. M. 2009. Using Geochemistry and Neural Networks to map Geology under Glacial Cover *Geoscience BC* **Project 2008-003**.

BELPERIO A. P. 2007. ASX Release: Tunkillia Oxide Gold - Further Good Drilling Results. <http://www.asx.com.au/asxpdf/20070501/pdf/3127c6z5qmx515.pdf>.

BELPERIO A. P. 2009a. ASX Report: Gold exploration at Tunkillia, South Australia. *Minotaur Exploration Ltd.*

BELPERIO A. P. 2009b. ASX Report: Update of Gold and Silver Resource Tunkillia, Gawler Craton, SA. *Minotaur Exploration Ltd.*

BELPERIO A. P. 2010. ASX Report: Positive results from drill testing of gold biogeochemical target. *Minotaur Exploration Ltd.*

BERMAN M., BISCHOF L. & HUNTINGTON J. 1999. Algorithms and software for the automated identification of minerals using field spectra or hyperspectral imagery. *Proceedings of the 13th International Conference on Applied Geologic Remote Sensing,* Vancouver, Canada, pp. 222-232.

BLISSETT A. H., CREASER R. A., DALY S. J., FLINT R. B. & PARKER A. J. 1993. Mesoproterozoic. *In:* Drexel J. F., Preiss W. V. & Parker A. J. eds., *The Geology of South Australia Volume 1. The Precambrian* (Bulletin 54 edition), pp 107-170, Geological Survey of South Australia.

BONWICK C. M. 1997. Discovery of Challenger Gold Deposit Implications for further exploration on the Gawler Craton. *New Generation Gold Mines '97. Case Histories of Discovery,* Glenside, Australia, pp. 7-1 to 7-15.

BROOKS R. R., CHAMBERS M. F., NICKS L. J. & ROBINSON B. H. 1998. Phytomining. *Trends in Plant Science* **3**, 359-362.

BROYER T. C., JOHNSON C. N. & PAULL R. E. 1972. Some aspects of lead in plant nutrition. *Plain Soil* **36**, 301-313.

BUDD A. R. & SKIRROW R. G. 2007. The Nature and Origin of Gold Deposits of the Tarcoola Goldfield and Implications for the Central Gawler Gold Province, South Australia. *Economic Geology* **102**, 1541-1563.

BURGESS S. S. O., ADAMS M. A., TURNER N. C., DON A. W. & ONG C. K. 2001. Tree Roots: Conduits for Deep Recharge of Soil Water. *Oecologia* **126**, 158-165.

BURGESS S. S. O., ADAMS M. A., TURNER N. C. & ONG C. K. 1998. The Redistribution of Soil Water by Tree Root Systems. *Oecologia* **115**, 306-311.

BUTT C. R. M., SCOTT K., CORNELIUS M. & ROBERTSON I. D. M. 2009. Regolith sampling for geochemical exploration. *In:* Scott K. & Pain C. eds., *Regolith Science*, pp 341-376, CSIRO Publishing; Springer, Collingwood.

CALDWELL M. M. & RICHARDS J. H. 1986. Competing root systems: morphology and models of absorbtion. *In:* Givnish T. J. ed., *On the Economy of Plant Form and Function*, pp 251-273, Cambridge University Press.

CALLEN R. A. 1983. Late Tertiary 'grey billy' and the age and origin of surficial silicifications (silcrete) in South Australia. *Journal of the Geological Society of Australia* **30**, 393-410.

CAMPBELL N. A. & REECE J. B. 2005. *Biology* (7th edition). Pearson Education Inc., San Francisco.

CANADELL J., JACKSON R. B., EHLERINGER J. R., MOONEY H. A., SALA O. E. & SCHULZE E. D. 1996. Maximum Rooting Depth of Vegetation Types at the Global Scale. *Oecologia* **108**, 583-595.

CARLISLE D. 1980. Possible variations on the calcrete-gypcrete uranium model. *United States Department of Energy* **GJBX-53(80)**.

CARLISLE D., MERIFIELD P. M., ORME A. R., KOHL M. S. & KOLKER O. 1978. Distribution of calcretes and gypcretes in southwestern United States and their uranium favorability: Based on a study of deposits in Western Australia and South West Africa (Namibia). *United States Department of Energy* **GJBX-29(78)**.

CERLING T. E. 1984. The stable isotopic composition of modern soil carbonate and its relationship to climate. *Earth and Planetary Science Letters* **71**, 229-240.

CHALMERS N. C., STEWART J. R. & BETTS P. G. 2007. Yarlbrinda and Yerda shear zones: structural and relative temporal constraints. *MESA Journal* **46**, 40-46.

CHEN X. Y. 2002a. Morphology and occurrence. *In:* Chen X. Y., Lintern M. J. & Roach I. C. eds., *Calcrete: characteristics, distribution and use in mineral exploration*, pp 5-7, CRC LEME, Canberra.

CHEN X. Y. 2002b. Origins. *In:* Chen X. Y., Lintern M. J. & Roach I. C. eds., *Calcrete: characteristics, distribution and use in mineral exploration*, pp 8-15, CRC LEME, Canberra.

CHEN X. Y., LINTERN M. J. & ROACH I. C. 2002a. *Calcrete: characteristics, distribution and use in mineral exploration*. CRC LEME, Canberra.

CHEN X. Y., MCKENZIE N. J. & ROACH I. C. 2002b. Distribution in Australia: calcrete landscapes. *In:* Chen X. Y., Lintern M. J. & Roach I. C. eds., *Calcrete: characteristics, distribution and use in mineral exploration*, pp 110-138, CRC LEME, Perth.

CHEN X. Y. & ROACH I. C. 2002. Introduction. *In:* Chen X. Y., Lintern M. J. & Roach I. C. eds., *Calcrete: characteristics, distribution and use in mineral exploration*, pp 1-4, CRC LEME, Perth.

COHEN D. R., HOFFMAN E. L. & NICHOL I. 1987. Biogeochemistry: A geochemical method for gold exploration in the Canadian Shield. *Journal of Geochemical Exploration* **29**, 49-73.

COHEN D. R., SHEN X. C., DUNLOP A. C. & RUTHERFORD N. F. 1998. A comparison of selective extraction soil geochemistry and biogeochemistry in the Cobar area, New South Wales. *Journal of Geochemical Exploration* **61**, 173-189.

COHEN D. R., SILVA-SANTISTEBAN C. M., RUTHERFORD N. F., GARNETT D. L. & WALDRON H. M. 1999. Comparison of vegetation and stream sediment geochemical patterns in northeastern New South Wales. *Journal of Geochemical Exploration* **66**, 469-489.

COPPENS K. T. 1997. A geochemical study of the Hopefull Hill Basalt and Lake Harris Komatiite, the relationship between them and their economic potential for nickel and gold. Honours thesis, Geology and Geophysics, University of Adelaide, Adelaide (unpubl.).

COWLEY W. M. & FLINT R. B. 1993. Archean. *In:* Drexel J. F., Preiss W. V. & Parker A. J. eds., *The Geology of South Australia Volume 1. The Precambrian* (Bulletin 54 edition), pp 142-147, Geological Survey of South Australia.

CSIRO 2010a. Automated Spectral Interpretation <http://www.thespectralgeologist.com/automated_interps.htm>. (retrieved 25/1/2013).

CSIRO 2010b. Discovering Australia's mineral resources <http://www.csiro.au/Organisation-Structure/Flagships/Minerals-Down-Under-Flagship/Discovering-mineral-resources.aspx>. (retrieved April 3 2012).

CUNNINGHAM G. M., MULHAM W. E., MILTHORPE P. L. & LEIGH J. H. 1981. *Plants of western New South Wales* Soil Conservation Service, NSW.

DALY S. J. & FANNING C. M. 1993. Archean. *In:* Drexel J. F., Preiss W. V. & Parker A. J. eds., *The Geology of South Australia Volume 1. The Precambrian* (Bulletin 54 edition), Geological Survey of South Australia.

DART R. C. 2009. Gold-in-calcrete: A continental to profile scale study of regolith carbonates and their association with gold mineralisation. Doctor of Philosophy thesis, Geology and Geophysics, University of Adelaide, Adelaide (unpubl.).

DART R. C., BAROVICH K., CHITTLEBOROUGH D. & HILL S. M. 2007. Calcium in regolith carbonates of central and southern Australia: Its source and implications for the global carbon cycle. *Palaeogeography, Palaeoclimatology, Palaeoecology* **249**, 322-334.

DAVIES M. B. 2003. Harris Greenstone Domain bedrock drilling Phase 2: June-August 2002. *Primary Industries and Resources South Australia* **Report Book 2002/029**.

DIGNAM R. 2008. Brownfields exploration through transported regolith: a comparative study of plant biogeochemical and soil geochemical techniques at the Pinnacles Ag-Pb-Zn deposit, Broken Hill, NSW. Honours thesis, Geology and Geophysics, University of Adelaide, Adelaide (unpubl.).

DMITRE 2006a. Mineral deposit information: Tunkillia Area 191 <https://egate.pir.sa.gov.au/minerals/new/pages/PrintMineralDepositDetail/getData?DEPOSIT_NO=3128&DEPOSIT_NAME=TUNKILLIA+AREA+191>. (retrieved December 6 2012).

DMITRE 2006b. Mineral deposit information: Tunkillia Tomahawk <https://egate.pir.sa.gov.au/minerals/new/pages/MineralDepositDetail/getData?DEPOSIT_NO=3127&S_DEPOSIT_NAME=tunkillia&S>. (retrieved December 6 2012).

DORR K. V. H., HOOVER D. B., OFFIELD T. N. & SHACKLETTE H. T. 1971. The application of geochemical, botanical, geophysicals, and remote sensing mineral prospecting techniques to tropical areas: Start of the art and needed research. *U.S. Geological Survey*.

DREW G. J. 1992. *Goldfields of South Australia*. Department of Mines and Energy. Primary Industries and Resources of South Australia.

DROWN C. 2003. The Barns Gold Project: Discovery in an emerging district. *MESA Journal* **28**, 4-9.

DROWN C. G. 2002. Barns Gold Project, Eyre Peninsula, South Australia. *Gawler Craton 2002: State of Play,* Adelaide. Department of Primary Industries and Resources.

DUNN C. E. 1986. Biogeochemistry as an aid to exploration for gold, platinum and palladium in the northern forests of Saskatchewan, Canada. *Journal of Geochemical Exploration* **25**, 21-40.

DUNN C. E. 2007. *Biogeochemistry in mineral exploration* (1st edition). (Handbook of exploration and environmental geochemistry, Vol. Volume 9). Elsevier, Amsterdam.

DUNN C. E. 2011. *Successful applications of plant biogeochemistry in mineral exploration*. van der Hoek B. G.

DUNN C. E., HALL G. E. M., COHEN D., CATT P. & LINTERN M. J. 1995. Applied biogeochemistry in mineral exploration and environmental studies. *17th International Geochemical Exploration Symposium* Townsville, Australia. The Association of Exploration Geochemists.

DUNN C. E., THOMPSON R. I., ANDERSON R. G. & PLOUFFE A. 2009. Element Distribution Patterns and Mineral Discoveries using Biogeochemical Methods. *Proceedings of the 24th International Applied Geochemistry Symposium,* Fredericton, New Brunswick, Canada, pp. 31-34.

EDGECOMBE D. 1997. Challenger gold deposit: Exploration case history. *MESA Journal* **4**, 8-11.

EGGLETON R. A. 2001. *The Regolith Glossary* (Surficial geology, soils and landforms). CSIRO, Canberra.

EGGLETON R. A. 2009. Regolith Mineralogy. *In:* Scott K. & Pain C. eds., *Regolith Science*, pp 45-72, CSIRO Publishing; Springer, Collingwood.

FABRIS A. J. 2009. *Is CHIM a potential exploration method in South Australia?* PIRSA.

FABRIS A. J. 2010. Investigation of partial leach soil surveys at the Tunkillia Gold prospect, SA. *Primary Industries and Resources South Australia* **Report Book 2010/01**.

FABRIS A. J. & KEELING J. L. 2010. Soil geochemistry to explore through aeolian cover: results from the Tunkillia gold prospect, Great Victoria Desert. *MESA Journal* **57**, 16-21.

FAIRCLOUGH M. C. & SCHWARZ M. P. 2003. Gawler Craton 2003: State of Play, The Excursion. *DMITRE* **Report Book 2003/17**.

FARMER A. M. 1993. The effects of dust on vegetation—a review. *Environmental Pollution* **79**, 63-75.

FERRIS G., SCHWARZ M. P., FAIRCLOUGH M. C., HEITHERSAY P. S., J D. S. & MORRIS B. J. 2003. *The Mineral Prospectivity of Yellabinna Region, Western Gawler Craton, South Australia*. Department of Primary Industries and Resources, South Australia.

FERRIS G. & WILSON M. 2004. Tunkillia Project: Proterozoic shear-zone-hosted gold mineralisation within the Yarlbrinda Shear Zone. *MESA Journal* **35**, 6-12.

FERRIS G. M. 2001. The geology and geochemistry of granitoids in the Childara region, western Gawler craton, South Australia—implications for the Proterozoic tectonic history of the western Gawler craton and the development of lode-style gold mineralization at Tunkillia. Masters thesis, University of Tasmania, Hobart (unpubl.).

FISHER L., CLEVERLEY J., BARNES S. & SCHMID S. 2011. DETCRC Report: Field Portable X-ray Fluorescence (pXRF) calibration and a proposed workflow for application to minerals exploration and mining. *CSIRO* **EP114660**.

FLEET E., DEER W. A., ZUSSMAN J. & HOWIE R. A. 2003. *Rock Forming Minerals*. Geological Society Publishing House.

FLINT R. 2009. *Exploration strategies for gold mineralisation in the Tunkillia area. SA Resources Conference, 27 Nov 2009*.

FRADD W. P. 1988. Earea Dam goldfield, historical review and production records. *Department of Mines and Energy South Australia* **Report Book 88/40**.

FRANCESCHI V. 2001. Calcium Oxalate in Plants. *Trends in Plant Science* **6**, 331.

FRANCESCHI V. & SCHUEREN A. M. 1986. Incorporation of Strontium into Plant Calcium Oxalate Crystals. *Protoplasma* **130**, 199-205.

FRASER G. L., SKIRROW R. G., SCHMIDT-MUMM A. & HOLM O. 2007. Mesoproterozoic Gold in the Central Gawler Craton, South Australia: Geology, Alteration, Fluids, and Timing. *Economic Geology* **102**, 1511-1539.

FRASER S. J. 1997. A regional overview of the Charters Towers-North Drummond Basin region: Geomorphic landform provinces. *CSIRO Exploration and Mining*.

FRASER S. J. 2006. *Making sense of complex data*. *Earthmatters: CSIRO exploration & mining magazine*. Brace M**:** 14-15. CSIRO.

FRASER S. J. 2012. SiroSOM Workshop. *CSIRO* **P2012/002**.

FRASER S. J. & DICKSON B. L. 2007. A New Method for Data Integration and Integrated Data Interpretation: Self-Organising Maps. *Fifth Decennial International Conference on Mineral Exploration,* Toronto, Canada, pp. 907-910.

FRASER S. J. & HODGKINSON J. H. 2009. An Investigation Using SiroSOM for the Analysis of QUEST Stream-Sediment and Lake-Sediment Geochemical Data. *CSIRO* **P2009/983**.

GARRETT R. G., REIMANN C., SMITH D. B. & XIE X. 2008. From geochemical prospecting to international geochemical mapping: a historical overview. *Geochemistry: Exploration, Environment, Analysis* **8**, 205-217.

GIBBONS L. 1997. Regolith study of the Old Well gold prospect, Tarcoola District, Gawler Craton. Honours thesis, Geology and Geophysics, University of Adelaide, Adelaide (unpubl.).

GILE L. H., PETERSON F. F. & GROSSMAN R. B. 1966. Morphological and genetic sequences of carbonate accumulation in desert soils. *Soil Science* **101**, 347-360.

GIRLING C. A., PETERSON P. J. & MINSKI M. J. 1978. Gold and arsenic concentrations in plants as an indication of gold mineralisation. *Science of The Total Environment* **10**, 79-85.

GOUDIE A. S. 1973. *Duricrusts in tropical and subtropical landscapes*. Clarendon Press, Oxford.

GOUDIE A. S. 1983. Calcretes. *In:* Goudie A. S. & Pye K. eds., *Chemical sediments and geomorphology: precipitates and residua in the near surface environment*, pp 93-132, Academic Press, London.

GRAY D. J. & LINTERN M. J. 1994. The solubility of gold in soils from semi-arid areas of Western Australia. *Exploration & Mining Research News* **1**, 8-9.

GRAY D. J. & LINTERN M. J. 1998. Chemistry of gold in the soils from the Yilgarn Craton, Western Australia. *The State of the Regolith. Proceedings of the Second Australian Conference on Landscape Evolution and Mineral Exploration. Springwood, NSW*, pp. 209-221. Geological Society of Australia Special Edition.

GRAY D. J. & PIRLO M. C. 2005. Hydrogeochemistry of the Tunkillia Gold Prospect, South Australia. *CRC LEME*.

GRENFEL RESOURCES NL 1997. Company Exploration Highlights. *In*, *MESA Journal*, Vol. 5, pp 12-13.

GULSON B., KORSCH M., DICKSON B., COHEN D., MIZON K. & MICHAEL DAVIS J. 2007. Comparison of lead isotopes with source apportionment models, including SOM, for air particulates. *Science of The Total Environment* **381**, 169-179.

HAWKES H. E. & WEBB J. S. 1962. *Geochemistry in Mineral Exploration* (Harper's Geoscience Series). Harper & Row, New York.

HICKS C. B. 2010. The Regolith Expression of Cu-Au mineralisation within the Northern region of the Project Mawson area, NE Eyre Peninsula, South Australia. Honours thesis, Geology and

Geophysics, University of Adelaide, Adelaide (unpubl.).

HILL L. J. 2002. Branching out into biogeochemical surveys: A guide to vegetation sampling. *In:* Roach I. C. ed., *Regolith and Landscapes in Eastern Australia*, pp 50-53, CRC LEME.

HILL L. J. 2004. Geochemical and biogeochemical dispersion and residence in landscapes of western New South Wales. Doctor of Philosophy thesis, Geology and Geophysics, The Australian National University, Canberra (unpubl.).

HILL P. & CROOKS A. F. 1991. Mineral occurrences of the Gairdner 1:250,000 map sheet area. *Department of Mines and Energy South Australia* **Report Book 91/89**.

HILL R. J. 2006. Unlocking South Australia's Mineral and Energy Potential - A Plan for Accelerating Exploration. Theme 2 (drilling partnerships with PIRSA and industry) : Year 2 partnership no. 33, Tunkillia Gold Project gradient IP mineral prospect. Project final report. *Primary Industries and Resources South Australia* **Open File Envelope No. 11,167**.

HILL S. M. & CHITTLEBOROUGH D. 2011. *Fowlers Gap Field Trip*. University of Adelaide.

HILL S. M., EGGLETON R. A. & TAYLOR G. 2003. Neotectonic disruption of silicified palaeovalley systems in an intraplate, cratonic landscape: Regolith and landscape evolution of the Mulculca range-front, Broken Hill Domain, New South Wales. *Australian Journal of Earth Sciences* **50**, 691-707.

HILL S. M., TAYLOR G., MCQUEEN K. G., ANAND R. R., PHANG C., WILDMAN J. E. & LINTERN M. J. 1998. Genesis of some calcretes in the southern Yilgarn Craton, Western Australia: Implications for mineral exploration. *Australian Journal of Earth Sciences* **45**, 177-182.

HINSINGER P., PLASSARD C. & JAILLARD B. 2006. Rhizosphere: A new frontier for soil biogeochemistry. *Journal of Geochemical Exploration* **88**, 210-213.

HOATSON D. M., SUN S.-S., DUGGAN M. B., DAVIES M. B., DALY S. J. & PURVIS A. C. 2005. Late Archean Lake Harris Komatiite, Central Gawler Craton, South Australia: Geologic Setting and Geochemistry. *Economic Geology* **100**, 349-374.

HOPKINSON A. L. 2009. Biogeochemical expression of the 'Tomahawk' Au-in-calcrete anomaly, Tunkillia, Gawler Craton, South Australia. Honours thesis, Geology and Geophysics, University of Adelaide, Adelaide (unpubl.).

HOU B. 2008. Palaeochannel studies related to the Harris Greenstone Belt, Gawler Craton, South Australia. *CSIRO CRC LEME Open File Report* **154**.

HOU B. & ALLEY N. 2003. A model for gold and uranium dispersion and concentration in residual and transported regolith along palaeodrainage systems: a case study from the central Gawler Craton. *MESA Journal* **30**, 49-53.

HULME K. A. 2010. *Eucalyptus camaldulensis* (river red gum) biogeochemistry: an innovative tool for mineral exploration in the Curnamona Province and adjacent regions. Doctor of Philosophy thesis, Geology and Geophysics, University of Adelaide, Adelaide (unpubl.).

HULME K. A. & HILL S. M. 2003. River red gums as a biological sampling medium in mineral exploration and environmental chemistry programs in the Curnamona Craton and adjacent regions of NSW and SA. *Advances in Regolith*, 205-210.

HULME K. A., HILL S. M. & DUNN C. E. 2006. Biogeochemistry for mineral exploration in Canada & Australia: A comparison based on international collaboration. *Regolith*.

JACKSON R. B., CANADELL J., EHLERINGER J. R., MOONEY H. A., SALA O. E. & SCHULZE E. D. 1996. A global analysis of root distributions for terrestrial biomes. *Oecologia* **108**, 389-411.

JACKSON R. B., MOORES L. A., HOFFMANN W. A., POCKMAN W. T. & LINDER C. R. 1999. Ecosystem rooting depth determined with caves and DNA. *Proceedings of the National Academy of Sciences* **96**, 11387-11392.

KABATA-PENDIAS A. & PENDIAS H. 2001. *Trace elements in soils and plants* (3rd ed. edition). CRC Press.

KEELING J. L. 2004. Metal ion dispersion through transported cover at Moonta, South Australia. *In:* Roach I. C., Aspandiar M. & Hill S. M. eds., *Regolith 2004: Proceedings of the CRC LEME Regional Regolith Symposia 2004*, pp 161-165, Cooperative Research Centre for Landscape Environments and Mineral Exploration, Bentley, WA.

KLAPPA C. F. 1983. A process-response model for the formation of pedogenic calcretes. *Geological Society, London, Special Publications* **11**, 211-220.

KLINGBERG L. L. 2009. Regolith-Landforms and regolith geochemistry of the 'Tomahawk' Au-in-calcrete anomaly: Tunkillia, Gawler Craton, South Australia. Honours thesis, Geology and Geophysics, University of Adelaide, Adelaide (unpubl.).

KLINGBERG L. L. 2010. *Regolith-Landforms and regolith geochemistry of the 'Tomahawk' Au-in-calcrete anomaly: Tunkillia, Gawler Craton, South Australia*. Sydney Mineral Exploration Discussion Group.

KNIGHT A. C. 2010. An evaluation of new mineral exploration technologies for effective mineral

exploration undercover near Broken Hill. Honours thesis, Geology and Geophysics, University of Adelaide, Adelaide (unpubl.).

KOHONEN T. 1990. The self-organizing map. *Proceedings IEEE* **78**, 1464-1480.

KOHONEN T. 1998. The self-organizing map. *Neurocomputing* **21**, 1-6.

KOVALEVSKII A. L. & KOVALEVSKAYA O. M. 1989. Biogeochemical haloes of gold in various species and parts of plants. *Applied Geochemistry* **4**, 369-374.

LAMPLUGH G. W. 1902. Calcrete. *Geological Magazine (Decade IV)* **9**, 575.

LANGFORD-SMITH T. 1978. *A select review of silcrete research in Australia*. *Silcrete in Australia*. Langford-Smith T. University of New England.

LEVINSON A. A. 1974. *Introduction to exploration geochemistry*. Applied Publishing Ltd., Calgary.

LINTERN M., HOUGH R. & RYAN C. 2011. Experimental studies on the gold-in-calcrete anomaly at Edoldeh Tank Gold Prospect, Gawler Craton, South Australia. *Journal of Geochemical Exploration*.

LINTERN M. J. 1997. Calcrete sampling for gold exploration. *MESA Journal* **5**, 5-8.

LINTERN M. J. 1999. *Study of the distribution of gold in soils at Mount Hope, Western Australia / M.J. Lintern* (Restricted report (CSIRO. Division of Exploration Geoscience) ; 24R 1989.). CRC LEME, Wembley, W.A. :.

LINTERN M. J. 2002. Calcrete sampling for mineral exploration. *In:* Chen X. Y., Lintern M. J. & Roach I. C. eds., *Calcrete: characteristics, distribution and use in mineral exploration*, CRC LEME.

LINTERN M. J. 2004a. Preliminary Biogeochemical Studies at Barns Gold Prospect, Gawler Craton, South Australia. *CSIRO CRC LEME Open File Report* **168**.

LINTERN M. J. 2004b. Preliminary regolith studies at Earea Dam Gold Prospect, Gawler Craton, South Australia. *CRC LEME Open File Report* **153**.

LINTERN M. J. 2005. Biogeochemical anomalies at Barns gold prospect (Eyre Peninsula, South Australia). *In:* Roach I. C. ed., *Regolith 2005 - Ten years of CRC LEME*, pp 195-196, CRC LEME.

LINTERN M. J. 2007. Vegetation controls on the formation of gold anomalies in calcrete and other materials at the Barns Gold Prospect, Eyre Peninsula, South Australia. *Geochemistry: Exploration, Environment, Analysis* **7**, 249-266.

LINTERN M. J. & BUTT C. R. M. 1993. Pedogenic Carbonate: An important samping medium for gold exploration in semi-arid areas. *Exploration Research News* **7**, 7-11.

LINTERN M. J., BUTT C. R. M. & SCOTT K. M. 1997. Gold in vegetation and soil - three case studies from the goldfields of south Western Australia. *Journal of Geochemical Exploration* **58**, 1-14.

LINTERN M. J., CRAIG M. A., WALSH D. M. & SHERIDAN N. C. 2001. The distribution of gold & other elements in surficial materials from the Higginsville palaeochannel gold deposits, Norseman, Western Australia. *CSIRO CRC LEME Open File Report* **102**.

LINTERN M. J., HOUGH R. M., RYAN C. G., WATLING J. & VERRALL M. 2009. Ionic gold in calcrete revealed by LA-ICP-MS, SXRF and XANES. *Geochimica et Cosmochimica Acta* **73**, 1666-1683.

LINTERN M. J. & SCOTT K. M. 1998. The distribution of gold and other elements in soils and vegetation at Panglo, Western Australia. *CSIRO CRC LEME Open File Report* **44**.

LINTERN M. J., SHEARD M. J. & CHIVAS A. R. 2006a. The source of pedogenic carbonate associated with gold-calcrete anomalies in the western Gawler Craton, South Australia. *Chemical Geology* **235**, 299-324.

LINTERN M. J., SHEARD M. J. & GOUTHAS G. 2006b. Regolith studies at the Boomerang Gold Prospect, Central Gawler Craton, South Australia. *CRC LEME Open File Report* **203**.

LOTTERMOSER B. G., ASHLEY P. M. & MUNKSGAARD N. C. 2008. Biogeochemistry of Pb–Zn gossans, northwest Queensland, Australia: Implications for mineral exploration and mine site rehabilitation. *Applied Geochemistry* **23**, 723-742.

LOWREY J. R. 2007. Plant biogeochemical expression of Au-mineralisation buried by an aeolian dunefield: Tunkillia, South Australia. Honours thesis, Geology and Geophysics, University of Adelaide, Adelaide (unpubl.).

LOWREY J. R. & HILL S. M. 2006. Plant biogeochemistry of Au-mineralisation buried by an aeolian dunefield: Tunkillia, S.A. *Regolith* **2006**, 217-220.

LUNGWITZ E. E. 1900. The lixiviation of gold deposits by vegetation and its geological importance. *Mining Journal (London)* **69**, 500-502.

MANN A. W. 2009. Ligand Based Soil Extraction Geochemistry <http://www.sgs.com/~/Media/Global/Documents/Third%20Party%20Documents/Third%20Party%20Technical%20and%20Research%20Papers/SGS-MIN-WA205-Ligand-Geochemistry-EN-11>. (retrieved 20/1/2013).

MANN A. W., BIRRELL R. D., FEDIKOW M. A. F. & DE SOUZA H. A. F. 2005. Vertical ionic migration: mechanisms, soil anomalies, and sampling depth for mineral exploration. *Geochemistry: Exploration, Environment, Analysis* **5**, 201-210.

MANN A. W., BIRRELL R. D., MANN A. T., HUMPHREYS D. B. & PERDRIX J. L. 1998. Application of the mobile metal ion technique to routine geochemical exploration. *Journal of Geochemical Exploration* **61**, 87-102.

MARTIN A. R. 1997. The discovery of gold mineralisation at Tunkillia in the Gawler Craton. *Helix Resources NL*.

MATSCHULLAT J., OTTENSTEIN R. & REIMANN C. 2000. Geochemical background – can we calculate it? *Environmental Geology* **39**, 990-1000.

MCCONACHY G. W. 2001. Grenfell Resources Ltd. Partial Relinquishment Report EL 2413. *Primary Industries and Resources South Australia* **Open File Envelope No. 9707**.

MCCULLEY R. L., JOBBÁGY E. G., POCKMAN W. T. & JACKSON R. B. 2004. Nutrient Uptake as a Contributing Explanation for Deep Rooting in Arid and Semi-Arid Ecosystems. *Oecologia* **141**, 620-628.

MCINNES B. I. A., DUNN C. E., CAMERON E. M. & KAMEKO L. 1996. Biogeochemical exploration for gold in tropical rain forest regions of Papua New Guinea. *Journal of Geochemical Exploration* **57**, 227-243.

MCKENZIE N. 2004. *Australian Soils and Landscapes: An Illustrated Compendium*. CSIRO Pub.

MCQUEEN K. G. 2005a. Identifying geochemical anomalies. *CRC LEME*.

MCQUEEN K. G. 2005b. Ore deposits and their primary expressions. *In:* Butt C. R. M., Robertson I. D. M., Scott K. M. & Cornelius M. eds., *Regolith expression of Australian ore systems*, pp 1-14, CRC LEME, Perth.

MCQUEEN K. G. 2006a. Calcrete geochemistry in the Cobar-Girilambone region, New South Wales. *CRC LEME Open File Report* **200**.

MCQUEEN K. G. 2006b. Unravelling the regolith with geochemistry. *In:* Fitzpatrick R. W. & Shand P. eds., *Regolith 2006: Consolidation and Dispersion of Ideas*, pp 230-235, CRC LEME, Perth, Western Australia.

MCQUEEN K. G. 2009. Regolith Geochemistry. *In:* Scott K. & Pain C. eds., *Regolith Science*, pp 73-104, CSIRO Publishing; Springer, Collingwood.

MCQUEEN K. G., HILL S. M. & FOSTER K. A. 1999. The nature and distribution of regolith carbonate accumulations in southeastern Australia and their potential as a sampling medium in geochemical exploration. *Journal of Geochemical Exploration* **67**, 67-82.

MEINZER O. E. 1923. *Outline of Ground-water Hydrology with Definitions*. U.S. Government Printing Office.

MEINZER O. E. 1927. *Plants as indicators of ground water*. U.S. Govt. Print. Off.

MERRY N., PONTUAL S. & GAMSON P. 1998. The relevance to geochemical surveys of mapping the regolith with field portable spectrometers. Regolith 1998: New approaches to an Old Continent, Kalgoorlie (unpubl.).

MINOTAUR EXPLORATION LTD, MITHRIL RESOURCES LTD & TORO ENERGY LTD 2010. EL 3107/EL4197, Glenloth, First partial relinquishment report for the period 11/7/2003 to 2/11/2009. *Primary Industries and Resources South Australia* **Open File Envelope No. 12,035**.

MITCHELL C. 2010. The Regolith Expression of IOCG mineralisation within the southern region of the Project Mawson area, NE Eyre Peninsula, South Australia. Honours thesis, Geology and Geophysics, University of Adelaide, Adelaide (unpubl.).

MORONI M. T. 2012. Aspects of forest carbon management in Australia – A discussion paper. *Forest Ecology and Management* **275**, 111-116.

MORRIS D. F. C. & SHORT E. L. 1969. Rhenium. *In:* Wedepohl K. H. ed., *Handbook of geochemistry*, pp 75.A.71 - 75.O.75, Springer Verlag, Berlin.

MORTON S. R., STAFFORD SMITH D. M., DICKMAN C. R., DUNKERLEY D. L., FRIEDEL M. H., MCALLISTER R. R. J., REID J. R. W., ROSHIER D. A., SMITH M. A., WALSH F. J., WARDLE G. M., WATSON I. W. & WESTOBY M. 2011. A fresh framework for the ecology of arid Australia. *Journal of Arid Environments* **75**, 313-329.

MUNGANA GOLDMINES LTD. 2011. Mungana to Acquire Controlling Interest in the Tunkillia Gold Project. *Mungana Gold Mines Ltd.*

MUNGANA GOLDMINES LTD. 2012. September 2012 Quarterly Report <http://www.asx.com.au/asxpdf/20121029/pdf/429rnzpc0ccf2p.pdf>. (retrieved Nov 28, 2012).

NAKATA P. A. 2003. Advances in our understanding of calcium oxalate crystal formation and function in plants. *Plant Science* **164**, 901-909.

NAUDÉ T. W. & NAIDOO V. 2007. *Oxalates-containing plants*. *Veterinary Toxicology*. Gupta R. C.**:** 880-891. Elsevier.

NESBITT H. W. 1979. Mobility and fractionation of rare earth elements during weathering of a granodiorite. *Nature* **279**, 206-210.

NESBITT H. W. & YOUNG G. M. 1989. Formation and Diagenesis of Weathering Profiles. *The Journal of Geology* **97**, 129-147.

NETTERBERG F. 1980. Geology of southern African calcretes. I. Terminology, description, macrofeatures and classification. *Transactions of the Geological Society of South Africa*, 255-283.

NETTERBERG F. & CAIGER J. H. 1983. A Geotechnical classification of calcretes and other pedocretes. *Geological Society, London, Special Publications* **11**, 235-243.

NIKNAM S. R. & MCCOMB J. 2000. Salt tolerance screening of selected Australian woody species -- a review. *Forest Ecology and Management* **139**, 1-19.

NOY-MEIR I. 1973. Desert Ecosystems: Environment and Producers. *Annual Review of Ecology and Systematics* **4**, 25-51.

OLYMPUS INNOV-X 2011. Periodic Table of Detectable Elements <http://www.olympus-ims.com/en/.downloads/download/?file=285213158&fl=en_US>. (retrieved 24/1/2013).

OVERALL R. A. & PARRY D. L. 2004. The uptake of uranium by Eleocharis dulcis (Chinese water chestnut) in the Ranger Uranium Mine constructed wetland filter. *Environmental Pollution* **132**, 307-320.

PAIN C. 2009. Regolith description and mapping. *In:* Scott K. & Pain C. eds., *Regolith Science*, pp 281-305, CSIRO Publishing; Springer, Collingwood.

PAIN C. F., CHAN R., CRAIG M., GIBSON D., KILGOUR P. & WILFORD J. 2007. RTMAP Regolith Database Field Book and Users Guide. *CRC LEME Open File Report* **231**.

PIRSA 2006. Gold <http://outernode.pir.sa.gov.au/minerals/geology/minerals_mines_and_quarries/commodities/gold>. (retrieved 10/12/2011).

PIRSA 2011. Gawler Calcrete Re-Analysis Project <http://www.pir.sa.gov.au/minerals/geology/geological_provinces/gawler_craton/gawler_calcrete>. (retrieved 23/12/2011).

PONTUAL S. 2007. Characterisation of regolith profiles by infrared spectroscopy. *In:* Cooper B. J. & Keeling J. L. eds., *5th Sprigg Symposium, November 2007: Regolith, Mineral Deposits and Environment*, Vol. 87, pp 67-70, Geological Society of Australia Abstracts, Adelaide.

PONTUAL S. 2009. Introduction to spectral geology a workshop manual. *Primary Industries and Resources South Australia, Alteration Mapping - HyLogger Workshop. Course manual, ASEG 09* **Report Book 2009/6**.

POTMA W. & SKIRROW R. 2006. Tunkillia modelling: Preliminary Results & some Predictive Targeting Outcomes. *CSIRO* **P2006/121**.

POTMA W. & ZHANG Y. 2006. Regional Thermal-Fluid-Flow Modelling: Preliminary Results & some Predictive Targeting Outcomes. *CSIRO* **P2006/120**.

QUADE J., CHIVAS A. R. & MCCULLOCH M. T. 1995. Strontium and carbon isotope tracers and the origins of soil carbonate in South Australia and Victoria. *Palaeogeography, Palaeoclimatology, Palaeoecology* **113**, 103-117.

RAJAGOPALAN S., ZHIQUN S. & MAJOR R. 1993. Geophysical Investigations of Volcanic Terrains: A Case History from the Gawler Range Volcanic Province, South Australia. *Exploration Geophysics* **24**, 769-778.

REID N. 2008. Phyto-exploration in arid subtropical, arid mediterranean and tropical savanna environments: Biogeochemical mechanisms and implications fo mineral exploration. Doctor of Philosophy thesis, Geology and Geophysics, University of Adelaide, Adelaide (unpubl.).

REID N., HILL S. M. & LEWIS D. M. 2009. Biogeochemical expression of buried gold mineralization in semi-arid northern Australia: penetration of transported cover at the Titania Gold Prospect, Tanami Desert, Australia. *Geochemistry: Exploration, Environment, Analysis* **9**, 267-273.

REID N., LINTERN M. J., ANAND R. R., PINCHAND T., GRAY D. J., NOBLE R. R. P., SUTTON G. & JARRETT R. 2010. *North East Yilgarn Biogeochemistry Project (MERIWA)* (Record 2010/4 edition). Geological Survey of Western Australia.

REIMANN C. 2005. Geochemical mapping: technique or art? *Geochemistry: Exploration, Environment, Analysis* **5**, 359-370.

REIMANN C. & FILZMOSER P. 2000. Normal and lognormal data distribution in geochemistry: death of a myth. Consequences for the statistical treatment of geochemical and environmental data. *Environmental Geology* **39**, 1001-1014.

RHODES E., CHAPPELL J., FUJIOKA T., FITZSIMMONS K., MAGEE J., AUBERT M. & HEWITT D. 2005. The history of aridity in Australia: Chronological developments. *In:* Roach I. C. ed., *Regolith 2005 - Ten years of CRC LEME*, pp 265-268, CRC LEME.

RICHARDS J. H. & CALDWELL M. M. 1987. Hydraulic Lift: Substantial Nocturnal Water Transport

between Soil Layers by Artemisiatridentata Roots. *Oecologia* **73**, 486-489.

RINGROSE C. 2011. High-grade, zinc discovery at surface in the "TL Property" south east British Columbia, Canada. *Cullen Resources Ltd. ASX Announcement*.

RISELY A. L. 2009. Soil geochemical expression of geophysical targets buried by an aeolian dunefield: 'BRAVO' prospect, Tunkillia, South Australia. Honours thesis, Geology and Geophysics, University of Adelaide, Adelaide (unpubl.).

ROBINSON J. & POTMA W. 2007. Tunkillia deposit scale modelling: Predictive Targeting Outcomes. *CSIRO* **P2007/587**.

RODUSHKIN I. & AXELSSON M. D. 2000. Application of double focusing sector field ICP-MS for multielemental characterization of human hair and nails. Part I. Analytical methodology. *Science of The Total Environment* **250**, 83-100.

ROLLINSON H. R. 1993. *Using geochemical data: evaluation, presentation, interpretation* (Geochemistry series). Pearson Education Ltd., Essex, England.

SALOMONS W. & MOOK W. G. 1986. Isotope geochemistry of carbonates in the weathering zone. *In:* Fritz P. & Fontes J. C. eds., *Handbook of Environmental Isotope Geochemistry*, Vol. 2, pp 239-269, Elsevier, Amsterdam, New York.

SCHMIDT MUMM A., CLARK C. & SKIRROW R. 2006. Mineral exploration under cover: Characterizing mineralizing fluid systems. *Journal of Geochemical Exploration* **89**, 359-362.

SCHMIDT MUMM A. & REITH F. 2007. Biomediation of calcrete at the gold anomaly of the Barns prospect, Gawler Craton, South Australia. *Journal of Geochemical Exploration* **92**, 13-33.

SCHWARZ M. P., MORRIS B. J., SHEARD M. J., FERRIS G. M., DALY S. J. & DAVIES M. B. 2010. *Chapter 4: Gawler Craton*. *South Australian mineral explorers guide*.

SCOTT K. M. 2009. Appendix 2: Regolith geochemistry of elements. *In:* Scott K. & Pain C. eds., *Regolith Science*, pp 433-452, CSIRO Publishing; Springer, Collingwood.

SGS 2011a. Mobile Metal Ions (MMI™) <http://www.sgs.com/en/Mining/Analytical-Services/Geochemistry/Mobile-Metal-Ions-MMI.aspx>. (retrieved February 21 2012).

SGS 2011b. Mobile Metal Ions (MMI™) Sampling Guide <http://www.sgs.com/~/media/Global/Documents/Flyers%20and%20Leaflets/SGS-MIN-WA002-MMI-Sampling-Guide-EN-11.pdf>. (retrieved March 23 2012).

SHEARD M. J., KEELING J. L., LINTERN M. J., HOU B., MCQUEEN K. G. & HILL S. M. 2007. *A guide for mineral exploration through the regolith of the central Gawler Craton, South Australia*. CRC LEME c/o CSIRO Exploration and Mining, Perth.

SHEARD M. J., LINTERN M. J., PRESCOTT J. R. & HUNTLEY D. J. 2006. Optical luminescence dating of sands from the Great Victoria Desert; South Australia's oldest desert dune system? *Regolith*, 318-321.

SHEARD M. J. & ROBERTSON I. D. M. 2004. Regolith characterisation and geochemistry as an aid to mineral exploration in the Harris Greenstone Belt, Central Gawler Craton, South Australia. *CSIRO CRC LEME Open File Report* **155**.

SLATER J. A., HAASE J., HEADY B., KROENUNG G. & LITTLE J. 2006. The SRTM Data "Finishing" Process and Products. *Photogrammetric Engineering & Remote Sensing* **72**, 237-247.

SMEE B. W. & STANLEY C. R. 1988. A test in pattern recognition: defining anomalous patterns in surficial samples which exhibit severe nugget effects. *Explore - Association of Exploration Geochemists Newsletter* **63**, 12-14.

SPECHT R. L. 1994. Biodiversity and conservation. *In:* Groves R. H. ed., *Australian Vegetation* (Second edition), pp 525-555, Cambridge University Press.

STEDNICK J. D., KLEM R. B. & RIESE W. C. 1987. Temporal variation of metal concentrations in biogeochemical samples over the Royal Tiger Mine, Colorado, part I: Within year variation. *Journal of Geochemical Exploration* **29**, 75-88.

STYLES G. 1980. Tarcoola Tertiary Drilling Project: Final Report On Drilling, March/April 1980. *PIRSA* **Open File Envelope No. 05234**.

SWAIN G., WOODHOUSE A., HAND M., BAROVICH K., SCHWARZ M. & FANNING C. M. 2005. Provenance and tectonic development of the late Archaean Gawler Craton, Australia; U–Pb zircon, geochemical and Sm–Nd isotopic implications. *Precambrian Research* **141**, 106-136.

TANTI D. J. 2011. Biogeochemical and Regolith expression of buried nonferrous mineralisation in the Northern Middleback Ranges, Iron Knob North, South Australia. Honours thesis, Geology and Geophysics, University of Adelaide, Adelaide (unpubl.).

TAYLOR G. & EGGLETON R. A. 2001. *Regolith geology and geomorphology*. John Wiley & Sons, NY, Brisbane.

THIRY Y., SCHMIDT P., VAN HEES M., WANNIJN J., VAN BREE P., RUFYIKIRI G. & VANDENHOVE H. 2005. Uranium distribution and cycling in Scots pine (Pinus sylvestris L.) growing on a revegetated U-mining heap. *Journal of Environmental Radioactivity* **81**, 201-219.

THOMAS L. 2011. Regolith-Landforms and plant biogeochemical expression of buried mineralization targets in the Northern Middleback Ranges, Iron Knob South, South Australia. Honours thesis, Geology and Geophysics, University of Adelaide, Adelaide (unpubl.).

THOMAS M. 2004. Biogeochemical data ranges from Tunkillia Prospect, central Gawler Craton, South Australia. *Regolith 2004: Proceedings of the CRC LEME Regional Regolith Symposia 2004,* CRC LEME, pp. 362-364. Bentley.

THOMAS M., MAUGER A. & HUNTINGTON J. 2006. *New Central Gawler Gold Hylogger Results*. Geoscience Australia.

VAN DER HOEK B. G., HILL S. M. & DART R. C. 2011. Regolith carbonate geochemical and plant biogeochemical inter-relationships for the expression of deeply buried mineralisation at the Tunkillia gold prospect, central Gawler Craton, Australia. International Applied Geochemistry Symposium, Rovaniemi, Finland (unpubl.).

VAN DER HOEK B. G., HILL S. M. & DART R. C. 2012. Calcrete and plant inter-relationships for the expression of concealed mineralization at the Tunkillia gold prospect, central Gawler Craton, Australia. *Geochemistry: Exploration, Environment, Analysis* **12**, 361-372.

VASEY B. S. S. 2009. Biogeochemical expression of geophysical targets within the Yarlbrinda Shear Zone south of Tunkillia, Gawler Craton, South Australia. Honours thesis, Geology and Geophysics, University of Adelaide, Adelaide (unpubl.).

VERBOOM W. H. & PATE J. S. 2006a. Bioengineering of soil profiles in semiarid ecosystems: the 'phytotarium' concept. A review. *Plant and Soil* **289**, 71-102.

VERBOOM W. H. & PATE J. S. 2006b. Evidence of active biotic influences in pedogenetic processes. Case studies from semiarid ecosystems of south-west Western Australia. *Plant and Soil* **289**, 103-121.

VESANTO J. 2005. SOM implementation in SOM Toolbox <http://www.cis.hut.fi/projects/somtoolbox/documentation/somalg.shtml>. (retrieved 10/1/2013).

WHITTEN G. F., WRIGHT R. G. & SOUTH R. 1976. Geochemical exploration in the Earea Dam Glenloth mining fields. *Mineral Resources Review* **No.144**.

WILLS K. J. A. 1997. Application of calcrete sampling in South Australia. *Adelaide Resources NL*.

WOODHEAD J. D., HELLSTROM J., HERGT J. M., GREIG A. & MAAS R. 2007. Isotopic and Elemental Imaging of Geological Materials by Laser Ablation Inductively Coupled Plasma-Mass Spectrometry. *Geostandards and Geoanalytical Research* **31**, 331-343.

WOPFNER H. 1978. Silcretes of northern South Australia and adjacent regions. *In:* Langford-Smith T. ed., *Silcrete in Australia*, pp 93-141, University of New England.

WOTTON N. J. 1992. Broadscale distribution patterns of the pearl bluebush (*Maireana sedifolia*) in northern South Australia. *Proceedings of the 7th Australian Rangeland Society Biennial Conference*, pp. 239-240. Australian Rangeland Society.

WRIGHT V. P. 2008. Calcrete. *In:* Nash D. J. & McLaren S. J. eds., *Geochemical Sediments and Landscapes*, pp 10-45, Blackwell Publishing Ltd.

WRIGHT V. P. & TUCKER M. E. 1991. Calcretes: An Introduction. *In:* Wright V. P. & Tucker M. E. eds., *Calcretes*, Blackwell Scientific Publications, Oxford.

XUEJING X. & BINCHUAN Y. 1993. Geochemical patterns from local to global. *Journal of Geochemical Exploration* **47**, 109-129.

APPENDIX A: Raw data

Raw data are included on the attached disk. The metadata for each dataset is listed in the table below. Coordinate systems are GDA94 Zone 53.

Data type	Material	Laboratory	Chapter(s)	File path
Geochemistry	Calcrete	Genalysis, Perth ALS, Adelaide	6.4	A - Calcrete geochemistry.xlsx
Geochemistry	Calcrete	University of Adelaide	5.5	B - Geochemistry of calcrete THKLK075 by LAICPMS.xlsx
Biogeochemistry	Plants	Acme Analytical Laboratories, Canada	5.2, 5.3, 5.4, 6.1.2, 6.3, 6.4, 6.5	C - Biogeochemistry all data.xlsx
Geochemistry	Rock powders	Acme Analytical Laboratories, Canada	5.1	D - Geochemistry of rock powders from Tunkillia.xlsx
Hylogger™/Hyper-spectral	Rock powders	DMITRE, Glenside, South Australia	5.1	E - Hylogger data

Laboratory reference data

Table A1: V14 certificate of analysis, Acme Analytical Laboratories Ltd. Internal Reference Material for 1VE Vegetation Digestion (2007)

ELEMENT	unit	Detection Limit	Expected Value	Standard Deviation**
Au	ppb	0.2	8.6	7.0
Ag	ppb	2	24	3
Al	%	0.01	0.15	0.01
As	ppm	0.1	11.3	2.9
B	ppm	1	17	1
Ba	ppm	0.1	1.4	0.1
Bi	ppm	0.02	0.09	0.01
Ca	%	0.01	0.67	0.03
Cd	ppm	0.01	0.23	0.01
Co	ppm	0.01	0.83	0.05
Cr	ppm	0.1	1.2	0.2
Cs*	ppm	0.005	0.029	0.001
Cu	ppm	0.01	5.17	0.21
Fe	%	0.001	0.016	0.001
Ga	ppm	0.1	0.1	0.0
Hg	ppb	1	52	4
K	%	0.01	0.51	0.03
La	ppm	0.01	0.03	0.01
Mg	%	0.001	0.079	0.004
Mn	ppm	1	2145	105
Mo	ppm	0.01	0.07	0.05
Na	%	0.001	0.002	0.001
Ni	ppm	0.1	1.5	0.2
P	%	0.001	0.093	0.008
Pb	ppm	0.01	0.88	0.07
S	%	0.01	0.06	0.02
Sb	ppm	0.02	0.07	0.01
Sc	ppm	0.1	0.1	0.0
Se	ppm	0.1	0.2	0.1
Sr	ppm	0.5	6.7	0.4
Te	ppm	0.02	< 0.02	
Th	ppm	0.01	< 0.01	
Ti	ppm	1	7	1
Tl	ppm	0.02	0.04	0.01
U	ppm	0.01	< 0.01	
V	ppm	2	< 2	
W	ppm	0.1	< 0.1	
Zn	ppm	0.1	15.8	1.0

*Optional elements not included in 1VE analytical package

Table A2: V16 certificate of analysis, Acme Analytical Laboratories Ltd. Internal Reference Material for 1VE Vegetation Digestion (2007)

Element	Unit	Detection Limit	Expected Value	Tolerance ± (%)
Au	ppb	0.2	0.9	130
Ag	ppb	2	32	25
Al	%	0.01	0.05	30
As	ppm	0.1	1.6	35
B	ppm	1	5	40
Ba	ppm	0.1	1.9	30
Be*	ppm	0.1	BDL	-
Bi	ppm	0.02	BDL	-
Ca	%	0.01	0.3	20
Cd	ppm	0.01	0.09	40
Ce*	ppm	0.01	0.1	35
Co	ppm	0.01	1.11	35
Cr	ppm	0.1	323.1	50
Cs*	ppm	0.005	0.036	25
Cu	ppm	0.01	6.69	30
Fe	%	0.001	0.413	45
Ga	ppm	0.1	0.2	65
Ge*	ppm	0.01	0.05	100
Hf*	ppm	0.001	0.006	100
Hg	ppb	1	41	30
In*	ppm	0.02	BDL	-
K	%	0.01	0.22	25
La	ppm	0.01	0.05	40
Li*	ppm	0.01	0.07	100
Mg	%	0.001	0.053	25
Mn	ppm	1	720	20
Mo	ppm	0.01	1.6	55
Na	%	0.001	0.002	100
Nb*	ppm	0.01	0.11	60
Ni	ppm	0.1	7.4	50
P	%	0.001	0.049	25
Pb	ppm	0.01	3	20
Pd*	ppb	2	BDL	-
Pt*	ppb	1	BDL	-
Rb*	ppm	0.1	1.7	25
Re*	ppb	1	BDL	-
S	%	0.01	0.02	260
Sb	ppm	0.02	0.07	60
Sc	ppm	0.1	BDL	-
Se	ppm	0.1	BDL	-
Sn*	ppm	0.02	0.23	45
Sr	ppm	0.5	11.2	25
Ta*	ppm	0.001	BDL	-
Te	ppm	0.02	BDL	-
Th	ppm	0.01	BDL	-
Ti	ppm	1	12	30
Tl	ppm	0.02	BDL	-
U	ppm	0.01	BDL	-
V	ppm	2	BDL	-
W	ppm	0.1	BDL	-
Y*	ppm	0.001	0.043	35
Zn	ppm	0.1	39.2	20
Zr*	ppm	0.01	0.018	45
*Optional elements not included in 1VE analytical package				

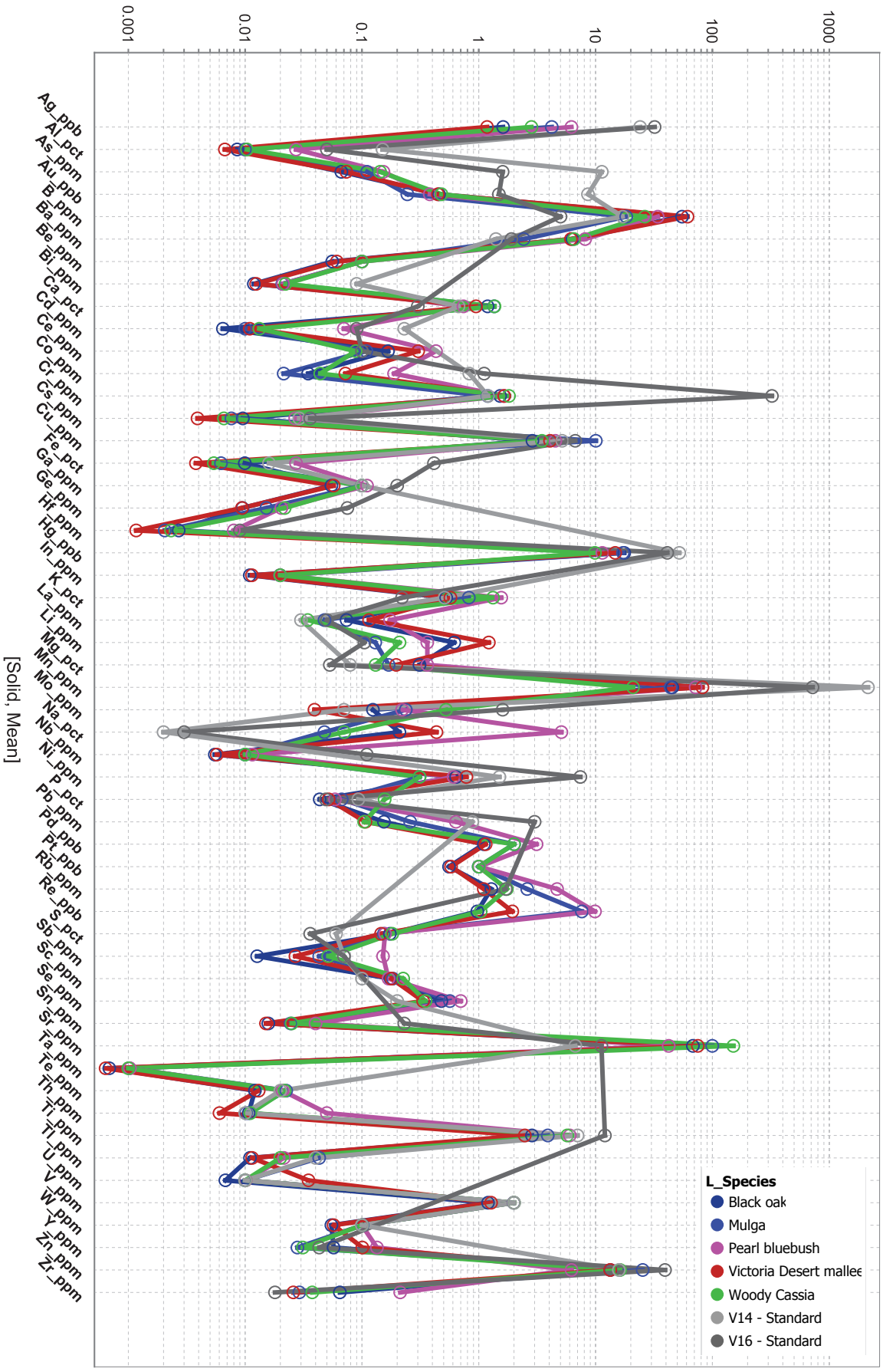

Figure A1: Parallel coordinate plot of average species biogeochemistry. Grey lines represent the standards used by Acme: V14 and V16. Note that the concentrations of some elements in the standards are up to an order of magnitude higher than in the samples.

Regolith profiles (Section 5.1)

Tables are a geochemical summary (presented to 2 significant figures) of the twelve clusters derived from Self-Organizing Map analysis and K-means clustering. Concentration of major elements are in wt. %. Gold concentrations are in PPB. Concentrations of all other elements are in PPM.

	Cluster 1			Cluster 2			Cluster 3			Cluster 4			Cluster 5			Cluster 6		
	Aeolian sand			Calc. sediment			Area-223 Upper			Area-223 Mid			Area-223 Oxide			Area-223 Lower		
	Min.	Max.	Avg.	Min.	Max.	Avg.	Min.	Max.	Avg.	Min.	Max.	Avg.	Min.	Max.	Avg.	Min.	Max.	Avg.
q-error	2.9	11	6.8	3.3	6.4	4.7	2	4.8	2.9	2.2	3.8	2.8	4.6	11	6.6	1.7	3.9	2.7
SiO_2	45	76	56	64	73	67	64	77	71	67	75	72	59	73	66	73	74	73
Al_2O_3	2.6	12	7.2	10	19	16	12	21	16	13	18	15	13	17	15	14	15	14
Fe_2O_3	1.2	2.7	2.1	3.4	4.3	3.8	1.7	2.7	2	2.1	2.4	2.2	2.1	9.7	5.9	1.1	1.3	1.2
CaO	8	18	13	0.22	2.4	0.99	0.01	0.68	0.09	0.02	0.04	0.033	0.06	0.09	0.075	0.11	0.12	0.12
MgO	1.6	3.3	2.7	0.34	1	0.66	0.6	0.94	0.8	0.82	0.94	0.9	0.38	1	0.71	0.15	0.21	0.17
Na_2O	0.13	0.5	0.32	0.25	0.5	0.4	0.23	1	0.51	0.33	0.49	0.4	1.1	1.3	1.2	2.9	3.5	3.1
K_2O	0.34	0.68	0.56	0.33	1	0.77	3.5	4.9	4.3	4.5	5.8	5.1	4.2	6.3	5.2	5.4	5.5	5.5
MnO	0.01	0.02	0.013	0.01	0.01	0.01	0.01	0.03	0.02	0.02	0.02	0.02	0.02	0.04	0.03	0.01	0.01	0.01
TiO2	0.17	0.32	0.27	0.36	0.45	0.41	0.25	0.69	0.35	0.28	0.4	0.35	0.3	0.63	0.47	0.08	0.11	0.1
P_2O_5	0.01	0.02	0.013	0.01	0.02	0.013	0.01	0.05	0.018	0.05	0.09	0.068	0.11	0.19	0.15	0.06	0.09	0.07
Cr_2O_3	0.005	0.008	0.007	0.002	0.012	0.008	0.001	0.006	0.003	0.001	0.005	0.003	0.001	0.002	0.002	0.001	0.002	0.001
Ba	0.01	0.26	0.12	0.05	0.14	0.11	0.07	0.15	0.11	0.11	0.2	0.14	0.1	0.13	0.12	0.11	0.11	0.11
LOI	9.9	22	17	8.4	11	9.8	3	6.8	4.6	2.9	4.5	3.5	2.2	5.9	4.1	1.6	1.9	1.8
SUM	99	100	99	100	100	100	100	100	100	99	100	100	99	100	99	100	100	100
TOT/C	2.5	4.5	3.5	0.11	0.84	0.37	0.02	0.28	0.063	0.03	0.13	0.083	0.06	0.06	0.06	0.03	0.29	0.17
TOT/S	0.02	0.13	0.083	0.02	0.06	0.043	0.02	0.15	0.066	0.07	0.16	0.12	0.06	0.09	0.075	0.02	0.02	0.02
Au*	30	110	69	17	110	56	18	340	63	13	47	23	7.6	12	9.6	1.8	4.3	2.8
Mo	0.1	0.6	0.31	0.1	0.7	0.32	0.1	1.3	0.34	0.1	0.3	0.15	0.3	7.3	3.7	0.2	1.2	0.5
Cu	5.1	12	8.4	6	13	9.9	0.6	5.3	1.8	0.9	4.1	2	7.3	74	38	2.7	13	5.3
Pb	3.8	11	5.9	5.5	20	9.4	13	100	43	4.3	18	10	15	33	24	20	76	36
Zn	6	120	28	3	33	13	2	19	4.7	5	38	18	28	52	37	9	47	26
Ni	4.3	10	5.9	2.4	8.4	5.7	0.2	2.4	1	0.6	1.2	0.81	1	7.3	3.9	0.7	4.5	1.9
As	1	3.9	1.9	2.1	14	5.6	0.5	1.6	0.78	0.5	0.5	0.5	0.5	3.2	1.8	0.5	0.8	0.54
Cd	0.1	0.4	0.14	0.1	0.1	0.1	0.1	0.1	0.1	0.1	0.1	0.1	0.1	0.1	0.1	0.1	0.1	0.1
Sb	0.1	0.1	0.1	0.1	0.1	0.1	0.1	0.1	0.1	0.1	0.1	0.1	0.1	0.2	0.13	0.1	0.1	0.1
Bi	0.1	0.1	0.1	0.1	0.2	0.12	0.1	0.3	0.15	0.1	0.2	0.11	0.1	0.3	0.2	0.1	0.1	0.1
Ag	0.1	0.1	0.1	0.1	0.1	0.1	0.1	0.4	0.19	0.1	0.5	0.26	0.1	0.6	0.25	0.5	1.2	0.79
Hg	0.01	0.02	0.013	0.01	0.01	0.01	0.01	0.01	0.01	0.01	0.01	0.01	0.01	0.01	0.01	0.01	0.01	0.01
Tl	0.1	0.1	0.1	0.1	0.1	0.1	0.1	0.6	0.15	0.1	0.1	0.1	0.3	1.1	0.58	0.1	0.1	0.1
Se	0.5	0.5	0.5	0.5	2.1	1.3	0.5	0.5	0.5	0.5	0.5	0.5	0.5	0.5	0.5	0.5	0.5	0.5
Ba	120	2500	590	480	1400	930	680	1500	1100	980	1900	1400	830	1200	1000	850	1000	910
Be	1	2	1.1	1	4	2	1	7	2.4	1	5	3	2	8	4.3	1	6	3
Co	2.3	4.7	3.3	2.5	8.2	4.7	0.2	1.1	0.39	0.2	0.6	0.3	0.2	2.7	1.3	0.2	1.5	0.79
Cs	0.8	1.9	1.3	1.5	4	2.5	3.8	8.3	5.4	3.8	5.3	4.7	6.6	20	13	3.5	6.5	4.9
Ga	2.2	19	6.1	11	32	22	15	20	18	16	19	17	13	19	16	14	16	15
Hf	2.9	6.1	4.1	3.1	6.6	4.4	3.2	5.9	4.2	3.8	4.8	4.5	4.5	6.9	5.8	4.5	5.9	5.2
Nb	2.6	7	4.1	6.3	11	8.9	6	14	9.1	6.3	9.9	8.6	8.3	15	12	15	20	17
Rb	13	31	21	20	63	42	170	230	200	210	270	240	230	260	250	190	210	200
Sn	1	3	1.3	2	3	2.2	1	3	1.9	1	2	1.6	1	2	1.3	1	3	2.3
Sr	85	1300	490	70	230	160	27	190	75	210	420	300	300	680	530	230	530	350
Ta	0.2	0.5	0.31	0.5	0.8	0.66	0.5	1.1	0.82	0.5	1	0.7	0.6	0.8	0.7	1.4	1.7	1.5
Th	2.3	5.6	3.4	3.9	12	6.7	5.4	9.2	6.6	11	28	20	14	21	18	23	33	27
U	0.6	2.5	1.1	1.2	3.3	2.1	1.1	1.7	1.4	1.4	2.1	1.7	3.9	7.1	5.3	4.6	5.7	5
V	8	71	30	71	180	100	10	79	32	43	59	50	25	98	62	8	17	11
W	0.5	1.4	0.87	1.3	2.6	1.8	3.5	7.3	5.2	6.3	15	9.5	4.5	8.6	6.2	1	2.5	1.8
Zr	120	260	160	120	240	160	120	210	160	140	180	160	180	280	220	150	170	160
Y	5.1	20	8.7	3.9	9.6	6.2	4.1	7.6	6	5.9	11	8.3	14	27	20	18	48	33
La	5.7	19	9.1	3.9	14	9.5	3.6	67	24	38	91	67	40	72	57	49	58	53
Ce	12	21	15	5.8	25	16	5.4	77	24	62	160	120	81	160	120	100	130	110
Pr	1.2	4.3	2	0.57	2.7	1.5	0.46	5.5	1.7	6	15	11	9.1	20	15	12	15	13
Nd	3.2	16	7.5	2.1	11	5.9	1.3	12	4.5	17	43	32	35	82	60	46	54	49
Sm	0.87	3.4	1.5	0.44	1.7	0.96	0.42	1.7	0.78	2.1	4.4	3.6	5.2	15	9.6	7.8	12	9.5
Eu	0.11	0.73	0.32	0.07	0.39	0.21	0.07	0.31	0.16	0.38	0.76	0.6	0.98	3.1	1.9	1.5	2.3	1.8
Gd	0.84	3.5	1.5	0.46	1.7	0.94	0.46	1.5	0.74	1.3	2.9	2.2	3.3	9.4	6.2	5.7	10	8
Tb	0.13	0.5	0.22	0.08	0.27	0.15	0.11	0.18	0.14	0.2	0.38	0.28	0.5	1.1	0.79	0.82	1.6	1.2
Dy	0.88	2.6	1.4	0.56	1.8	1.1	0.76	1.5	0.99	1.1	2.1	1.6	2.6	5.3	4.1	4.1	9	6.6
Ho	0.17	0.61	0.28	0.12	0.34	0.22	0.13	0.27	0.21	0.2	0.42	0.29	0.52	1.1	0.77	0.74	1.7	1.1
Er	0.55	1.8	0.89	0.37	1.2	0.73	0.46	0.95	0.71	0.63	1.4	1	1.4	3.2	2.2	1.8	4.2	3
Tm	0.08	0.23	0.12	0.06	0.19	0.11	0.07	0.15	0.11	0.11	0.21	0.14	0.21	0.48	0.34	0.25	0.56	0.4
Yb	0.58	1.4	0.89	0.56	1.3	0.82	0.57	1.2	0.87	0.79	1.4	1	1.2	3.3	2.2	1.7	3.6	2.5
Lu	0.08	0.24	0.13	0.09	0.18	0.13	0.06	0.17	0.13	0.11	0.25	0.15	0.2	0.49	0.35	0.24	0.52	0.37

	Cluster 7			Cluster 8			Cluster 9			Cluster 10			Cluster 11			Cluster 12		
	Area-191 Upper			Area-191 Mid			Area-191 Lower			Tomahawk Upper			Tomahawk Mid			Tomahawk Lower		
	Min.	Max.	Avg.	Min.	Max.	Avg.	Min.	Max.	Avg.	Min.	Max.	Avg.	Min.	Max.	Avg.	Min.	Max.	Avg.
q-error	1.7	4.4	2.8	1.3	3.1	1.9	1.3	6.1	2.2	1.5	2.8	2.2	1.3	3.1	2.3	1.4	3.6	2.2
SiO_2	64	78	68	65	71	68	69	74	72	64	67	65	68	76	70	67	71	69
Al_2O_3	13	24	21	17	21	19	12	16	15	21	22	21	13	20	17	17	20	19
Fe_2O_3	0.38	0.46	0.42	0.38	0.51	0.43	0.53	3	1.5	0.5	2.3	1	0.35	0.78	0.56	0.46	0.74	0.57
CaO	0.02	0.06	0.04	0.03	0.07	0.043	0.1	0.61	0.27	0.02	0.11	0.075	0.02	0.79	0.2	0.1	0.53	0.3
MgO	0.1	0.13	0.12	0.09	0.14	0.12	0.09	0.41	0.22	0.25	0.7	0.38	0.16	0.42	0.29	0.1	0.29	0.18
Na_2O	0.43	0.81	0.6	0.48	2.8	1	2.7	4.6	3.8	0.36	0.88	0.59	0.41	1.6	0.76	0.66	2.4	1.5
K_2O	0.3	2.4	0.99	3.2	4.4	3.8	3.6	4.6	4.2	0.98	2.1	1.4	3	4.7	3.8	3.6	4.9	4.2
MnO	0.01	0.01	0.01	0.01	0.01	0.01	0.01	0.02	0.012	0.01	0.01	0.01	0.01	0.01	0.01	0.01	0.01	0.01
TiO2	0.23	0.36	0.29	0.18	0.26	0.23	0.15	0.23	0.18	0.21	0.39	0.27	0.14	0.19	0.16	0.18	0.3	0.22
P_2O_5	0.01	0.01	0.01	0.01	0.02	0.011	0.02	0.32	0.071	0.01	0.01	0.01	0.01	0.02	0.014	0.02	0.03	0.025
Cr_2O_3	0.001	0.002	0.002	0.001	0.008	0.002	0.001	0.009	0.002	0.001	0.002	0.001	0.001	0.007	0.002	0.001	0.005	0.002
Ba	0.01	0.11	0.048	0.14	0.17	0.15	0.11	0.24	0.16	0.03	0.07	0.048	0.07	0.15	0.1	0.12	0.19	0.15
LOI	6.8	10	8.6	5	7.3	6.4	1.8	3.7	2.8	8.1	10	9.1	4.5	6.9	6.3	3.5	5.9	5
SUM	99	100	100	99	100	100	99	100	100	99	100	100	99	100	100	99	100	100
TOT/C	0.02	0.07	0.038	0.02	0.03	0.023	0.02	0.02	0.02	0.05	0.24	0.12	0.03	0.64	0.17	0.03	0.26	0.088
TOT/S	0.03	0.07	0.045	0.02	0.07	0.043	0.02	0.27	0.058	0.03	0.07	0.05	0.05	0.17	0.07	0.02	0.04	0.022
Au*	0.5	26	7.1	0.5	4.5	2	0.5	1.8	1.1	5.8	85	31	2.7	11	4.8	2.5	9.3	5.4
Mo	0.1	0.5	0.16	0.1	0.2	0.11	0.1	0.4	0.19	0.1	0.3	0.14	0.1	1.3	0.41	0.1	3.6	1.1
Cu	0.8	4.1	1.4	0.9	3.3	1.9	3.8	23	11	0.5	9.2	3.5	0.3	7.5	1.9	0.8	3.8	2.3
Pb	4.4	8.7	7.2	2.7	11	5.8	0.7	3.6	1.8	3.2	7.8	4.4	3.2	16	7.1	4.4	34	19
Zn	1	3	1.4	1	16	2.1	2	50	23	1	5	2.3	1	8	3.2	1	6	2.9
Ni	0.7	2	1.3	0.5	2.3	1.2	1.2	5.5	2.4	0.5	2.2	1.1	0.5	3	1.4	0.5	1.8	1
As	0.5	0.7	0.53	0.5	0.5	0.5	0.5	0.5	0.5	0.5	1.3	0.74	0.5	0.5	0.5	0.5	0.5	0.5
Cd	0.1	0.1	0.1	0.1	0.1	0.1	0.1	0.1	0.1	0.1	0.1	0.1	0.1	0.1	0.1	0.1	0.1	0.1
Sb	0.1	0.1	0.1	0.1	0.1	0.1	0.1	0.1	0.1	0.1	0.1	0.1	0.1	0.1	0.1	0.1	0.1	0.1
Bi	0.1	0.1	0.1	0.1	0.1	0.1	0.1	0.1	0.1	0.1	0.1	0.1	0.1	0.1	0.1	0.1	0.1	0.1
Ag	0.1	0.1	0.1	0.1	0.1	0.1	0.1	0.1	0.1	0.1	0.1	0.1	0.1	0.1	0.1	0.1	0.1	0.1
Hg	0.01	0.01	0.01	0.01	0.01	0.01	0.01	0.01	0.01	0.01	0.01	0.01	0.01	0.01	0.01	0.01	0.01	0.01
Tl	0.1	0.1	0.1	0.1	0.1	0.1	0.1	0.1	0.1	0.1	0.1	0.1	0.1	0.1	0.1	0.1	0.2	0.11
Se	0.5	1.8	0.66	0.5	0.5	0.5	0.5	0.5	0.5	0.5	0.5	0.5	0.5	0.5	0.5	0.5	0.5	0.5
Ba	190	1100	440	1200	1700	1500	1000	2500	1500	280	820	480	610	1500	1000	930	1900	1300
Be	1	2	1.1	1	2	1.2	1	3	1.5	1	4	1.6	1	4	1.5	1	4	1.8
Co	0.2	0.7	0.44	0.2	1	0.46	0.7	3.7	2.2	0.2	3.3	1.1	0.2	1.1	0.49	0.2	1.9	0.88
Cs	0.6	1.1	0.91	1.1	2.1	1.6	1.7	4.8	3.1	1.1	2.6	1.7	1.4	2.8	2.1	1.1	3.8	1.8
Ga	17	28	22	14	21	17	13	16	14	20	31	26	13	19	17	13	21	18
Hf	3.3	4.6	3.9	3.4	4.8	4	2.5	3.9	3.2	2.7	3.8	3.1	2.1	3.4	2.7	2.4	3.6	3
Nb	8.5	13	11	7.8	11	9	4.7	8.3	6.9	7.6	12	11	6.8	11	8.6	5.3	10	7.4
Rb	17	59	29	79	130	100	91	140	120	33	78	56	77	150	130	100	180	120
Sn	1	2	1.8	1	2	1.1	1	2	1	1	2	1.9	1	4	1.6	1	2	1.3
Sr	11	120	40	140	250	180	230	1900	570	28	88	52	88	200	140	83	410	280
Ta	0.7	1	0.8	0.4	0.9	0.64	0.3	0.7	0.5	0.5	1	0.81	0.6	1.1	0.86	0.5	1.2	0.81
Th	2.6	3.9	3.2	3.9	6	4.7	7.8	16	11	4.3	12	6.6	5.5	12	8.3	5	20	15
U	0.7	1.2	0.81	0.7	1	0.86	1	2.1	1.5	0.9	1.7	1.2	0.8	1.6	1.1	0.8	2.2	1.7
V	8	24	16	8	17	9.6	8	25	11	25	79	45	10	33	18	13	82	31
W	1.4	2.4	1.9	0.6	1.9	1.3	1.2	4.7	1.8	1.1	2.3	1.6	0.5	1.4	0.88	0.9	4.4	2.3
Zr	130	150	140	120	170	140	94	140	110	98	120	110	75	110	92	81	130	110
Y	2.9	3.6	3.3	2.7	3.9	3.1	4.3	12	8.2	5.7	11	8.1	8.3	19	12	6.6	16	11
La	0.9	1.8	1.3	2.4	12	5.8	15	58	36	6.2	27	15	13	30	21	16	52	40
Ce	1.6	3.6	2.2	2.9	18	7.2	34	140	68	11	49	26	21	60	40	28	100	78
Pr	0.16	0.34	0.21	0.23	1.7	0.61	3.5	14	6.8	0.91	4.9	2.4	2	6.4	4.1	2.6	10	7.9
Nd	0.5	1.5	0.9	0.8	4.7	1.9	9.8	48	23	3.1	16	7.9	6.7	23	14	9.2	34	26
Sm	0.17	0.31	0.23	0.22	0.81	0.34	1.6	7.6	3.5	0.52	2.6	1.4	1.3	3.5	2.4	1.4	5.5	4.1
Eu	0.05	0.13	0.086	0.09	0.25	0.17	0.45	1.6	0.77	0.13	0.31	0.24	0.25	0.45	0.33	0.28	0.88	0.69
Gd	0.2	0.47	0.3	0.21	0.55	0.37	1.1	5.3	2.5	0.58	2.4	1.2	1.1	3.1	2	1.1	3.9	2.9
Tb	0.05	0.06	0.055	0.04	0.09	0.055	0.17	0.53	0.3	0.12	0.28	0.19	0.2	0.46	0.3	0.18	0.51	0.4
Dy	0.37	0.57	0.45	0.31	0.61	0.41	0.93	2.8	1.6	0.92	1.8	1.3	1.4	3	2	1	2.8	2.1
Ho	0.07	0.14	0.1	0.07	0.14	0.1	0.15	0.4	0.27	0.21	0.35	0.27	0.3	0.5	0.39	0.26	0.58	0.41
Er	0.31	0.5	0.4	0.26	0.43	0.34	0.44	1.1	0.77	0.66	1.1	0.88	0.86	1.7	1.2	0.76	1.7	1.2
Tm	0.05	0.08	0.064	0.04	0.08	0.053	0.05	0.15	0.11	0.07	0.16	0.12	0.12	0.26	0.17	0.12	0.25	0.18
Yb	0.42	0.59	0.51	0.33	0.69	0.49	0.54	1.3	0.81	0.67	1.2	0.97	0.97	1.9	1.3	0.66	1.7	1.2
Lu	0.07	0.1	0.085	0.05	0.1	0.074	0.07	0.15	0.11	0.09	0.15	0.13	0.13	0.27	0.19	0.12	0.24	0.18

Component-plane plots

All variables used in the Self-Organising Maps analysis. Red = high value/contribution, blue = low value/contribution to the nodes on the map.

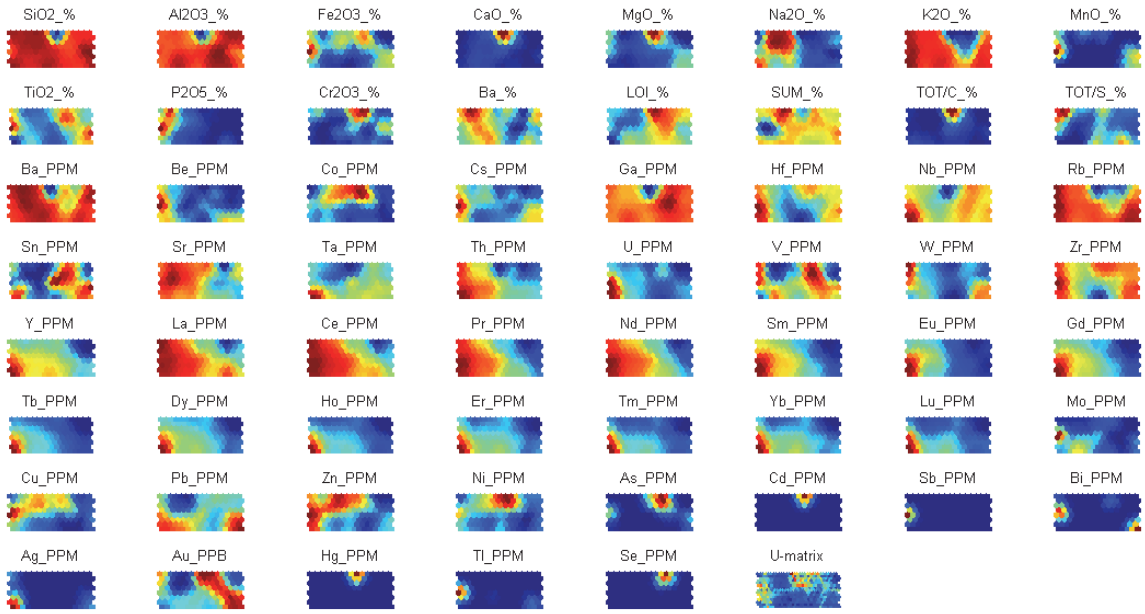

1. Aeolian sand
2. Indurated sediments
3. Area-223 Upper saprolite
4. Area-223 Middle saprolite
5. Area-223 Oxide zone
6. Area-223 Lower saprolite
7. Area-191 Upper saprolite
8. Area-191 Middle saprolite
9. Area-191 Lower saprolite
10. Tomahawk Upper saprolite
11. Tomahawk Middle saprolite
12. Tomahawk Lower saprolite

APPENDIX B: Miscellaneous

Challenger deposit

The Challenger Au mine open pit exposes the weathering profile that is typical of much of the central Gawler Craton. At the base of the pit is fresh Archean bedrock. The weathering front, as indicated by the sub-horizontal dashed line, marks an abrupt change in colour and texture. The pallid zone has relic primary lithology viz. lamprophyre and mafic dykes. The mafic dykes (inset) are up to several metres wide and are visible within the saprolite to the surface. The soil at the top of the profile hosts the calcrete that is attributable to the discovery of the deposit. Iron-stained saprolite is likely from the downward percolation of Fe solutes from the transported regolith.

This profile is an excellent example of why and how the saprolite can be used as a sampling material for mineral exploration in the central Gawler Craton. This holds particularly true for the Tunkillia Au Prospect where thousands of air-core drill holes terminate at the base of this weathered profile and have had minimal geochemical analysis. There is potential for the saprolite to be reinvestigated using a mineralogical and litho-geochemical approach.

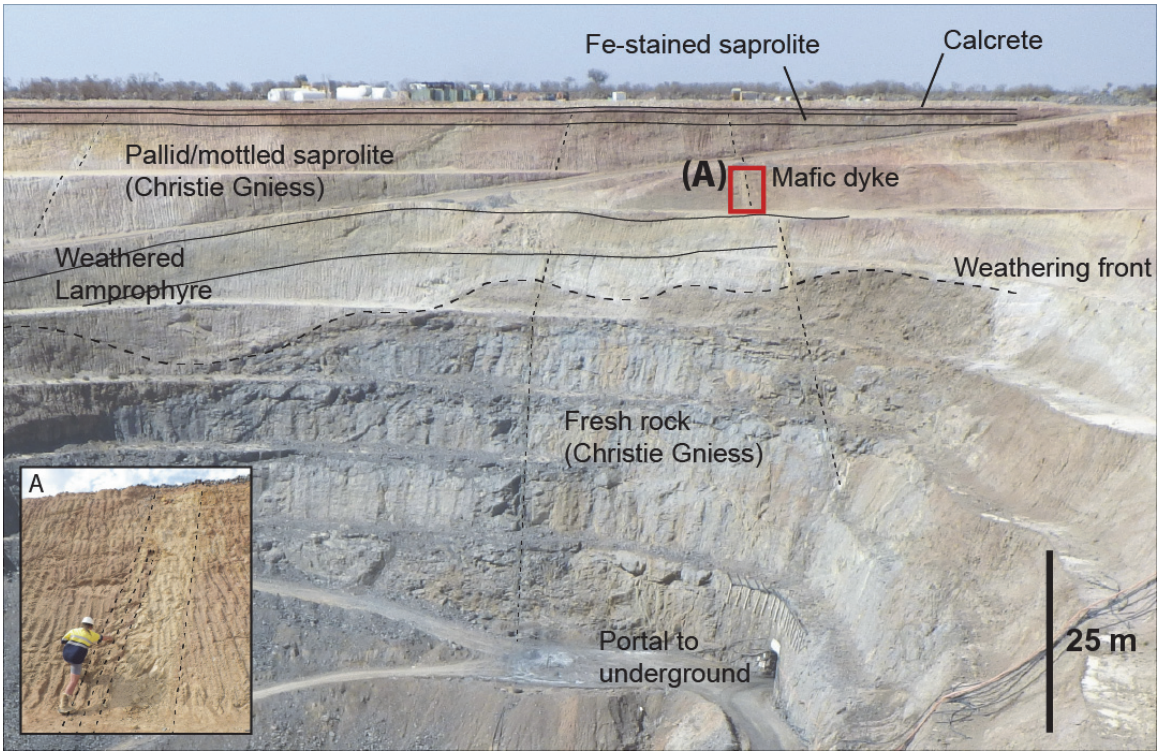

Regional Regolith Landform Map

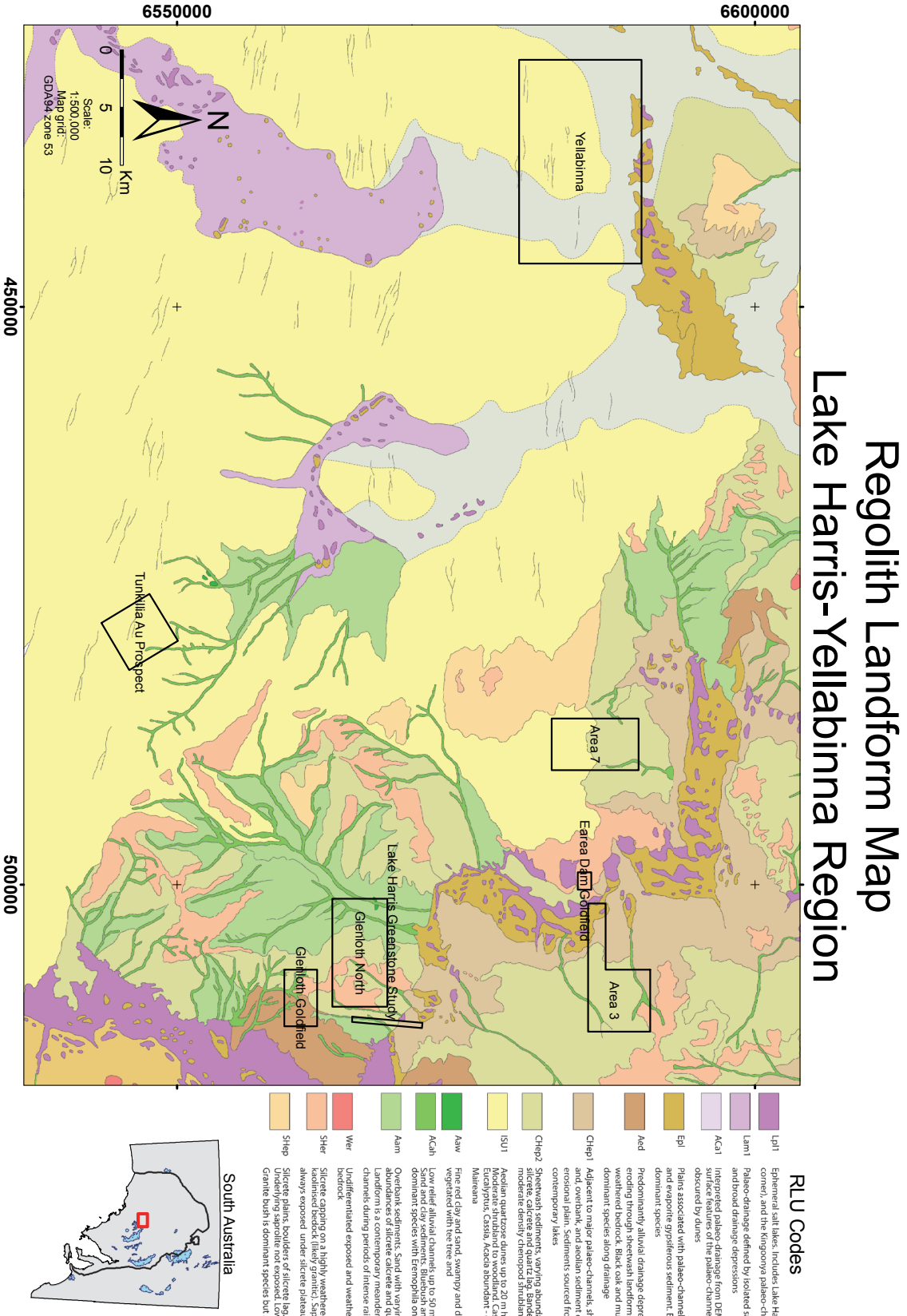

Biogeochemical summary of species

The table below contains the average concentration ± the standard deviation of each element for each plant species that were sampled in the biogeochemical surveys: Tunkillia Au Prospect, Yellabinna Regional Reserve, Glenloth and Earea Dam goldfields, Lake Harris, Area-3, Area-7 and Glenloth North.

	Black oak (574)	Mulga (216)	Pearl bluebush (563)	Victoria Desert mallee (335)	Woody cassia (28)
Ag (ppb)	1.6 ± 8.3	4.2 ± 2.4	3.8 ± 8.8	1.2 ± 0.45	2.8 ± 2
Al (%)	0.0085 ± 0.0045	0.01 ± 0.00048	0.018 ± 0.017	0.0067 ± 0.0033	0.01 ± 0.0019
As (ppm)	0.067 ± 0.046	0.11 ± 0.039	0.13 ± 0.078	0.073 ± 0.056	0.14 ± 0.069
Au (ppb)	0.46 ± 0.67	0.24 ± 0.13	0.5 ± 0.96	0.45 ± 0.69	0.48 ± 0.43
B (ppm)	55 ± 19	18 ± 4.8	48 ± 23	61 ± 33	26 ± 7.7
Ba (ppm)	6.3 ± 2.9	2.4 ± 1.6	7.2 ± 4.3	6.1 ± 3.1	6.5 ± 3.7
Be (ppm)	0.056 ± 0.017	0.1 ± 0.0048	0.1 ± 0.01	0.061 ± 0.03	0.1 ± 0
Bi (ppm)	0.012 ± 0.011	0.021 ± 0.0065	0.021 ± 0.0078	0.012 ± 0.0075	0.022 ± 0.0057
Ca (%)	1.2 ± 0.31	1.4 ± 0.38	0.95 ± 0.35	0.95 ± 0.36	1.4 ± 0.34
Cd (ppm)	0.0064 ± 0.02	0.01 ± 0.00084	0.031 ± 0.037	0.011 ± 0.017	0.013 ± 0.0086
Ce (ppm)	0.17 ± 0.072	0.11 ± 0.056	0.31 ± 0.31	0.3 ± 0.37	0.088 ± 0.061
Co (ppm)	0.035 ± 0.021	0.021 ± 0.013	0.11 ± 0.1	0.072 ± 0.083	0.044 ± 0.022
Cr (ppm)	1.5 ± 0.91	1.2 ± 0.38	1.7 ± 1.6	1.7 ± 1.3	1.8 ± 0.46
Cs (ppm)	0.0095 ± 0.0028	0.0076 ± 0.0037	0.016 ± 0.016	0.0039 ± 0.0024	0.0066 ± 0.0024
Cu (ppm)	2.9 ± 1	10 ± 3.1	3.7 ± 1.3	4.1 ± 1.4	3.5 ± 0.89
Fe (%)	0.0099 ± 0.0034	0.0062 ± 0.002	0.016 ± 0.016	0.0038 ± 0.0017	0.0054 ± 0.0032
Ga (ppm)	0.055 ± 0.015	0.1 ± 0.0048	0.1 ± 0.029	0.057 ± 0.018	0.1 ± 0
Ge (ppm)	0.0095 ± 0.0078	0.015 ± 0.009	0.016 ± 0.011	0.0094 ± 0.007	0.022 ± 0.012
Hf (ppm)	0.0027 ± 0.002	0.0021 ± 0.0013	0.0048 ± 0.0055	0.0012 ± 0.001	0.0023 ± 0.0022
Hg (ppb)	18 ± 5.9	17 ± 4.6	14 ± 6.6	15 ± 8.6	9.9 ± 2.4
In (ppm)	0.011 ± 0.0029	0.02 ± 0.00096	0.02 ± 0.0	0.011 ± 0.0035	0.02 ± 0
K (%)	0.52 ± 0.16	0.82 ± 0.16	0.98 ± 0.61	0.57 ± 0.16	1.3 ± 0.21
La (ppm)	0.074 ± 0.034	0.048 ± 0.027	0.13 ± 0.12	0.11 ± 0.14	0.034 ± 0.026
Li (ppm)	0.62 ± 0.37	0.13 ± 0.11	0.64 ± 0.56	1.2 ± 0.83	0.21 ± 0.13
Mg (%)	0.31 ± 0.062	0.17 ± 0.044	0.3 ± 0.095	0.2 ± 0.047	0.13 ± 0.024
Mn (ppm)	45 ± 22	44 ± 23	59 ± 35	82 ± 60	21 ± 4.8
Mo (ppm)	0.12 ± 0.14	0.24 ± 0.52	0.15 ± 0.15	0.039 ± 0.1	0.52 ± 0.29
Na (%)	0.21 ± 0.087	0.048 ± 0.024	2.2 ± 2.4	0.43 ± 0.15	0.07 ± 0.042
Nb (ppm)	0.0055 ± 0.0015	0.01 ± 0.00048	0.011 ± 0.0039	0.0057 ± 0.0018	0.01 ± 0
Ni (ppm)	0.64 ± 0.58	0.31 ± 0.15	0.63 ± 0.73	0.78 ± 0.84	0.31 ± 0.14
P (%)	0.043 ± 0.0081	0.067 ± 0.013	0.054 ± 0.025	0.052 ± 0.01	0.16 ± 0.04
Pb (ppm)	0.15 ± 0.15	0.26 ± 0.17	0.33 ± 0.58	0.11 ± 0.14	0.1 ± 0.068
Pd (ppb)	1.1 ± 0.32	2 ± 0.18	2.4 ± 1.6	1.1 ± 0.35	2 ± 0
Pt (ppb)	0.56 ± 0.16	1 ± 0.048	1 ± 0.075	0.58 ± 0.18	1 ± 0
Rb (ppm)	1.3 ± 0.53	2.6 ± 0.93	2.6 ± 2	1.1 ± 0.57	1.7 ± 0.44
Re (ppb)	0.97 ± 1.4	7.6 ± 38	4.6 ± 6.1	1.9 ± 2.4	1 ± 0.19
S (%)	0.17 ± 0.048	0.15 ± 0.024	0.17 ± 0.047	0.15 ± 0.046	0.18 ± 0.04
Sb (ppm)	0.013 ± 0.017	0.043 ± 0.21	0.068 ± 0.35	0.027 ± 0.098	0.051 ± 0.06
Sc (ppm)	0.18 ± 0.091	0.18 ± 0.066	0.19 ± 0.1	0.18 ± 0.099	0.23 ± 0.12
Se (ppm)	0.48 ± 0.2	0.57 ± 0.23	0.53 ± 0.25	0.33 ± 0.14	0.35 ± 0.16
Sn (ppm)	0.016 ± 0.016	0.024 ± 0.014	0.03 ± 0.037	0.015 ± 0.012	0.025 ± 0.0096
Sr (ppm)	68 ± 29	100 ± 51	61 ± 32	75 ± 34	150 ± 51
Ta (ppm)	0.00069 ± 0.00025	0.001 ± 0.00016	0.001 ± 0.00013	0.00064 ± 0.00029	0.001 ± 0
Te (ppm)	0.012 ± 0.0055	0.022 ± 0.0071	0.021 ± 0.0032	0.013 ± 0.0074	0.022 ± 0.0048
Th (ppm)	0.011 ± 0.0072	0.01 ± 0.0014	0.03 ± 0.041	0.006 ± 0.0028	0.011 ± 0.0042
Ti (ppm)	2.9 ± 0.64	3.9 ± 0.71	4.2 ± 2.7	2.5 ± 0.55	5.7 ± 1.9
Tl (ppm)	0.011 ± 0.0031	0.043 ± 0.052	0.021 ± 0.0025	0.011 ± 0.0035	0.02 ± 0
U (ppm)	0.0068 ± 0.0091	0.01 ± 0.00048	0.016 ± 0.025	0.035 ± 0.045	0.01 ± 0
V (ppm)	1.2 ± 0.51	2 ± 0.096	2.2 ± 0.8	1.3 ± 0.54	2 ± 0
W (ppm)	0.055 ± 0.015	0.1 ± 0.021	0.1 ± 0.0	0.057 ± 0.018	0.1 ± 0
Y (ppm)	0.057 ± 0.029	0.028 ± 0.017	0.1 ± 0.091	0.1 ± 0.11	0.031 ± 0.032
Zn (ppm)	13 ± 5.1	25 ± 7.6	10 ± 5.7	13 ± 4.2	16 ± 4.1
Zr (ppm)	0.065 ± 0.027	0.029 ± 0.013	0.12 ± 0.13	0.026 ± 0.013	0.038 ± 0.023

Element abundances in plants

Element abundances in plants (dry weight) as a bulk composition are presented in sources from Markert (1994), in Dunn (2007).

Element	Units	Concentration
C	%	44.5
O	%	42.5
H	%	6.5
N	%	2.5
K	%	1.9
Ca	%	1
S	%	0.3
P	%	0.2
Mg	%	0.2
Cl	%	0.2
Si	%	0.1
Ag	ppb	20
Al	ppm	80
As	ppm	0.1
Au	ppb	0.2
B	ppm	40
Ba	ppm	40
Be	ppb	1
Bi	ppb	10
Br	ppm	4
Cd	ppb	50
Ce	ppm	0.5
Co	ppm	0.2
Cr	ppm	1.5
Cs	ppm	0.2
Cu	ppm	10
Dy	ppb	30
Er	ppb	20
Eu	ppb	8
F	ppm	2
Fe	ppm	150
Ga	ppm	0.1
Gd	ppb	40
Ge	ppb	10
Hf	ppb	50
Hg	ppb	20
Ho	ppb	8
I	ppm	3
In	ppb	1
Ir	ppb	0.01
La	ppm	0.2

Element	Units	Concentration
Li	ppm	0.2
Lu	ppb	3
Mn	ppm	200
Mo	ppm	0.5
Na	ppm	150
Nb	ppb	50
Nd	ppm	0.2
Ni	ppm	1.5
Os	ppb	0.0015
Pa	ppb	?
Pb	ppm	1
Pd	ppb	0.1
Po	ppb	?
Pr	ppb	50
Pt	ppb	0.005
Ra	ppb	?
Rb	ppm	50
Re	ppb	0.1
Rh	ppb	0.01
Ru	ppb	0.1
Sb	ppm	0.1
Sc	ppb	20
Se	ppb	20
Sm	ppb	40
Sn	ppm	0.2
Sr	ppm	50
Ta	ppb	1
Tb	ppb	8
Te	ppb	20
Th	ppb	5
Ti	ppm	5
Tl	ppb	20
Tm	ppb	4
U	ppb	10
V	ppm	0.5
W	ppm	0.2
Y	ppm	0.2
Yb	ppb	20
Zn	ppm	50
Zr	ppm	0.1

Tunkillia dataset

The diagram below illustrates drilling pattern at the Tunkillia Au Prospect and the relationship to the biogeochemical and regolith geochemical studies. The drill grid is visible from the aerial image although it is masked in this diagram by the drill collars (X). The drill hole data are supplied by Minotaur Exploration Ltd. and Mungana Goldmines Ltd. to assist with the interpretation of biogeochemical and regolith geochemical data and are not supplied with this thesis.

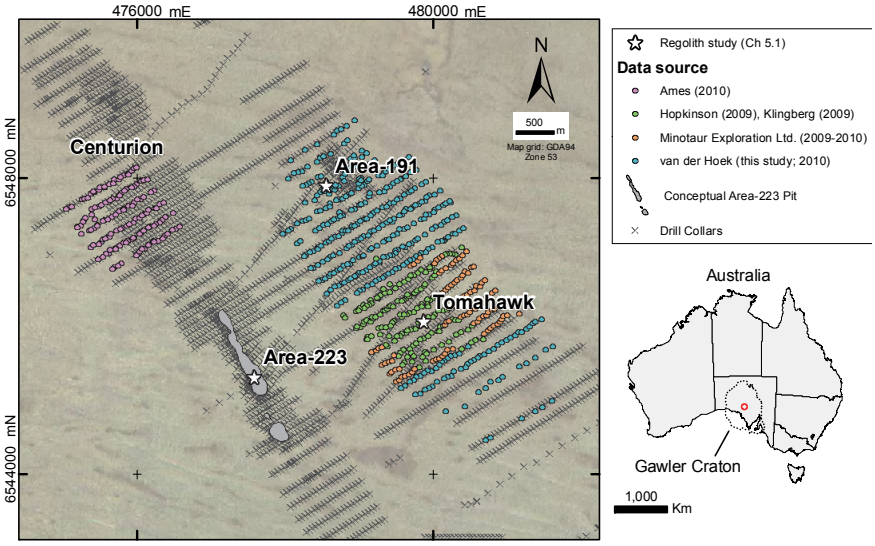

The diagram below illustrates the high-density calcrete geochemical sampling program over the Tunkillia Au Prospect. These data were used to produce the Au-in-calcrete contours that are discussed in Sections 5.3 and 5.5. The regional Au-in-calcrete contours that highlight the northward palaeo-drainage were produced using the regional Au-in-calcrete data that typically has 500 m spacing (e.g., surrounding the high-density sampling grid in the diagram below). The high density data are supplied by Minotaur Exploration Ltd. to assist with the interpretation of biogeochemical and regolith geochemical data and are not supplied with this thesis.

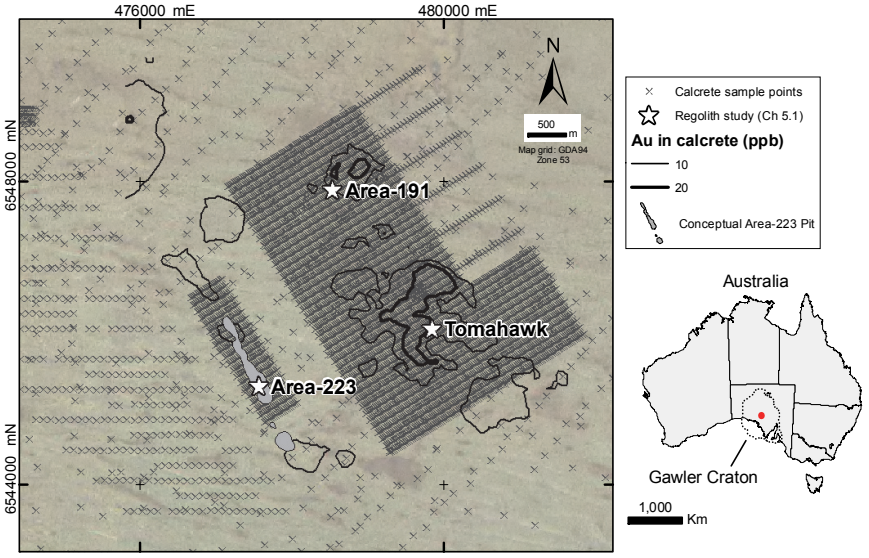

SOM terminology

General SOM and SiroSOM-specific terminology associated with the graphical user interface and used for the interpretation of output data are described in detail in Fraser & Dickson (2007), and Fraser (2012). A summary of the definitions derived from these sources is included in the table below.

B.M.U	Best matching unit (interchangeable with ***cell*** or ***node***) is a group of similar/related observations
U-Matrix	The Unified distance matrix is the map of BMUs. Adjacent BMUs on the map may have no geospatial association. Colours are representative of the similarity of adjacent hexagonal cells: cool colours are more similar than warm colours, and increasing darkness is representative of a strong association.
QER	Quantization Error is the distance of data from the BMU that represents it. Samples with a high QER are 'anomalous' and can be a result of variables that have values higher or lower than those of the BMU.
Training	Node vectors are 'trained' to represent the original data distribution. The n-dimensional space is defined by the input variables (i.e., 50-60 elements). The space is seeded randomly with seed-vectors – the number of seed-vectors is determined by the size of the map. In the case of the data used for this study, the optimum map dimensions are 15 x 30, which equates to 450 seed-vectors. An iterative process is applied to the input samples, where the seed-vectors a trained to represent the structure of the input samples in n-dimensional space.
Cluster	Clusters are defined by the lowest achieved David-Boudin index. At the lowest index value, the variance of data within clusters is minimised and the variance of data between clusters is maximised arriving at an estimated number of true populations within the data. The number of clusters is variable due to initial random seeding and the number of iterations. Five iterations is the default input and may need alteration to achieve a lower index and appropriate number of clusters. Clusters have an advantage over PCA as they are easier to back-analyse.
Component plane plots (variables)	Nodes can be presented as a U-matrix that shows node, and therefore sample, similarity. Because the node vectors are defined in the data space by the input variables, is possible to visualise individual element contribution to each node by colouring the map to produce "component plane plots". Examples of the component plane plots are included in Appendix A.

Flow path modelling procedure

Flow direction models were generated from the 1-arc second (30 m) SRTM digital elevation model using the hydrology tools in ArcToolbox in ArcGIS 9.3:

1) Run fill tool
   a) Input raster: DEM
   b) Output raster: DEM_fill
2) Run Flow direction tool
   a) Input raster: DEM_fill
   b) Output raster: DEM_flowdir
3) Run Flow accumulation tool
   a) Input raster: DEM_flowdir
   b) Output raster: DEM_flowacc
4) Spatial analyst raster calculator
   a) Input raster: DEM_flowacc
   b) Calculation: [DEM_flowacc] > 30*
   c) Output: flow paths

* A low number (30) was chosen such that low flows in the water course were represented, whereas an arbitrarily large number (5,000) would clip the results to riverbeds only. Calculations using < 30 produced a visually complex map. This value was deemed to be the most appropriate for the scale of map produced.

PSD of aeolian sands in the Yellabinna Regional Reserve

Particle size distribution (PSD) of aeolian material was investigated at three locations along the Yellabinna Regional Reserve boundary track as a follow-up to the Yellabinna surveys (*Section 6.5*). Samples were collected using the same technique described for mobile metal ion analysis of soil samples by Mann *et al*. (2005). The objective was to compare the MMI™ technique on bulk samples with the partial extraction of different size fractions (< 75 µm and < 200 µm) conducted at Tunkillia (Fabris 2010).

A 200-g bulk soil subsample was dried and sieved using a 200 µm and 75 µm mesh and a mechanical sieve shaker for 150 seconds. PSD data are included in the table below.

Particle size distribution of aeolian sediments in the Yellabinna Regional Reserve

Sample_ID	Easting (GDA 94 Z53)	Northing (GDA 94 Z53)	Bulk (g)	< 75 µm fraction (%)	< 200 µm fraction (%)	> 200 µm fraction (%)
Yel1 (east)	444911	6588988	155.7	1.2	41.8	57.9
Yel2	437978	6590620	186.8	4.2	57.5	42.3
Yel3 (west)	428813	6590566	140.1	3.1	48.4	51.5
Average ± 1SD	-	-	-	2.8 ± 0.9	49.2 ± 4.6	50.5 ± 4.5

Guidelines for the use of MMI™ methods, suggest to collect 250 – 350 g of bulk soil and to avoid sieving to prevent cross-contamination of samples (SGS 2011b).

The calculated average < 75 µm fraction of soil at the three sites in the Yellabinna Regional Reserve is 2.8 ± 0.9%. Assuming the large fractions are barren quartz, and Au is likely associated with clays in the fine fractions, normalising the MMI™ data from the Yellabinna using the average with low-end error (1.99%) transforms the highest Au in bulk from 0.4 ppb to 20.1 ppb (best case). While the MMI™ method used is different to the partial leach studies at Tunkillia by Fabris *et al*. (2010), it allows for a fraction comparison, albeit crude. A 20 ppb Au peak in the Yellabinna is near-background concentration at Tunkillia (peak of 155 pbb Au) for the same size fraction.

Investigating grain size distribution of aeolian sand samples from three locations (10 – 20 cm depth) within the Yellabinna (*Section 6.5*), found the < 200 µm fraction to account for 50% of the total mass. At < 200 µm, a substantial mass of barren quartz (likely 50%) would be diluting any potential trace element expressions of mineralisation. Practicality becomes an important factor with in-field sieving (pre-concentration). Fine fractions < 80 µm constitute < 5% of total soil mass. To collect a sufficient mass would through manual sieving would be laborious and problematic where soil moisture content would block the sieve mesh.

APPENDIX C: Publications

van der Hoek B.G., Hill S.M. & Dart R.C. (2012). Calcrete and plant inter-relationships for the expression of concealed mineralization at the Tunkillia gold prospect, central Gawler Craton, Australia.
Geochemistry: Exploration, Environment, Analysis, 12(4), 361-372.